

**ON THE METHODOLOGIES FOR DETERMINING THE ELASTIC AND  
PLASTIC MATERIAL PROPERTIES OF SMALL SCALE STRUCTURES  
USING INDENTATION TESTING**

by

Jayanta Kumar Phadikar

A dissertation submitted to the Faculty of the University of Delaware in partial fulfillment of the requirements for the degree of Doctor of Philosophy in Mechanical Engineering

Summer 2014

© 2014 Jayanta Kumar Phadikar  
All Rights Reserved

UMI Number: 3637294

All rights reserved

INFORMATION TO ALL USERS

The quality of this reproduction is dependent upon the quality of the copy submitted.

In the unlikely event that the author did not send a complete manuscript and there are missing pages, these will be noted. Also, if material had to be removed, a note will indicate the deletion.



UMI 3637294

Published by ProQuest LLC (2014). Copyright in the Dissertation held by the Author.

Microform Edition © ProQuest LLC.

All rights reserved. This work is protected against unauthorized copying under Title 17, United States Code



ProQuest LLC.  
789 East Eisenhower Parkway  
P.O. Box 1346  
Ann Arbor, MI 48106 - 1346

**ON THE METHODOLOGIES FOR DETERMINING THE ELASTIC AND  
PLASTIC MATERIAL PROPERTIES OF SMALL SCALE STRUCTURES  
USING INDENTATION TESTING**

by

Jayanta Kumar Phadikar

Approved: \_\_\_\_\_  
Suresh G. Advani, Ph.D.  
Chair of the Department of Mechanical Engineering

Approved: \_\_\_\_\_  
Babatunde A. Ogunnaike, Ph.D.  
Dean of the College of Engineering

Approved: \_\_\_\_\_  
James G. Richards, Ph.D.  
Vice Provost for Graduate and Professional Education

I certify that I have read this dissertation and that in my opinion it meets the academic and professional standard required by the University as a dissertation for the degree of Doctor of Philosophy.

Signed:

---

Anette M. Karlsson, Ph.D.  
Professor in charge of dissertation

I certify that I have read this dissertation and that in my opinion it meets the academic and professional standard required by the University as a dissertation for the degree of Doctor of Philosophy.

Signed:

---

Travis A. Bogetti, Ph.D.  
Adviser and Member of dissertation committee

I certify that I have read this dissertation and that in my opinion it meets the academic and professional standard required by the University as a dissertation for the degree of Doctor of Philosophy.

Signed:

---

Michael H. Santare, Ph.D.  
Member of dissertation committee

I certify that I have read this dissertation and that in my opinion it meets the academic and professional standard required by the University as a dissertation for the degree of Doctor of Philosophy.

Signed:

---

Mark R. VanLandingham, Ph.D.  
Member of dissertation committee

## ACKNOWLEDGMENTS

Much more than a stepping stone in the development of my academic career, these four years served as a wonderful experience and an impactful aid in the growth of my personal and social life.

My advisors, Dr. Anette M. Karlsson and Dr. Travis A. Bogetti have always given me freedom on how to proceed in the research work. This made my journey comfortable and joyful because I could act according to my instinct of understanding the subject and developing intelligent techniques instead of getting caught by too much computations or experiments. They never demanded unreasonable amount of results, therefore I could work peacefully according to my capacity. At the same time, there were watchful about my work, so I could not be neglectful.

Both Dr. Karlsson and Dr. Bogetti, especially Dr. Karlsson has helped me in learning the art of communicating my research/thoughts in a nice and comprehensive way to others. Her innumerable corrections in the papers and presentations have helped me to become more considerate about others' understandings. Dr. Karlsson's morality and Dr. Bogetti's honesty in doing research have always inspired me. Apart from these, both Dr. Karlsson and Dr. Bogetti have helped me by their suggestions during the course of the research work and in developing my academic career.

I thank Dr. Michael Santare (Department of Mechanical Engineering, University of Delaware) and Dr. Mark R. VanLandingham (Weapons and Materials Research Directorate, U.S. Army Research Laboratory, Aberdeen Proving Ground, MD) for agreeing to be my committee members. Dr. Santare's attitude of deeply

understanding the subject has always inspired me. His intelligent questions during the group meetings have urged me to properly understand my research topic. Dr. VanLandingham provided very helpful comments regarding the practical applications of my work. In addition, I would like to thank Dr. Victor N Kaliakin (Department of Civil Engineering, University of Delaware) for the finite element course he taught which helped during the course of my research work.

I would like to thank our department coordinators Letita Toto, Lisa Katzmire and Roger Stahl for providing numerous helps time to time which made my journey smooth.

During the stay in UD, I have come across wonderful friends and well-wishers including Parag G Nittur, Gaurav Pandey, Rahul Bhambure, Guoliang Ding, Hang Yu, Dattatrya Sahane, Narendar Singh Khatra to whom I am grateful. My parents' well-wishing attitude and support have always comforted me.

I wish a happy life to all of you.

## TABLE OF CONTENTS

LIST OF TABLES .....	x
LIST OF FIGURES .....	xix
ABSTRACT .....	xxiv
Chapter	
1 INTRODUCTION .....	1
1.1 Useful Mathematical Concepts.....	6
1.1.1 Uniqueness, sensitivity and condition number .....	6
1.1.2 Buckingham PI theorem .....	11
1.1.3 Solution of a system of nonlinear equations.....	13
1.2 Geometry and Material Properties.....	15
1.3 Oliver-Pharr Method .....	20
1.4 Single Indentation.....	21
1.5 Non-uniqueness of Force-displacement Relationship .....	25
1.6 Dual Indentation .....	27
1.7 Indentation of Anisotropic Materials.....	30
1.8 Outline of the Dissertation Work .....	33
2 INDENTATION OF NON-FLAT SUBSTRATES: CONICAL INDENTATION OF A SPHERE .....	35
2.1 Indentation of a Sphere Made of Linear-elastic, Perfectly-plastic Material .....	36
2.1.1 Theoretical preliminaries.....	36
2.1.2 Establishing the functional forms .....	42
2.1.2.1 Finite element model .....	42
2.1.2.2 Functional form for the first method (based on unloading slope) .....	45
2.1.2.3 Functional forms for the second method (based on reverse analysis) .....	48

2.1.3	Numerical verification.....	54
2.1.4	Sensitivity analysis.....	58
2.1.5	Synopsis: linear-elastic, perfectly-plastic sphere .....	62
2.2	Indentation of a Sphere Made of Viscoelastic Material .....	63
2.2.1	Viscoelastic solution using the elastic solution.....	63
2.2.1.1	Elastic solution.....	63
2.2.1.2	Viscoelastic solution.....	64
2.2.2	Numerical verification.....	68
2.2.2.1	Elastic indentation .....	68
2.2.2.2	Viscoelastic indentation.....	72
2.2.3	Synopsis: indentation of a visco-elastic sphere.....	73
2.3	Summary.....	74
3	A GENERAL METHODOLOGY TO IDENTIFY MATERIAL PARAMETERS WITH IDENTICAL FORCE-DISPLACEMENT RELATIONSHIP .....	76
3.1	Methodology.....	77
3.2	Iso-lines and Surfaces.....	80
3.2.1	Isotropic, linear-elastic, strain hardening plastic materials .....	81
3.2.2	Transversely isotropic, linear-elastic, perfectly plastic material.....	84
3.3	Functional Forms from Finite Element Analysis .....	85
3.4	Results .....	89
3.4.1	Isotropic, linear-elastic, power-law strain hardening plastic material.....	90
3.4.2	Isotropic, linear-elastic, linear strain hardening plastic material.....	101
3.4.3	Transversely isotropic, linear-elastic, perfectly plastic material.....	104
3.5	Application to Experiments in the Literature .....	108
3.6	Summary.....	113

4	ASSESSMENT OF THE SENSITIVITY OF INDENTATION TESTING USING CONDITION NUMBER AND SENSITIVITY ANALYSIS.....	115
4.1	Application of Condition Number to Indentation Technique.....	116
4.2	Condition Numbers of Single and Dual Indentation Techniques.....	124
4.2.1	Modified condition number .....	125
4.2.2	Computational procedure .....	126
4.2.3	Condition numbers for single indentation .....	127
4.2.4	Condition numbers for dual indentation.....	129
4.3	Sensitivity Analysis.....	136
4.3.1	Analysis procedure .....	136
4.3.2	Sensitivity of dual indentation techniques.....	138
4.3.2.1	Dual conical indentation ( $\alpha_1 = 50^\circ$ , $\alpha_2 = 80^\circ$ ).....	139
4.3.2.2	Dual spherical indentation: $(h_m/R_i)_1 = 10\%$ , $(h_m/R_i)_2 = 40\%$ .....	142
4.3.2.3	Dual spherical indentation: $(h_m/R_i)_1 = 10\%$ and $1\%$ , $(h_m/R_i)_2 = 100\%$ .....	145
4.3.2.4	Dual conical-spherical indentation: $\alpha_1 = 80^\circ$ , $(h_m/R_i)_2 = 100\%$ ; and $(h_m/R_i)_1 = 1\%$ , $\alpha_2 = 50^\circ$ .....	147
4.3.2.5	Sensitivity behavior across material range.....	149
4.4	Sensitivity of Dual Indentation for Transversely Isotropic, Linear-elastic, Perfectly-plastic Materials .....	151
4.4.1	Condition numbers and sensitivity .....	151
4.5	Summary.....	156
5	CONCLUDING REMARKS AND FUTURE WORK.....	158
5.1	Concluding Remarks .....	158
5.1.1	Geometry .....	158
5.1.2	Reliability .....	159
5.1.3	Material properties.....	160
5.2	Suggested Future Work .....	161
5.3	Summary.....	164

REFERENCES .....	166
------------------	-----

Appendix

A	FUNCTIONAL FORMS AND FITTING COEFFICIENTS .....	177
A.1	Isotropic, Linear-elastic, Power-law Strain Hardening Plastic Materials .....	177
A.1.1	Conical indentation of a half-space .....	178
A.1.2	Spherical indentation of a half-space .....	184
A.1.3	Conical indentation of a sphere .....	192
A.1.4	Spherical indentation of a sphere .....	192
A.2	Isotropic, Linear-elastic, Linear-hardening Material.....	193
A.2.1	Conical indentation of a half-space .....	194
A.2.2	Spherical indentation of a half-space .....	194
A.3	Transversely Isotropic, Linear-elastic, Perfectly-plastic Material .....	195

## LIST OF TABLES

Table 1.1:	Correlation between condition number and the sensitivity to perturbation in four linear systems.....	9
Table 1.2:	Dimensional matrix of the parameters involved in Eq. (1.2).....	12
Table 1.3:	Various combinations of shape functions, half-angles (conical indentation) and depth-to-radius ratios (spherical indentation) used by previous researchers. ....	29
Table 2.1:	The coefficients $a_{ij}$ used in Eq. (2.15c).....	49
Table 2.2:	The coefficients $b_{ij}$ used in Eq. (2.19c).....	51
Table 2.3:	Comparison of input material properties with that obtained using the two methods for selected indentation depths .....	56
Table 2.4:	Comparison of input material properties with that obtained using the two methods for selected half-angles of indentation.....	57
Table 3.1:	Material parameter sets that lead to identical $W_t$ and $W_e$ for conical ( $\alpha = 70.3^\circ$ ) indentation of a half-space and a sphere (radius 23 $\mu\text{m}$ ) modeled by linear-elastic, power law hardening plastic material model. Force displacement relationships are shown in Figure 3.6. ....	92
Table 3.2:	Material parameter sets that lead to identical $W_t$ and $W_e$ for spherical (radius 3 $\mu\text{m}$ ) indentation of a half-space modeled by linear-elastic, power law hardening plastic material model with depth-to-radius ratio of 20% and 100%. Force displacement relationships are shown in Figure 3.8.....	95
Table 3.3:	Material parameter sets leading to identical $W_t$ , $P_m$ and $W_e$ for spherical (radius 3 $\mu\text{m}$ ) indentation of a half-space modeled by linear-elastic, power law hardening plastic material model with depth-to-radius ratio of 100%. Force displacement relationships are shown in Figure 3.9.....	98

Table 3.4:	Material parameter sets leading to identical $(W_t, W_e)$ and $(W_t, P_m, W_e)$ for spherical (radius 3 $\mu\text{m}$ ) indentation of a sphere (radius 23 $\mu\text{m}$ ) modeled by linear-elastic, power law hardening plastic material model. Force displacement relationships are shown in Figure 3.10. ....	99
Table 3.5:	Material parameter sets leading to identical $W_t$ and $W_e$ for conical ( $\alpha = 70.3^\circ$ ) and spherical indentation (radius 3 $\mu\text{m}$ ) of a half-space modeled by linear-elastic, linear hardening plastic material model. Force displacement relationships are shown in Figure 3.12. ....	102
Table 3.6:	Material parameter sets leading to identical $W_t$ for conical ( $\alpha = 70.3^\circ$ ) and spherical (radius 3 $\mu\text{m}$ ) indentation of a half-space modeled by transversely isotropic, linear-elastic, perfectly-plastic material model. Poisson's ratios are assumed to be constant: $\nu_{xz} = 0.05$ and $\nu_{xy} = 0.2$ . Force displacement relationships are shown in Figure 3.14 .....	106
Table 3.7:	Material parameter sets leading to identical $(W_t, W_e)$ and $(W_t, P_m, W_e)$ with that of the experimental (Taljat et al., 1998) material. Force displacement relationships are shown in Figure 3.17.....	111
Table 4.1:	Condition numbers for single indentation technique for various combinations of shape functions .....	128
Table 4.2a:	Condition numbers for various combinations of shape functions of dual conical indentation arranged in ascending order (rank 1-50).....	131
Table 4.2b:	Condition numbers for various combinations of shape functions of dual conical indentation arranged in ascending order (rank 51-100)....	132
Table 4.3a:	Condition numbers for various combinations of shape functions of dual spherical indentation arranged in ascending order (rank 1-50)....	133
Table 4.3b:	Condition numbers for various combinations of shape functions of dual spherical indentation arranged in ascending order (rank 51-100).	134
Table 4.4:	Condition numbers for various choices of half-angles (for conical indentation) and depth-to-radius ratios (for spherical indentation) for the shape function combination $(W_e^2, S_u^1, W_e^1)$ .....	136
Table 4.5:	Errors in calculated material properties based on Monte Carlo, One Factor and Uniform Factors sensitivity analysis for conical dual indentation with $\alpha_1 = 50^\circ$ and $\alpha_2 = 80^\circ$ and shape function combination $(W_e^2, S_u^1, W_e^1)$ , $\kappa_m^{avg} = 5.8248$ . $\kappa_m^{avg} = 5.8248$ .....	140

Table 4.6:	Errors in calculated material properties based on Monte Carlo sensitivity analysis procedure for conical dual indentation with $\alpha_1 = 50^\circ$ and $\alpha_2 = 80^\circ$ and shape function combination $(h_f^2, S_u^1, W_e^1), \kappa_m^{avg} = 42.715$ and $(h_f^2, W_t^1, P_m^1), \kappa_m^{avg} = 322.06$ . . . . .	142
Table 4.7:	Errors in calculated material properties based on Monte Carlo, One Factor and Uniform Factors sensitivity analysis procedure for spherical dual indentation with $(h_m/R_i)_1 = 10\%$ and $(h_m/R_i)_2 = 40\%$ and shape function combination $(W_e^2, S_u^1, W_e^1), \kappa_m^{avg} = 7.6837$ . $\kappa_m^{avg} = 7.6837$ . . . . .	144
Table 4.8:	Errors in calculated material properties based on Monte Carlo sensitivity analysis procedure for spherical dual indentation with $(h_m/R_i)_1 = 10\%$ and $(h_m/R_i)_2 = 40\%$ and shape function combination $(W_t^2, W_t^1, h_f^1), \kappa_m^{avg} = 65.825$ and $(h_f^2, W_e^1, h_f^1), \kappa_m^{avg} = 253.09$ . . . . .	145
Table 4.9:	Errors in calculated material properties based on Monte Carlo sensitivity analysis procedure for spherical dual indentation with $(h_m/R_i)_1 = 10\%$ ; $(h_m/R_i)_2 = 100\%$ ; shape function combination $(W_e^2, S_u^1, W_e^1), \kappa_m^{avg} = 4.1113$ and $(h_m/R_i)_1 = 1\%$ ; $(h_m/R_i)_2 = 100\%$ ; shape function combination $(W_e^2, S_u^1, W_e^1), \kappa_m^{avg} = 2.6237$ . . . . .	147
Table 4.10:	Errors in calculated material properties based on Monte Carlo sensitivity analysis for dual conical-spherical indentation with $\alpha_1 = 80^\circ$ , $(h_m/R_i)_2 = 100\%$ ; and $(h_m/R_i)_1 = 1\%$ , $\alpha_2 = 50^\circ$ with shape function combination $(W_e^2, S_u^1, W_e^1)$ . Condition numbers are 4.1599 and 4.7386 respectively. . . . .	149
Table 4.11:	Errors in calculated material properties based on Monte Carlo sensitivity analysis for 9 selected materials spanning the $E/Y-n$ space for spherical dual indentation with $(h_m/R_i)_1 = 1\%$ and $(h_m/R_i)_2 = 100\%$ and shape function combination $(W_e^2, S_u^1, W_e^1)$ . . . . .	150
Table 4.12:	Condition numbers for various combinations of half-angles (conical indentation) and depth-to-radius ratios (spherical indentation). As the difference between half-angles or depth-to-radius ratio increases, sensitivity to experimental error decreases. . . . .	153

Table 4.13: Condition numbers for various combinations of shape functions arranged in ascending order .....	155
Table A.1: Fitting coefficients for Eq. (A.1) for the normalized total energy, $W_t$ , for $\alpha = 50^\circ$ .....	178
Table A.2: Fitting coefficients for Eq. (A.1) for the normalized maximum load, $P_m$ , for $\alpha = 50^\circ$ .....	178
Table A.3: Fitting coefficients for Eq. (A.1) for the normalized unloading slope, $S_u$ , for $\alpha = 50^\circ$ .....	179
Table A.4: Fitting coefficients for Eq. (A.1) for the normalized elastic energy, $W_e$ , for $\alpha = 50^\circ$ .....	179
Table A.5: Fitting coefficients for Eq. (A.1) for the normalized final depth, $h_f$ , for $\alpha = 50^\circ$ .....	179
Table A.6: Fitting coefficients for Eq. (A.1) for the normalized unloading slope, $S_u$ , for $\alpha = 60^\circ$ .....	180
Table A.7: Fitting coefficients for Eq. (A.1) for the normalized unloading energy, $W_e$ , for $\alpha = 60^\circ$ .....	180
Table A.8: Fitting coefficients for Eq. (A.1) for the normalized total energy, $W_e$ , for $\alpha = 70^\circ$ .....	180
Table A.9: Fitting coefficients for Eq. (A.1) for the normalized maximum load, $P_m$ , for $\alpha = 70^\circ$ .....	181
Table A.10: Fitting coefficients for Eq. (A.1) for the normalized unloading slope, $S_u$ , for $\alpha = 70^\circ$ .....	181
Table A.11: Fitting coefficients for Eq. (A.1) for the normalized unloading energy, $W_e$ , for $\alpha = 70^\circ$ .....	181
Table A.12: Fitting coefficients for Eq. (A.1) for the normalized final depth, $h_f$ , for $\alpha = 70^\circ$ .....	182
Table A.13: Fitting coefficients for Eq. (A.1) for the normalized total energy, $W_t$ , for $\alpha = 70.3^\circ$ .....	182
Table A.14: Fitting coefficients for Eq. (A.1) for the normalized elastic energy, $W_e$ , for $\alpha = 70.3^\circ$ .....	182

Table A.15: Fitting coefficients for Eq. (A.1) for the normalized total energy, $W_t$ , for $\alpha = 80^\circ$ .....	183
Table A.16: Fitting coefficients for Eq. (A.1) for the normalized maximum load, $P_m$ , for $\alpha = 80^\circ$ .....	183
Table A.17: Fitting coefficients for Eq. (A.1) for the normalized unloading slope, $S_u$ , for $\alpha = 80^\circ$ .....	183
Table A.18: Fitting coefficients for Eq. (A.1) for the normalized elastic energy, $W_e$ , for $\alpha = 80^\circ$ .....	184
Table A.19: Fitting coefficients for Eq. (A.1) for the normalized final depth, $h_f$ , for $\alpha = 80^\circ$ .....	184
Table A.20: Fitting coefficients for Eq. (A.1) for the normalized unloading slope, $S_u$ , for $(h_m/R_s) = 1\%$ .....	185
Table A.21: Fitting coefficients for Eq. (A.1) for the normalized unloading energy, $W_e$ , for $(h_m/R_s) = 1\%$ .....	185
Table A.22: Fitting coefficients for Eq. (A.1) for the normalized total energy, $W_t$ , for $(h_m/R_s) = 10\%$ .....	185
Table A.23: Fitting coefficients for Eq. (A.1) for the normalized maximum load, $P_m$ , for $(h_m/R_s) = 10\%$ .....	186
Table A.24: Fitting coefficients for Eq. (A.1) for the normalized unloading slope, $S_u$ , for $(h_m/R_s) = 10\%$ .....	186
Table A.25: Fitting coefficients for Eq. (A.1) for the normalized elastic energy, $W_e$ , for $(h_m/R_s) = 10\%$ .....	186
Table A.26: Fitting coefficients for Eq. (A.1) for the normalized final depth, $h_f$ , for $(h_m/R_s) = 10\%$ .....	187
Table A.27: Fitting coefficients for Eq. (A.1) for the normalized total energy, $W_t$ , for $(h_m/R_s) = 20\%$ .....	187
Table A.28: Fitting coefficients for Eq. (A.1) for the normalized maximum load, $P_m$ , for $(h_m/R_s) = 20\%$ .....	187
Table A.29: Fitting coefficients for Eq. (A.1) for the normalized unloading slope, $S_u$ , for $(h_m/R_s) = 20\%$ .....	188

Table A.30: Fitting coefficients for Eq. (A.1) for the normalized unloading energy, $W_e$ , for $(h_m/R_s) = 20\%$ .....	188
Table A.31: Fitting coefficients for Eq. (A.1) for the normalized final depth, $h_f$ , for $(h_m/R_s) = 20\%$ .....	188
Table A.32: Fitting coefficients for Eq. (A.1) for the normalized unloading slope, $S_u$ , for $(h_m/R_s) = 30\%$ .....	189
Table A.33: Fitting coefficients for Eq. (A.1) for the normalized elastic energy, $W_e$ , for $(h_m/R_s) = 30\%$ .....	189
Table A.34: Fitting coefficients for Eq. (A.1) for the normalized total energy, $W_t$ , for $(h_m/R_s) = 40\%$ .....	189
Table A.35: Fitting coefficients for Eq. (A.1) for the normalized maximum load, $P_m$ , for $(h_m/R_s) = 40\%$ .....	190
Table A.36: Fitting coefficients for Eq. (A.1) for the normalized unloading slope, $S_u$ , for $(h_m/R_s) = 40\%$ .....	190
Table A.37: Fitting coefficients for Eq. (A.1) for the normalized elastic energy, $W_e$ , for $(h_m/R_s) = 40\%$ .....	190
Table A.38: Fitting coefficients for Eq. (A.1) for the normalized final depth, $h_f$ , for $(h_m/R_s) = 40\%$ .....	191
Table A.39: Fitting coefficients for Eq. (A.1) for the normalized unloading slope, $S_u$ , for $(h_m/R_s) = 100\%$ .....	191
Table A.40: Fitting coefficients for Eq. (A.1) for the normalized elastic energy, $W_e$ , for $(h_m/R_s) = 100\%$ .....	191
Table A.41: Fitting coefficients for Eq. (A.1) for the normalized total energy, $W_t$ , for $\alpha = 70.3^\circ$ and $(h_m/R_s) = 20\%$ .....	192
Table A.42: Fitting coefficients for Eq. (A.1) for the normalized elastic energy, $W_e$ , for $\alpha = 70.3^\circ$ and $(h_m/R_s) = 20\%$ .....	192
Table A.43: Fitting coefficients for Eq. (A.1) for the normalized total energy, $W_t$ , for $h_m/R_i = 38.33\%$ and $h_m/R_s = 5\%$ .....	193
Table A.44: Fitting coefficients for Eq. (A.1) for the normalized elastic energy, $W_e$ , for $h_m/R_i = 38.33\%$ and $h_m/R_s = 5\%$ .....	193

Table A.45: Fitting coefficients for Eq. (A.2) for the normalized total energy, $W_t$ , for $\alpha = 70.3^\circ$ .....	194
Table A.46: Fitting coefficients for Eq. (A.2) for the normalized elastic energy, $W_e$ , for $\alpha = 70.3^\circ$ .....	194
Table A.47: Fitting coefficients for Eq. (A.2) for the normalized total energy, $W_t$ , for $h_m/R_s = 3\%$ .....	195
Table A.48: Fitting coefficients for Eq. (A.2) for the normalized elastic energy, $W_e$ , for $h_m/R_s = 3\%$ .....	195
Table A.49: Equations of the seven surfaces used in the regression analysis (Figure 3.4) for transversely isotropic, linear-elastic, perfectly plastic material.	196
Table A.50: The assignment of $x$ , $y$ and $z$ of the equations in Table A.49 to the non-dimensional material properties groups $(E_z/E_x)$ , $(E_x/G_{xz})$ and $(E_x/Y)$ .....	197
Table A.51: The equations used in the regression analysis for various shape functions for conical indentation of a half-space .....	198
Table A.52: The equations used in the regression analysis for various shape functions for spherical indentation of a half-space .....	199
Table A.53: Polynomial fitting coefficients for the coefficients of the surface for the normalized total energy, $W_t$ , for $\alpha = 45^\circ$ .....	200
Table A.54: Polynomial fitting coefficients for the coefficients of the surface for the normalized maximum load, $P_m$ , for $\alpha = 45^\circ$ .....	200
Table A.55: Polynomial fitting coefficients for the coefficients of the surface for the normalized unloading slope, $S_u$ , for $\alpha = 45^\circ$ .....	200
Table A.56: Polynomial fitting coefficients for the coefficients of the surface for the normalized elastic energy, $W_e$ , for $\alpha = 45^\circ$ .....	201
Table A.57: Polynomial fitting coefficients for the coefficients of the surface for the normalized final depth, $h_f$ , for $\alpha = 45^\circ$ .....	201
Table A.58: Polynomial fitting coefficients for the coefficients of the surface for the normalized total energy, $W_t$ , for $\alpha = 80^\circ$ .....	202

Table A.59: Polynomial fitting coefficients for the coefficients of the surface for the normalized maximum load, $P_m$ , for $\alpha = 80^\circ$ .....	202
Table A.60: Polynomial fitting coefficients for the coefficients of the surface for the normalized unloading slope, $S_u$ , for $\alpha = 80^\circ$ .....	203
Table A.61: Polynomial fitting coefficients for the coefficients of the surface for the normalized elastic energy, $W_e$ , for $\alpha = 80^\circ$ .....	203
Table A.62: Polynomial fitting coefficients for the coefficients of the surface for the normalized final depth, $h_f$ , for $\alpha = 80^\circ$ .....	204
Table A.63: Polynomial fitting coefficients for the coefficients of the surface for the normalized total energy, $W_t$ , for $(h_m/R) = 1\%$ .....	204
Table A.64: Polynomial fitting coefficients for the coefficients of the surface for the normalized maximum load, $P_m$ , for $(h_m/R) = 1\%$ .....	205
Table A.65: Polynomial fitting coefficients for the coefficients of the surface for the normalized unloading slope, $S_u$ , for $(h_m/R) = 1\%$ .....	205
Table A.66: Polynomial fitting coefficients for the coefficients of the surface for the normalized elastic energy, $W_e$ , for $(h_m/R) = 1\%$ .....	206
Table A.67: Polynomial fitting coefficients for the coefficients of the surface for the normalized final depth, $h_f$ , for $(h_m/R) = 1\%$ .....	206
Table A.68: Polynomial fitting coefficients for the coefficients of the surface for the normalized total energy, $W_t$ , for $(h_m/R) = 100\%$ .....	206
Table A.69: Polynomial fitting coefficients for the coefficients of the surface for the normalized maximum load, $P_m$ , for $(h_m/R) = 100\%$ .....	207
Table A.70: Polynomial fitting coefficients for the coefficients of the surface for the normalized unloading slope, $S_u$ , for $(h_m/R) = 100\%$ .....	207
Table A.71: Polynomial fitting coefficients for the coefficients of the surface for the normalized elastic energy, $W_e$ , for $(h_m/R) = 100\%$ .....	208
Table A.72: Polynomial fitting coefficients for the coefficients of the surface for the normalized final depth, $h_f$ , for $(h_m/R) = 100\%$ .....	208
Table A.73: Polynomial fitting coefficients for the coefficients of the surface for the normalized total energy, $W_t$ , for $\alpha = 50^\circ$ .....	208

Table A.74: Polynomial fitting coefficients for the coefficients of the surface for the normalized elastic energy, $W_e$ , for $\alpha = 50^\circ$ .	209
Table A.75: Polynomial fitting coefficients for the coefficients of the surface for the normalized total energy, $W_t$ , for $\alpha = 60^\circ$ .	209
Table A.76: Polynomial fitting coefficients for the coefficients of the surface for the normalized elastic energy, $W_e$ , for $\alpha = 60^\circ$ .	210
Table A.77: Polynomial fitting coefficients for the coefficients of the surface for the normalized total energy, $W_t$ , for $\alpha = 70^\circ$ .	210
Table A.78: Polynomial fitting coefficients for the coefficients of the surface for the normalized elastic energy, $W_e$ , for $\alpha = 70^\circ$ .	211
Table A.79: Polynomial fitting coefficients for the coefficients of the surface for the normalized unloading slope, $S_u$ , for $\alpha = 80^\circ$ .	211
Table A.80: Polynomial fitting coefficients for the coefficients of the surface for the normalized elastic energy, $W_e$ , for $\alpha = 80^\circ$ .	212
Table A.81: Polynomial fitting coefficients for the coefficients of the surface for the normalized unloading slope, $S_u$ , for $(h_m/R) = 20\%$ .	212
Table A.82: Polynomial fitting coefficients for the coefficients of the surface for the normalized elastic energy, $W_e$ , for $(h_m/R) = 20\%$ .	213
Table A.83: Polynomial fitting coefficients for the coefficients of the surface for the normalized maximum load, $P_m$ , for $(h_m/R) = 40\%$ .	213
Table A.84: Polynomial fitting coefficients for the coefficients of the surface for the normalized elastic energy, $W_e$ , for $(h_m/R) = 40\%$ .	214
Table A.85: Polynomial fitting coefficients for the coefficients of the surface for the normalized maximum load, $P_m$ , for $(h_m/R) = 60\%$ .	214
Table A.86: Polynomial fitting coefficients for the coefficients of the surface for the normalized elastic energy, $W_e$ , for $(h_m/R) = 60\%$ .	215
Table A.87: Polynomial fitting coefficients for the coefficients of the surface for the normalized maximum load, $P_m$ , for $(h_m/R) = 80\%$ .	215
Table A.88: Polynomial fitting coefficients for the coefficients of the surface for the normalized elastic energy, $W_e$ , for $(h_m/R) = 80\%$ .	216

## LIST OF FIGURES

Figure 1.1:	A typical nanoindenter (Hysitron Triboindenter): (a) outside view and (b) inside view .....	3
Figure 1.2:	(a) Isometric view of a typical indentation experiment (b) Cross-sectional view of an indentation experiment (c) force-displacement relationship obtained from a typical indentation experiment .....	4
Figure 1.3:	Three systems of straight lines (examples a, b and c of Table 1.1: the original or unperturbed systems) with increasing condition number and sensitivity. As the condition number increases, the straight lines approach each other and finally overlap.....	11
Figure 1.4:	A cantilever beam problem used for illustrating Buckingham PI theorem.....	12
Figure 1.5:	Algorithm used to solve the nonlinear set of equations arising in indentation analyses .....	15
Figure 1.6:	The two widely used indenters: a) conical indenter with half-angle $\alpha$ and b) spherical indenter with radius $R_i$ .....	16
Figure 1.7:	Three time-independent material models: (a) Isotropic, linear-elastic, power-law hardening material (b) isotropic, linear-elastic, linear hardening material (c) transversely isotropic, linear-elastic, perfectly-plastic material ( $x$ - $y$ is the plane of isotropy) .....	18
Figure 1.8:	Three selected models for viscoelastic materials: (a) Maxwell element (b) Kelvin-Voigt element and (c) standard three parameter model.....	20
Figure 1.9:	Procedure for obtaining material properties from an indentation experiment (single indentation).....	23
Figure 2.1:	Conical indentation of a sphere resting on a fixed rigid plate .....	38
Figure 2.2:	Solving the cone-sphere contact problem via superposition: (a) the complete problem; (b) the upper half model; (c) the lower half model. .	39
Figure 2.3:	Finite element model in ABAQUS, including enlargements of the refined meshes (plotted at the same scale) at the top of the sphere (conical indentation) and the bottom of the sphere (contact with the rigid surface).....	44

Figure 2.4: Comparison of the force displacement relationship obtained using the finite element method and the superposition techniques. For a linear-elastic material (assumed here), the loading and unloading curves are identical. ....	46
Figure 2.5: The function $\rho(a_t)$ defined in Eq. (2.5) as function of $a_t$ , the projected contact area for a $75^\circ$ half-angle indenter indenting a sphere of radius $23 \mu\text{m}$ .....	47
Figure 2.6: Graphs of functions $\phi_1$ and $\theta_1$ of Eqs. (2.13) and (2.14) for $\alpha = 70.3^\circ$ and $0.05 < h_m/R_s < 0.20$ : (a) $\frac{S_u}{Yh_m} = \phi_1\left(\frac{E}{Y}, \frac{h_m}{R_s}\right)$ (b) $\frac{S_u}{W_t} h_m^2 = \theta_1\left(\frac{E}{Y}, \frac{h_m}{R_s}\right)$ .....	50
Figure 2.7: Graphs of functions $\phi_2$ and $\theta_2$ of Eqs. (2.17) and (2.18) for $h_m/R = 0.10$ and $45^\circ \leq \alpha \leq 90^\circ$ : (a) $\frac{S_u}{Yh_m} = \phi_2\left(\frac{E}{Y}, \alpha\right)$ (b) $\frac{S_u}{W_t} h_m^2 = \theta_2\left(\frac{E}{Y}, \alpha\right)$ .....	52
Figure 2.8: Flowchart of the second methodology (based on reverse analysis) to determine material properties of a sphere by conical indentation.....	54
Figure 2.9: Sensitivity in determining the elastic modulus, $E$ , with respect to imposing a small error in (a) the unloading slope, $S_u$ , and (b) the projected contact radius, $a_t$ , using the first method (the method based on elastic unloading). ....	59
Figure 2.10: Sensitivity in determining the elastic modulus, $E$ , and the yield strength, $Y$ , with respect to imposing a small error in (a) the unloading slope, $S_u$ , and (b) the total energy, $W_t$ , using the second method (finite element based reverse analysis). ....	61
Figure 2.11: Assumed constitutive behavior of the viscoelastic material and the loading function: (a) standard three-element solid model for deviatoric behavior, (b) spring element for spherical (volumetric) behavior, and (c) triangular loading.....	66
Figure 2.12: The (a) original and (b) normalized force-displacement relationships for the elastic indentation problem, for selected Poisson's ratios as obtained from geometrically nonlinear finite element analysis .....	70
Figure 2.13: Comparison of force-displacement relationships obtained using the proposed semi-analytical approach and ABAQUS for four selected loading times, $T$ . ....	72

Figure 3.1:	Schematics of three sets of loading curves with (a) identical $W_t$ but different $P_m$ , (b) identical $W_t$ and $P_m$ , and (c) identical $P_m$ , $W_t^1$ and $W_t^2$ .	80
Figure 3.2:	Schematic of a iso- $(W_t/W_e)$ line in $E / Y - \bar{\xi}$ space .....	83
Figure 3.3:	Finite element model of a half-space being indented by a spherical indenter .....	86
Figure 3.4:	Schematic of the regression analysis used for expressing the normalized shape functions as functions of material properties for transversely isotropic materials (Eqs. (1.13)).....	89
Figure 3.5:	Few iso- $(W_t/W_e)$ lines for conical indentation of a half-space with $\alpha = 70.3^\circ$ .....	92
Figure 3.6:	Force-displacement relationships corresponding to five material parameter sets that lead to identical $W_t$ and $W_e$ for conical ( $\alpha = 70.3^\circ$ ) indentation of (a) a half-space and (b) a sphere (radius 23 $\mu\text{m}$ ) modeled by linear-elastic, power law hardening plastic material model. The curves overlap within the resolution of the figure. ....	93
Figure 3.7:	Stress-strain relationships corresponding to five material parameter sets that lead to identical $W_t$ and $W_e$ for conical ( $\alpha = 70.3^\circ$ ) indentation of (a) a half-space and (b) a sphere (radius 23 $\mu\text{m}$ ) modeled by linear-elastic, power law hardening plastic material model. ....	94
Figure 3.8:	Force-displacement relationships corresponding to five material sets that lead to identical $W_t$ and $W_e$ for spherical (radius 3 $\mu\text{m}$ ) indentation of a half-space modeled by linear-elastic, power law hardening plastic material model with depth-to-radius ratio of (a) 20% and (b) 100%. The curves do not overlap completely. The difference in force-displacement relationships is clearer for depth-to-radius ratio of 100% than of 20%. ....	96
Figure 3.9:	Force-displacement relationships corresponding to five material parameter sets that lead to identical $W_t$ , $P_m$ and $W_e$ for spherical (of radius 3 $\mu\text{m}$ ) indentation of a half-space modeled by linear-elastic, power-law hardening plastic material model with depth-to-radius ratio of 100%. The force-displacement relationships almost overlap. ....	98

Figure 3.10: Force-displacement relationships corresponding to five material parameter sets leading to (a) identical $W_t$ and $W_e$ and (b) identical $W_t$ , $P_m$ and $W_e$ , for spherical (radius 3 $\mu\text{m}$ ) indentation of a sphere (radius 23 $\mu\text{m}$ ). Although the curves with identical $W_t$ and $W_e$ do not overlap, curves for with identical $W_t$ , $P_m$ and $W_e$ do overlap. ....	100
Figure 3.11: Iso- $(W_t/W_e)$ lines for conical ( $\alpha = 70.3^\circ$ ) indentation of a half-space made of linear elastic, linear strain hardening plastic material .....	101
Figure 3.12: Force-displacement relationships corresponding to five material parameter sets leading to identical $W_t$ and $W_e$ for (a) conical ( $\alpha = 70.3^\circ$ ) and (b) spherical (radius 3 $\mu\text{m}$ ) indentation of a half-space modeled by linear-elastic, linear hardening plastic material model. The curves overlap within the resolution of the figure. ....	103
Figure 3.13: A iso- $(W_t/W_e)$ surface for (a) conical ( $\alpha = 70.3^\circ$ ) and (b) spherical (radius 3 $\mu\text{m}$ ) indentation of a half-space made of transversely isotropic, linear-elastic, perfectly plastic material.....	105
Figure 3.14: Force-displacement relationships corresponding to five material parameter sets that lead to identical $W_t$ and $W_e$ for (a) conical ( $\alpha = 70.3^\circ$ ) and (b) spherical (radius 3 $\mu\text{m}$ ) indentation of a half-space made of transversely isotropic, linear-elastic, perfectly plastic material model. The curves almost overlap on each other. ....	107
Figure 3.15: Comparison of force-displacement relationships obtained from experiment (Taljat et al., 1998) and simulation for spherical (radius 0.788 mm) indentation of a half-space .....	109
Figure 3.16: Iso- $(W_t/W_e)$ lines corresponding to the geometry of indentation experiment performed by Taljat et al. (1998). The iso-line corresponding to the experimental material is indicated. ....	110
Figure 3.17: Comparison of the experimentally (Taljat et al., 1998) obtained force-displacement relationship and the force-displacement relationships of five material parameter sets leading to (a) $W_t$ and $W_e$ and (b) $W_t$ , $P_m$ and $W_e$ identical to the experimental material .....	112
Figure 4.1: Selected iso- $(P_m/S_u h_m)$ lines for (a) $\alpha = 50^\circ$ ; (b) $\alpha = 50^\circ$ and $\alpha = 80^\circ$ ; (c) $\alpha = 50^\circ$ and $\alpha = 70^\circ$ ; (d) $\alpha = 50^\circ$ and $\alpha = 60^\circ$ . As the iso-lines from two tests approach each other, the system becomes increasingly sensitive to experimental errors.....	122

Figure 4.2: Selected iso- $(P_m/S_u h_m)$  lines passing through the point  $E/Y = 500$ ,  $n = 0.25$  for four selected conical indenters..... 124

## ABSTRACT

Instrumented indentation is a popular technique used to determine the elastic and plastic material properties of small scale structures. In this dissertation, an attempt is made to advance the indentation research in three areas:

- i) Indentation of non-flat substrates;
- ii) Uniqueness and sensitivity of indentation testing;
- iii) Indentation of anisotropic materials.

Regarding indentation of non-flat substrates, conical indentation of a sphere made of isotropic, linear-elastic, perfectly-plastic material and viscoelastic material is investigated. For the sphere with time-independent properties, a semi-analytical method and a finite element based reverse analysis technique are proposed to determine the material properties. It is shown that the methods can predict the material properties quite accurately. For the viscoelastic sphere, a semi-analytical method is developed to obtain the force-displacement relationship of the sphere. The method can be used to obtain the force-displacement relationship of a viscoelastic sphere much faster than the finite element simulation, thus saving computational cost for a possible reverse analysis. The methodologies proposed for the sphere can inspire similar methodologies for other non-flat substrates.

Regarding the non-uniqueness and sensitivity due to experimental error of indentation testing, it is shown comprehensively that the two phenomena are not independent, rather non-uniqueness is an extreme case of sensitivity. A methodology is developed to systematically identify the materials which will result in identical force-displacement relationship. The concept of condition number is employed to quantify and rank the sensitivity of different indentation methodologies due to experimental error. Thus, guidelines are provided regarding the selection of test conditions to improve the sensitivity. The guidelines obtained from the condition number are verified by explicit sensitivity analysis. It appears that, in general, indentation tests need to be very accurate to determine the material properties accurately.

Regarding indentation of anisotropic materials, various possible dual indentation methodologies have been considered for indentation of a transversely isotropic, linear-elastic, perfectly-plastic material. The methodologies developed for uniqueness and sensitivity analysis are applied to the material. It appears that the sensitivity for transversely isotropic materials is higher compared to the isotropic materials.

## Chapter 1

### INTRODUCTION

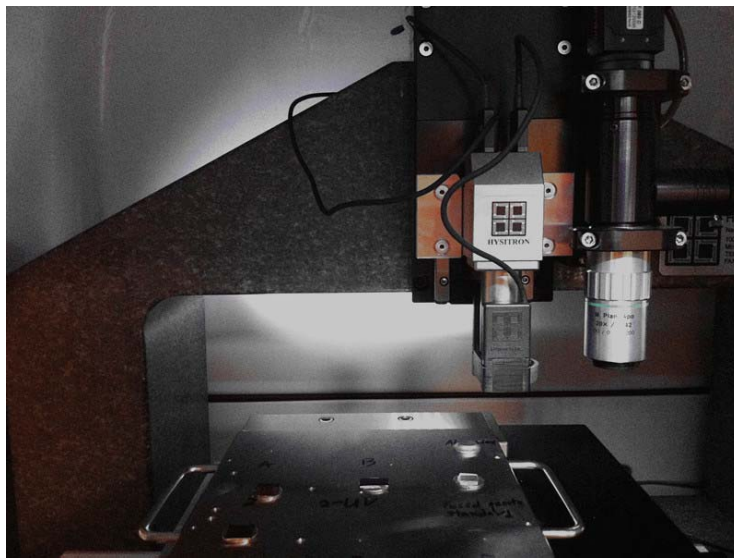
Small scale structures such as thin films, micro-fibers and micro-spheres are frequently used in many engineering components such as solar panels, MEMS, medical devices and so on. Determination of the mechanical properties of such small scale structures is a key step in designing such engineering devices. Conventional testing methods, such as tensile testing and bending testing are primarily designed for much larger scale structures. Thus, with the growing applications of small scale structures, there is a need for developing testing methods for determining mechanical properties at the micro scale. A popular technique for determining the mechanical properties of bulk materials available in small volume is indentation testing (Cheng and Cheng, 2004; Green, 2005; Oliver and Pharr, 1992; Johnson, 1987; Jackson et al., 2010; Yan et al., 2007a, 2007b). Originally, the technique was developed to measure material hardness, but in last few decades, methodologies have been developed to measure more sophisticated mechanical properties such as elastic and plastic material properties through instrumented indentation testing (see the review by Cheng and Cheng (2004)).

Figure 1.1 shows a typical nanoindenter (Hysitron Triboindenter). During an indentation experiment (Figure 1.2a and 1.2b), a rigid indenter is pushed into and then removed from the surface of a solid substrate, while the indentation force,  $P$ , and depth of penetration,  $h$ , are continuously measured during loading and unloading periods. Thus, a “force-displacement relationship” is obtained from the indentation

testing (Figure 1.2c). Methodologies are being developed to extract the elastic and plastic properties of the substrate material using the force-displacement relationship. Two steps are involved in such methodologies. In the first step, a correlation is obtained between the force-displacement relationship and the material properties using analytical or numerical methods. For example, a finite element model for a particular indenter and substrate geometry can be created and the material properties can be varied systematically to obtain the force-displacement relationships for a range of materials. Based on the results, a regression analysis can be used to express the characteristic quantities quantifying the force-displacement relationships in terms of the material properties, that is, the constitutive equations for the tested system. This step is known as forward analysis. In the second step, the correlation obtained in the first step is inverted to express the material properties in terms of the force-displacement relationship. Since the constitutive equations are now known, the force-displacement relationship obtained from an actual indentation experiment can be used to extract the material properties of the substrate. This step is known as reverse analysis.



(a)



(b)

Figure 1.1: A typical nanoindenter (Hysitron Triboindenter): (a) outside view and (b) inside view

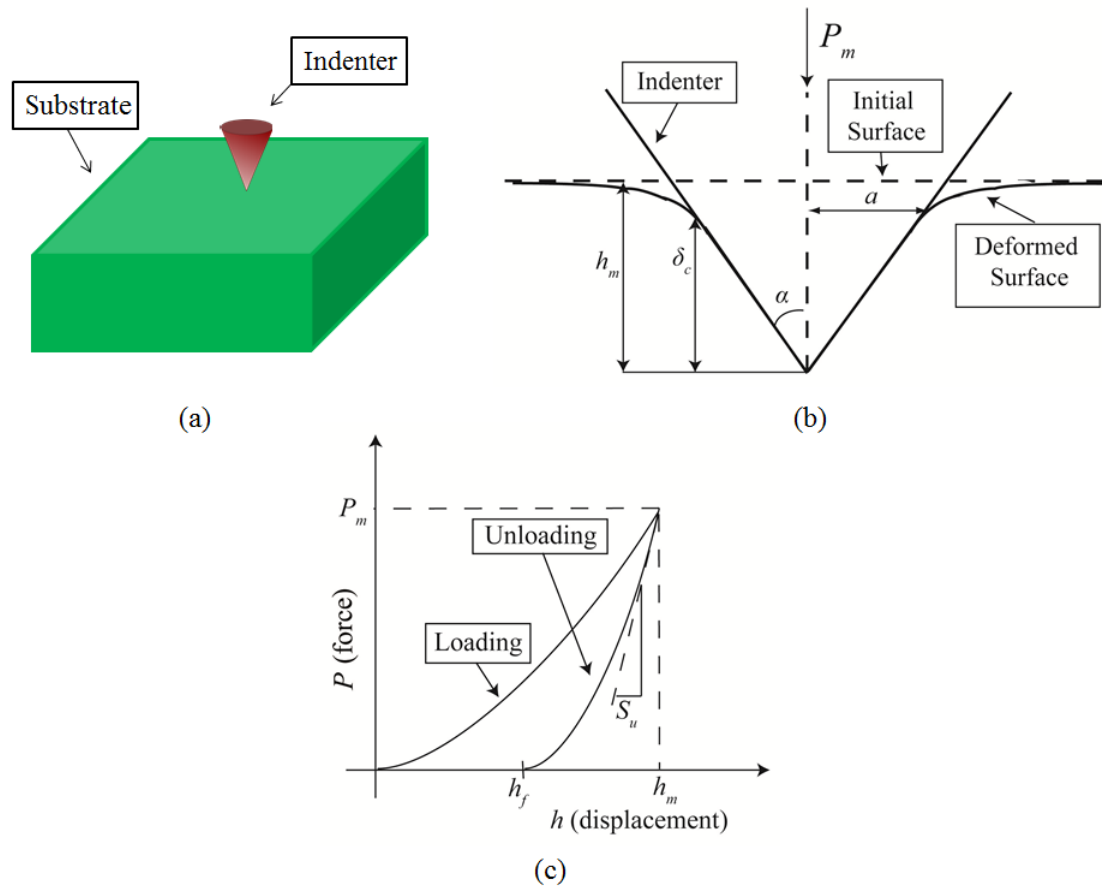


Figure 1.2: (a) Isometric view of a typical indentation experiment (b) Cross-sectional view of an indentation experiment (c) force-displacement relationship obtained from a typical indentation experiment

Currently, indentation tests are used to determine the material properties of substrates over a wide range of geometries and material types. These include substrates with flat surfaces e.g., thin films (Zhao et al., 2007), spherical surfaces e.g., living cells (Cao et al., 2004) and cylindrical surfaces e.g., micro-fibers (McAllister et al, 2012). Different material types include isotropic (Cao et al., 2005), anisotropic (McAllister et al., 2012) and visco-elastic materials (Vandamme and Ulm, 2006). However, in some cases, more than one material can yield indistinguishable force-

displacement relationships (Cheng and Cheng, 1999; Capehart and Cheng, 2003; Tho et al., 2004; Alkorta et al., 2005, Chen et al., 2007, Liu et al., 2009, Wang et al., 2010). Thus, a unique relationship between the material properties and the force-displacement relationship is not guaranteed. In addition, Hyun et al. (2011) found that in certain cases, a small experimental error can lead to very large error in the determined material properties. Thus, non-uniqueness and sensitivity to experimental error may determine the practical effectiveness of indentation testing. A literature review will be presented below (sections 1.2-1.7) to elucidate the following scope of improvements in indentation research. In summary, the works published in the open literature show:

1. Most of the methodologies are limited to flat substrates and thus new methodologies need to be developed for non-flat substrates.
2. Sporadic works are available regarding non-uniqueness and sensitivity of indentation testing and thus a systematic investigation of these two issues for different substrate geometries and material types needs to be developed.
3. Limited works are available for anisotropic material and thus methodologies need to be extended to include this material type.

In section 1.1, selected basic mathematical concepts that will be used in this dissertation will be presented. In sections 1.2-1.7, a description of the essential concepts involved in an indentation analysis will be presented along with a literature review. This will be followed, in section 1.8, by a description of the current work and the organization of the remaining chapters.

## 1.1 Useful Mathematical Concepts

### 1.1.1 Uniqueness, sensitivity and condition number

A sensitivity analysis of a system investigates how much perturbation is required in the input/solution to produce a particular amount of change in the output/data. The sensitivity of a system can be quantified by condition number (Datta, 2010). The condition number gives a measure of the ratio of the error in the solution to the error in the data. Thus, for a system, a large condition number implies that a small deviation in the data is cause for a large deviation in the solution. Therefore, a system with a large condition number is sensitive to experimental errors and is called ill-conditioned. Similarly, a small condition number implies that the system is not sensitive to perturbations in data (experimental errors) and is well-conditioned. The condition number is an inherent property of the system and does not depend on the algorithm that is used to solve the system, defined as follows.

Consider the general system (linear or nonlinear) of equations,  $f(x) = y$ , where  $x$  is the input/solution vector and  $y$  the output/data vector. With the perturbations in the solution and the data, the system of equations can be written as  $f(x + \Delta x) = y + \Delta y$ . For the special case of a linear system, the system of equations,  $f(x) = y$  can be expressed as  $Ax = y$ , where  $A$  is a two-dimensional matrix. With perturbations, it becomes  $A(x + \Delta x) = y + \Delta y$ .

There are two definitions of condition number (Higham, 1996; Rheinbott, 1976): one relates to the absolute error in the data or the solution, and the other to the relative error. Since the relative error tends to be more useful than the absolute error, the second condition number is used more widely than the first condition number. For

the system,  $f(\mathbf{x}) = \mathbf{y}$ , the second condition number at a point  $\mathbf{z}$ , of the domain (of input,  $\mathbf{x}$ ), is given by:

$$\kappa = u_1(\mathbf{f}, C, \mathbf{z}) / u_2(\mathbf{f}, C, \mathbf{z}) \quad (1.1a)$$

with

$$\begin{aligned} u_1(\mathbf{f}, C, \mathbf{z}) &= \inf_{\mathbf{x} \text{ in } C} \{t \text{ in } [0, \infty); \|f(\mathbf{x}) - f(\mathbf{z})\| \leq t \|\mathbf{x} - \mathbf{z}\|\} \\ u_2(\mathbf{f}, C, \mathbf{z}) &= \sup_{\mathbf{x} \text{ in } C} \{t \text{ in } [0, \infty); \|f(\mathbf{x}) - f(\mathbf{z})\| \geq t \|\mathbf{x} - \mathbf{z}\|\} \end{aligned} \quad (1.1b)$$

where  $C$  is a sub-domain enclosing the point  $\mathbf{z}$  and  $\|\cdot\|$  denotes the second norm. For the linear system, the second condition number reduces to a simpler expression, which is given by:

$$\kappa = \|A\| \|A^{-1}\| \quad (1.1c)$$

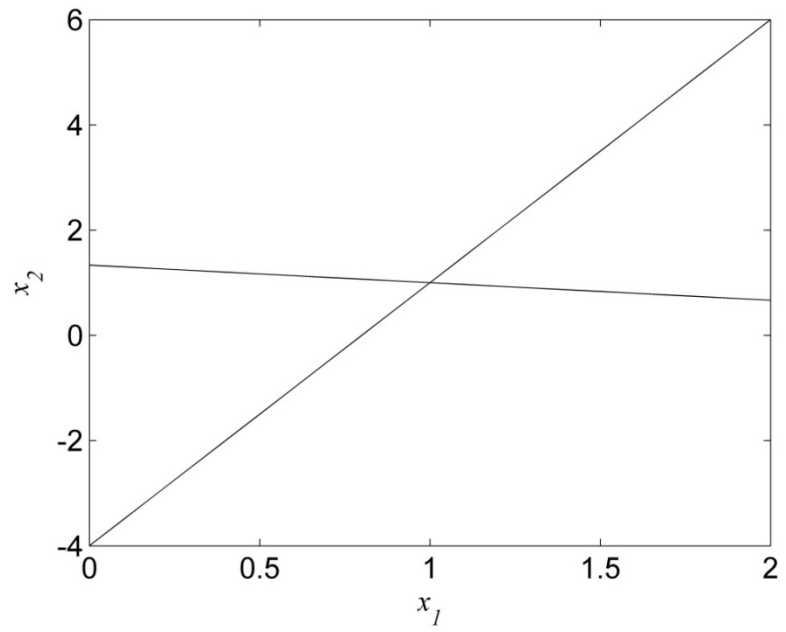
It can be shown that (Higham, 1996; Rheinboldt, 1976), small  $\kappa$  implies  $\|A\mathbf{x}\| / \|\mathbf{x}\|$  is small for a given  $\|A\mathbf{y}\| / \|\mathbf{y}\|$  and vice versa. Well-conditioned systems have condition numbers close to 1, which is the case of tensile testing.

To illustrate how the condition number can quantify the sensitivity of a system, four simple linear systems are considered (Table 1.1). Perturbations were applied to the original systems (for all the four examples) by changing the first element of the data vector,  $\mathbf{y}$ , by 1%. The solutions of the original and perturbed systems were computed and percentage differences were determined. Table 1.1 shows that the error in the solution increases as the condition number increases. The fourth example is of a non-unique system and for this system, the condition number is infinity. Figure 1.3 provides a graphical representation of the four systems. The graphs of the linear systems (examples a, b and c of Table 1.1) will be straight lines in the  $x_1$ - $x_2$  plane and the original systems (unperturbed) are plotted in Figures 1.3a, 1.3b and 1.3c,

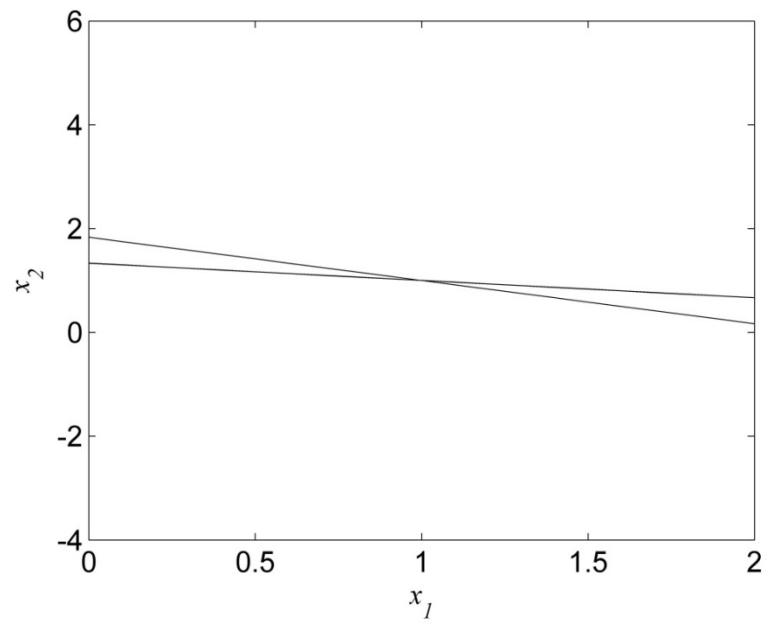
respectively. As the condition number of the system increases, the straight lines get closer to each other. For the third example, the straight lines are so close that it appears they have overlapped. Finally, in the fourth example, when the two straight lines actually overlap, the solution becomes non-unique (a figure for this situation has not been shown due to its triviality). Thus, the uniqueness and the extent of the sensitivity of a system can be quantified using the condition number and the non-uniqueness can be considered as an extreme case of a highly sensitive system. These concepts will be used later to study the sensitivity due to experimental errors for a range of indentation methodologies.

Table 1.1: Correlation between condition number and the sensitivity to perturbation in four linear systems.

Example	System ( $Ax = y$ )	Solution	Condition number	Percentage change in the solution
a	Original $\begin{bmatrix} 1 & 3 \\ 5 & -1 \end{bmatrix} \begin{bmatrix} x_1 \\ x_2 \end{bmatrix} = \begin{bmatrix} 4 \\ 4 \end{bmatrix}$ Perturbed $\begin{bmatrix} 1 & 3 \\ 5 & -1 \end{bmatrix} \begin{bmatrix} x_1 \\ x_2 \end{bmatrix} = \begin{bmatrix} 4.04 \\ 4 \end{bmatrix}$	$x_1 = 1$ $x_2 = 1$  $x_1 = 1.0025$ $x_2 = 1.0125$	1.6400	$x_1: 0.25$ $x_2: 1.25$
b	Original $\begin{bmatrix} 1 & 3 \\ 5 & 6 \end{bmatrix} \begin{bmatrix} x_1 \\ x_2 \end{bmatrix} = \begin{bmatrix} 4 \\ 11 \end{bmatrix}$ Perturbed $\begin{bmatrix} 1 & 3 \\ 5 & 6 \end{bmatrix} \begin{bmatrix} x_1 \\ x_2 \end{bmatrix} = \begin{bmatrix} 4.04 \\ 11 \end{bmatrix}$	$x_1 = 1$ $x_2 = 1$  $x_1 = 0.9733$ $x_2 = 1.0222$	7.7606	$x_1: 2.67$ $x_2: 2.22$
c	Original $\begin{bmatrix} 1000 & 999 \\ 999 & 998 \end{bmatrix} \begin{bmatrix} x_1 \\ x_2 \end{bmatrix} = \begin{bmatrix} 1999 \\ 1997 \end{bmatrix}$ Perturbed $\begin{bmatrix} 1000 & 999 \\ 999 & 998 \end{bmatrix} \begin{bmatrix} x_1 \\ x_2 \end{bmatrix} = \begin{bmatrix} 2019 \\ 1997 \end{bmatrix}$	$x_1 = 1$ $x_2 = 1$  $x_1 = -1.995E4$ $x_2 = 1.997E4$	3.99E6	$x_1: 1.995E6$ $x_2: -1.997E6$
d	$\begin{bmatrix} 5 & 6 \\ 5 & 6 \end{bmatrix} \begin{bmatrix} x_1 \\ x_2 \end{bmatrix} = \begin{bmatrix} 11 \\ 11 \end{bmatrix}$	Non-unique	Infinity	--



(a)



(b)

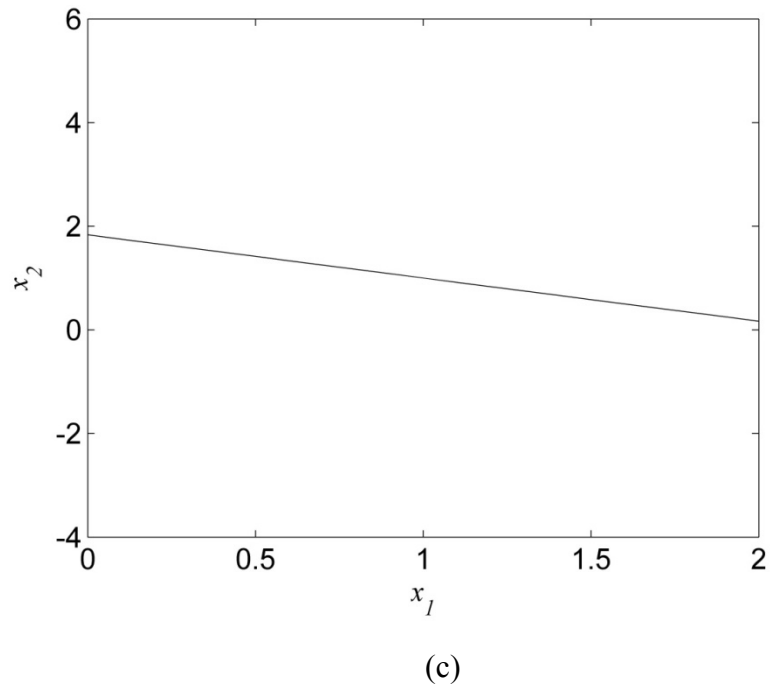


Figure 1.3: Three systems of straight lines (examples a, b and c of Table 1.1: the original or unperturbed systems) with increasing condition number and sensitivity. As the condition number increases, the straight lines approach each other and finally overlap.

### 1.1.2 Buckingham PI theorem

Buckingham PI theorem (Buckingham, 1914) is an important theorem regarding dimensional analysis and is used in indentation analysis to reduce the computational cost. According to this theorem, if there are  $n$  physical variables, and  $k$  is the rank of the dimensional matrix, then the equation is equivalent to an equation involving a set of  $p = n - k$  dimensionless parameters constructed from the original variables. The theorem is illustrated below by a simple example.

Consider the problem of the elastic cantilever beam deflection as shown in Figure 1.4 with the following parameters: beam length:  $l$ , elastic modulus:  $E$  and

radius of the circular cross-section:  $r$ . A point load of magnitude  $P$  is applied on the tip of the beam and the corresponding tip deflection is  $\delta$ . The tip deflection is a function of the material properties, geometric parameters and the force. Thus the deflection can be written as:

$$\delta = f(P, l, E, R) \quad (1.2)$$

To obtain the functional form of  $f$  using finite element simulations, the four parameters need to be varied systematically.

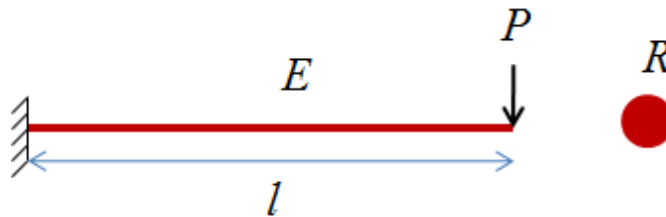


Figure 1.4: A cantilever beam problem used for illustrating Buckingham PI theorem.

The dimensional matrix can be formed from the units of the parameters in Eq. (1.2) and is shown in Table 1.2 (M, L and T denote the indices corresponding to mass, length and time, respectively, in the units of the parameters).

Table 1.2: Dimensional matrix of the parameters involved in Eq. (1.2).

	$P$	$l$	$E$	$R$	$\delta$
M	1	0	1	0	0
L	1	1	-1	1	1
T	-2	0	-2	0	0

The rank of the above matrix can be computed to be 2 (procedure for computing rank of a matrix can be found in standard books on Linear Algebra e.g. (Datta, 2010)) and thus according to Buckingham's PI theorem, there are  $5 - 2 = 3$  independent non-dimensional groups. By inspection, three non-dimensional groups can be formed as  $(\delta/l)$ ,  $(P/ER^2)$  and  $(l/R)$  and, consequently, Eq. (1.2) can be written in its non-dimensional form as follows:

$$\frac{\delta}{l} = g\left(\frac{P}{ER^2}, \frac{l}{R}\right) \quad (1.3)$$

Thus, Eq. (1.3) implies that only two non-dimensional parameters need to be varied, instead of four, to obtain the functional form of  $f$ . In this way, Buckingham PI theorem can be used to save computational cost and is used in indentation analyses frequently.

### 1.1.3 Solution of a system of nonlinear equations

In indentation analyses, a system of nonlinear equation arises which needs to be solved in order to obtain the material properties from an indentation experiment. The solution procedure used in this thesis will be described in this section.

Consider the set of nonlinear equations:

$$\begin{aligned} y_1 &= f_1(x_1, x_2, x_3) \\ y_2 &= f_2(x_1, x_2, x_3) \\ y_3 &= f_3(x_1, x_2, x_3) \end{aligned} \quad (1.4)$$

In this set of equations, the quantities on the left hand side, and the functions  $f_1, f_2$  and  $f_3$  are known. The quantities on the right hand side,  $x_1, x_2$  and  $x_3$  are to be determined. The functions,  $f_1, f_2$  and  $f_3$  appearing in this thesis are highly nonlinear functions. Non-linear systems can be solved numerically using an iterative process. The predicted solution,  $x_1^{pr}, x_2^{pr}, x_3^{pr}$ , is the one for which the residual or the distance between the

vectors  $(y_1, y_2, y_3)$  and  $(f_1(x_1^{pr}, x_2^{pr}, x_3^{pr}), f_2(x_1^{pr}, x_2^{pr}, x_3^{pr}), f_3(x_1^{pr}, x_2^{pr}, x_3^{pr}))$  is minimized. The residual can be defined in various ways, but will be defined in this thesis as

$$\delta = \sqrt{\left(\frac{y_1 - y_1^{pr}}{y_1}\right)^2 + \left(\frac{y_2 - y_2^{pr}}{y_2}\right)^2 + \left(\frac{y_3 - y_3^{pr}}{y_3}\right)^2} \quad (1.5)$$

The ordinary line search and golden section line search (Arora, 2012) methods were impractical to use for solving the nonlinear systems of this thesis because of the very high computational cost involved. Although, the Newton-Raphson method (Arora, 2012) converged much faster, the convergence was dependent on the initial starting point. Further, although the Newton-Raphson method works well for a well-posed system, it does not converge at all for an ill-posed system. Due to these problems, a combination of the three methods was used to solve the set of nonlinear equations in the present work. The algorithm is schematically shown in Figure 1.5. At first, an ordinary line search is employed to determine the solution. The predicted solution is used as an initial guess to a Newton-Raphson algorithm. If the solution converges, the algorithm is ended. If it does not converge after 1000 Newton-Raphson iterations, a golden section line search is employed thereafter starting from the solution of the ordinary line search.

The system of equations considered may have multiple solutions. Multiple solutions can exist either discretely or continuously over a region. In indentation analyses, if multiple solutions exist, they were found to exist over a continuous region only. In such a case, the Newton-Raphson method does not converge. The golden section line search algorithm will converge to one of the multiple solutions, and thus, all the solutions cannot be obtained using the proposed algorithm. However, this was

found to be sufficient for this study and other methods were employed (will be discussed later in Chapter 3) to determine all the solutions.

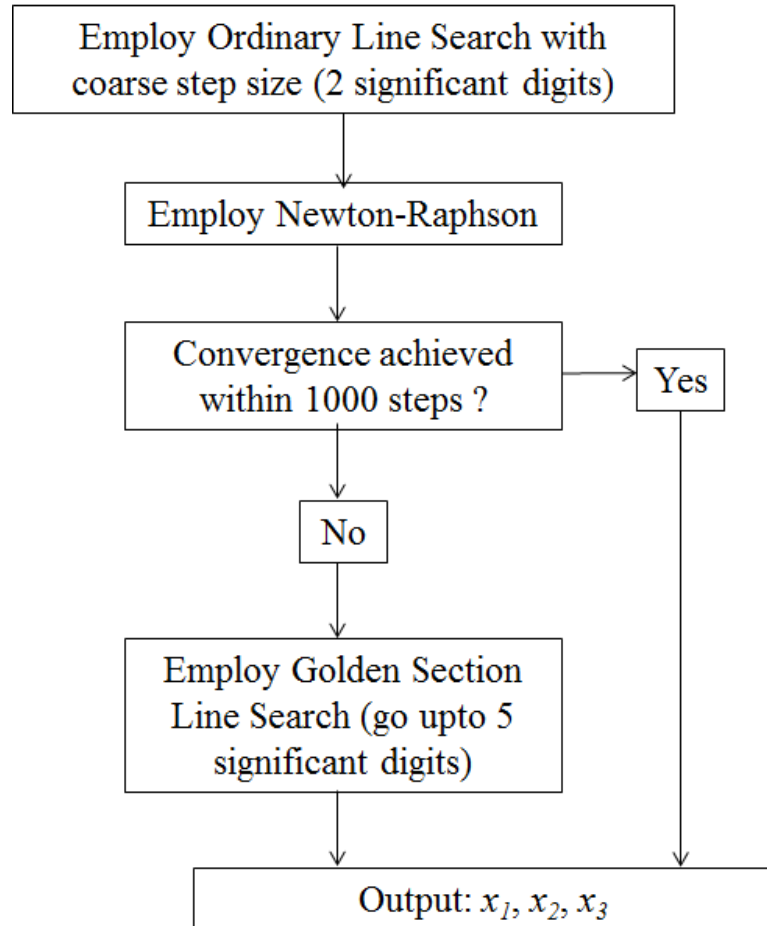


Figure 1.5: Algorithm used to solve the nonlinear set of equations arising in indentation analyses

## 1.2 Geometry and Material Properties

Indenters of various shapes are used in indentation testing and three important types: conical, spherical and flat indenters are considered here. A conical indenter can

be characterized by the half-angle,  $\alpha$ , and a spherical indenter can be characterized by the radius,  $R_i$  (see Figure 1.6). The widely used indenter, the Berkovich indenter can be represented by a conical indenter with half-angle,  $\alpha = 70.3^\circ$  (Lichinchi et al., 1998).

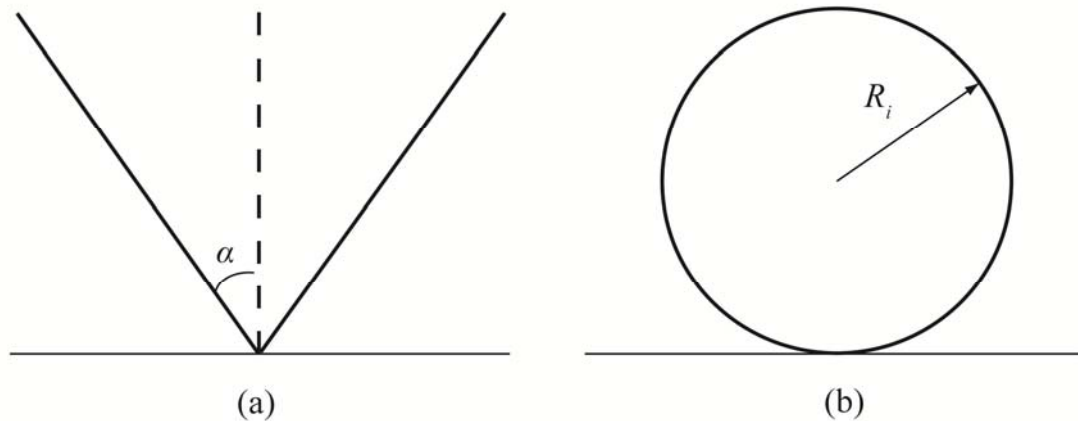


Figure 1.6: The two widely used indenters: a) conical indenter with half-angle  $\alpha$  and b) spherical indenter with radius  $R_i$ .

Most of the indentation literature is devoted to indentation on substrates with flat surfaces. Specific examples of such substrates include thin films (Wang et al., 2010) and single crystals (Brookes et al., 1971; Aguilar-Santillan, 2008; Viswanath et al., 2007). Substrates with spherical shapes (radius will be denoted by  $R_s$ ) requiring material characterization include micron-sized metal coated polymer particles used in the manufacturing of anisotropic conductive adhesives (Kristiansen et al., 2001), polymer latex particles for controlling the mechanical properties of latex films used in the synthetic latex materials (Misawa et al., 1991; Tamai et al., 1989) and living cells

(Dao et al., 2003). Micro and nano-fibers (McAllister et al., 2012; Ebenstein and Wahl, 2006) are examples of substrates with cylindrical surfaces.

A suitable material model for many metals or metallic alloys is the isotropic, linear-elastic, power-law strain hardening plastic model shown in Figure 1.7a (Dieter and Bacon, 1986; Lubliner, 1990). According to this, the uniaxial stress-strain relationship of a material can be expressed as:

$$\sigma = \begin{cases} E\varepsilon & \text{for } \varepsilon \leq \frac{Y}{E} \\ K\varepsilon^n & \text{for } \varepsilon \geq \frac{Y}{E} \end{cases} \quad (1.6)$$

where  $\sigma$  and  $\varepsilon$  correspond to the stress and the strain, respectively, and  $E$ ,  $Y$  and  $n$  denote the elastic modulus, the yield strength and the strain hardening exponent of the material, respectively. The strength coefficient,  $K$ , can be written as  $K = E^n Y^{1-n}$ . Apart from power-law hardening plasticity, another widely adopted model for metal is linear strain hardening plasticity, as illustrated in Figure 1.7b (Dieter, 1986). The constitutive relation for this material model can be written as:

$$\sigma = \begin{cases} E\varepsilon & \text{for } \varepsilon \leq \frac{Y}{E} \\ Y + E_p \left( \varepsilon - \frac{Y}{E} \right) & \text{for } \varepsilon \geq \frac{Y}{E} \end{cases} \quad (1.7)$$

where  $E_p$  is the hardening rate. In the simplified linear-elastic, perfectly-plastic model, (Figure 1.7a or 1.7b) the hardening is assumed to be zero, i.e.,  $n = 0$  (power-law hardening) or  $E_p = 0$  (linear hardening). In this case, the constitutive relation becomes:

$$\sigma = \begin{cases} E\varepsilon & \text{for } \varepsilon \leq \frac{Y}{E} \\ Y & \text{for } \varepsilon \geq \frac{Y}{E} \end{cases} \quad (1.8)$$

Poisson's ratios are assumed to be constant in this work for simplicity since they are minor factors in indentation testing (Cheng and Cheng, 2004).

The simplest possible anisotropic material is the transversely isotropic, linearly-elastic, perfectly-plastic material. Assuming that  $x$ - $y$  is the plane of isotropy (Figure 1.7c), we have the following material parameters: Young's moduli:  $E_x = E_y$ ,  $E_z$ ; Poisson's ratio:  $\nu_{xz} = \nu_{yz}$ ,  $\nu_{xy}$ ; shear moduli:  $G_{xz} = G_{yz}$ ,  $G_{xy} = E_x/(2(1+\nu_{xy}))$  and yield strength:  $Y$ .

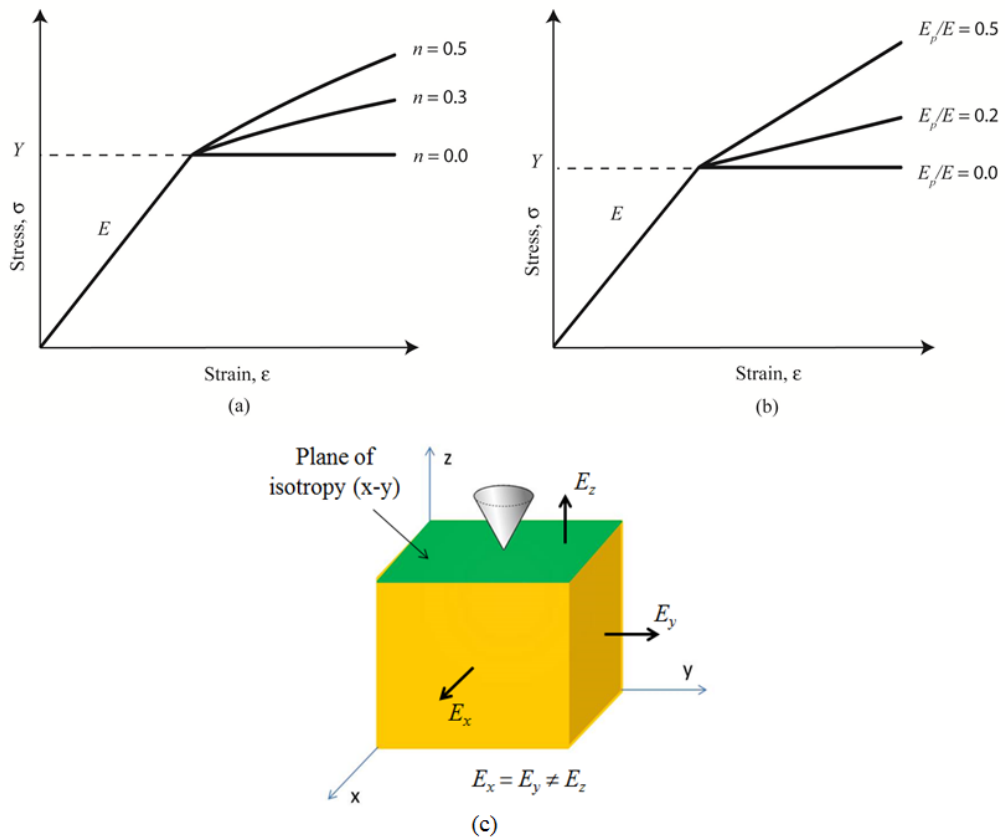


Figure 1.7: Three time-independent material models: (a) Isotropic, linear-elastic, power-law hardening material (b) isotropic, linear-elastic, linear hardening material (c) transversely isotropic, linear-elastic, perfectly-plastic material ( $x$ - $y$  is the plane of isotropy)

The material properties of viscoelastic materials are discussed in many text books, see for example, (Haddad, 1995). Viscoelastic materials exhibit both elastic solid and viscous fluid behavior. The general constitutive equation of a viscoelastic material can be written as (where  $t$  denotes time):

$$\sigma + p_1 \frac{d\sigma}{dt} + p_2 \frac{d^2\sigma}{dt^2} + p_3 \frac{d^3\sigma}{dt^3} + \dots = q_0 \varepsilon + q_1 \frac{d\varepsilon}{dt} + q_2 \frac{d^2\varepsilon}{dt^2} + \dots \quad (1.9)$$

Many models of viscoelastic materials are available with various combinations of springs (representing elastic behavior) and dashpots (representing viscous behavior). The constitutive equations associated with these models retain different terms from left and right hand sides of the general constitutive relation, Eq. (1.9). Two very simple models are Maxwell's element and Kelvin-Voigt elements which are shown in Figure 1.8a and 1.8b, respectively. The most widely used model is the standard three parameter model shown in Figure 1.8c. The constitutive relation for this model is given by:

$$\sigma + p_1 \frac{d\sigma}{dt} = q_0 \varepsilon + q_1 \frac{d\varepsilon}{dt} \quad (1.10)$$

To model a viscoelastic material, the constitutive behavior is divided into spherical and deviatoric components, and suitable representation from the above described models are assigned to those components. This will be discussed in more details in Chapter 2.

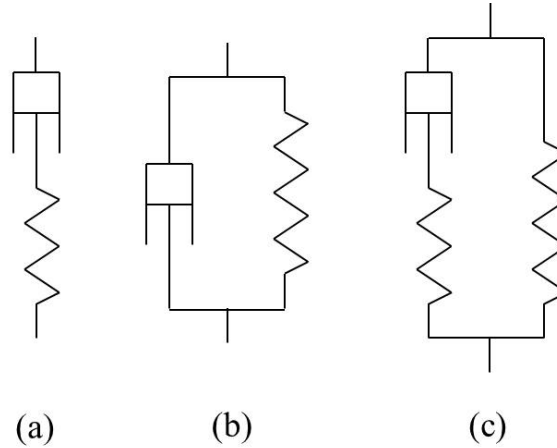


Figure 1.8: Three selected models for viscoelastic materials: (a) Maxwell element (b) Kelvin-Voigt element and (c) standard three parameter model

### 1.3 Oliver-Pharr Method

The force-displacement response obtained from an indentation experiment can be characterized by various functions such as the total energy during loading (the area under the loading curve),  $W_t$ , maximum force,  $P_m$ , unloading slope,  $S_u$ , elastic energy (the area under the unloading curve),  $W_e$ , maximum indentation depth,  $h_m$ , and residual or final depth,  $h_f$  (Yan et. al., 2007a, 2007b ; Dao et al., 2003; Ogasawara et al., 2009; Cao et al., 2005; Phadikar et al., 2012). These functions are typically referred to as “shape functions.”

The most widely used method for determining the elastic modulus for a flat semi-infinite isotropic substrate using indentation technique is the so-called “Oliver-Pharr method” (Oliver and Pharr, 1992). This method assumes that the initial unloading is elastic and thus uses the elastic solution for the problem to express the unloading slope,  $S_u$ , in terms of elastic modulus, Poisson’s ratio and contact radius

(radius of projected area of contact at maximum depth of penetration). Accordingly, the relationship is given by:

$$S_u = \left. \frac{dP}{dh} \right|_{h=h_m} = 2\beta a \frac{E}{1-\nu^2} = 2\beta a E_r \quad (1.11a)$$

where  $a$  is the contact radius at maximum load,  $E$  and  $\nu$  are elastic modulus and Poisson's ratio, respectively, of the substrate material, and  $\beta$  is a correction factor.  $E_r$  is known as the plane strain reduced modulus of the material. One disadvantage of this method is the need of the contact radius,  $a$ , which is difficult to measure experimentally (Chen et al., 2006; Johnson, 1987). A common method to determine the contact radius is to use the contact depth,  $\delta_c$ , which can be determined from the following equation:

$$\delta_c = h_m - \omega \frac{P_m}{S_u} \quad (1.11b)$$

where  $\omega$  is a dimensionless constant which depends on the indenter geometry, for example  $\omega = 0.75$  for a Berkovich indenter (Oliver and Pharr, 1992). However, this relationship is not applicable to a range of cases (Cheng and Cheng, 2004; Pharr, 1998). Moreover, the Oliver-Pharr method does not give any information about the inelastic properties of the material.

Due to these limitations, several authors have attempted to use other shape functions to determine the elastic and plastic properties (Cao and Lu, 2004; Xu and Li, 2005; Yan et al., 2007a, 2007b; Zhao et al., 2006). This will be described next.

#### 1.4 Single Indentation

Considering conical indentation of an elastic half-space made of isotropic, linear-elastic, power-law strain hardening material, the force-displacement relationship

depends on the material properties, such as  $E$ ,  $Y$  and  $n$ , and geometrical parameters, such as  $h_m$  and  $\alpha$ . The shape functions,  $\Pi_i$  can be written as (Phadikar et al., 2013b):

$$\Pi_i = F_i^{ph}(E, Y, n, \alpha, h_m); \quad i = 1-5 \quad (1.12a)$$

where  $\Pi_1 = W_t$ ,  $\Pi_2 = P_m$ ,  $\Pi_3 = S_u$ ,  $\Pi_4 = W_e$ ,  $\Pi_5 = h_f$ . The superscript  $ph$  indicates power-law hardening material. Using the above relations, various combinations of the shape functions can also be expressed in terms of the material and geometric parameters, for example,

$$\begin{aligned} P_m / S_u &= F_6^{ph}(E, Y, n, \alpha, h_m); & S_u / W_t &= F_7^{ph}(E, Y, n, \alpha, h_m); \\ W_t / W_e &= F_8^{ph}(E, Y, n, \alpha, h_m); & S_u / h_f &= F_9^{ph}(E, Y, n, \alpha, h_m) \end{aligned} \quad (1.12b)$$

Applying dimensional analysis and Buckingham's PI theorem (Buckingham, 1914) to Eq. (1.12a), the relations can be simplified as follows (Phadikar et al., 2013b):

$$\Psi_i = \bar{F}_i^{ph}\left(\frac{E}{Y}, n, \alpha\right); \quad i = 1-5 \quad (1.13)$$

where  $\Psi_1 = W_t / Yh_m^3$ ,  $\Psi_2 = P_m / Yh_m^2$ ,  $\Psi_3 = S_u / Yh_m$ ,  $\Psi_4 = W_e / Yh_m^3$ ,  $\Psi_5 = h_f / h_m$  and the overhead bar indicates normalized form. In an indentation experiment, the geometrical parameters are known. Thus, for fixed geometric parameters ( $\alpha$  and  $h_m$ ), Eqs. (1.12a) & (1.13) can be written as

$$\Pi_i = G_i^{ph}(E, Y, n); \quad i = 1-5 \quad (1.14a)$$

$$\Psi_i = \bar{G}_i^{ph}\left(\frac{E}{Y}, n\right); \quad i = 1-5 \quad (1.14b)$$

The functions  $\bar{G}_i^{ph}$  can be determined using finite element analysis. For this, finite element models simulating indentation experiments can be built and shape functions can be extracted from the force-displacement relationships by systematically varying the material properties. Then by regression analysis, the functions  $\bar{G}_i^{ph}$  can be

obtained. Once the functions are obtained, three shape functions obtained from a real indentation experiment can be selected and substituted in Eq. (1.14a) or (1.14b) to determine the three material properties. The procedure is illustrated in Figure 1.9.

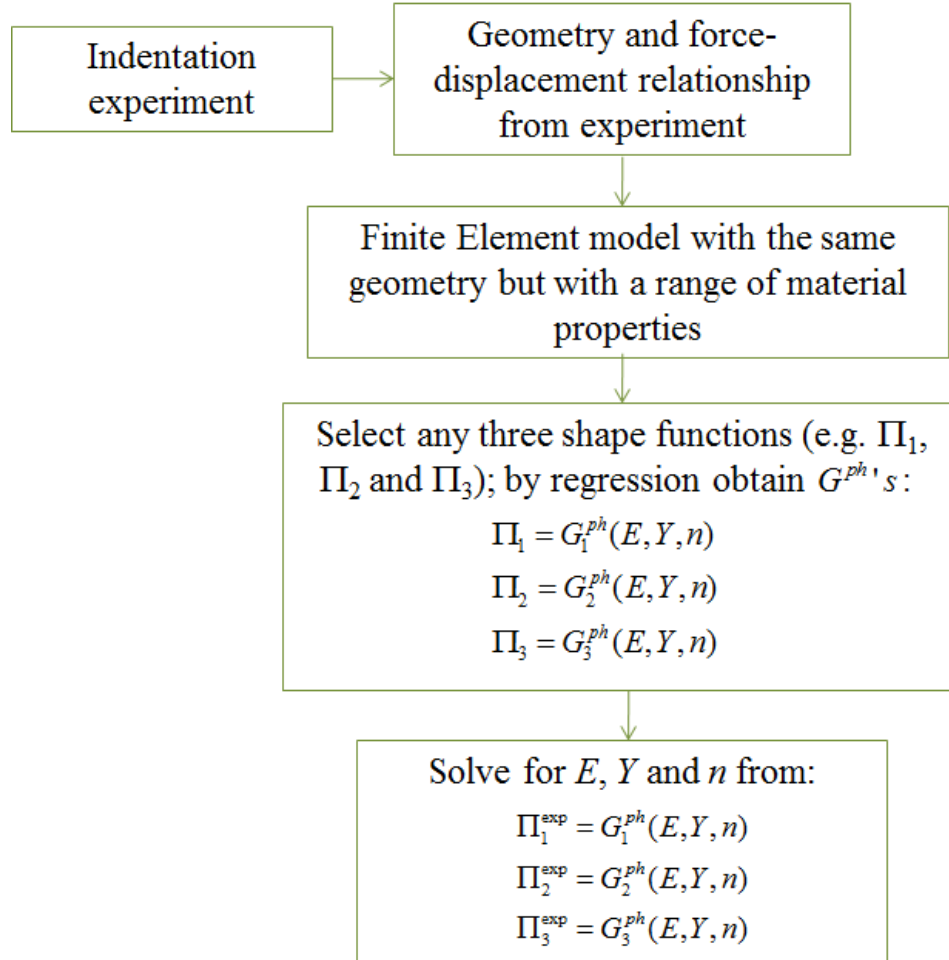


Figure 1.9: Procedure for obtaining material properties from an indentation experiment (single indentation)

Eqs. (1.12)-(1.14) represent the relationships between the shape functions and material properties for conical indentation of a half-space made of isotropic, linear-

elastic, power-law strain hardening material. Similar relationship can be derived for other indenter/substrate geometries and material models. For isotropic, linear-elastic, linear hardening material, the relationship between the normalized shape functions and material properties takes the following form (superscript *lh* indicates linear hardening) (Phadikar et al., 2013d):

$$\Psi_i = \bar{G}_i^{lh} \left( \frac{E}{Y}, \frac{E_p}{E} \right); \quad i = 1-5 \quad (1.15)$$

For transversely isotropic, linear-elastic, perfectly-plastic material, the relationships take the following form (Phadikar et al., 2013e):

$$\Psi_i^{tp} = \bar{G}_i^{tp} \left( \frac{E_x}{E_z}, \frac{E_z}{G_{xz}}, \frac{E_z}{Y} \right); \quad i = 1-5 \quad (1.16)$$

where,  $\Psi_1^{tp} = W_t / E_x h_m^3$ ,  $\Psi_2^{tp} = P_m / E_x h_m^2$ ,  $\Psi_3^{tp} = S_u / E_x h_m$ ,  $\Psi_4^{tp} = W_e / E_x h_m^3$ ,  $\Psi_5^{tp} = h_f / h_m$ , superscript *tp* stands for transversely isotropic material. For conical indentation of a half-space, Eqs. (1.14) – (1.16) are valid for fixed half-angle  $\alpha$ . It can be shown in similar ways that for other indenter/substrate geometries the relationships are valid for the following fixed parameters: i) spherical indentation of a half-space: fixed depth-to-radius ratio,  $h_m/R_i$ ; ii) conical indentation of a sphere: fixed half-angle,  $\alpha$  and depth-to-radius ratio,  $h_m/R_s$ ; and iii) spherical indentation of a sphere: fixed depth-to-substrate radius ratio,  $h_m/R_s$  and indenter radius-to-substrate radius ratio:  $R_i/R_s$ .

Several research groups (Cheng and Cheng, 1999; Capehart and Cheng, 2003; Tho et al., 2004; Alkorta et al., 2005, Chen et al., 2007, Liu et al., 2009, Wang et al., 2010) have reported that more than one material can result in indistinguishable force-displacement relationships. Thus, a one-to-one relationship between the material properties and the experimentally obtained force-displacement relationship is not

guaranteed. Consequently, a single indentation technique described in the previous section cannot be used to determine the material properties of a substrate. Several researchers have attempted to systematically identify materials that yield identical force-displacement relationships and a brief review is presented in the following section. That will be followed by a review of dual indentation methodologies which are proposed to overcome the limitation of single indentation technique.

### **1.5 Non-uniqueness of Force-displacement Relationship**

Different researchers have proposed different methodologies for systematic identification of materials with identical force-displacement relationships, for specific geometries and material properties.

Cheng and Cheng (1999), Capehart and Cheng (2003), Tho et al. (2004), Alkorta et al. (2005), Chen et al. (2007) and Liu et al. (2009), investigated the non-uniqueness of force-displacement relationship for conical indentation of flat substrates made of isotropic, linear elastic, power law hardening materials. They used the self-similarity of the specific indentation problem and showed that out of two shape functions of the loading curve (loading energy,  $W_l$ , and maximum load,  $P_m$ ), only one is independent and can be used to characterize the entire loading curve. Thus, by obtaining materials with identical  $P_m$ , they obtained materials with identical loading curves. However, self-similarity does not exist for other commonly used indentation geometries, such as spherical indentation of a half-space (Cao and Lu, 2004; Zhao et al., 2006), conical indentation of a sphere (Phadikar et al., 2012) and spherical indentation of a sphere (Zhou and Lu, 2010). Thus, the methodologies may not be applicable for these indentation geometries.

As an alternative to identify materials with identical loading curves discussed above, various efforts on identifying materials with identical *unloading* curves have been explored. For example, Alkorta et al (2005), Tho et al. (2004), Liu et al. (2008) and Chen et al. (2008) showed that the unloading curve can be described by a power law expression (known as “potential law,” Oliver and Pharr (1992)) to identify materials with identical unloading curves and thus obtained materials with identical force-displacement relationship. However, the potential unloading law (Oliver and Pharr (1992)), is shown to be valid for conical indentation of a half-space made of isotropic materials, but not for other indentation geometries or for anisotropic or viscoelastic materials. Cheng and Cheng (1999) showed that for given total loading energy,  $W_t$ , a correlation exists between elastic energy,  $W_e$  and final depth,  $h_f$ . Further, they demonstrated numerically that materials with identical  $W_e$  also results in identical unloading slope,  $S_u$ . Thus, they showed that out of the three possible shape functions describing the unloading curve, only one is independent. Thereby, they obtained materials with identical  $W_e$  (or  $S_u$  and  $h_f$ ) and the materials were found to have identical unloading curves. However, a clear explanation of whether identical  $W_e$  (or  $S_u$  and  $h_f$ ) will always result in identical unloading curve was not provided. Capehart and Cheng (2003) obtained materials with identical unloading curves by using a statistical method utilizing a large number of points in the unloading curve. In addition to conical indentation of a half-space made of isotropic, linear elastic, power-law strain hardening plastic materials, Liu et al. (2009) considered bilinear hardening plastic materials and spherical indentation. For conical indentation of a half-space made of linear hardening plastic materials, self-similarity and “potential law” descriptions were used for obtaining materials with identical loading and unloading

curves, respectively. For spherical indentation of a half-space, they attempted to identify materials with identical loading curves by comparing the quantity  $C = P_m / h_m^2$ . Although the materials with identical value of  $C$  resulted in identical loading curves for shallow indentation, the loading curves differed considerably for deep indentation. Wang et al. (2010) attempted to identify elastic moduli of a transversely isotropic, linear-elastic thin film using finite element based reverse analysis and concluded that several materials can result in identical force-displacement relationship.

Thus, it can be concluded that a general method for obtaining materials with identical force-displacement relationship for different material types and indentation geometries is not developed yet.

To overcome the problem of non-uniqueness in single indentation, several researchers have proposed dual indentation in which two indenters are utilized instead of a single indenter. This will be described next.

## 1.6 Dual Indentation

To address the shortcoming of the single indentation methodology, dual indentation methodologies have been proposed by several authors (Table 1.3). In dual indentation methodologies, two indenter geometries are utilized giving two additional shape functions. Considering conical indentation of a half-space made of isotropic, linear-elastic, power-law hardening material, only three equations are needed and the premise is that two sets of half-angles will provide distinct displacement responses. Thus, it will be possible to uniquely determine the material properties. For two sets of fixed geometrical parameters, Eq. (1.14b) can be written as (Phadikar et al., 2013b):

$$\Psi_{ij} = \bar{G}_{ij}^{ph} \left( \frac{E}{Y}, n, \alpha_j \right); \quad i = 1 - 5; j = 1, 2 \quad (1.17)$$

where superscripts  $j = 1$  and  $2$  correspond to test 1 and test 2, respectively. For linear hardening material, the relationships become:

$$\Psi_{ij} = \bar{G}_{ij}^{lh} \left( \frac{E}{Y}, \frac{E}{E_p}, \alpha_j \right); \quad i = 1-5; j = 1, 2 \quad (1.18)$$

For transversely isotropic, linear-elastic, perfectly-plastic material, the relationships become:

$$\Psi_{ij}^{tp} = \bar{G}_{ij}^{tp} \left( \frac{E_x}{E_z}, \frac{E_z}{G_{xz}}, \frac{E_z}{Y}, \alpha_j \right); \quad i = 1-5; j = 1, 2 \quad (1.19)$$

In a dual indentation technique for isotropic material, three equations from Eq. (1.17) are selected, along with two half-angles,  $\alpha_1$  and  $\alpha_2$ , (conical indentation of a half-space). Thus, for isotropic material, two shape functions can be selected from half-angle  $\alpha_1$  and one shape function can be selected from half-angle  $\alpha_2$ . Alternately, one shape function can be selected from half-angle  $\alpha_1$  and two shape functions can be selected from half-angle  $\alpha_2$ . Similarly, for transversely isotropic materials, the shape functions can be selected in three ways: i) one shape function from  $\alpha_1$  and three shape functions from  $\alpha_2$ ; ii) two shape functions from  $\alpha_1$  and two shape functions from  $\alpha_2$  and iii) three shape functions from  $\alpha_1$  and one shape function from  $\alpha_2$ . Therefore, there are numerous ways to conduct a dual indentation experiment. The shape functions and half-angle (for conical indentation of a half-space) or depth-to-radius ratio (for spherical indentation of a half-space) combinations selected by previous researchers are tabulated in Table 1.3.

Table 1.3: Various combinations of shape functions, half-angles (conical indentation) and depth-to-radius ratios (spherical indentation) used by previous researchers.

Geometry	Shape function combination	Ref.
<b>Conical Indentation</b>	$S_u _{70.3^\circ}, P_m _{70.3^\circ}, P_m _{45^\circ}$	Le (2008)
	$S_u _{70.3^\circ}, h_f _{70.3^\circ}, P_m _{70.3^\circ}, P_m _{60^\circ}$	Chollacoop et. al. (2003)
	$(S_u / P_m) _{70.3^\circ}, P_m _{70.3^\circ}, P_m _{60^\circ}$	
	and	Lan and Venkatesh (2007)
	$(W_t / W_e) _{70.3^\circ}, P_m _{70.3^\circ}, (W_t / W_e) _{60^\circ}$	
	$S _{70.3^\circ}, (P_m / S) _{70.3^\circ}, (P_m / S) _{80.5^\circ}$	Wang et. al. (2005)
	$(W_e / W_t) _{60^\circ}, P_m _{60^\circ}, (W_e / W_t) _{70.3^\circ}, P_m _{70.3^\circ}$	Swaddiwudhipong et. al. (2005)
	$S _{70.3^\circ}, h_f _{70.3^\circ}, P_m _{70.3^\circ}, P_m _{60^\circ, 50^\circ, 42.3^\circ}$	Bucaille et. al. (2003)
	Any two of	
	$P_m _{60^\circ}, P_m _{63.14^\circ}, P_m _{70.3^\circ}$	Yan et. al. (2007)
	( $E$ was assumed to be known)	
<b>Spherical indentation</b>	$P_m _{13\%}, P_m _{30\%}, S_u _{30\%}$	Zhao et. al. (2006)
	$P_m _{1\%}, P_m _{6\%}$	Cao and Lu (2004)
	( $E$ was assumed to be known)	
	$P_m _{10\%}, P_m _{30\%}$	Ogasawara (2009)
	( $E$ was assumed to be known)	
	$P_m _{15\%}, P_m _{3\%}, \frac{W_e}{W_t} _{15\%}, \frac{W_e}{W_t} _{3\%}$	Cao et. al. (2007)

However, Chen et al. (2007) showed that certain groups of materials exist which result in identical force-displacement relationships even for dual indentation testing. They showed that generally materials with low values of  $E/Y$  and  $n$  fall into

this category. Thus, unfortunately a dual indentation technique does not guarantee a unique data reduction scheme for all materials.

Closely related to uniqueness is the issue regarding sensitivity to experimental errors (Chollacoop et al., 2003; Lan and Venkatesh, 2007; Le, 2008; Hyun et al., 2011; Cao and Lu, 2004a; Cao and Lu, 2004b; Swaddiwudhipong, 2005). In fact, the sensitivity due to experimental errors can be quite high for certain cases. For example, Le, (2009) reported that an error of order 1% in experimental data can result in an error of 70% in the determined material properties. Cao and Lu (2004a) demonstrated for selected cases of conical indentation, sensitivity due to experimental error can be decreased by selecting indenters with large difference in half-angles. Similarly, for spherical indentation, Cao and Lu (2004b) demonstrated that sensitivity can be decreased by increasing the difference between two selected depth-to-radius ratios. However, no such guidelines are available regarding the selection of shape function combinations. Thus, a complete and systematic investigation of the uniqueness and sensitivity to experimental error in dual indentation methodologies has not been developed.

Compared to isotropic materials, only limited works have been done on determining the material properties of anisotropic materials using indentation. A review will be presented next.

### **1.7 Indentation of Anisotropic Materials**

The indentation technique is used to characterize small scale anisotropic structures such as single crystals (Brookes et al., 1971; Aguilar-Santillan, 2008; Viswanath et al., 2007; McCann, 2004; Yeap et al., 2011; Kearney et al., 2006; Zambaldi et al., 2006; Zambaldi et al., 2010; Vlassak, 1994), fibers(McAllister et al.,

2012; Ebenstein and Wahl, 2006), thin films (Wang et al., 2010) and biological structures (Cui et al., 1994; Reisinger et al., 2011; Cox et al., 2008; Rosa et al., 2012; Carnelli et al., 2011; Swadener et al., 2001; Gindl and Schoberl, 2004; Gindl and Gupta, 2002; Fan et al., 2002; Franzoso, 2008). The indentation modulus,  $M$ , of a general anisotropic material is defined by (Vlassak, 1994),

$$S_u = 2aM \quad (1.20)$$

where  $S_u$  is the unloading slope and  $a$  is the contact radius. For isotropic materials,  $M$  reduces to the plain strain elastic modulus,  $E_r$  (see Eq. (1.11a)). Exact and approximate simplified expressions of  $M$  in terms of the anisotropic material constants have been developed for a range of geometries, for example see (Vlassak, 1994; Swadener and Pharr, 2001; Delafargue and Ulm, 2004). The mechanical characterizations of anisotropic materials using indentation testing include: (i) measurement of indentation moduli along different directions of anisotropy (Viswanath et al., 2007; McCann, 2004; Yeap et al., 2011; Fan et al., 2002; Franzoso, 2008; Vlassak, 1994; Swadener et al., 2001), (ii) measurement of hardness along different directions of anisotropy (Cui et al., 1994; Brookes et al., 1971; Aguilar-Santillan, 2008; Viswanath et al., 2007; McCann, 2004; Yeap et al., 2011; Franzoso, 2008; McCann, 2004), and (iii) investigation of pile up pattern to predict delamination (Kearney et al., 2006; Zambaldi et al., 2012).

In addition, multiple attempts have been made to determine the anisotropic elastic and plastic material properties. Various researchers, for example see (Amitay-Sadovsky et al., 1999; Ebenstein and Wahl, 2006; Gindl and Gupta, 2002; Rosa et al., 2012; Gindl and Schoberl, 2004), attempted to determine Young's moduli in different directions of anisotropy by assuming the indentation modulus,  $M$ , to be the same as

the isotropic reduced modulus,  $E_r$ , in different directions. However, only approximate values can be obtained through these studies, since the indentation modulus is dependent on all the elastic moduli in anisotropic materials. Jiang and Batra (2009) considered indentation of an anisotropic elastic half-space of a Face Centered Cubic material (having three Young's moduli), indented by an infinite cylinder and determined the three Young's moduli using indentation in three directions of anisotropy.

Only a limited number of researchers, e.g., (Wang et al., 2010; McAllister et al., 2012; Carnelli et al., 2011) have considered indentation of transversely isotropic materials. Carnelli et al. (2011) attempted to determine the three elastic parameters by indenting in one direction and using a finite element based reverse analysis technique. However, they found that several materials can result in identical force-displacement relationships. McAllister et al. (2012), performed indentation tests in two directions of anisotropy to determine the indentation moduli in their respective directions. Then, Young's moduli in two directions were determined by using an inverse analysis which utilizes analytical expressions for the indentation moduli in terms of the three material parameters (shear modulus was assumed to be known). Wang et al. (2010) adopted a similar approach with a simplified expression of the shear modulus. Yonezu et al. (2009) and Yonezu et al. (2010) determined the plastic properties, such as yield strengths, in two directions and the strain hardening exponent using spherical indentation of an anisotropic half-space (elastic properties were assumed to be known). Nakamura and Gu (2007) investigated dual conical-spherical indentation on transversely isotropic materials in one direction and attempted to determine five independent anisotropic material parameters, such as Young's moduli and yield

strengths in two directions and the strain hardening exponent. However, they concluded that the material parameters determined will only be of approximate values. Therefore, this method can only be used to gain insights about the anisotropic characteristics and a more rigorous study would be required to determine the parameters more accurately.

Thus, systematic dual indentation methodologies along with the uniqueness and sensitivity analysis, as described in section 1.6 for isotropic materials, have not been developed for anisotropic materials.

## **1.8 Outline of the Dissertation Work**

Considering the above scopes for improvement in indentation research, this dissertation focuses on the following three aspects:

- i) Investigating selected methods to evaluate indentation on non-flat substrates;
- ii) Systematic analysis of uniqueness and sensitivity; and
- iii) Investigating selected indentation methodologies for anisotropic materials.

The work is presented in three chapters as described below.

In chapter 2, conical indentation of a sphere is considered. A sphere can be considered as one of the simplest non-flat structures. Two material types, namely isotropic, linear-elastic, perfectly-plastic and viscoelastic materials are considered.

In chapter 3, a general methodology for identifying materials with identical force-displacement relationship is presented. The methodology is illustrated for a wide range of indentation geometries and substrate material models.

In chapter 4, a method to demonstrate the relationship between uniqueness and sensitivity in indentation testing has been presented. Then, the concept of condition

number and explicit sensitivity analysis has been used for systematic investigation of sensitivity of different dual indentation methodologies.

Lastly, concluding remarks and scopes for further improvements are discussed in chapter 5.

## **Chapter 2**

### **INDENTATION OF NON-FLAT SUBSTRATES: CONICAL INDENTATION OF A SPHERE**

As discussed in Chapter 1, currently indentation literature is dedicated mostly to indentation on flat substrates. However, several authors (Jackson and Green, 2005; Lin and Lin, 2006; Malayalamurthi and Marappan, 2008; Sahoo et al., 2009) have investigated the indentation of a hemisphere by a flat punch. Moreover, Zhou and Lu (2010) investigated indentation of a sphere by a spherical indenter. Examples of spherical substrates requiring material characterizations include micron-sized metal coated polymer particles used in the manufacturing of anisotropic conductive adhesives (Kristiansen et al., 2001), polymer latex particles for controlling the mechanical properties of latex films (Misawa et al., 1991; Tamai et al., 1989) used in the synthetic latex materials and living cells (Dao et al., 2003). To our knowledge, there are no studies on indentation of a sphere by a conical indenter available in the open literature. Thus, in this chapter, conical indenter of a sphere made of isotropic, linear-elastic, perfectly-plastic material and viscoelastic material are considered. The work contained in this chapter is based on our published work Phadikar et al., 2012 and Phadikar et al., 2013a.

## 2.1 Indentation of a Sphere Made of Linear-elastic, Perfectly-plastic Material

### 2.1.1 Theoretical preliminaries

Isotropic, linear-elastic, perfectly-plastic material can be characterized by two material parameters, namely, the elastic modulus,  $E$ , and the yield strength,  $Y$ , see Chapter 1, section 1.2. Two methodologies are proposed to determine the elastic modulus and yield strength of a sphere by conical indentation testing. The first method is a semi-analytical method which is similar to the “Oliver-Pharr method” (discussed in Chapter 1, section 1.3) and utilizes the concept of elastic unloading. The second method is a finite element based reverse analysis technique. Both methodologies will converge to indentation of a flat half-space when the radius of the substrate is very large compared to maximum indentation depth.

Oliver and Pharr (1992) made the assumption that the indentation response is elastic during unloading and used the contact equations of a flat half-space indented by a conical indenter to express Young’s modulus in terms of the shape functions. The procedure is briefly described here. The classical Galin-Sneddon’s solution for the force-displacement and contact depth-displacement relationship of a flat semi-infinite substrate indented by a rigid conical indenter is given by Galin (1961) and Sneddon (1965):

$$P = E_r \frac{2 \tan \alpha}{\pi} h^2 \quad (2.1)$$

$$\frac{\delta_c}{h} = \frac{2}{\pi} \quad (2.2)$$

where  $P$ ,  $E_r$ ,  $\alpha$ ,  $h$  and  $\delta_c$  denote the force, reduced modulus, half-angle, displacement and the contact depth (Figure 1.2b), respectively. The projected contact radius can be expressed in terms of the contact depth as:

$$a = \delta_c \tan \alpha \quad (2.3)$$

Differentiating Eq. (2.1) with respect to the indentation depth,  $h$ , and utilizing Eqs. (2.2) and (2.3),

$$\frac{S_u}{E_r} = \frac{1}{E_r} \left. \frac{dP}{dh} \right|_{h=h_m} = 2a \quad (2.4)$$

Later various correction factors have been introduced in the above equation to incorporate various effects (see the review by Oliver and Pharr (1994)).

Inspired by the above approach, we adopt the concept of elastic unloading of the sphere (of radius  $R_s$ ) resting on a rigid flat plate and indented by a rigid conical indenter, Figure 2.1. Similar to the Oliver-Pharr approach, we propose that there exists a functional relationship between the unloading slope, projected contact radius and reduced elastic modulus:

$$\frac{S_u}{E_r} = \rho(a_t) \quad (2.5)$$

Eq. (2.5) simplifies to Eq. (2.4) for a flat substrate with  $\rho(a) = 2a$ . If the characteristic function  $\rho$  can be found, the elastic modulus can be computed by determining  $S_u$  and  $a_t$  experimentally. This is equivalent to using Oliver-Pharr method with a suitable correction factor ( $\psi$ ) as follows:

$$E_r = \frac{S_u}{2a_t \psi}; \quad \psi = \frac{\rho(a_t)}{2a_t} \quad (2.6)$$

This function will be determined next.

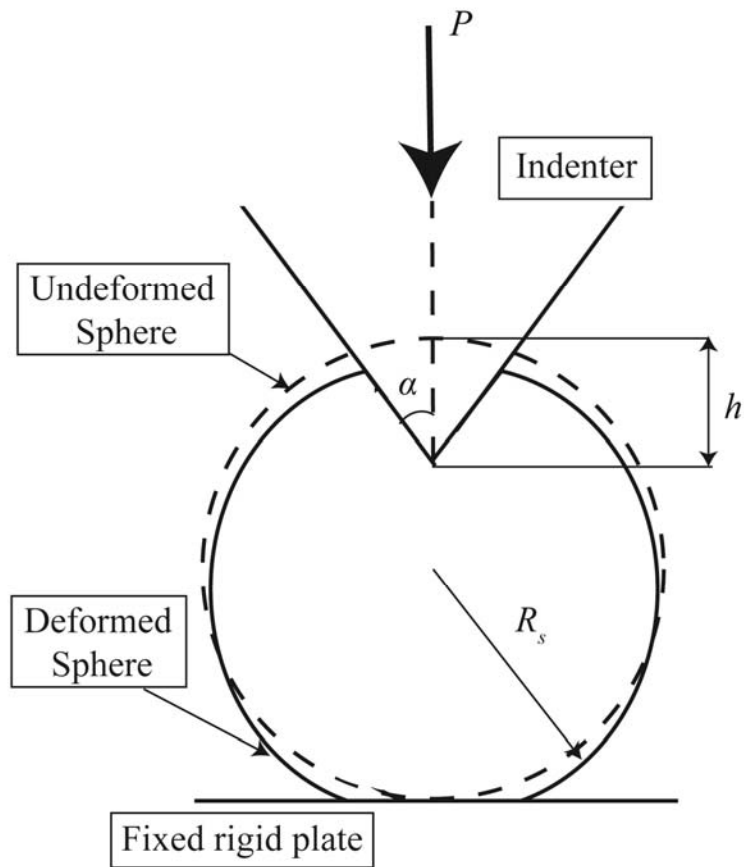


Figure 2.1: Conical indentation of a sphere resting on a fixed rigid plate

Assuming small and elastic displacements, the problem of conical indentation of a sphere resting on a rigid flat plate can be solved as superposition of two problems as shown in Figure 2.2. The first part is the conical indentation of a hemisphere resting on a fixed rigid plate and the displacement of the conical indenter tip is  $h_c$  (Figure 2.2b). The second part is a hemisphere-flat punch contact problem where the rigid flat punch is fixed and the top surface of the hemisphere is displaced by  $h_s$  (Figure 2.2c). Using Newton's second and third laws, it is evident that the indentation force,  $P$  is acting on the two sub-problems as indicated in Figure 2.2b and 2.2c. Using

superposition, the overall displacement of the conical indenter tip can be expressed as the sum of displacements of the two sub-problems, i.e.,  $h = h_c + h_s$ . A solution for the first sub-problem, i.e., the indentation of an elastic hemisphere by a conical indenter (Figure 2.2b), is reported by Fu (2007):

$$a_c = -\frac{R_s}{4} \left( \pi \cot \alpha - \sqrt{(\pi \cot \alpha)^2 + \frac{16h_c}{R_s}} \right) \quad (2.7a)$$

$$P = E_r \left( 2a_c h_c - \frac{\pi a_c^2 \cot \alpha}{2} - \frac{2a_c^3}{3R_s} \right) \quad (2.7b)$$

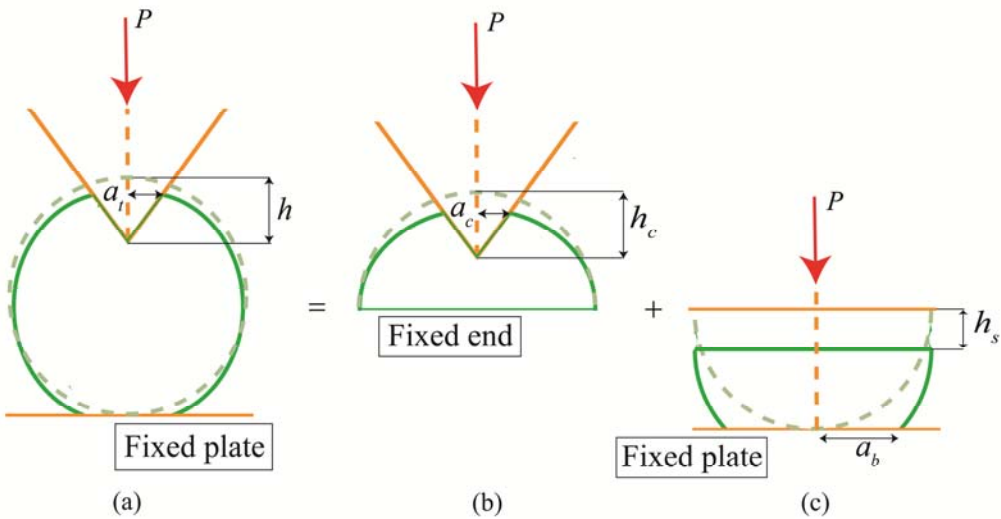


Figure 2.2: Solving the cone-sphere contact problem via superposition: (a) the complete problem; (b) the upper half model; (c) the lower half model.

To the knowledge of the author, two analytical solutions are available in the literature for the second sub-problem (indentation of a hemisphere by a flat punch), reported by

Hertz (Johnson, 1987) and by Tataru (1989, 1991). Hertz's solution (Johnson, 1987) for this problem is given by:

$$a_b = \sqrt{h_s R_s} \quad (2.8a)$$

$$P = \frac{4}{3} E_r R_s^{1/2} h_s^{3/2} \quad (2.8b)$$

Tataru's solution (Tataru, 1989, 1991) for this problem is given by:

$$a_b = \left[ \frac{3R_s P}{4E_r} \right]^{1/3} \quad (2.9a)$$

$$h_s = \frac{3P}{4a_b E_r} - \frac{P}{\pi E_r \sqrt{a_b^2 + 4R_s^2}} \left[ 1 + \frac{2R_s^2}{(a_b^2 + 4R_s^2)(1-\nu)} \right] \quad (2.9b)$$

Hertz's solution is based on small displacement formulation whereas Tataru's solution is based on large displacement formulation. Thus, Tataru's solution is expected to be more accurate than Hertz's solution as the load (or deformation) is increased.

Eqs. (2.6)-(2.8) cannot be inverted analytically to form a closed-form force-displacement ( $P-h$ ) relationship of the overall system. However, using the above relations for two sub-problems, the following numerical algorithm can be used to establish the characteristic function defined in Eq. (2.5) for known values of sphere radius,  $R_s$ , and indenter half angle,  $\alpha$ :

**Step 1:** Assume a value of the indentation depth for the first sub-problem,  $h_c$ .

**Step 2:** Determine the contact radius,  $a_c$ , and the ratio  $P/E_r$  using Eq. (2.7)

**Step 3:** Utilizing the computed value of  $P/E_r$ , determine the deformation of the hemisphere,  $h_s$  using Eq. (2.8) (Hertz's solution) or Eq. (2.9) (Tataru's solution).

**Step 4:** Determine the total displacement of the indenter,  $h = h_c + h_s$ .

**Step 5:** Repeat Steps 1-4 with a value of indentation depth  $h_c + \Delta h_c$  in Step 1 where  $\Delta h_c$  is a very small change in  $h_c$ . Thus, obtain  $P/E_r + \Delta(P/E_r)$  from Step 2 and  $h + \Delta h$  from Step 4.

**Step 6:** Compute  $S_u/E_r$  using the forward difference formula for numerical differentiation as  $\Delta(P/E_r) / \Delta h$

**Step 7:** Repeat Steps 1-6 for a range of values of  $h_c$ . Thus, obtain extended sets of  $S_u/E_r$  (from Step 6) and  $a_c$  (from Step 2) which can be used to develop an empirically established function  $S_u/E_r = \rho(a_c)$

It can be easily shown that Eq. (2.4) is obtained (i.e.  $\rho(a) = 2a$ ) when the algorithm is applied for indentation of a flat substrate. Since the contact radius is generally difficult to measure experimentally, Oliver and Pharr (1992) derived a formula (Eq. (1.11b), Chapter 1, section 1.3) to compute the contact depth and the contact radius. A similar formula cannot be readily derived for the present problem, and thus imposes a limitation of the proposed methodology.

Next, we consider the second method in which a finite element based reverse analysis methodology will be utilized. The functional relationships between the normalized shape functions (characteristic functions from the force-displacement response) and the material properties were determined in Chapter 1, sections 1.4 and 1.6 for isotropic, linear-elastic, power law and linear strain hardening materials, respectively. Since, out of five shape functions, only two are independent, it is not possible to determine the material properties for such materials uniquely using single indentation. In the present case, since the sphere is made of a linear-elastic, perfectly-plastic material, it is possible however to determine the material properties uniquely using a single indentation test. For this we propose to utilize the following two shape

functions: total energy,  $W_t$  (from the loading curve) and unloading slope,  $S_u$  (from the unloading curve). The relationships similar to Eq. (1.13) (Chapter 1, section 1.4) can be derived and take the following form (Phadikar et al., 2012):

$$\frac{W_t}{Yh_m^3} = \bar{F}_1^{pp} \left( \frac{E}{Y}, \frac{h_m}{R_s}, \alpha \right) \quad (2.10)$$

$$\frac{S_u}{Yh_m} = \bar{F}_3^{pp} \left( \frac{E}{Y}, \frac{h_m}{R_s}, \alpha \right) \quad (2.11)$$

where the superscript  $pp$  indicates elastic, perfectly-plastic material. The quantity  $h_m/R_s$  appears because the substrate is a sphere and not a half-space. Dividing Eq. (2.10) by Eq. (2.11), we obtain:

$$\frac{S_u}{W_t} h_m^2 = \bar{F}_7^{pp} \left( \frac{E}{Y}, \frac{h_m}{R_s}, \alpha \right) \quad (2.12)$$

Eqs (2.11) and (2.12) can be used to establish the elastic-plastic properties of a sphere using experimentally obtained values of  $S_u$ ,  $W_t$ ,  $h_m$  and  $R_s$ . This will be discussed in section 2.1.3.

## 2.1.2 Establishing the functional forms

### 2.1.2.1 Finite element model

Finite element simulations were performed using the commercial finite element code ABAQUS (Dassault Systemes, 2009). A two-dimensional axisymmetric model was adopted and approximately 24,000 ‘‘CAX4R’’ elements were used to model the sphere. A homogeneous material with isotropic, linear-elastic, perfectly-plastic material properties was assigned to the substrate sphere. Poisson’s ratio was taken as 0.2. The sphere is assumed to rest on a fixed rigid plate. Both the flat surface and the

indenter are modeled using the “analytical rigid” option in ABAQUS. Coulomb’s friction law is used and the friction coefficient between the two pairs of surfaces is taken to be 0.2 (Taljat et al, 1998). Due to Poisson’s ratio effect, the surface nodes which come into contact with the rigid surface during the loading period continue to move away from the axis of symmetry after the initial contact. Thus, frictional force acts between the sphere-rigid plate pair as well. Several simulations with refined meshes and time increments (i.e., the step size of each simulation increment along the load path) were investigated for the convergence study. The model used, shown in Figure 2.3, gave the same results as a finer mesh and time increment. Thus, the selected refinement is sufficient to capture the mechanism of indentation. This model is used for most of the simulations whereas slightly different meshes were adopted for simulating large indentation depth-to-radius ratios. The surface nodes of the sphere were kept traction free and the nodes along the axis of symmetry were constrained in the direction normal to indenter displacement to simulate symmetry conditions.

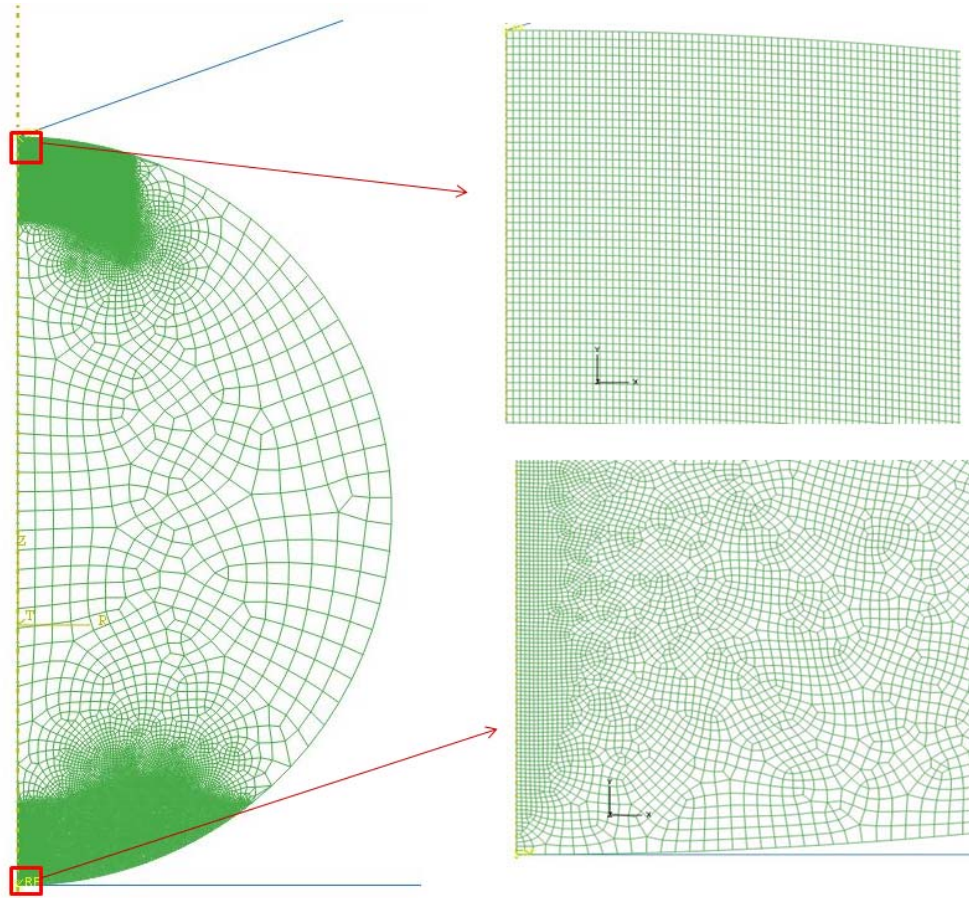


Figure 2.3: Finite element model in ABAQUS, including enlargements of the refined meshes (plotted at the same scale) at the top of the sphere (conical indentation) and the bottom of the sphere (contact with the rigid surface).

The model simulates indentation testing by pushing the rigid indenter into the sphere to a predefined position, and then bringing it back to the original position. The reaction force at the indenter tip and the indenter displacement are recorded continuously over the loading and unloading sequence, similar to a real indentation experiment. Based on the force-displacement relationships obtained, the total energy,  $W_t$ , and the initial unloading slope,  $S_u$ , can be obtained. In all cases,  $S_u$  was computed

using the two points, which are associated with the maximum load and 90% of the maximum load.

#### **2.1.2.2 Functional form for the first method (based on unloading slope)**

This algorithm discussed in section 2.1.1 provides the force-displacement relationship within the linear-elastic loading range for a sphere subjected to conical indentation. To investigate the viability of the algorithm, the force-displacement relationship obtained from the algorithm will be compared with the results from finite element simulations. A sphere of radius,  $R_s = 23 \mu\text{m}$  with elastic modulus,  $E = 100 \text{ GPa}$  and Poisson's ratio,  $\nu = 0.2$  is considered. The indenter half-angle is taken to be  $\alpha = 75^\circ$ . The force-displacement relationships computed using the algorithm and finite element simulation are shown in Figure 2.4. Thus, they are in good agreement with each other, where (within the resolution of the figure) the two analytical results overlap. Thus, the proposed algorithm gives reliable force-displacement relationships.

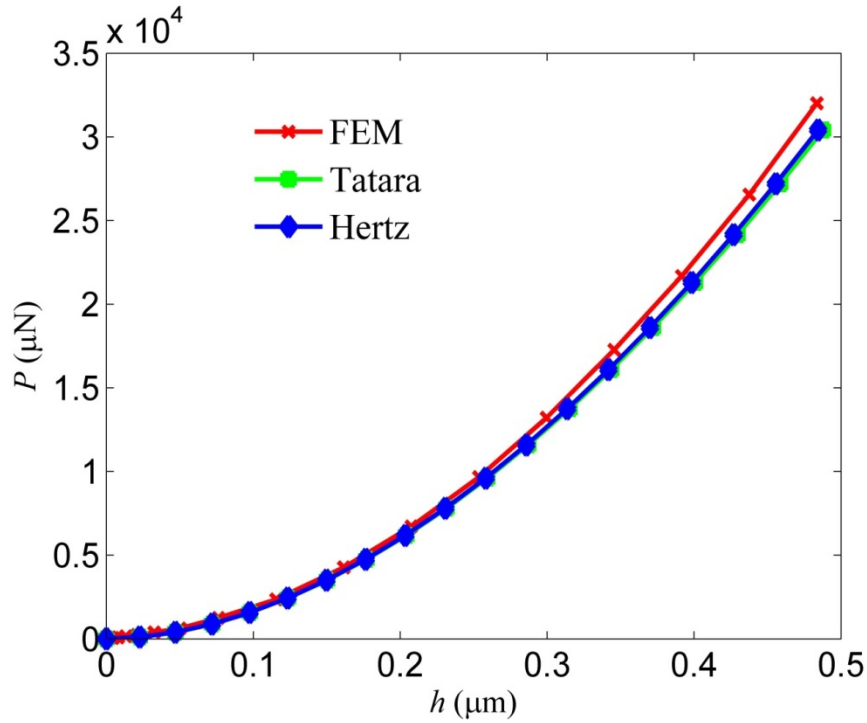


Figure 2.4: Comparison of the force displacement relationship obtained using the finite element method and the superposition techniques. For a linear-elastic material (assumed here), the loading and unloading curves are identical.

As discussed in section 2.1.1, the technique is based on developing a function,  $\rho$ , that relates the unloading slope,  $S_u$ , to the projected contact area,  $a_t$ , and the reduced modulus,  $E_r$ , as defined in Eq. (2.5). The function obtained by the proposed algorithm for the sphere and indenter considered in the above paragraph is shown in Figure 2.5. If the “Oliver-Pharr method,” Eq. (2.4), is used for this problem, it will predict  $\rho(a_t) = 2a_t$  which is also shown in Figure 2.5. Thus, from the graph and Eq. (2.5), it can be concluded that the Oliver-Pharr method will significantly under-predict the elastic modulus if it is used for evaluating material properties of a spherical substrate. The erroneous result is not a surprise, since that method is formulated to evaluate material

properties of a flat substrate. As seen from Figure 2.5, for a given  $a_t$ , Hertz's model predicts a slightly smaller  $\rho(a_t)$  compared to Tatara's model, and thus from Eq. (2.5), Hertz's model will predict slightly larger elastic modulus compared to Tatara's model. The accuracy of the proposed algorithm for predicting elastic modulus will be discussed later.

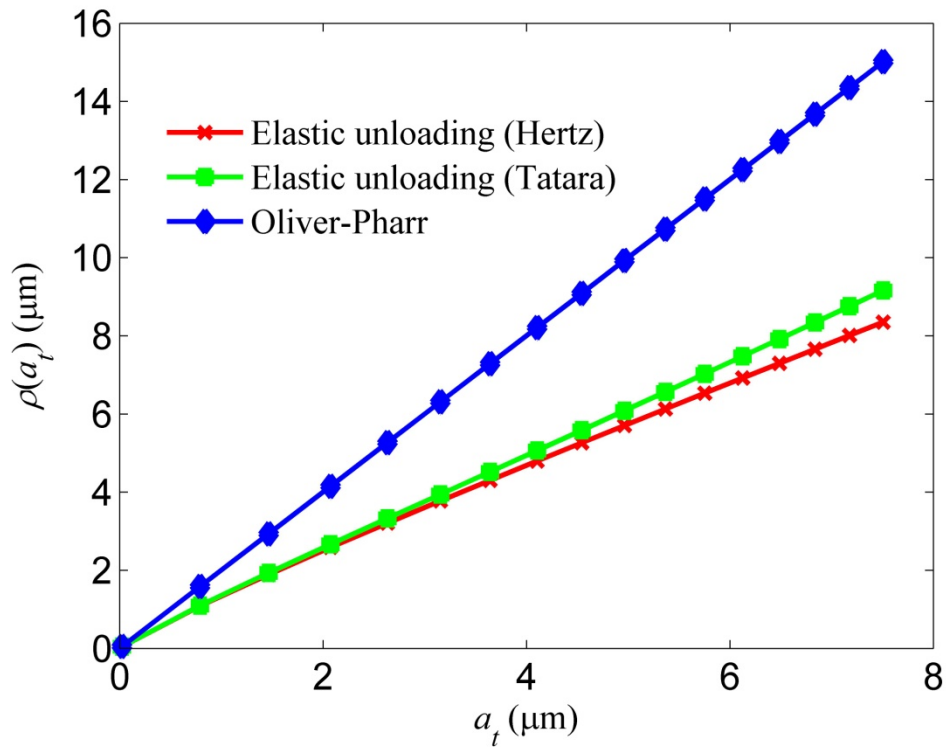


Figure 2.5: The function  $\rho(a_t)$  defined in Eq. (2.5) as function of  $a_t$ , the projected contact area for a  $75^\circ$  half-angle indenter indenting a sphere of radius  $23 \mu\text{m}$ .

### 2.1.2.3 Functional forms for the second method (based on reverse analysis)

To develop the functional forms of Eqs. (2.11) and (2.12), a material set with elastic modulus,  $E$ , and yield stress,  $Y$ , varying from 20 GPa to 220 GPa and 0.2 GPa to 0.8 GPa, respectively, was chosen to cover a wide range of  $E/Y$  ratios. For simplicity, first we assume a fixed indenter (i.e., constant half-angle,  $\alpha$ ) and various indentation depth-to-radius ratios. In this case, Eqs. (2.11) and (2.12) can be written as:

$$\frac{S_u}{Yh_m} = \phi_1 \left( \frac{E}{Y}, \frac{h_m}{R_s} \right) \quad (2.13)$$

$$\frac{S_u}{W_t} h_m^2 = \theta_1 \left( \frac{E}{Y}, \frac{h_m}{R_s} \right) \quad (2.14)$$

An indenter with  $\alpha = 70.3^\circ$  half-angle is assumed, which represents the widely used Berkovich indenter<sup>1</sup>. A sphere of radius,  $R_s = 23 \mu\text{m}$  was chosen and the range of  $0.05 \leq h_m/R_s \leq 0.20$  was investigated. The numerical results are plotted in Figure 2.6.

The surfaces can be fitted with the following equations:

$$\frac{S_u}{Yh_m} = A_1 \frac{E}{Y} + A_2 \quad (2.15a)$$

$$\frac{S_u}{W_t} h_m^2 = A_3 \frac{E}{Y} + A_4 \quad (2.15b)$$

Here,

$$A_i = \sum_{j=0}^5 a_{ij} \left( \frac{h_m}{R_s} \right)^{5-j} ; \text{ for } i = 1, 2, 3, 4 \quad (2.15c)$$

---

<sup>1</sup> The Berkovich and conical indenter with half-angle  $70.3^\circ$  are equivalent since they have same projected contact area (Cheng and Cheng, 2004; Lichinchi et al., 1998). We assume that this equivalency holds for a spherical substrate, at least within the range of deformations considered.

The coefficients  $a_{ij}$  are tabulated in Table 2.1.<sup>2</sup>

Table 2.1: The coefficients  $a_{ij}$  used in Eq. (2.15c)

$a_{ij}$	$j=0$	$j=1$	$j=2$	$j=3$	$j=4$	$j=5$
$i=1$	-8.903E3	7.831E3	-2.5945E3	4.133E2	-3.465E1	3.770
$i=2$	8.270E	-5.380E6	1.335E6	-1.566E5	8.676E3	-2.117E2
$i=3$	2.783E2	-7.716E1	-6.998	3.393	4.4684E-1	9.551E-2
$i=4$	6.34E5	-4.090E5	1.005E5	-1.160E4	6.169E2	-6.416

Solving Eqs. (2.15a) and (2.15b) for  $E$  and  $Y$ , we get the following closed form equations relating  $E$  and  $Y$  with  $S_u$ ,  $W_t$ ,  $h_m$  and  $R_s$ :

$$E = \frac{S_u (S_u h_m^2 - A_4 W_t)}{h_m \{A_1 (S_u h_m^2 - A_4 W_t) + A_2 A_3 W_t\}} \quad (2.16a)$$

$$Y = \frac{S_u A_3 W_t}{h_m \{A_1 (S_u h_m^2 - A_4 W_t) + A_2 A_3 W_t\}} \quad (2.16b)$$

Eq. (2.15) assumes a Berkovich indenter tip for a range of indentation depths-to-radius ratios.

---

<sup>2</sup> In this case 20 coefficients are needed to describe the functions. This may seem like a large number of parameters, and note that we are **not** striving to develop a relationship where the parameters can be interpreted as physical parameters, but we are just interested in finding “fitting parameters” that describe the intricate response. This method is commonly adopted in reverse analysis, see for example (Cao and Lu, 2004; Chen et al., 2006; Hyun et al., 2011; Le, 2008).

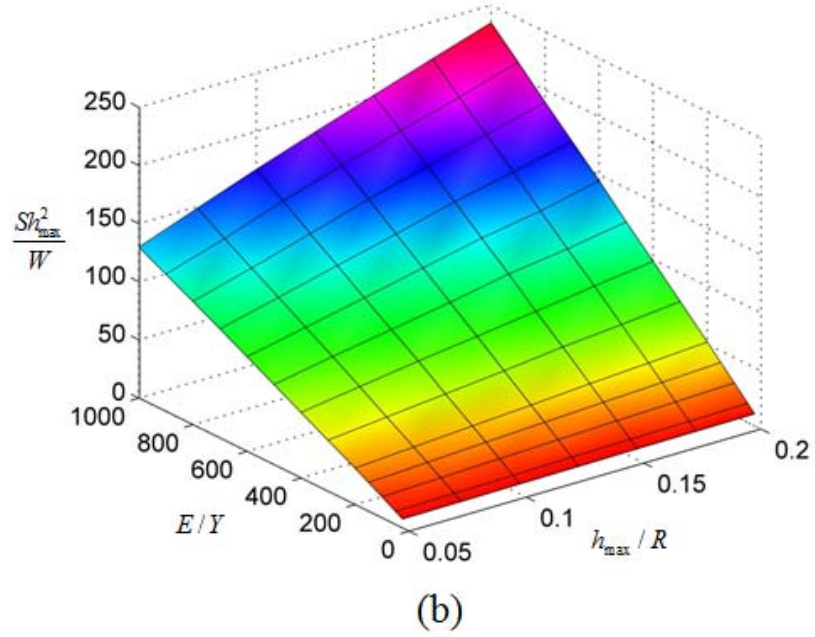
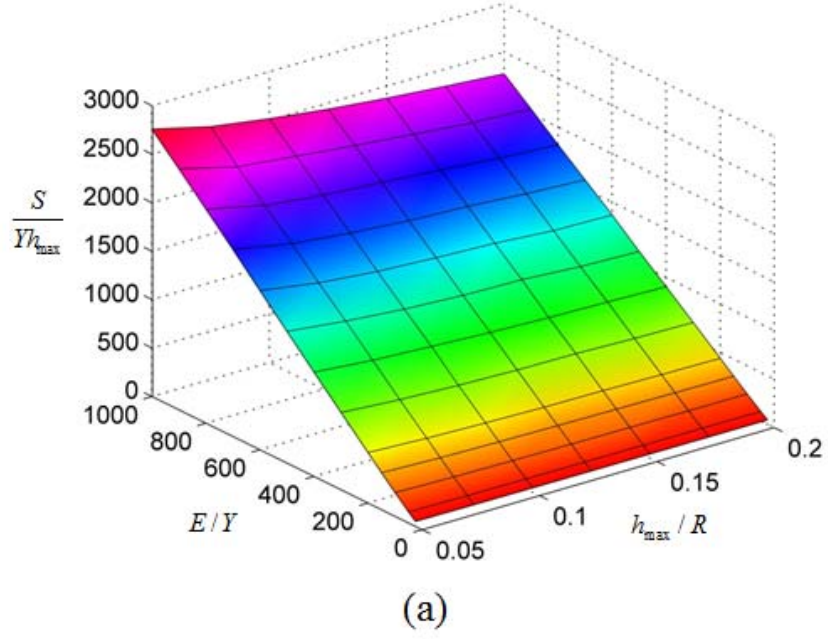


Figure 2.6: Graphs of functions  $\phi_l$  and  $\theta_l$  of Eqs. (2.13) and (2.14) for  $\alpha = 70.3^\circ$  and  $0.05 < h_m/R_s < 0.20$ : (a)  $\frac{S_u}{Y h_m} = \phi_l \left( \frac{E}{Y}, \frac{h_m}{R_s} \right)$  (b)  $\frac{S_u}{W_l} h_m^2 = \theta_l \left( \frac{E}{Y}, \frac{h_m}{R_s} \right)$

Next, we keep the depth-to-radius ratio fixed, and use various indenter half-angles. In this case, Eqs. (2.11) and (2.12) can be written as:

$$\frac{S_u}{Yh_m} = \varphi_2\left(\frac{E}{Y}, \alpha\right) \quad (2.17)$$

$$\frac{S_u}{W_t} h_m^2 = \theta_2\left(\frac{E}{Y}, \alpha\right) \quad (2.18)$$

These functional forms can be determined using the previously described procedure except that in this case  $\alpha$  is varied while  $h_m/R_s$  is kept constant. A depth-to-radius ratio 0.10 was considered and the range of half-angle was set to  $45^\circ \leq \alpha \leq 90^\circ$  to produce the characteristic functions in Eqs. (2.17) and (2.18). The numerical results are plotted in Figure 2.7 and the surfaces can be fitted as:

$$\frac{S_u}{Yh_m} = B_1 \frac{E}{Y} + B_2 \quad (2.19a)$$

$$\frac{S_u}{W_t} h_m^2 = B_3 \frac{E}{Y} + B_4 \quad (2.19b)$$

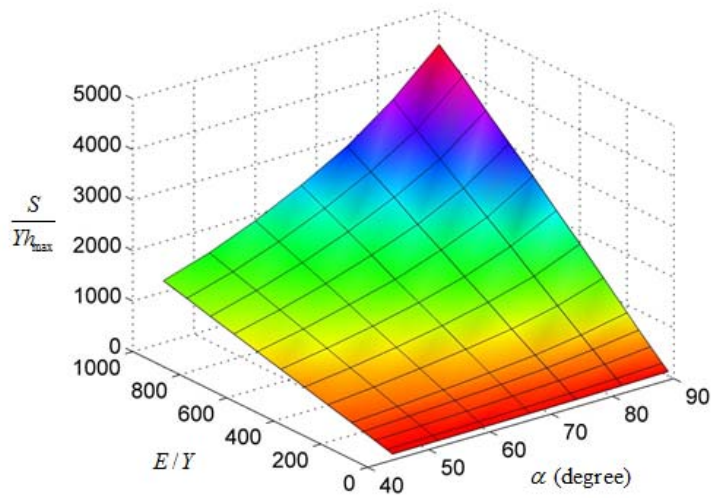
where,

$$B_i = \sum_{j=0}^5 b_{ij} \left(\frac{\pi\alpha}{180}\right)^{5-j}; \text{ for } i = 1, 2, 3, 4 \quad (2.19c)$$

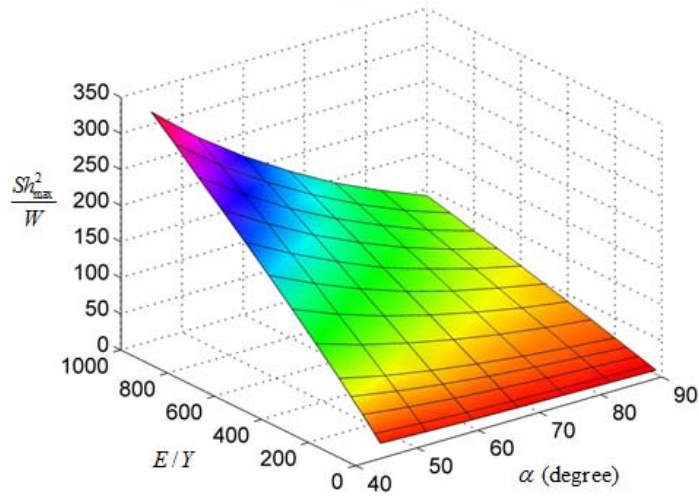
and the coefficients  $b_{ij}$  are tabulated in Table 2.2.

Table 2.2: The coefficients  $b_{ij}$  used in Eq. (2.19c)

$b_{ij}$	$j = 0$	$j = 1$	$j = 2$	$j = 3$	$j = 4$	$j = 5$
$i = 1$	6.388	-3.259E1	6.600E1	-6.413E1	3.1645E1	-5.548
$i = 2$	-2.098E3	1.221E4	-2.764E4	3.039E4	-1.629E4	3.419E3
$i = 3$	-3.196E-1	2.350E-1	-6.717E-1	1.082	-1.262	8.790E-1
$i = 4$	-5.410	1.035E1	4.642	6.113	-5.642E1	4.834E1



(a)



(b)

Figure 2.7: Graphs of functions  $\phi_2$  and  $\theta_2$  of Eqs. (2.17) and (2.18) for  $h_m/R = 0.10$  and  $45^\circ \leq \alpha \leq 90^\circ$ : (a)  $\frac{S_u}{Y h_m} = \phi_2\left(\frac{E}{Y}, \alpha\right)$  (b)  $\frac{S_u}{W_t} h_m^2 = \theta_2\left(\frac{E}{Y}, \alpha\right)$

Solving for  $E$  and  $Y$ , we get following closed form equations relating  $E$  and  $Y$  with  $S_u$ ,  $W_t$ ,  $h_m$  and  $R_s$ :

$$E = \frac{S_u (S_u h_m^2 - B_4 W_t)}{h_m \{B_1 (S_u h_m^2 - B_4 W_t) + B_2 B_3 W_t\}} \quad (2.20a)$$

$$Y = \frac{S_u B_3 W_t}{h_m \{B_1 (S_u h_m^2 - B_4 W_t) + B_2 B_3 W_t\}} \quad (2.20b)$$

The overall procedure for obtaining  $E$  and  $Y$  from a conical indentation experiment on a sphere is presented in a flowchart in Figure 2.8.

If it is not possible to conduct the indentation testing for the range of indentation depths or half-angles considered in the flowchart of Figure 2.8 (for example, it might be required to do an indentation testing with  $h_m/R_s = 15\%$  and  $\alpha = 60^\circ$ ), for such cases, a general procedure will be presented next. In this procedure, a finite element model needs to be built with experimentally used values of  $h_m$ ,  $R_s$  and  $\alpha$ . Since  $h_m$ ,  $R_s$  and  $\alpha$  are fixed, Eqs. (2.11) and (2.12) can be rewritten as:

$$\frac{S_u}{Y h_m} = \varphi \left( \frac{E}{Y} \right) \quad (2.21)$$

$$\frac{S_u}{W_t} h_m^2 = \theta \left( \frac{E}{Y} \right) \quad (2.22)$$

Once the functional forms are established, properties such as  $E$  and  $Y$  can be determined based on experimentally obtained values for  $S_u$  and  $W_t$  using the following steps:

**Step 1:** The left hand side of Eq. (2.22) can be determined from the experiment.

Determine  $E/Y$  using function  $\theta$ , where  $\theta$  is determined by the finite element simulation procedure described above.

**Step 2:** Substitute the obtained value of  $E/Y$  into the function  $\varphi$  which is determined by the finite element simulation. As  $S_u$  and  $h_m$  are known from the experiments, calculate  $Y$  using Eq. (2.21).

**Step 3:** Using the obtained value of  $Y$ , compute  $E$  using the value of  $E/Y$  obtained in Step 1.

The accuracy of the proposed method will be described next.

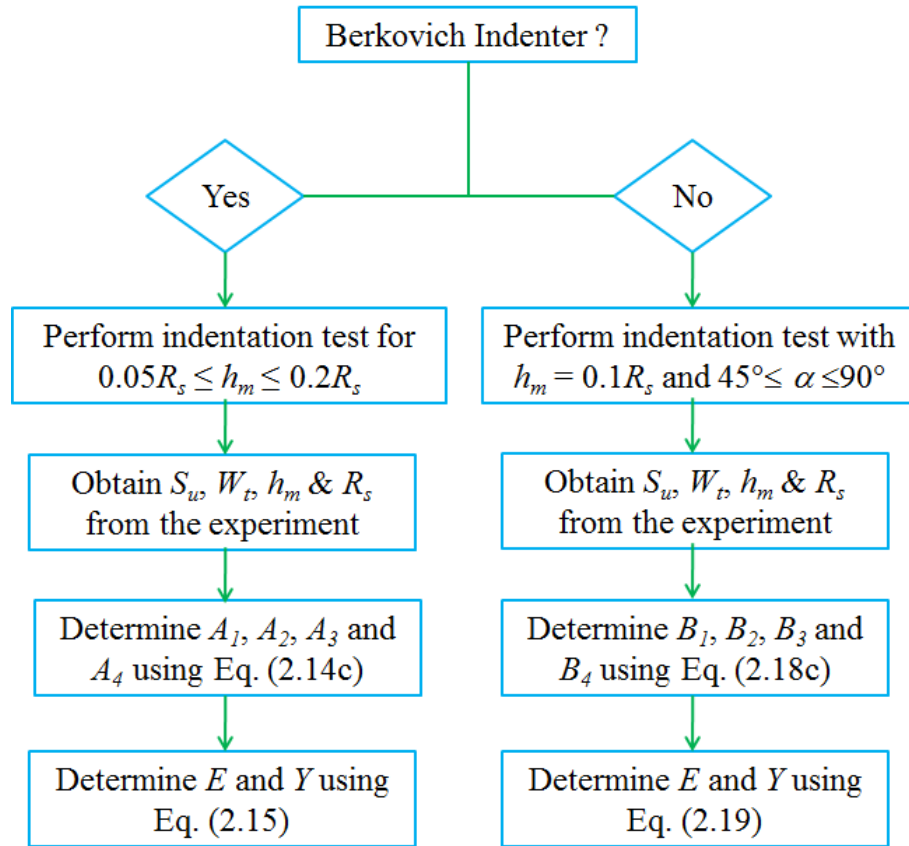


Figure 2.8: Flowchart of the second methodology (based on reverse analysis) to determine material properties of a sphere by conical indentation

### 2.1.3 Numerical verification

To the author’s knowledge, at this time, no comprehensive experimental data are available to verify the proposed schemes. Thus, numerical simulations which can be regarded as “exact experiments” are used to investigate the validity of the proposed

methods. Three sample materials (used by Yan et al., 2007a, 2007b) are used for this purpose. The material properties of these materials were excluded from the range of the properties that was used to develop the functional forms of Eqs. (2.15) and (2.19).

Numerical simulations were conducted in which an indenter with  $\alpha = 70.3^\circ$  indents the spheres made of the three sample materials. From these simulations (which act as “numerical experiments”), the force-displacement relationships are obtained and the unloading slope,  $S_u$ , and the total energy,  $W_t$ , are extracted. The elastic modulus obtained using the method based on elastic unloading presented in sections 2.1.1-2.1.2 are tabulated in Table 2.3 along with the original input material properties. Hertz’s solution predicts slightly higher elastic modulus than Tatara’s solution (this was explained in section 2.1.2). The error in the predicted elastic modulus lies within 12%. The elastic modulus,  $E$ , and yield strength,  $Y$ , obtained using Eq. (2.16) (the second method, the finite element based reverse analysis), are also tabulated in Table 2.3. This method predicts  $E$  and  $Y$  quite accurately, with errors less than 3%.

Table 2.3: Comparison of input material properties with that obtained using the two methods for selected indentation depths

Input Material Properties	$h_m/R_s$	Elastic Unloading		Functional Form from FEA	
		Hertz	Tatara		
		$E$ (% error)	$E$ (% error)	$E$ (% error)	$Y$ (% error)
<b>Bulk Ti</b> $E = 130$ GPa $Y = 600$ Mpa	0.06	126 (3.08)	121 (6.92)	128 (1.54)	584 (2.67)
	0.11	135 (3.85)	127 (2.31)	129 (0.77)	588 (2.00)
	0.16	145 (11.5)	133 (2.31)	129 (0.77)	591 (1.50)
<b>Bulk Ti-Al-Fe</b> $E = 110$ GPa $Y = 795$ MPa	0.06	107 (2.73)	103 (6.36)	108 (1.82)	780 (1.89)
	0.11	115 (4.55)	109 (0.91)	109 (0.91)	780 (1.89)
	0.16	122 (10.9)	113 (2.73)	108 (1.82)	784 (1.38)
<b>Bulk Steel</b> $E = 210$ GPa $Y = 500$ MPa	0.06	198 (5.71)	190 (9.52)	208 (0.95)	493 (1.40)
	0.11	219 (3.81)	204 (2.86)	209 (0.48)	495 (1.00)
	0.16	232 (10.5)	214 (1.90)	209 (0.48)	497 (0.60)

In a similar manner, the accuracy of the proposed methods is evaluated for a fixed depth-to-radius ratio of 0.10. The same sample materials are used in the finite element simulations to extract  $S_u$  and  $W_t$  for the three selected indenter shapes. The half-angles that are chosen are  $63.14^\circ$  (the cross-sectional area is half of that of the Berkovich indenter),  $70.3^\circ$  (the cross-sectional area is same as the Berkovich indenter) and  $75.79^\circ$  (the cross-sectional area is twice of that of the Berkovich indenter). The resultant  $E$  based on the method of elastic unloading, and  $E$  and  $Y$  obtained from Eq. (2.20), along with the original input material properties are tabulated in Table 2.4. Thus, in this case as well, the proposed reverse analysis method predicts the values of

$E$  and  $Y$  quite accurately with errors less than 3% for the later approach and the former within 8% error.

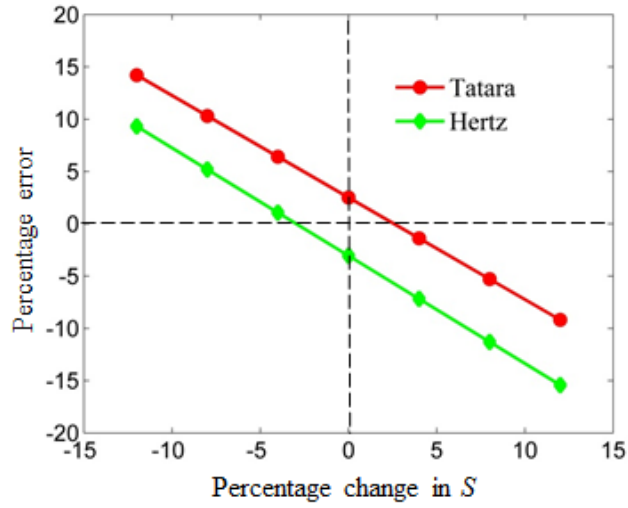
Table 2.4: Comparison of input material properties with that obtained using the two methods for selected half-angles of indentation.

Input Material Properties	Half-angle	Elastic Unloading		Functional Form from FEA	
		Hertz	Tatara	$E$	$Y$
		$E$ (% error)	$E$ (% error)	$E$ (% error)	$Y$ (% error)
<b>Bulk Ti</b> $E = 130 \text{ GPa}$ $Y = 600 \text{ MPa}$	63.14	126 (3.08)	120 (7.69)	129 (0.77)	589 (1.83)
	70.3	134 (3.08)	127 (2.31)	129 (0.77)	587 (2.17)
	75.79	140 (7.69)	131 (0.77)	128 (1.54)	585 (2.50)
<b>Bulk Ti-Al-Fe</b> $E = 110 \text{ GPa}$ $Y = 795 \text{ MPa}$	63.14	109 (0.91)	103 (6.36)	109 (0.91)	783 (1.51)
	70.3	113 (2.73)	107 (2.73)	109 (0.91)	779 (2.01)
	75.79	119 (8.18)	112 (1.82)	108 (1.82)	779 (2.01)
<b>Bulk Steel</b> $E = 210 \text{ GPa}$ $Y = 500 \text{ MPa}$	63.14	201 (4.29)	191 (9.05)	210 (0.00)	495 (1.00)
	70.3	215 (2.38)	202 (3.81)	210 (0.00)	495 (1.00)
	75.79	225 (7.14)	211 (0.48)	209 (0.48)	494 (1.20)

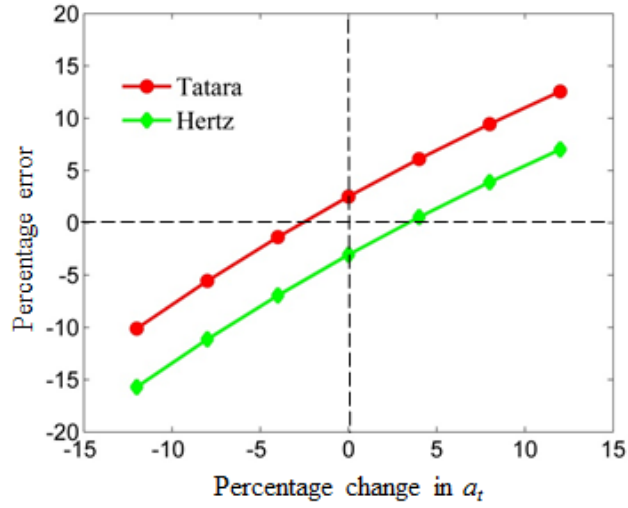
#### 2.1.4 Sensitivity analysis

Real physical experiments always contain some degree of experimental error. To investigate the sensitivity of the proposed methodologies to such errors, we will present a sensitivity analysis.

For the first method, i.e. the method based on elastic unloading, a sphere with radius,  $R_s = 23 \mu\text{m}$  is indented numerically by an indenter with half-angle,  $\alpha = 70.3^\circ$  with a maximum depth of penetration,  $h_m = 2.3 \mu\text{m}$  ( $h_m/R_s = 0.10$ ). The input material properties used are typical for bulk Ti-Al-Fe alloy and are assumed linear-elastic, perfectly-plastic. To examine the sensitivity of the first method with respect to  $S_u$  and  $a_t$ , these two output parameters are varied within  $\pm 12\%$  and the corresponding errors obtained in calculated  $E$  are noted. For 12% difference in  $S_u$  or  $a_t$ , the percentage error in calculating  $E$  lies between 5-15% i.e. the same order of magnitude as the error imposed.



(a)

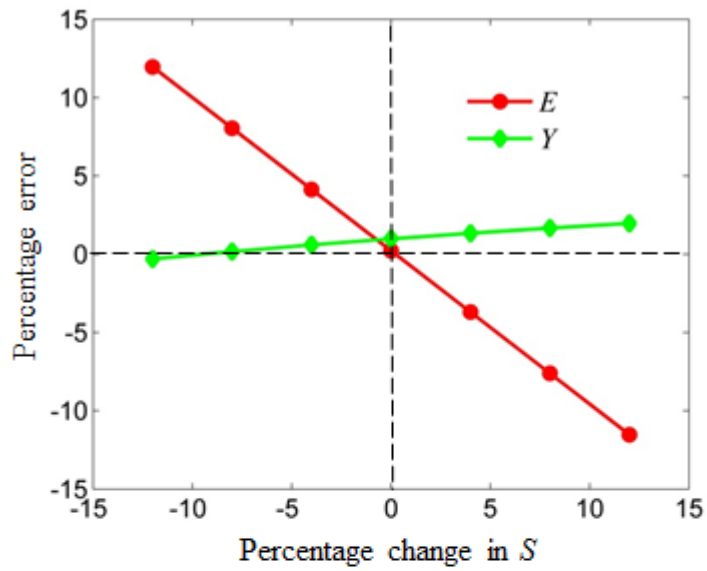


(b)

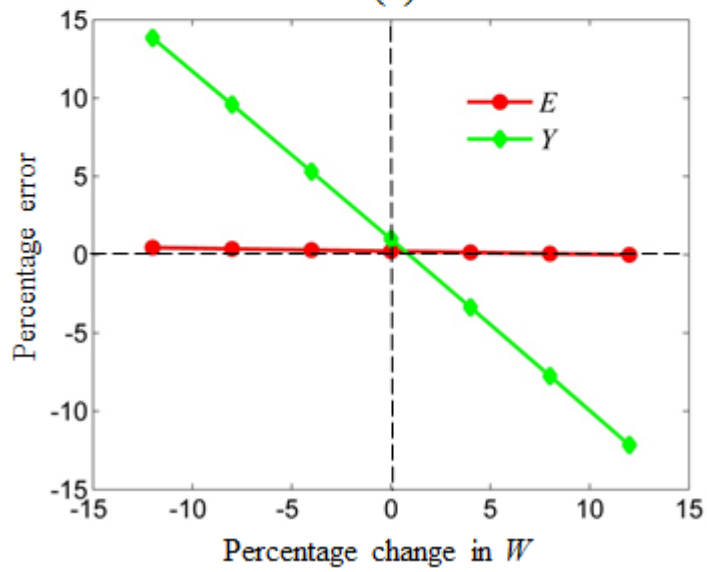
Figure 2.9: Sensitivity in determining the elastic modulus,  $E$ , with respect to imposing a small error in (a) the unloading slope,  $S_u$ , and (b) the projected contact radius,  $a_t$ , using the first method (the method based on elastic unloading).

For the second method, a sphere with  $R_s = 23 \mu\text{m}$  is indented numerically by an indenter with  $\alpha = 63.14^\circ$  up to  $h_m = 2.3 \mu\text{m}$  ( $h_m/R_s = 0.10$ ). The input material is

taken as typical properties for steel and linear-elastic, perfectly-plastic material is assumed. To examine the sensitivity of the second method with respect to  $S_u$  and  $W_t$ , these two output parameters are varied within  $\pm 12\%$  and the corresponding errors obtained in calculated  $E$  and  $Y$  are noted. Figure 2.10 shows that the error in  $S_u$  does not affect the calculated value of  $Y$  considerably, whereas the error in  $W_t$  does not affect the calculated value of  $E$  considerably. This may be expected since the unloading slope is determined from the elastic unloading behavior and the loading work is governed by yielding. Further, it can be noted that for a 12% difference in  $S_u$  (or  $W_t$ ) the percentage error in calculating  $E$  (or  $Y$ ) lies between 10-15% i.e. the same order of magnitude as the error imposed.



(a)



(b)

Figure 2.10: Sensitivity in determining the elastic modulus,  $E$ , and the yield strength,  $Y$ , with respect to imposing a small error in (a) the unloading slope,  $S_u$ , and (b) the total energy,  $W_t$ , using the second method (finite element based reverse analysis).

### **2.1.5 Synopsis: linear-elastic, perfectly-plastic sphere**

Two methodologies, a semi-analytical method and a finite element based reverse analysis technique, are presented as data reduction schemes to determine the elastic modulus and yield strength of a sphere via conical indentation.

In the first method, a relationship between the initial unloading slope, projected contact radius and elastic modulus is developed which can be used to obtain the elastic modulus based on the experimental data. By comparing the results obtained from the proposed method with results from finite element simulations, we show that this method predicts the elastic modulus with an error less than 12%. It was shown that, the “Oliver-Pharr method” which is developed for flat surfaces will significantly under-predict the elastic modulus if it is applied for a sphere.

In the second method, finite element simulations are used to correlate the non-dimensional shape functions with material properties. For the particular scheme shown in this work using a Berkovich indenter, the experiment has to be performed by keeping the maximum indentation depth between 5% and 20% of the radius of the sphere whereas for a non-Berkovich indenter, the maximum indentation depth has to be kept at 10% of the radius. A general method is also presented for other indenters and depth-to-radius ratios but a finite element software is required for that. By comparing the results obtained from the proposed method with results from the finite element simulations, it is shown that this method predicts the elastic modulus and yield strength with a less than 3% error.

A sensitivity analysis was conducted in which the shape functions obtained from the (numerical) experiment were perturbed to simulate experimental errors, and the properties predicted by the two methods were recorded. The results suggest that the error obtained when determining the material properties is of same order of

magnitude of error in the experimental data. In the proposed sensitivity analysis, one shape function was perturbed at a time. Some more sophisticated schemes will be discussed in Chapter 3.

## **2.2 Indentation of a Sphere Made of Viscoelastic Material**

Although several researchers (Cheng et al., 2005; Vandamme and Ulm, 2006; Francius et al., 2007; Cheng and Cheng, 2005; Zhou and Lu, 2010) have investigated indentation of a flat substrate made of viscoelastic material, to the authors' knowledge, only one study is available in the literature regarding the indentation of non-flat viscoelastic substrates (Zhou and Lu (2010)). Their methodology relies on Hertz-type solutions (Johnson, 1987), and thus the procedure is limited to shallow indentation depths. In this section, we investigate the indentation of a viscoelastic sphere by a conical indenter as shown in Figure 2.1, with the ultimate goal of developing a reliable evaluation technique for indentation testing of viscoelastic spherical particles. For this purpose, a semi-analytical technique is developed for the forward analysis of the indentation problem, which is then verified by a geometrically nonlinear finite element analysis. The technique will be shown to be applicable for moderate indentation depths and can be extended easily for other non-flat substrates as well.

### **2.2.1 Viscoelastic solution using the elastic solution**

#### **2.2.1.1 Elastic solution**

Lee and Radok (Lee and Radok, 1960) developed the “method of functional equations” for solving viscoelastic indentation problems from a corresponding linear-elasticity solution. In this approach, the elastic constants in an elastic solution are replaced by equivalent viscoelastic operators to obtain the viscoelastic solution. Here,

we first determine the elastic solution of the cone-sphere contact problem by geometrically nonlinear finite element analysis. For a particular indenter half-angle,  $\alpha$ , the indenter force,  $P$ , is in general, a function of the indentation depth,  $h$ , the radius of the sphere,  $R_s$ , the elastic modulus,  $E$ , and Poisson's ratio,  $\nu$ , of the material. Thus,

$$P = f_1(E, h, R_s, \nu) \quad (2.23)$$

Applying dimensional analysis and utilizing Buckingham's PI theorem (see Chapter 1, section 1.1.2), the above equation can be written in its non-dimensional form as follows:

$$\frac{P}{ER_s^2} = f_2\left(\frac{h}{R_s}, \nu\right) \quad (2.24)$$

We assume the following specific form of Eq. (2.24):

$$\frac{P}{E_r R_s^2} = f_3\left(\frac{h}{R_s}\right) \quad (2.25)$$

In this equation  $E_r$  is the plane strain reduced modulus (see Chapter 1, section 1.3).

The validity of the above assumption, as well as the functional form of the function  $f_3$  will be established using finite element analysis in a later section. The reduced modulus  $E_r$  generally appears in indentation problems where contact interference is very small compared to the dimensions of the contacting bodies. However, it will be shown later that even for quite large indentation depths, the elastic modulus and Poisson's ratio can be combined into the reduced modulus  $E_r$  for this particular case.

### 2.2.1.2 Viscoelastic solution

Applying the "method of functional equations" (Lee and Radok, 1960) to the elastic solution given by Eq. (2.25), the following relationship between force and

displacement in Laplace domain can be obtained easily for the corresponding viscoelastic problem:

$$\frac{P(s)}{R_s^2 E_r(s)} = \Gamma \left[ f_3 \left( \frac{h(t)}{R_s} \right) \right] \quad (2.26)$$

where  $P(s)$  is Laplace transform of the loading function ( $s$  denotes the Laplace domain parameter) and  $E_r(s)$  is the reduced elastic modulus of the viscoelastic material in Laplace domain (it can be determined when the constitutive relation is known and will be described in a later section). Eq. (2.26) can easily be inverted to determine the indenter displacement as a function of time as follows:

$$h(t) = R_s f_3^{-1} \left[ \frac{1}{R_s^2} \Gamma^{-1} \left( \frac{P(s)}{E_r(s)} \right) \right] \quad (2.27)$$

Thus, for a given radius of the sphere, loading history and constitutive equation, Eq. (2.27) can be used to determine the indenter displacement as a function of time. It follows that the force-displacement relationship for a specific viscoelastic indentation problem can thus be obtained. An example will be presented next to illustrate the methodology.

A brief description of the viscoelastic material properties was presented in Chapter 1, section 1.7. Here we consider a viscoelastic material with the four-parameter Kelvin-Voigt deviator creep model (Haddad, 1995) shown in Figure 2.11a and 2.11b. In this model, the shear behavior is modeled by the standard three-element solid model (Figure 2.11a) where  $G_1$  and  $G_2$  are the moduli of the two spring elements and  $\eta$  is the viscosity of the dashpot element. The bulk behavior is modeled by a linear time independent spring (Figure 2.11b) with modulus  $K$ . To express the constitutive

relation for this model, the stress and strain tensors need to be decomposed into deviatoric and spherical (volumetric) components as:

$$\begin{aligned}\sigma_{ij} &= \sigma_{ij}^D + \sigma_{ij}^V \\ \varepsilon_{ij} &= \varepsilon_{ij}^D + \varepsilon_{ij}^V\end{aligned}\tag{2.28a}$$

where the indicial notation is used, with  $i, j = 1, 2, 3$ .

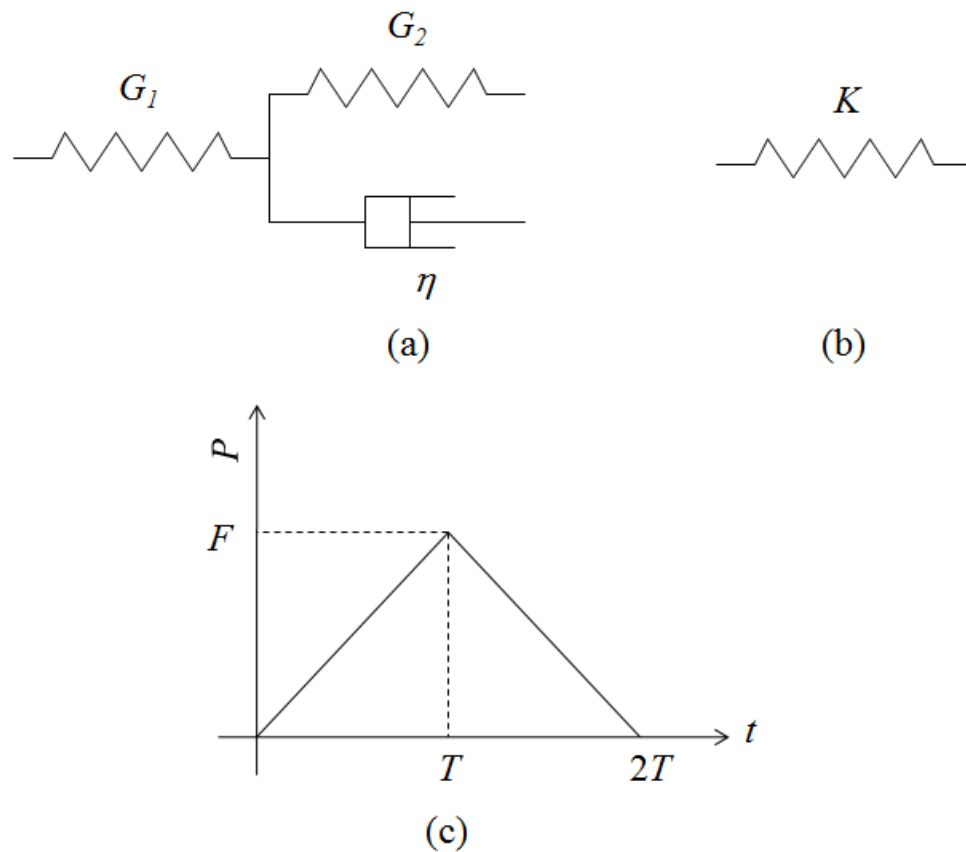


Figure 2.11: Assumed constitutive behavior of the viscoelastic material and the loading function: (a) standard three-element solid model for deviatoric behavior, (b) spring element for spherical (volumetric) behavior, and (c) triangular loading

The deviatoric and spherical components in terms of stress and strain tensors are given by:

$$\begin{aligned}\sigma_{ij}^D &= \sigma_{ij} - \frac{1}{3}\sigma_{kk}\delta_{ij}; & \sigma_{ij}^V &= \frac{1}{3}\sigma_{kk}\delta_{ij} \\ \varepsilon_{ij}^D &= \varepsilon_{ij} - \frac{1}{3}\varepsilon_{kk}\delta_{ij}; & \varepsilon_{ij}^V &= \frac{1}{3}\varepsilon_{kk}\delta_{ij}\end{aligned}\quad (2.28b)$$

where  $\delta_{ij}$  is the Kronecker delta function. In the time ( $t$ ) domain, the constitutive relation for Kelvin-Voigt deviator creep model can be written as (Haddad, 1995):

$$\sigma_{ij}^D + \frac{\eta}{G_1 + G_2} \frac{d\sigma_{ij}^D}{dt} = \frac{G_1 G_2}{G_1 + G_2} 2\varepsilon_{ij}^D + \frac{G_1 \eta}{G_1 + G_2} \frac{d(2\varepsilon_{ij}^D)}{dt} \quad (2.29a)$$

$$\sigma_{ij}^V = 3K\varepsilon_{ij}^V \quad (2.29b)$$

Employing Laplace transforms, the constitutive relations take the following form in the Laplace domain (Haddad, 1995):

$$\sigma_{ij}^D(s) = 2G(s)\varepsilon_{ij}^D(s) \quad (2.30a)$$

$$\sigma_{ij}^V(s) = 3K(s)\varepsilon_{ij}^V(s) \quad (2.30b)$$

where

$$G(s) = \frac{G_1 G_2 + G_1 \eta s}{G_1 + G_2 + \eta s} \quad (2.30c)$$

$$K(s) = K \quad (2.30d)$$

The reduced modulus in Laplace domain can now be written in terms of viscoelastic material properties as follows:

$$\begin{aligned}E_r(s) &= \frac{E(s)}{1 - \nu(s)^2} = \frac{4G(s)\{3K(s) + G(s)\}}{3K(s) + 4G(s)} \\ \Rightarrow E_r(s) &= 4G_1 \frac{(G_2 + s\eta)\{3K(G_1 + G_2 + s\eta) + G_1(G_2 + s\eta)\}}{(G_1 + G_2 + s\eta)\{3K(G_1 + G_2 + s\eta) + 4G_1(G_2 + s\eta)\}}\end{aligned}\quad (2.31)$$

In this example, a loading-unloading history with maximum force  $F$  and time period  $2T$  applied as a triangular ramp as shown in Figure 2.11c is considered. The loading function for this history can be written as:

$$P(t) = \frac{F}{T}t[H(t) - H(t-T)] + \left\{-\frac{F}{T}t + 2F\right\}[H(t-T) - H(t-2T)] \quad (2.32)$$

where  $F$  is the peak load,  $T$  is the time when the peak load is reached and  $H(t)$  is the Heaviside function. Taking the Laplace transform of Eq. (2.32) gives

$$P(s) = \frac{F}{Ts^2} \{1 - 2 \exp(-Ts) + \exp(2Ts)\} \quad (2.33)$$

Substituting  $E_r(s)$  from Eq. (2.31), and  $P(s)$  from Eq. (2.33) into Eq. (2.27), we obtain:

$$h(t) = R_s f_3^{-1} \left[ \frac{1}{R_s^2} \Gamma^{-1} \left( \frac{F \{1 - 2 \exp(-Ts) + \exp(2Ts)\}}{4Ts^2 G_1 (G_2 + s\eta)} \right) \frac{(G_1 + G_2 + s\eta) \{3K(G_1 + G_2 + s\eta) + 4G_1(G_2 + s\eta)\}}{\{3K(G_1 + G_2 + s\eta) + G_1(G_2 + s\eta)\}} \right] \quad (2.34)$$

By determining the inverse Laplace transform in the above expression, the displacement of the indenter can be computed as a function of time. The force-displacement relationship of the indentation problem can then be obtained by combining the loading and displacement history.

In the next section, we will use finite element analysis to investigate the accuracy of the proposed semi-analytical approach.

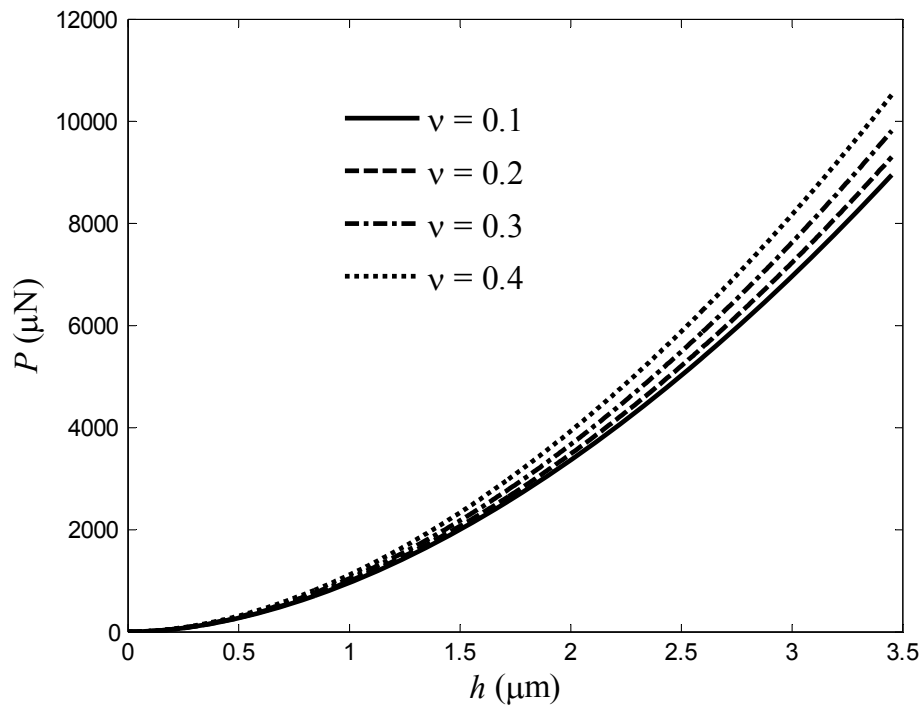
## 2.2.2 Numerical verification

### 2.2.2.1 Elastic indentation

The commercial finite element code ABAQUS (Dassault Systemes, 2009) is used to simulate the elastic indentation of the sphere by a conical indenter. The model

is the same as that used for linear-elastic, perfectly-plastic material (described in Chapter 2, section 1.2) except that visco-elastic material properties were used.

A sphere of radius  $R_s = 23 \mu\text{m}$  and made of a material with Young's modulus,  $E = 1000 \text{ MPa}$  was numerically indented by a conical indenter with half-angle  $\alpha = 70.3^\circ$ . To investigate the validity of the assumption used in section 2.1, the force-displacement relationships are plotted in Figure 2.12a for four selected Poisson's ratios up to a maximum indentation depth of 15% of the radius. Clearly there is significant difference between these curves.



(a)

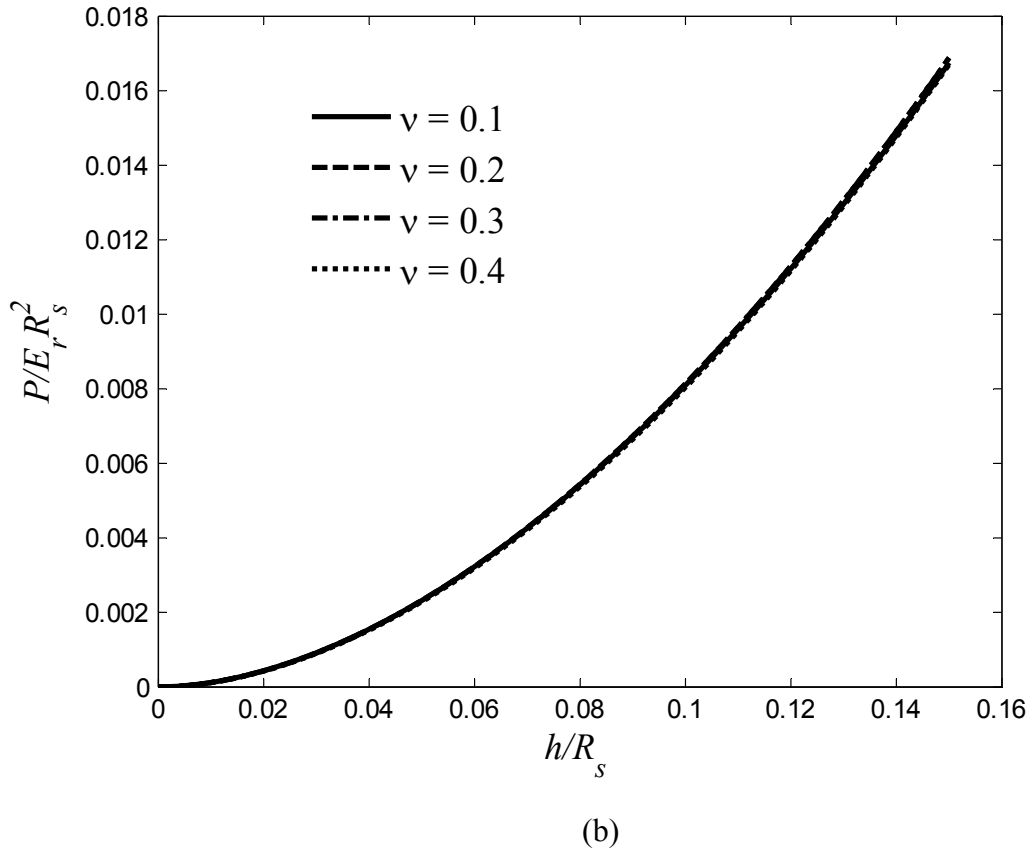


Figure 2.12: The (a) original and (b) normalized force-displacement relationships for the elastic indentation problem, for selected Poisson's ratios as obtained from geometrically nonlinear finite element analysis

The same data is represented in Figure 2.12b, where normalized force,  $P/E_r R_s^2$  is plotted as a function of the normalized indentation depth,  $h/R_s$  as in Eq. (2.25) for four selected Poisson's ratios. Within the resolution of Figure 2.12b, the results obtained for the investigated Poisson's ratios essentially overlap on each other, thus validating the assumption of writing Eq. (2.24) as Eq. (2.25). By curve-fitting, the function  $f_3$  in Eq. (2.25) was determined to be:

$$f_3\left(\frac{h}{R_s}\right) = 4.427\left(\frac{h}{R_s}\right)^4 - 2.079\left(\frac{h}{R_s}\right)^3 + 9.321\text{E-}1\left(\frac{h}{R_s}\right)^2 + 4.686\text{E-}3\left(\frac{h}{R_s}\right) - 1.025\text{E-}5 \quad (2.35)$$

The function  $f_3$  can be inverted and used in Eq. (2.34) to determine the force-displacement relationship of the viscoelastic indentation problem.

As an example, we considered a sphere of radius 23  $\mu\text{m}$  indented by an indenter of half-angle 70.3°. The viscoelastic material properties were taken as  $G_1 = 234.6 \text{ MPa}$ ,  $G_2 = 25.78 \text{ MPa}$ ,  $\eta = 257.78 \text{ Pa-s}$  and  $K = 687.6 \text{ MPa}$  (Dassault Systemes, 2009). For four values of  $T$  ( $T = 1\text{s}$ ,  $T = 10\text{s}$ ,  $T = 20\text{s}$  and  $T = 30\text{s}$ ) with  $F = 1000 \mu\text{N}$ , the force-displacement relationships obtained using the proposed semi-analytical approach are plotted in Figure 2.13. Since  $f_3$  is a fourth order polynomial, Eq. (2.33) resulted in four values of the displacement,  $h$ , (for a given  $t$ , since  $h$  is a function of  $t$ ) and the realistic positive values were selected ignoring the negative and imaginary roots. The curve fitting as well as other computations involved in solving Eq. (2.34) to determine the displacement,  $h$ , were performed using the commercial software MATLAB (MATLAB, 2011).

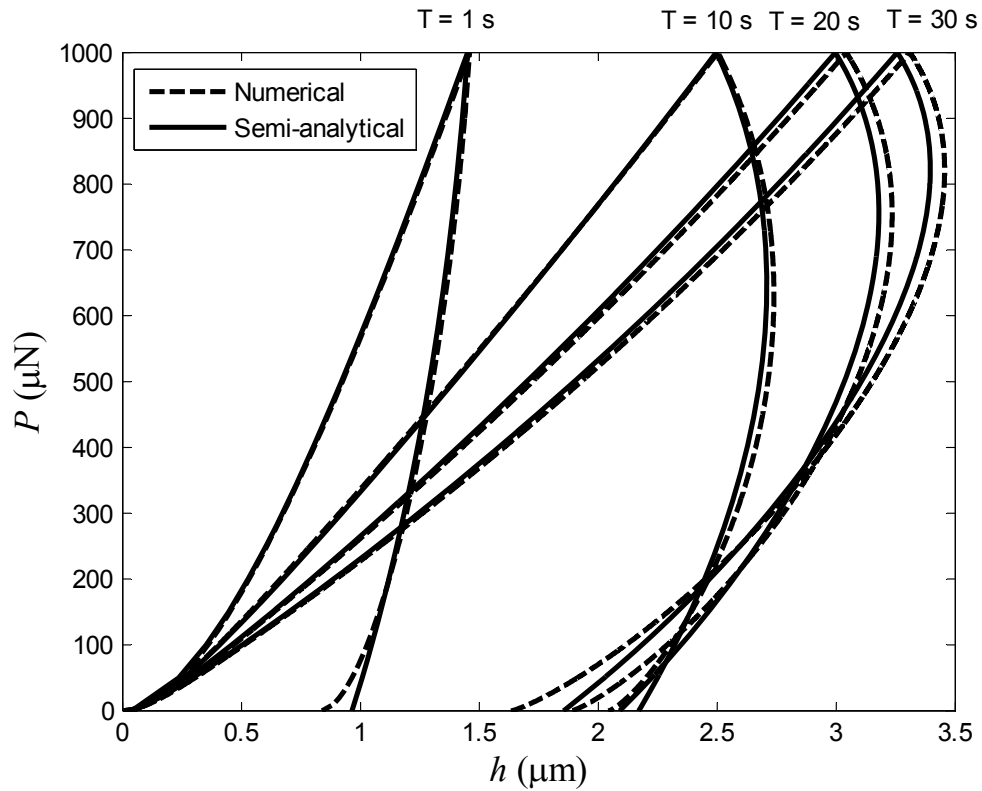


Figure 2.13: Comparison of force-displacement relationships obtained using the proposed semi-analytical approach and ABAQUS for four selected loading times,  $T$ .

### 2.2.2.2 Viscoelastic indentation

To verify the semi-analytical approach, we used finite element analysis (using ABAQUS) to simulate the viscoelastic problem numerically. The finite element model described in section 2.1.2.1 is adopted except that the viscoelastic material properties, in the form of Prony series, are used instead of elastic properties. The force-displacement relationships for the indentation problem with geometry and material properties described in section 2.1.2.1 are plotted in Figure 2.13. Figure 2.13 shows that the semi-analytical approach captures the loading curve quite accurately.

Relatively larger error for  $T = 20\text{s}$  and  $T = 30\text{s}$  can be due to the increase in inaccuracy

of regression used in Eq. (2.35), with increasing depth-to-radius ratio. The semi-analytical approach cannot capture the unloading part accurately, particularly near the end of the unloading curve. This is not surprising since the method of functional equations is valid only when the contact radius is a monotonically increasing function of time (Lee and Radok, 1960), which is not true during most of the unloading period.

There is a significant difference between the computational costs involved in obtaining the force-displacement relationships using the semi-analytical method and the direct finite element simulations. For example, for the case  $T = 30$  s, approximately 5 CPU hours was needed to obtain the force-displacement relationship using finite element simulation, whereas it took less than 1 CPU second for the semi-analytical method (excluding the elastic finite element analysis). Computations were performed in a DELL Precision T7400 workstation with two Intel(R) Xeon(R) X5472 @3GHz processors. Thus, the semi-analytical method is a viable method for obtaining the force-displacement relationships for viscoelastic spheres.

### **2.2.3 Synopsis: indentation of a visco-elastic sphere**

A semi-analytical approach is proposed to obtain the force-displacement relationship for conical indentation of a viscoelastic sphere. The proposed approach is based on “the method of functional equations” which was developed to obtain the viscoelastic solution of a problem from the corresponding elastic solution. The results obtained from the semi-analytical method and finite element simulations are compared for a specific viscoelastic material model and loading history. The results agree well for most of the loading and unloading parts. The proposed approach can easily be applied to other loading histories and viscoelastic material models. Since the computational cost involved in obtaining the force-displacement relationship is much

less for the proposed method compared to finite element simulation, it can be useful for the determination of viscoelastic material properties of spherical particles based on an indentation test.

### **2.3 Summary**

Currently, most of the indentation methodologies have been developed for flat substrates. Further, limited works are available for indentation of visco-elastic substrates. In this chapter, conical indentation of a sphere made of a linear-elastic, perfectly-plastic material and a viscoelastic material have been investigated.

For the sphere made of linear-elastic, perfectly-plastic material, two methodologies are proposed for determining the material properties. The first method is similar to the Oliver-Pharr method for flat substrates and utilizes the concept of elastic unloading. The second method is a finite element based reverse analysis technique. In this method, relationships between two selected shape functions and the material properties are established using finite element simulations for a given indenter shape. This corresponds to the constitutive equations of the system. This constitutive equation can now be used to obtain the material properties of an unknown material from the force-displacement response obtained from indentation testing with the relevant indenter shape. It is shown that both the methods can determine the material properties quite accurately

For the sphere made of viscoelastic material, a semi-analytical method is proposed to obtain the force-displacement relationship. It is shown that the force-displacement relationship obtained using the proposed semi-analytical method agrees well with the one obtained from a finite element simulation. Further, the

computational cost involved in using the semi-analytical method is much lower compared to the finite element simulation.

### Chapter 3

#### **A GENERAL METHODOLOGY TO IDENTIFY MATERIAL PARAMETERS WITH IDENTICAL FORCE-DISPLACEMENT RELATIONSHIP**

In chapter 2, conical indentation of a sphere made of i) isotropic, linear-elastic, perfectly-plastic and ii) viscoelastic materials were considered. Only two material properties are involved for linear-elastic, perfectly-plastic material (excluding Poisson's ratio). Therefore, it was possible to determine the material properties by single indentation technique. However, when hardening is considered (Chapter 1, section 1.5), it is not possible to determine the material properties using a single indentation technique, because only two of the five shape functions are independent and a linear-elastic with plastic hardening is described by three material parameters. An interesting phenomenon that evolves due to this is that more than one set of three material parameters can describe a single force-displacement relationship.

Several researchers have attempted to systematically identify the material parameters resulting in identical force-displacement relationships and a brief review was presented in Chapter 1, section 1.5. To summarize, the developed methodologies are limited to specific indenter/substrate geometries and material models. In this chapter, we attempted to develop a general and comprehensive methodology for identifying such material parameters. The methodology will be applied to identify material parameters with identical force-displacement relationship for a wide variety of material models such as i) isotropic, linear-elastic, power-law strain hardening plastic material; ii) isotropic, linear-elastic, linear strain hardening plastic material;

and iii) transversely isotropic, linear-elastic, perfectly plastic material (see Chapter 1, section 1.2 for descriptions of these material models). These material properties are studied for selected geometries such as i) conical indentation of a half-space; ii) spherical indentation of a half-space; iii) conical indentation on a sphere; and iv) spherical indentation on a sphere.

Single indentation test (described in section 1.4, Chapter 1) and the use of the corresponding shape functions can provide easy way to determine the material properties of a substrate material. However, as discussed in section 1.5, Chapter 1, several researchers have shown that for conical indentation of a half-space made of isotropic, power-law hardening materials, more than one material parameter can correspond to a single force-displacement relationship. Thus relatively complex dual indentation is necessary to determine the material properties uniquely. The study presented in this chapter will reveal whether single indentation test is sufficient for other commonly used indenter/substrate geometries and material types, or dual indentation is necessary. Further, this study is helpful in determining a range of the material properties of the substrate material from a single indentation test and gaining insight into the material parameter sets that result in identical force-displacement relationship. The content of this chapter is based on our work reported in Phadikar et al, 2013d.

### **3.1 Methodology**

In this section, the outline of the general methodology will be described. The methodology is based on comparing selected shape functions of the force-displacement relationships for two sets of material parameters.

Schematics of three non-identical loading curves (of possible force–displacement relationships) with various identical shape functions are considered in Figure 3.1: identical values of loading energy,  $W_t$ , but different values of maximum load,  $P_m$  (Figure 3.1a); identical values of  $W_t$  and  $P_m$  (Figure 3.1b); and identical values of  $P_m$ ,  $W_t^1$  and  $W_t^2$  (Figure 3.1c). For Figure 3.1c,  $W_t^1$  is the area under the loading curve between  $h = 0$  to  $h = h_m/2$  (that is,  $W_t^1 = \int_0^{h_m/2} P_l(h)dh$ , subscript  $l$  denotes the loading curve) whereas  $W_t^2$  is the area under the loading curve between  $h = h_m/2$  and  $h = h_m$  ( $W_t^2 = \int_{h_m/2}^{h_m} P_l(h)dh$ ). Similarly, corresponding to the unloading curve, we can define  $W_e^1 = \int_{h_f}^{(h_f+h_m)/2} P_u(h)dh$  and  $W_e^2 = \int_{(h_f+h_m)/2}^{h_m} P_u(h)dh$ , where subscript  $u$  indicates the unloading curve. To the author’s knowledge, loading curves with an inflexion point similar to the loading curve of Figure 3.1b have never been obtained from any indentation testing (both real experiment and simulation). Thus, we make the assumption that if the loading curves of two materials have identical values of  $W_t$  and  $P_m$ , they will have identical loading curves. The validity of this assumption will be illustrated through selected examples in later sections. Furthermore, existence of loading curves similar to the loading curve of Figure 3.1c with three inflexion points is questionable intuitively and has never been obtained from an indentation test to our knowledge. Thus, a stronger assumption would be that, if two materials have identical values of  $P_m$ ,  $W_t^1$ , and  $W_t^2$ , they have identical loading curves.

An approach similar to the loading curves can be constructed to identify materials with identical unloading curves, since to the author’s knowledge, unloading curves with inflexion point(s) (similar to Figures 3.1b and 3.1c for loading curves) have not been obtained from any indentation testing. In this case, similar to the

loading curve, the area under the unloading curves (physically the elastic energy),  $W_e$  or the areas under two segments of unloading curves,  $W_e^1$  and  $W_e^2$  need to be compared. Thus, similar to the previous paragraph, we make the assumption that if unloading curves corresponding to two sets of material parameters have identical values of  $P_m$  and  $W_e$ , they will have identical unloading curves. Similarly, a stronger assumption will be that if two sets of material parameters correspond to identical values of  $P_m$ ,  $W_e^1$ , and  $W_e^2$ , they have identical unloading curves. It follows that, a set of shape functions such as  $W_e$ ,  $(P_m, W_e)$  and  $(P_m, W_e^1, W_e^2)$  can be compared to determine material parameters with identical unloading curves. Thus, material parameters resulting in identical force-displacement relationships can be searched for by iterating over the material range and comparing either of the sets of shape functions such as  $(W_t, W_e)$ ,  $(W_t, P_m, W_e)$  and  $(W_t^1, W_t^2, P_m, W_e^1, W_e^2)$ . The computational cost involved in the search procedure and the complexity of regression analysis are lowest for the set  $(W_t, W_e)$ , and highest for the set  $(W_t^1, W_t^2, P_m, W_e^1, W_e^2)$  since they are proportional to the number of shape functions included. Since the assumptions listed above do not involve specific material model or geometry, these are applicable for any shape of the indenter/substrate and the material model. Note that, the method identifies material parameters that will lead to identical force-displacement relationship but there may not be any real material in existence corresponding to such material parameters.

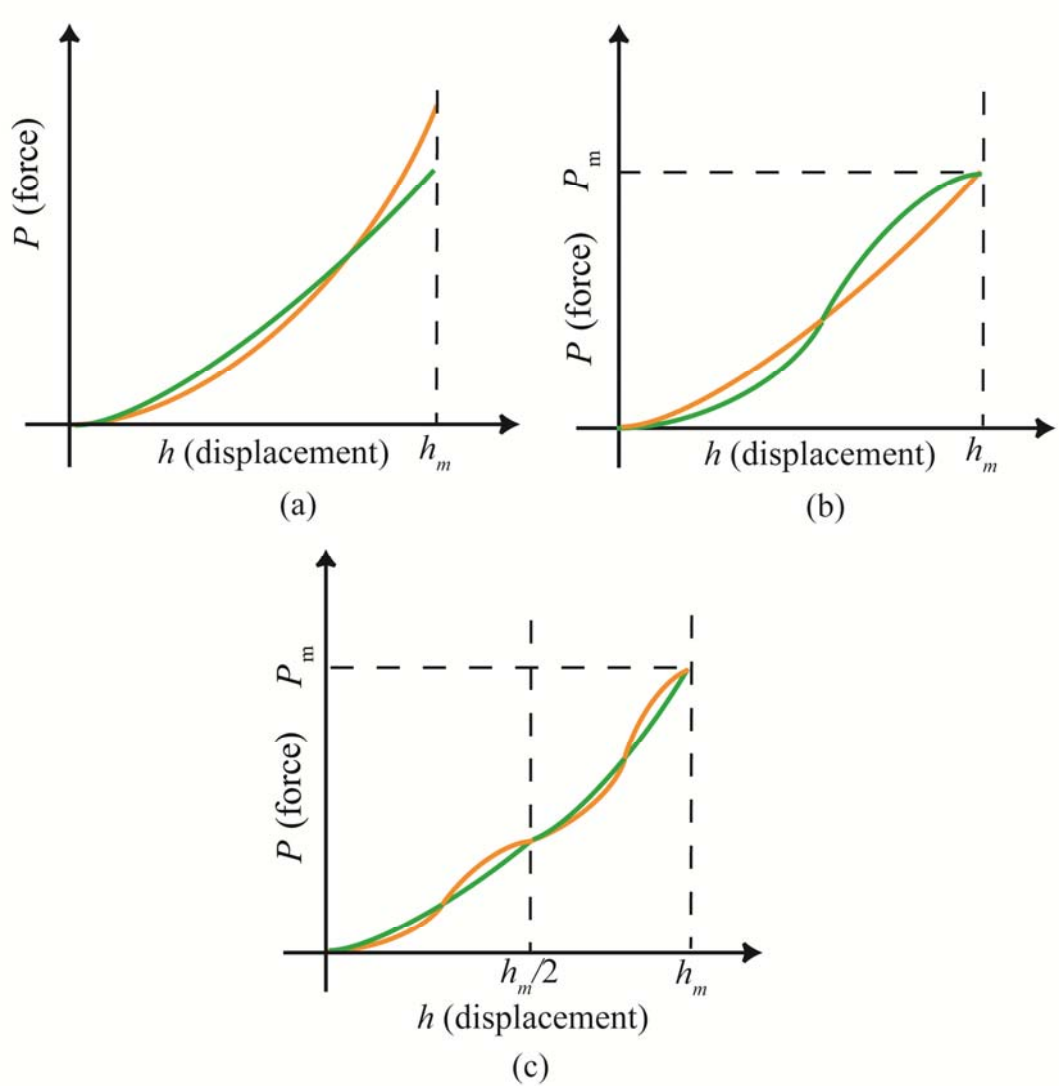


Figure 3.1: Schematics of three sets of loading curves with (a) identical  $W_t$  but different  $P_m$ , (b) identical  $W_t$  and  $P_m$ , and (c) identical  $P_m$ ,  $W_t^1$  and  $W_t^2$

### 3.2 Iso-lines and Surfaces

In this section we proceed to quantify the discussion in section 3.1. When the set  $(W_t, W_e)$  is compared for obtaining material parameters leading to identical force-displacement relationships, an existence map of the corresponding materials in the

material space can be constructed. The procedures will be explained in this section for four selected material models.

### 3.2.1 Isotropic, linear-elastic, strain hardening plastic materials

The isotropic, linear-elastic, strain hardening material models with two kinds of hardening, namely linear and power-law hardening are described in Chapter 1, section 1.2. Such materials can be characterized by three parameters, namely, elastic modulus,  $E$ , yield strength,  $Y$ , and hardening modulus,  $E_p$ , (for linear hardening) or hardening exponent,  $n$  (for power-law hardening).

The conditions for two materials (of same material model) having identical  $W_t$  and  $W_e$  are equivalent to the following conditions (two materials are denoted by subscripts 1 and 2):

$$(W_t)_1 = (W_t)_2 \quad (3.1a)$$

$$(W_t / W_e)_1 = (W_t / W_e)_2 \quad (3.1b)$$

The relationships between the normalized shape functions and material properties are described in Chapter 1, section 1.4. From Eq. (1.11b), the relationship for the total energy,  $W_t$  becomes:

$$\frac{W_t}{Yh_m^3} = \bar{G}_1 \left( \frac{E}{Y}, \bar{\xi} \right); \quad \bar{\xi} = \begin{cases} n & \text{for power-law hardening} \\ E_p/E & \text{for linear hardening} \end{cases} \quad (3.2a)$$

$$\text{or } W_t = Yh_m^3 \bar{G}_1 \left( \frac{E}{Y}, \bar{\xi} \right) \quad (3.2b)$$

Using Eq. (3.2b), the first condition, Eq. (3.1a) can be written as:

$$Y_1 h_m^3 \bar{G}_1 \left( \frac{E_1}{Y_1}, \bar{\xi}_1 \right) = Y_2 h_m^3 \bar{G}_1 \left( \frac{E_2}{Y_2}, \bar{\xi}_2 \right) \quad (3.3)$$

which gives the ratio of their yield strengths as follows:

$$r = \frac{Y_1}{Y_2} = \bar{G}_1 \left( \left( \frac{E}{Y} \right)_2, \bar{\xi}_2 \right) / \bar{G}_1 \left( \left( \frac{E}{Y} \right)_1, \bar{\xi}_1 \right) \quad (3.4)$$

Similar to Eq. (3.2a), the non-dimensional equation for elastic energy,  $W_e$ , can be written as:

$$\frac{W_e}{Yh_m^3} = \bar{G}_4 \left( \frac{E}{Y}, \bar{\xi} \right) \quad (3.5)$$

Combining Eqs. (3.2a) and (3.5), we obtain

$$\frac{W_t}{W_e} = \bar{G}_8 \left( \frac{E}{Y}, \bar{\xi} \right) \quad (3.6)$$

Using Eq. (3.6), the second condition, Eq. (3.1b) can be rewritten as:

$$\bar{G}_8 \left( \left( \frac{E}{Y} \right)_1, \bar{\xi}_1 \right) = \bar{G}_8 \left( \left( \frac{E}{Y} \right)_2, \bar{\xi}_2 \right) \quad (3.7)$$

The functions  $\bar{G}_1$ ,  $\bar{G}_2$  and  $\bar{G}_8$  can be determined via extensive finite element analysis.

Using the functional form of Eq. (3.6), the quantity  $W_t/W_e$  can be plotted as a surface in the  $E/Y - \bar{\xi}$  space and the corresponding iso- $(W_t/W_e)$  lines can be extracted. A schematic of a typical iso- $(W_t/W_e)$  line is shown in Figure 3.2. Since all the materials lying on a particular iso- $(W_t/W_e)$  line have identical value of  $W_t/W_e$ , it follows that any two materials selected from a particular iso- $(W_t/W_e)$  line will satisfy the second condition for identical force-displacement relationship, Eq. (3.1b) (or Eq. (3.7)). From such an iso-line, pairs of material parameter sets that will lead to identical force-displacement relationship can be found in the following steps (see Figure 3.2):

**Step 1:** Select any two points on a particular iso- $(W_t/W_e)$  line (as illustrated in Figure 3.2). This will give two sets of  $(E/Y)$  and  $\bar{\xi}$  that satisfy the second condition of identical force-displacement relationship, Eq. 3.7 (or Eq. (3.1b)).

**Step 2:** Determine the ratio  $r = Y_1/Y_2$  from Eq. (3.4) using the values of  $(E/Y)_1$ ,  $\bar{\xi}_1$ ,  $(E/Y)_2$  and  $\bar{\xi}_2$  obtained in Step 1. Since Eq. (3.4) is derived from Eq. (3.1a), the parameter sets now satisfy the first condition (Eq. 3.1a) as well.

**Step 3:** Assume any value of  $Y_2$  and determine  $Y_1$  using  $Y_1 = rY_2$ , from Step 2.

**Step 4:** Using  $Y_1$  and  $Y_2$  (obtained in Step 2), and  $(E/Y)_1$  and  $(E/Y)_2$  (obtained in Step 1), determine  $E_1$  and  $E_2$ .

**Step 5:** For power-law hardening materials, the strain hardening exponents can be obtained directly using  $n_1 = \bar{\xi}_1$ ,  $n_2 = \bar{\xi}_2$ . For linear hardening materials, the hardening moduli can be obtained using the relations,  $(E_p)_1 = E_1\bar{\xi}_1$ ,  $(E_p)_2 = E_2\bar{\xi}_2$ .

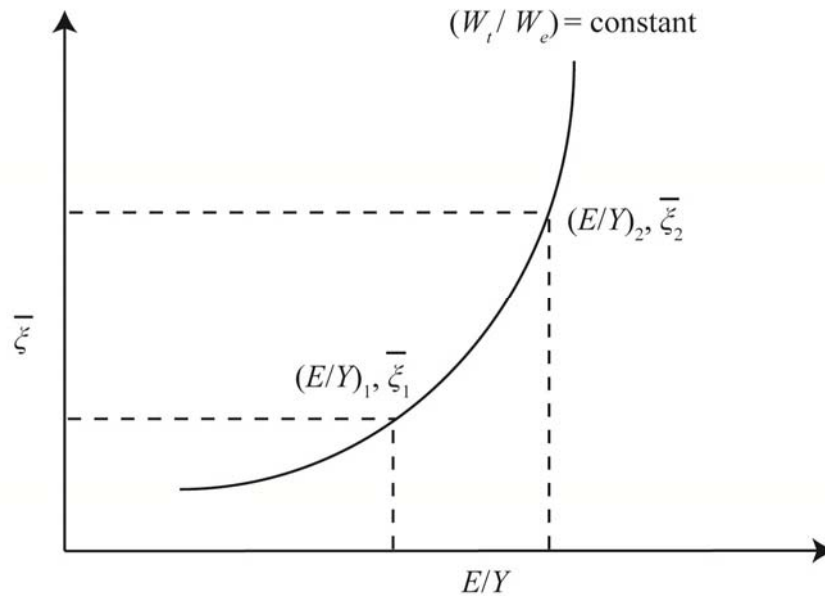


Figure 3.2: Schematic of a iso- $(W_t/W_e)$  line in  $E/Y - \bar{\xi}$  space

Since  $Y_2$  is selected arbitrarily, there exist infinite sets of material parameters that lead to identical force-displacement relationship, corresponding to any two points of a iso- $(W_t/W_e)$  line. Thus, it can be said that all materials lying on a particular iso- $(W_t/W_e)$  line will have identical force-displacement relationships with the constraint of Eq. (3.4).

The methodology is derived for conical indentation of a half-space. However, it can be easily shown that the method is applicable to other geometries such as spherical indentation of a half-space, conical indentation of a sphere and spherical indentation of a sphere.

### 3.2.2 Transversely isotropic, linear-elastic, perfectly plastic material

For transversely isotropic, linear-elastic, perfectly-plastic material, the relationships between the normalized energies,  $W_t$  and  $W_e$ , and the material properties can be written as follows (see Chapter 1, section 1.4):

$$\frac{W_t}{E_x h_m^3} = \bar{G}_1^{tp} \left( \frac{E_x}{E_z}, \frac{E_z}{G_{xz}}, \frac{E_z}{Y} \right) \quad (3.8)$$

$$\frac{W_e}{E_x h_m^3} = \bar{G}_4^{tp} \left( \frac{E_x}{E_z}, \frac{E_z}{G_{xz}}, \frac{E_z}{Y} \right) \quad (3.9)$$

$$\frac{W_t}{W_e} = \bar{G}_8^{tp} \left( \frac{E_x}{E_z}, \frac{E_z}{G_{xz}}, \frac{E_z}{Y} \right) \quad (3.10)$$

where subscript  $tp$  indicates transversely isotropic, elastic, perfectly-plastic material.

In this case, material parameters leading to identical force-displacement relationships can be obtained from iso- $(W_t/W_e)$  surfaces in three dimensional  $E_x/E_z$ - $E_z/G_{xz}$ - $E_z/Y$  space similar to the previous sections. This will be illustrated in a later section (section 3.4.3).

### 3.3 Functional Forms from Finite Element Analysis

In Eqs. (1.14)-(1.16), the relationships between normalized shape functions and material properties are described. To implement the methodology described in the above sections, functional forms of  $\bar{G}_i^{ph}$ ,  $\bar{G}_i^{lh}$  and  $\bar{G}_i^{lp}$  ( $i = 1-5$ ) used in those equations need to be found. The functional forms will be required in the later chapters of this thesis as well. The functional forms can be obtained by conducting virtual indentation testing via finite element simulations similar to Chapter 2, section 2.1.2.1.

Finite element simulations were performed using the commercial finite element program ABAQUS (Dassault Systemes, 2009). The half-space was modeled by a two-dimensional axisymmetric model with boundary conditions similar to the sphere in section 2.1.2.1. The model shown in Figure 3.3 was selected after a convergence study. For the spherical substrate, the model described in Chapter 2, section 2.1.2.1 is adopted. The conical or spherical indenters were modeled as two dimensional axisymmetric rigid bodies using the “analytical rigid” option in ABAQUS. Coulomb’s friction law with friction coefficient 0.15 (Bowden and Tabor, 2001) is used to model friction between the surfaces.

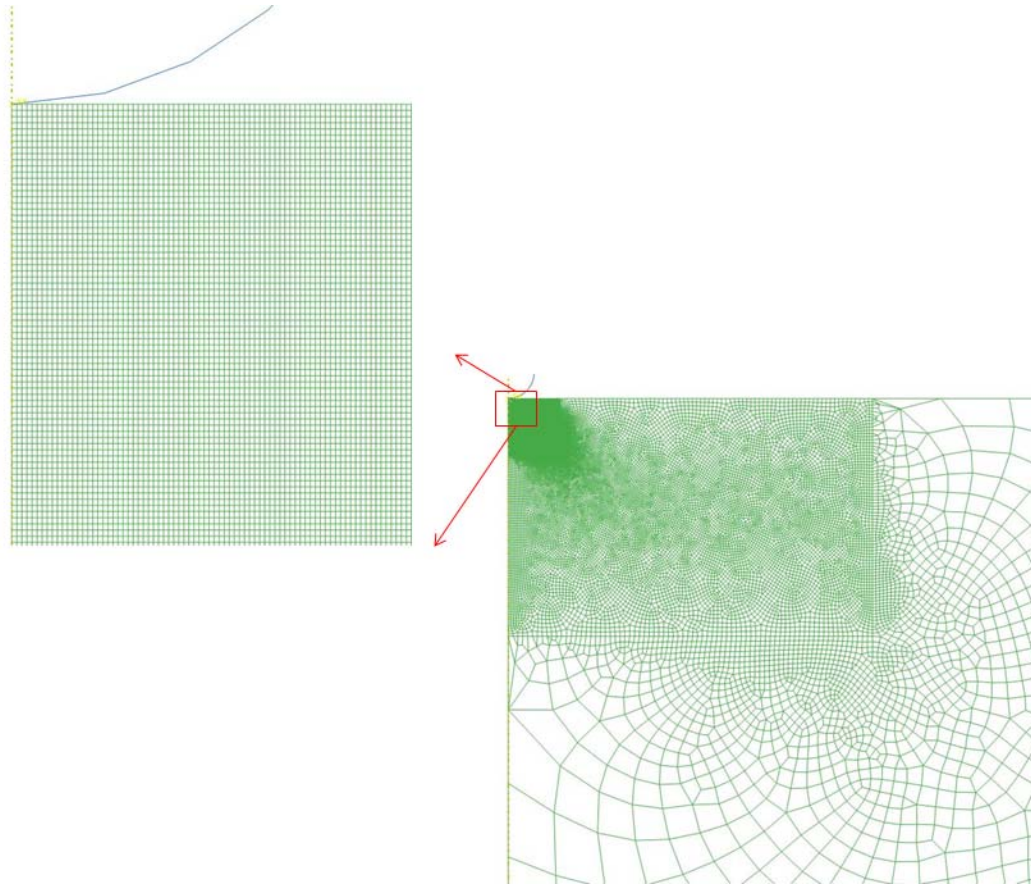


Figure 3.3: Finite element model of a half-space being indented by a spherical indenter

To develop the functional forms, finite element simulations for a range of materials were conducted to extract the shape functions. For isotropic materials, a material set with elastic modulus  $80 \leq E$  (GPa)  $\leq 300$  and yield stress  $0.1 \leq Y$  (GPa)  $\leq 2.0$  was chosen to cover a wide range of  $E/Y$  ratios ( $80 \leq E/Y \leq 1000$ ). For power-law hardening materials, the strain hardening exponent was taken to be  $0.0 \leq n \leq 0.5$ , which is common for metals (Chen et al., 2007). Similarly, for linear hardening materials, the range of  $E_p$  was taken such that  $0.0 \leq E_p/E \leq 0.5$ . Poisson's ratio was taken to be constant at 0.3. As previously noted, Poisson's ratio has only a minor

effect on the force-displacement response. For power law hardening materials (indicated by the subscript  $p$  in the fitting coefficients,  $C_p^{jk}$ ), the following form is used:

$$\Psi_i = \bar{G}_i^{ph} \left( \frac{E}{Y}, n \right) = \sum_{j=0}^{j_u} \sum_{k=0}^{k_u} C_p^{jk} \left( \frac{E}{Y} \right)^{5-j} n^{5-k}; \quad i = 1-5 \quad (3.11)$$

where  $j_u$  and  $k_u$  are the upper limits of  $j$  and  $k$ , respectively which is different for different geometries. The fitting coefficients, are tabulated in Tables A.1-44 for various indentation geometries and shape functions in Appendix A, section A.1. Similarly for linear hardening materials (indicated by the subscript  $l$  in the fitting coefficients,  $C_l^{jk}$ ), the following form is used:

$$\Psi_i = \bar{G}_i^{lh} \left( \frac{E}{Y}, n \right) = \sum_{j=0}^4 \sum_{k=0}^4 C_l^{jk} \left( \frac{E}{Y} \right)^{5-j} n^{5-k}; \quad i = 1-5 \quad (3.12)$$

The fitting coefficients, are tabulated in Tables A.45-48 for various indentation geometries and shape functions in Appendix A, section A.2.

For transversely isotropic material, the following range of material properties was chosen (Vinson, 1999; Bower, 2009):  $5 \leq E_x/E_y \leq 45$ ,  $1.5 \leq E_y/G_{xy} \leq 4$ ,  $45 \leq E_y/Y \leq 290$ . Poisson's ratios were taken to be constant:  $\nu_{xy} = 0.2$ ,  $\nu_{zx} = 0.05$ . As previously noted, Poisson's ratios are assumed to be constant for simplicity. Considering Eq. (1.13), the normalized shape functions of the left hand side were expressed as functions of  $E_z/E_x$ ,  $E_x/G_{xz}$  and  $E_x/Y$  for fixed values of  $\alpha$  (for conical indentation) or  $h_m/R$  (for spherical indentation). First, the normalized shape functions were used to attempt to fit with  $E_x/G_{xz}$  and  $E_x/Y$  for selected fixed values of  $E_z/E_x$ . Altogether 169 surface equations (taken from [www.zunzun.com](http://www.zunzun.com)) were tried for this purpose. For each surface, the values of the normalized shape function were computed at all data points

and the percentage differences between the computed and the original values were determined. Surfaces with maximum deviations more than 2.5% were rejected. For each selected surface, the coefficients of the fitted surface were then used to attempt to fit with  $E_z/E_x$ . A surface was rejected if all of the coefficients could not be fit with coefficient of determination,  $R^2 > 0.95$ . If none of the surface equations could be selected in the above manner, attempts were made by keeping  $E_x/G_{xz}$  or  $E_x/Y$  constant, instead. The outline is depicted comprehensively in Figure 3.4. Finally, seven surface equations (Table A.49) were found to be sufficient for fitting all the normalized shape functions with material properties (including results presented in other chapters). For conical and spherical indentation, the surface equations used for fitting the normalized shape functions are tabulated in Table A.51. The corresponding fitting coefficients are presented in Tables A.53-A.88. Some more details regarding the fitting procedure are presented in Appendix A, section A.3.

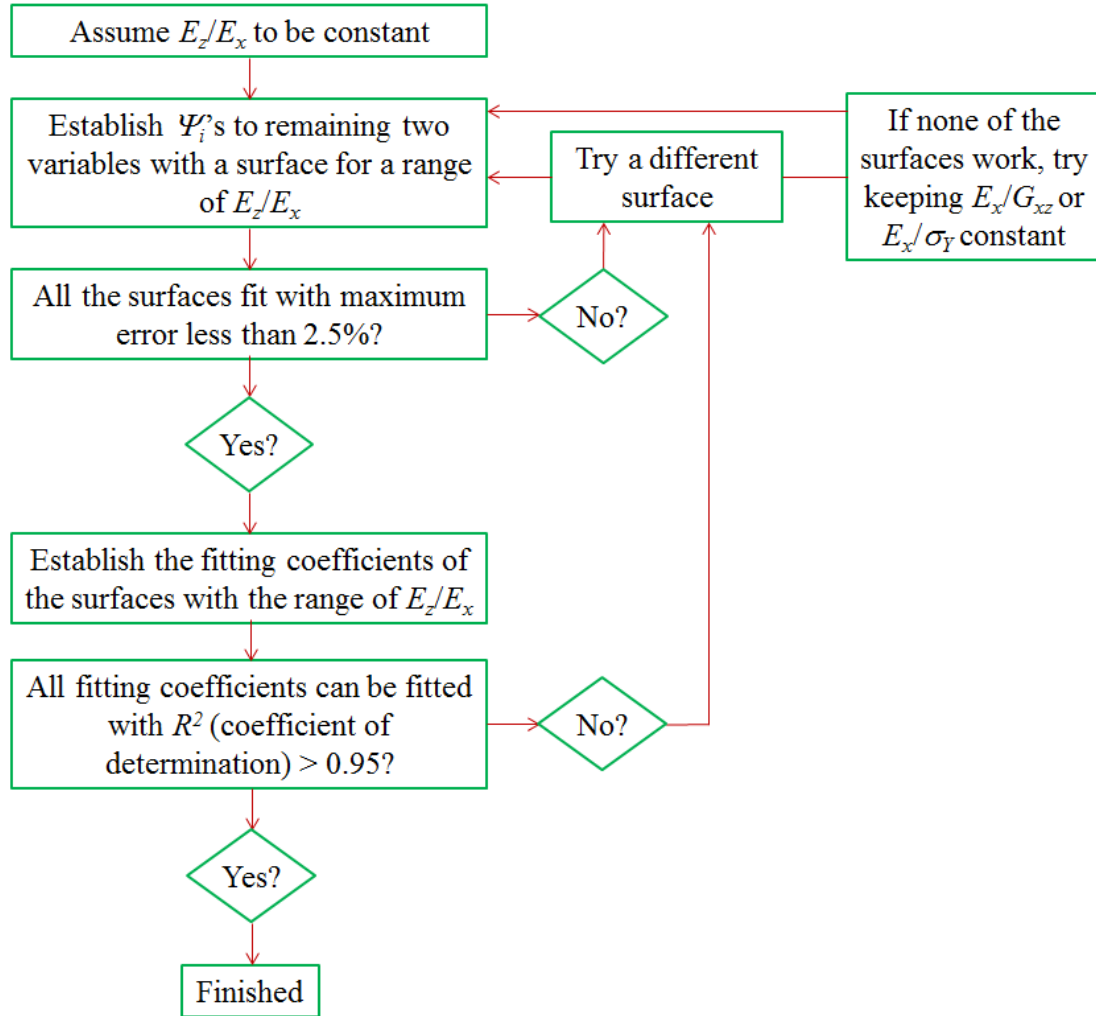


Figure 3.4: Schematic of the regression analysis used for expressing the normalized shape functions as functions of material properties for transversely isotropic materials (Eqs. (1.13))

### 3.4 Results

The proposed methodologies are applied to selected indenter/substrate geometries and material models to investigate the viability of the methodologies for identifying material parameters leading to identical force-displacement relationship. This will be presented next.

### 3.4.1 Isotropic, linear-elastic, power-law strain hardening plastic material

To illustrate the proposed methodology for an isotropic, linear-elastic, power-law strain hardening material model, finite element simulations of a half-space and a sphere (radius 23  $\mu\text{m}$ ) indented by a conical indenter with half-angle  $70.3^\circ$  are conducted. For indentation of a half-space, selected iso- $(W_t/W_e)$  lines extracted using the procedures outlined in section 3.1, are plotted in Figure 3.5. Five materials parameters with identical values of  $W_t$  and  $W_e$  are extracted for each case, and the force-displacement and stress-strain relationships of these materials are plotted in Figure 3.6 and 3.7, respectively. Figure 3.6 shows that the force-displacement relationships overlap. The material parameters are tabulated in Table 3.1. As discussed in Chapter 1, section 1.5, various authors (Cheng and Cheng, 1999; Tho et al., 2004; Alkorta et al., 2005) have shown that only two shape functions out of five are independent for conical indentation of a half-space composed of a isotropic, linear-elastic, power-law strain hardening plastic material. In the proposed methodology, the two independent shape functions are  $W_t$  and  $W_e$ . Thus, as expected, material parameters with identical  $W_t$  and  $W_e$  result in identical force-displacement relationships.

The material parameters leading to identical force-displacement relationship can be seen to have different values of elastic modulus (Table 3.1). Since the elastic modulus of the substrate material can be determined from Oliver-Pharr method, in this section, we will investigate if the range of the material parameters leading to identical force-displacement relationship becomes smaller, when the elastic modulus is kept constant. The force-displacement relationships in Figure 3.6 do not overlap completely and there are some small numerical differences among them. The difference between the total and elastic energy for material # 1 and material # 5 (denoted by superscript 1

and 5 respectively) for conical indentation of half-space was computed to be

$$\sqrt{\left[\frac{W_t^1 - W_t^5}{W_t^1}\right]^2 + \left[\frac{W_e^1 - W_e^5}{W_e^1}\right]^2} = 0.08\% .$$

Next a set of material parameters (material # 6) was searched in the range of  $350 < Y \text{ (MPa)} < 550$  and  $0.2 < n < 0.4$  by keeping the elastic modulus same as material # 1 ( $E = 300 \text{ GPa}$ ) that will lead to minimum deviation in the total and elastic energy,

$$\sqrt{\left[\frac{W_t^1 - W_t^6}{W_t^1}\right]^2 + \left[\frac{W_e^1 - W_e^6}{W_e^1}\right]^2} .$$

The set with  $Y = 549 \text{ MPa}$  and  $n = 0.304$  was found to lead minimum deviation of 2.88%. Since this amount of deviation is larger than for material # 5, it is concluded that the degree of non-uniqueness decreases as elastic modulus is kept fixed. Thus, when the elastic modulus of a material is known, the range of the possible values of its yield strength and strain hardening exponent that can be obtained from a single indentation test becomes smaller.

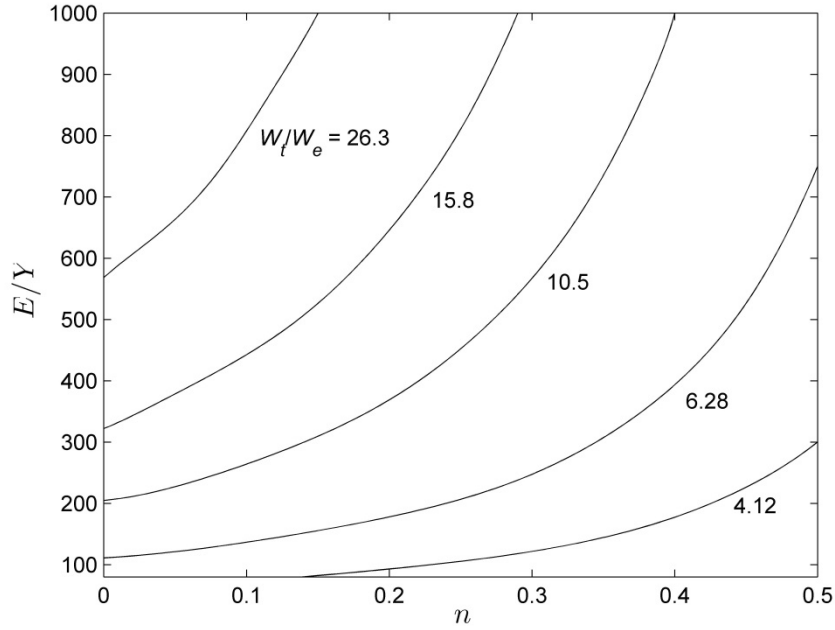
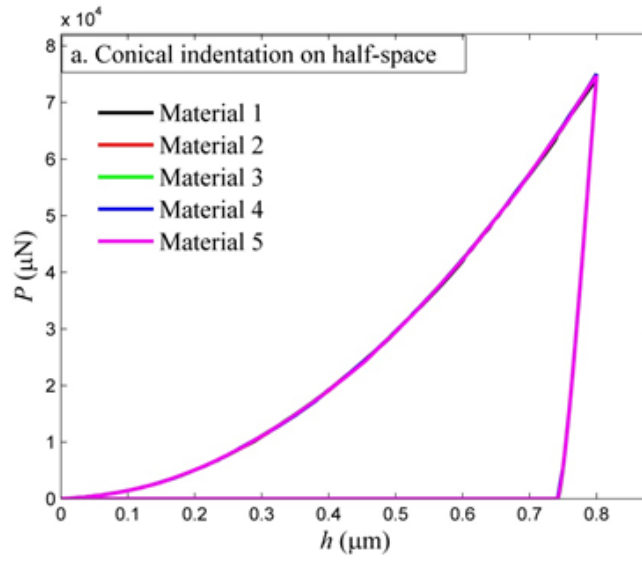


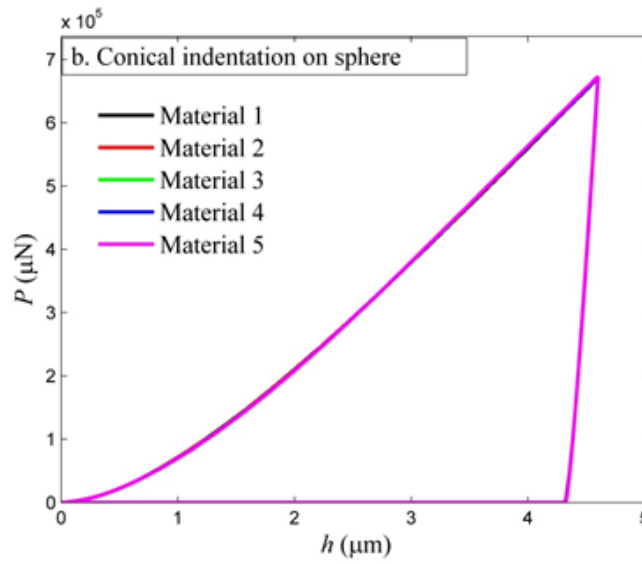
Figure 3.5: Few iso- $(W_t/W_e)$  lines for conical indentation of a half-space with  $\alpha = 70.3^\circ$

Table 3.1: Material parameter sets that lead to identical  $W_t$  and  $W_e$  for conical ( $\alpha = 70.3^\circ$ ) indentation of a half-space and a sphere (radius  $23 \mu\text{m}$ ) modeled by linear-elastic, power law hardening plastic material model. Force displacement relationships are shown in Figure 3.6.

Material #	Half-space			Sphere		
	$E$ (GPa)	$Y$ (MPa)	$n$	$E$ (GPa)	$Y$ (MPa)	$n$
1	300.00	1000.0	0.14030	300.00	1000.0	0.16474
2	308.93	772.31	0.22066	310.59	776.49	0.23622
3	315.68	631.37	0.27271	316.68	633.37	0.28580
4	319.63	532.71	0.31149	322.72	537.87	0.32084
5	322.73	461.04	0.34110	328.81	469.73	0.34714

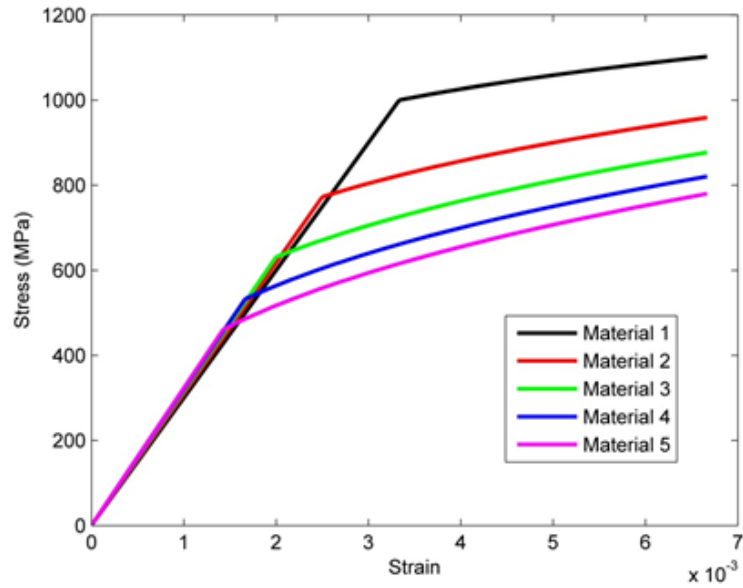


(a)

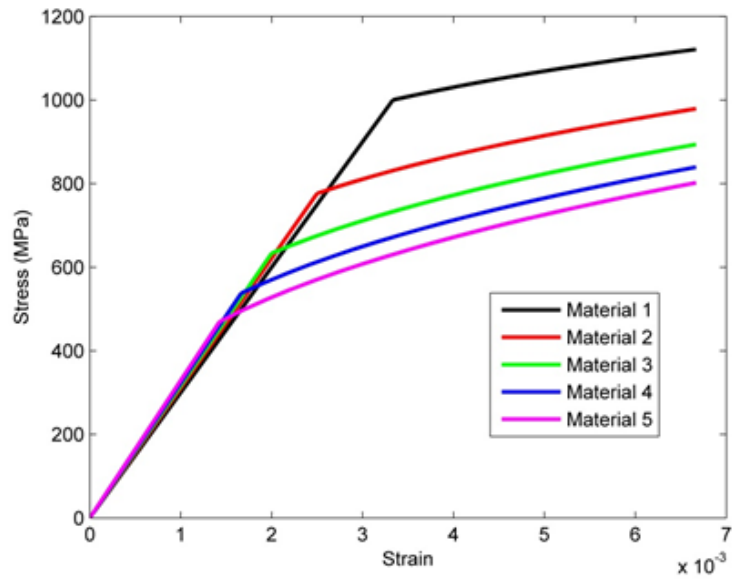


(b)

Figure 3.6: Force-displacement relationships corresponding to five material parameter sets that lead to identical  $W_i$  and  $W_e$  for conical ( $\alpha = 70.3^\circ$ ) indentation of (a) a half-space and (b) a sphere (radius  $23 \mu\text{m}$ ) modeled by linear-elastic, power law hardening plastic material model. The curves overlap within the resolution of the figure.



(a)



(b)

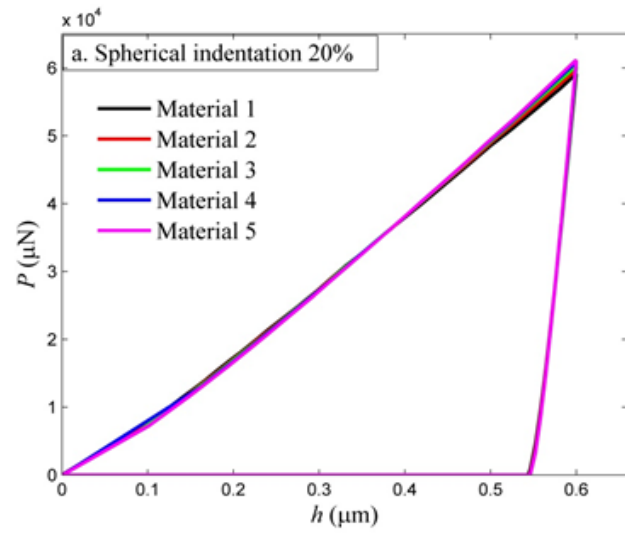
Figure 3.7: Stress-strain relationships corresponding to five material parameter sets that lead to identical  $W_i$  and  $W_e$  for conical ( $\alpha = 70.3^\circ$ ) indentation of (a) a half-space and (b) a sphere (radius  $23 \mu\text{m}$ ) modeled by linear-elastic, power law hardening plastic material model.

For spherical indentation of a half-space, a spherical indenter of radius  $3 \mu\text{m}$  is considered and finite element simulations of indentations with depth-to-radius ratios of 20% and 100% respectively, are conducted. Iso- $(W_t/W_e)$  lines are constructed and material parameters leading to identical values of  $W_t$  and  $W_e$  are extracted from a iso-line using the procedures outlined in section 3.1. The material parameters are tabulated in Table 3.2 and the force-displacement relationships are shown in Figure 3.8.

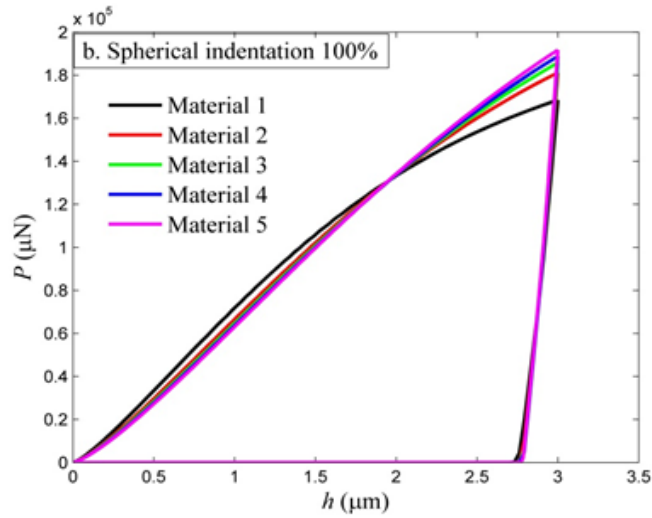
Although the unloading curves overlap, the loading curves do not completely overlap. This scenario for loading curves was predicted in section 3.1 and schematically shown in Figure 3.1a. The difference in loading curves is more prevalent for the larger indentation depth. Interestingly, for both 20% and 100% depth-to-radius ratios the loading curves have a common intersection point.

Table 3.2: Material parameter sets that lead to identical  $W_t$  and  $W_e$  for spherical (radius  $3 \mu\text{m}$ ) indentation of a half-space modeled by linear-elastic, power law hardening plastic material model with depth-to-radius ratio of 20% and 100%. Force displacement relationships are shown in Figure 3.8

Material #	Depth-to-radius ratio: 20%			Depth-to-radius ratio: 100%		
	$E$ (GPa)	$Y$ (MPa)	$n$	$E$ (GPa)	$Y$ (MPa)	$n$
1	300.00	1000.0	0.18131	100.00	1000.0	0.18636
2	314.70	786.74	0.24466	116.78	389.25	0.37741
3	324.25	648.50	0.28894	124.18	248.35	0.43796
4	330.52	550.87	0.32223	128.43	183.47	0.47271
5	335.79	479.70	0.34781	129.45	143.84	0.50000



(a)



(b)

Figure 3.8: Force-displacement relationships corresponding to five material sets that lead to identical  $W_i$  and  $W_e$  for spherical (radius  $3 \mu\text{m}$ ) indentation of a half-space modeled by linear-elastic, power law hardening plastic material model with depth-to-radius ratio of (a) 20% and (b) 100%. The curves do not overlap completely. The difference in force-displacement relationships is clearer for depth-to-radius ratio of 100% than of 20%.

For the depth-to-radius ratio of 100%, material parameters leading to identical  $W_t$ ,  $W_e$  and  $P_m$  are then searched for, following the methodology outlined in section 3.1. A reliable method similar to iso- $(W_t/W_e)$  lines could not be obtained for the three shape functions involved and thus a general searching procedure is used. To this end, a base material parameter set is first selected and material parameter sets leading to the shape functions set  $(W_t, P_m$  and  $W_e)$  identical to that of the base material parameter set are identified, in a region around the base material parameter set. The base material parameter set is selected as having elastic modulus,  $E = 180$  GPa, yield strength,  $Y = 1200$  MPa and strain hardening exponent,  $n = 0.3$  and the set  $(W_t, W_e, P_m)$  is computed using the functional forms presented in section 3.3. A grid of new sets of parameters is considered surrounding the base set by varying the parameters,  $E$ ,  $Y$  and  $n$ , within  $\pm 50\%$  of the original values and the set  $(W_t, P_m, W_e)$  corresponding to those new sets is computed. The following quantity is calculated for each of the new sets to quantify the difference between the set of shape functions  $(W_t, P_m, W_e)$  for the new sets and the base set:

$$\delta = \sqrt{\left(\frac{W_t^n - W_t^b}{W_t^b}\right)^2 + \left(\frac{P_m^n - P_m^b}{P_m^b}\right)^2 + \left(\frac{W_e^n - W_e^b}{W_e^b}\right)^2} \quad (3.14)$$

where the superscripts  $b$  and  $n$  indicate the shape functions for the base material parameter set and the new sets, respectively. The new material parameter sets with  $\delta < 0.01$  (1% tolerance) are obtained. Force-displacement relationships corresponding to some selected new sets are shown in Figure 3.9 along with that of the base set. The parameters corresponding to the new sets are tabulated in Table 3.3. Again, the force-displacement relationships overlap. The minor differences among the force-

displacement relationships are probably due to the inaccuracy of regression. These differences are likely to be within the margin of experimental errors.

Table 3.3: Material parameter sets leading to identical  $W_t$ ,  $P_m$  and  $W_e$  for spherical (radius  $3 \mu\text{m}$ ) indentation of a half-space modeled by linear-elastic, power law hardening plastic material model with depth-to-radius ratio of 100%. Force displacement relationships are shown in Figure 3.9.

Material #	$E$ (GPa)	$Y$ (MPa)	$n$
1	177.00	1320.0	0.2800
2	179.00	1260.0	0.2900
3	180.00	1200.0	0.300
4	181.00	1140.0	0.3100
5	184.00	1080.0	0.3200

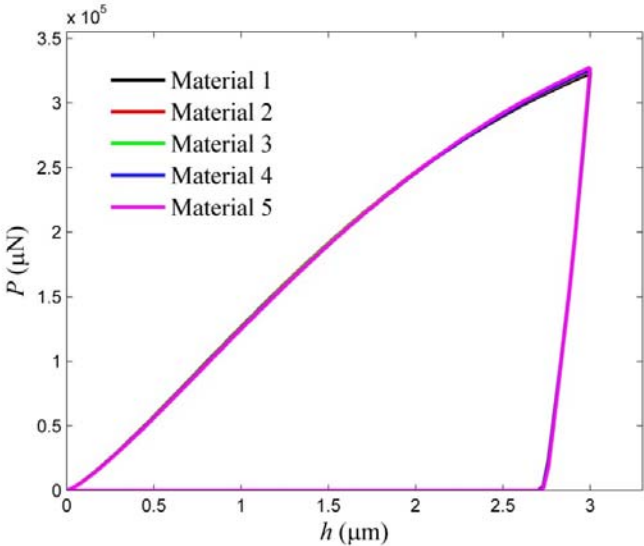
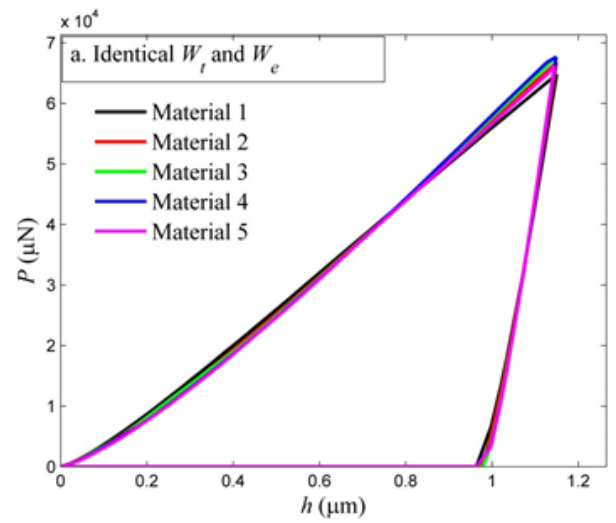


Figure 3.9: Force-displacement relationships corresponding to five material parameter sets that lead to identical  $W_t$ ,  $P_m$  and  $W_e$  for spherical (of radius  $3 \mu\text{m}$ ) indentation of a half-space modeled by linear-elastic, power-law hardening plastic material model with depth-to-radius ratio of 100%. The force-displacement relationships almost overlap.

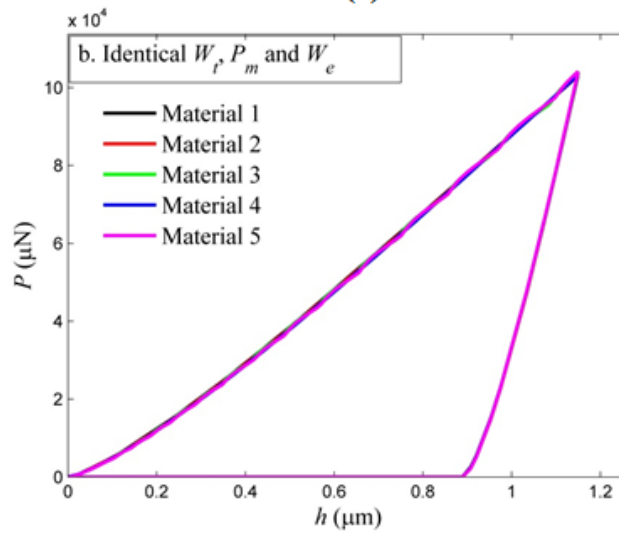
For spherical indentation on a sphere, a sphere of radius 23  $\mu\text{m}$  indented by another sphere of radius 3  $\mu\text{m}$  is considered and finite element simulation with maximum indentation depth,  $h_m = 1.15 \mu\text{m}$  is conducted. Iso- $(W_t/W_e)$  lines are drawn and material parameter sets leading to identical values of  $W_t$  and  $W_e$  are extracted from a iso-line using the procedures outlined in section 3.1. The obtained material parameters are tabulated in Table 3.4 and the corresponding force-displacement relationships are shown in Figure 3.10a. Similar to spherical indentation of a half-space, the loading curves do not completely overlap. Thus, as a next step, materials with identical  $W_t$ ,  $W_e$  and  $P_m$  are searched for following the methodology outlined in section 3.1 similar to spherical indentation of a half-space. Force-displacement relationships corresponding to one such set of material parameters are shown in Figure 3.10b and the material parameters are tabulated in Table 3.4. For these parameters sets, the force-displacement relationships overlap.

Table 3.4: Material parameter sets leading to identical  $(W_t, W_e)$  and  $(W_t, P_m, W_e)$  for spherical (radius 3  $\mu\text{m}$ ) indentation of a sphere (radius 23  $\mu\text{m}$ ) modeled by linear-elastic, power law hardening plastic material model. Force displacement relationships are shown in Figure 3.10.

Material #	Identical $W_t$ and $W_e$			Identical $W_t, P_m$ and $W_e$		
	$E$ (GPa)	$Y$ (MPa)	$n$	$E$ (GPa)	$Y$ (MPa)	$n$
1	150.00	1000.0	0.15335	177.00	1370.0	0.26000
2	161.60	538.66	0.32969	178.00	1280.0	0.28000
3	170.81	341.63	0.41798	178.00	1200.0	0.30000
4	174.90	249.86	0.46806	178.00	1120.0	0.32000
5	178.23	198.04	0.50000	179.00	1080.0	0.33000



(a)



(b)

Figure 3.10: Force-displacement relationships corresponding to five material parameter sets leading to (a) identical  $W_i$  and  $W_e$  and (b) identical  $W_i$ ,  $P_m$  and  $W_e$ , for spherical (radius  $3 \mu\text{m}$ ) indentation of a sphere (radius  $23 \mu\text{m}$ ). Although the curves with identical  $W_i$  and  $W_e$  do not overlap, curves for with identical  $W_i$ ,  $P_m$  and  $W_e$  do overlap.

### 3.4.2 Isotropic, linear-elastic, linear strain hardening plastic material

To illustrate the methodology for linear-elastic, linear strain hardening plastic materials, finite element simulations of a half-space indented by a conical indenter with half-angle  $70.3^\circ$  and a sphere with radius  $3 \mu\text{m}$  were conducted. Following the procedures outlined in section 3.2, selected iso- $(W_t/W_e)$  lines are plotted in Figure 3.11 for conical indentation of a half-space. Five sets of material parameters leading to identical values of  $W_t$  and  $W_e$  are extracted and the corresponding force-displacement relationships are plotted in Figure 3.12. The material parameters are listed in Table 3.5. Once again, the force-displacement relationships overlap.

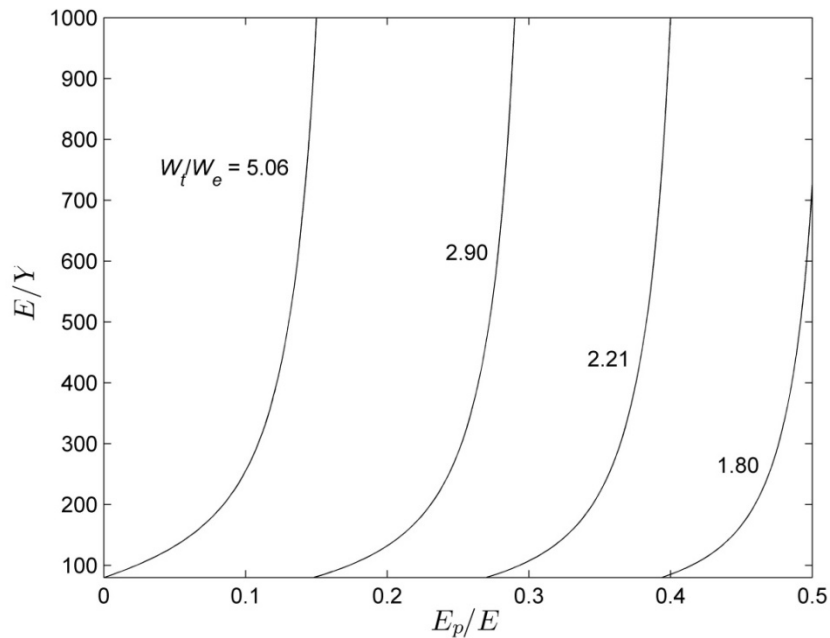
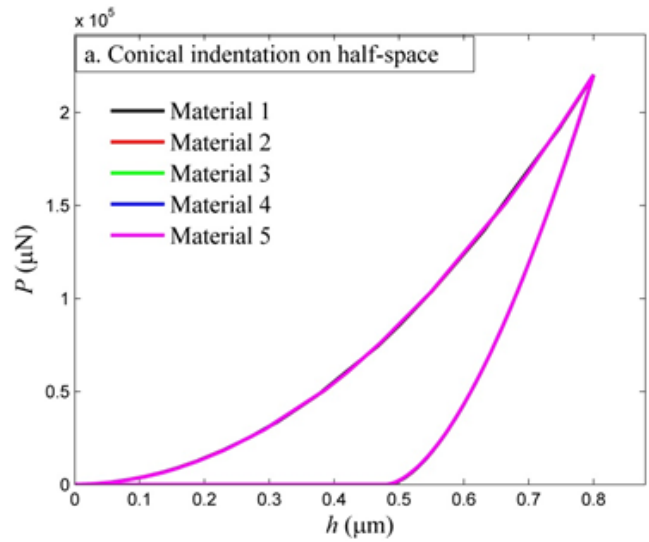


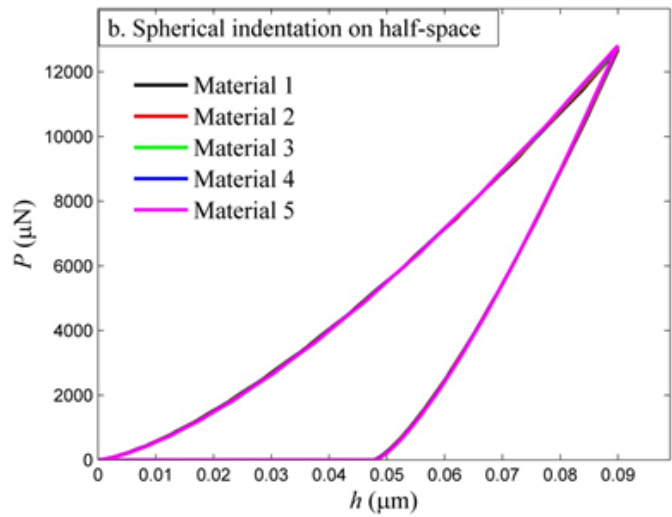
Figure 3.11: Iso- $(W_t/W_e)$  lines for conical ( $\alpha = 70.3^\circ$ ) indentation of a half-space made of linear elastic, linear strain hardening plastic material

Table 3.5: Material parameter sets leading to identical  $W_i$  and  $W_e$  for conical ( $\alpha = 70.3^\circ$ ) and spherical indentation (radius  $3 \mu\text{m}$ ) of a half-space modeled by linear-elastic, linear hardening plastic material model. Force displacement relationships are shown in Figure 3.12.

Material #	Conical indentation			Spherical indentation		
	$E$ (GPa)	$Y$ (MPa)	$E_p$ (GPa)	$E$ (GPa)	$Y$ (MPa)	$E_p$ (GPa)
<b>1</b>	300.00	1000	109.37	300.00	1000	99.648
<b>2</b>	304.61	761.54	114.42	307.07	767.68	108.68
<b>3</b>	307.99	615.99	117.95	312.28	624.55	114.95
<b>4</b>	310.54	517.56	120.56	316.15	526.91	119.56
<b>5</b>	312.48	446.40	122.55	319.07	455.82	123.04



(a)

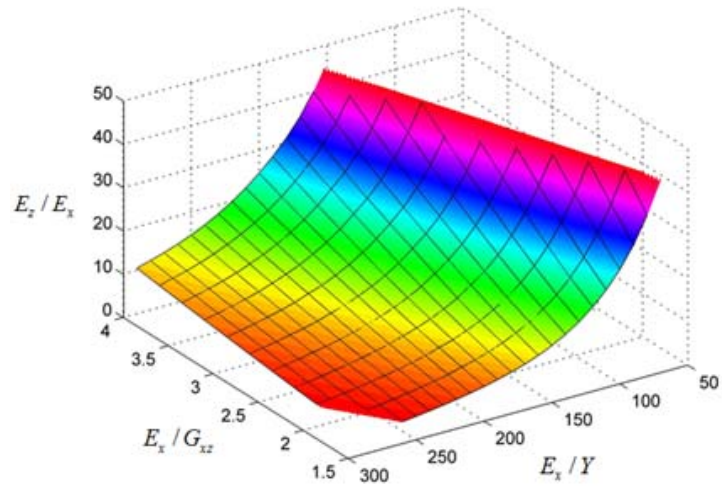


(b)

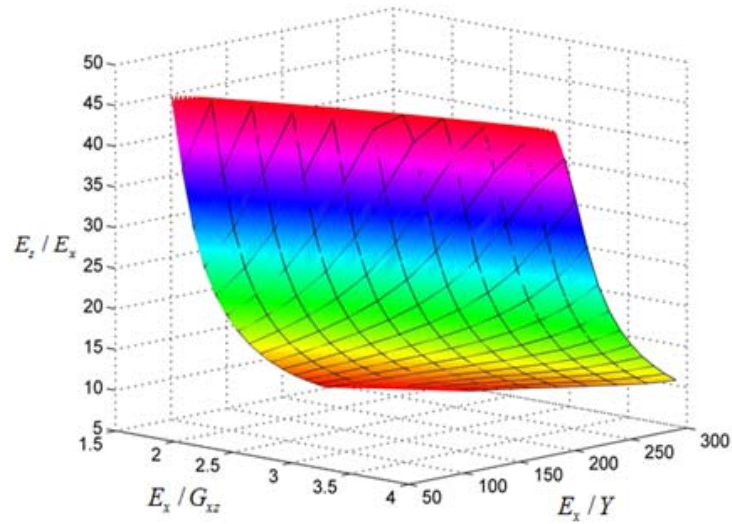
Figure 3.12: Force-displacement relationships corresponding to five material parameter sets leading to identical  $W_t$  and  $W_e$  for (a) conical ( $\alpha = 70.3^\circ$ ) and (b) spherical (radius  $3\mu\text{m}$ ) indentation of a half-space modeled by linear-elastic, linear hardening plastic material model. The curves overlap within the resolution of the figure.

### 3.4.3 Transversely isotropic, linear-elastic, perfectly plastic material

Finally, to illustrate the methodology for transversely isotropic, linear-elastic, perfectly-plastic material, finite element simulations of a half-space indented by a conical indenter with half-angle  $70.3^\circ$  and a spherical indenter with radius  $3 \mu\text{m}$  are conducted. An iso- $(W_i/W_e)$  surface is plotted in Figure 3.13 for each case and five material parameter sets leading to identical values of  $W_i$  and  $W_e$  are extracted. The material parameters are listed in Table 3.7 and the corresponding force-displacement relationships are plotted in Figure 3.14. The force-displacement relationships almost overlap.



(a)

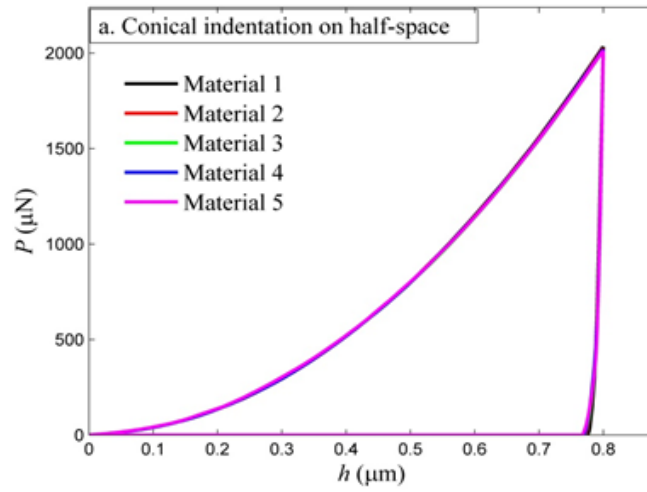


(b)

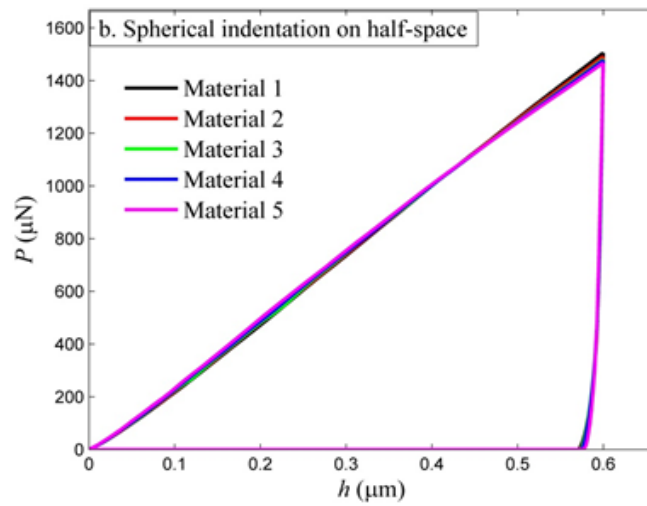
Figure 3.13: A iso- $(W_i/W_e)$  surface for (a) conical ( $\alpha = 70.3^\circ$ ) and (b) spherical (radius  $3 \mu\text{m}$ ) indentation of a half-space made of transversely isotropic, linear-elastic, perfectly plastic material.

Table 3.6: Material parameter sets leading to identical  $W_i$  for conical ( $\alpha = 70.3^\circ$ ) and spherical (radius  $3\mu\text{m}$ ) indentation of a half-space modeled by transversely isotropic, linear-elastic, perfectly-plastic material model. Poisson's ratios are assumed to be constant:  $\nu_{xz} = 0.05$  and  $\nu_{xy} = 0.2$ . Force displacement relationships are shown in Figure 3.14

Material #	Conical Indentation				Spherical Indentation			
	$E_z$ (GPa)	$E_x$ (GPa)	$G_{xz}$ (GPa)	$Y$ (MPa)	$E_z$ (GPa)	$E_x$ (GPa)	$G_{xz}$ (GPa)	$Y$ (MPa)
1	55.000	10.000	4.8958	35.336	187.50	5.0000	3.1451	45.454
2	112.17	7.4896	2.7235	37.636	174.24	6.1277	3.0638	43.769
3	96.341	4.9406	3.2937	41.195	332.70	7.6689	2.0451	42.605
4	173.23	7.2177	2.0162	38.290	256.18	8.5394	2.2772	41.889
5	142.31	3.7805	2.3628	45.275	107.89	10.9394	3.6465	40.516



(a)



(b)

Figure 3.14: Force-displacement relationships corresponding to five material parameter sets that lead to identical  $W_t$  and  $W_e$  for (a) conical ( $\alpha = 70.3^\circ$ ) and (b) spherical (radius  $3 \mu\text{m}$ ) indentation of a half-space made of transversely isotropic, linear-elastic, perfectly plastic material model. The curves almost overlap on each other.

### 3.5 Application to Experiments in the Literature

The proposed methodologies are applied to a real indentation experiment, and material parameter sets with force-displacement relationship identical to the experimentally obtained force-displacement relationship are obtained. This will be presented in this section.

Taljat et al. conducted spherical indentation experiments on A533-B steel. The radius of the indenter and the maximum indentation depth were 0.788 mm and 0.226 mm respectively. They presented the force-displacement relationship obtained from the indentation experiment, as well as the stress-strain curve of A533-B steel obtained from a separate compression test. Zhao et al., conducted regression analysis of the stress-strain curve reported by Taljat et al., and reported that it can be modeled as a isotropic, linear-elastic, power-law hardening material with material properties of, elastic modulus,  $E = 210$  GPa, yield strength,  $Y = 400$  MPa and strain hardening exponent,  $n = 0.127$ .

The spherical indentation experiments are simulated using the finite element model described in section 4.1 and the material properties described in the above paragraph. The substrate is modeled as a half-space. The Poisson's ratio is taken to be 0.3. The force-displacement relationships obtained from the experiment as well as from the present simulation are shown in Figure 3.15, showing reasonable agreement.

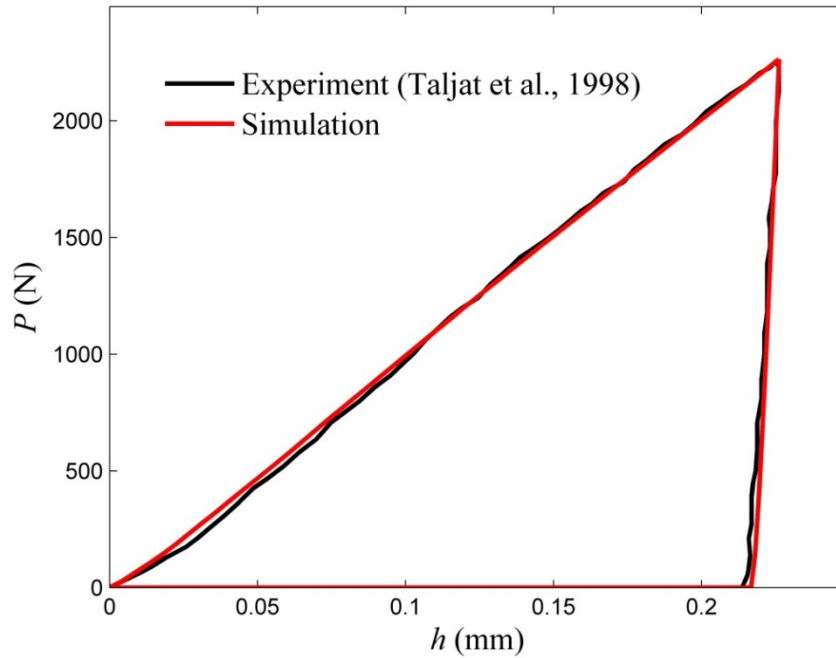


Figure 3.15: Comparison of force-displacement relationships obtained from experiment (Taljat et al., 1998) and simulation for spherical (radius 0.788 mm) indentation of a half-space

To identify material parameter sets leading to force-displacement relationship identical to the experimental force-displacement relationship shown in Figure 3.15, a material set with elastic modulus,  $80 \leq E \text{ (GPa)} \leq 300$ , yield stress  $0.1 \leq Y \text{ (GPa)} \leq 2.0$  and strain hardening exponent,  $0.0 \leq n \leq 0.5$  is considered. The maximum load,  $P_m$ , total energy,  $W_t$ , elastic energy,  $W_e$ , and the ratio,  $W_t/W_e$  for the experimental material were computed to be, 2263.5 N, 21.9 J, 0.79 J and 27.8, respectively. Since the force-displacement relationships obtained from the experiment and the simulation are almost identical, the force-displacement relationship obtained from the simulation is used for the computations of the shape functions mentioned above for accuracy. Following the procedure outlined in section 3.1, selected iso-lines are plotted in Figure 3.16 which

includes the iso-line corresponding to the experimental material. Five material parameter sets leading to values of  $W_t$  and  $W_e$  identical to that of the experimental material are extracted from the iso-line corresponding to the experimental material. The force-displacement relationships corresponding to the material parameter sets are plotted in Figure 3.17a and the parameters are tabulated in Table 3.7. The force-displacement relationships almost overlap. Next, as done previously, material parameter sets with identical  $W_t$ ,  $W_e$  and  $P_m$  are searched for following the methodology outlined in section 3.1 and 3.4.1. The force-displacement relationships corresponding to such sets are plotted in Figure 3.17b and the parameters are tabulated in Table 3.7. Again, the force-displacement relationships overlap.

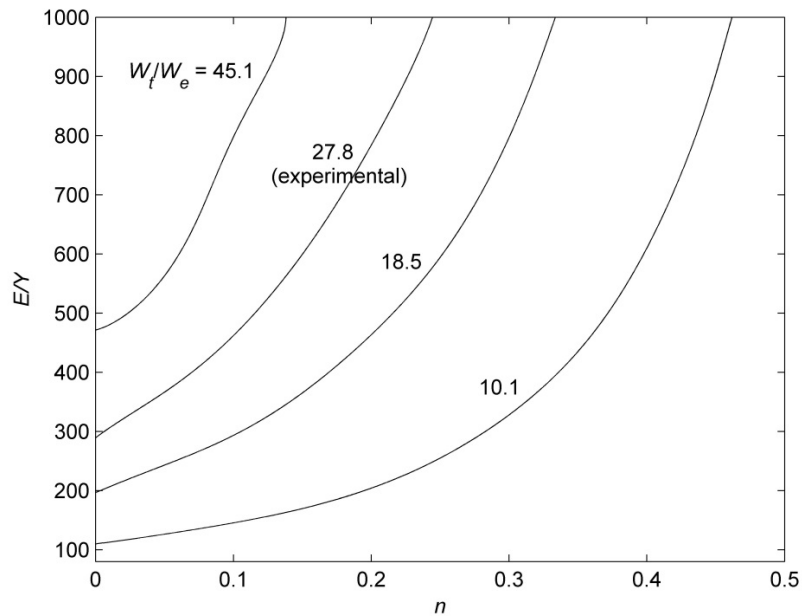
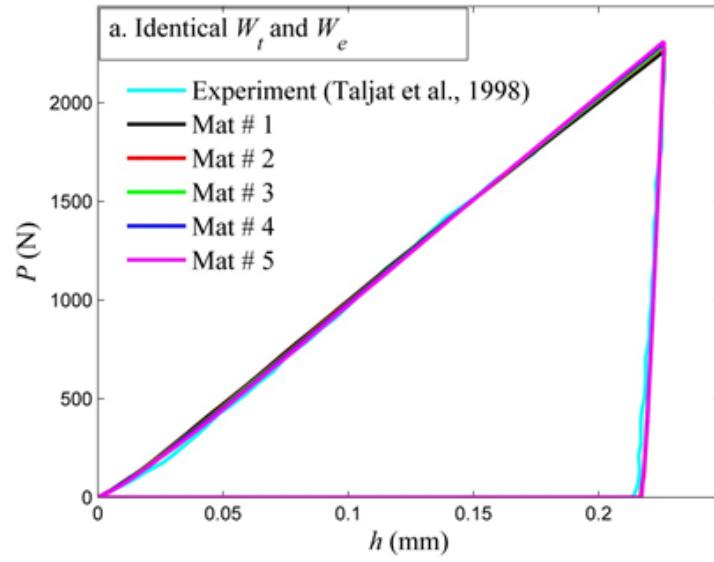


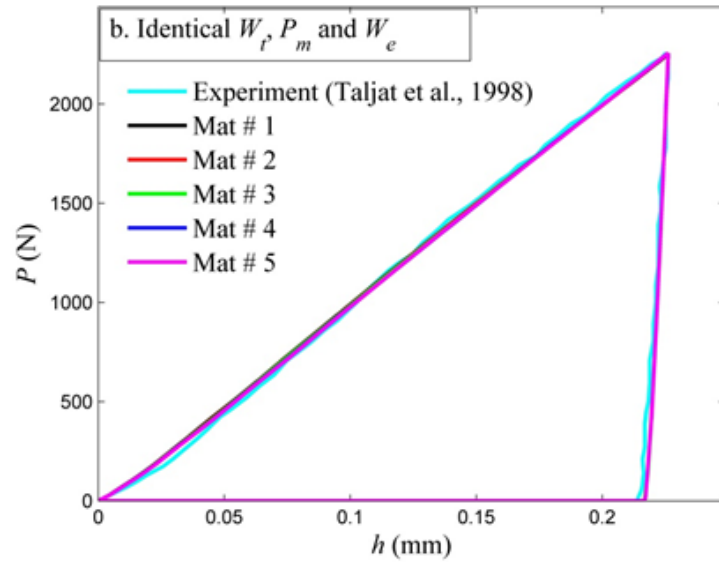
Figure 3.16: Iso- $(W_t/W_e)$  lines corresponding to the geometry of indentation experiment performed by Taljat et al. (1998). The iso-line corresponding to the experimental material is indicated.

Table 3.7: Material parameter sets leading to identical ( $W_i, W_e$ ) and ( $W_i, P_m, W_e$ ) with that of the experimental (Taljat et al., 1998) material. Force displacement relationships are shown in Figure 3.17.

Material #	Identical $W_i$ and $W_e$			Identical $W_i, P_m$ and $W_e$		
	$E$ (GPa)	$Y$ (MPa)	$n$	$E$ (GPa)	$Y$ (MPa)	$n$
1	500.00	1000.0	0.11568	207.00	410.00	0.12000
2	518.60	864.34	0.15022	208.00	393.00	0.13000
3	532.44	760.64	0.17891	209.00	377.00	0.14000
4	541.37	676.71	0.20392	211.00	360.00	0.15000
5	545.28	605.87	0.22635	213.00	345.00	0.16000



(a)



(b)

Figure 3.17: Comparison of the experimentally (Taljat et al., 1998) obtained force-displacement relationship and the force-displacement relationships of five material parameter sets leading to (a)  $W_t$  and  $W_e$  and (b)  $W_t$ ,  $P_m$  and  $W_e$  identical to the experimental material

### 3.6 Summary

In instrumented indentation, several material parameter sets can give rise to identical force-displacement relationships (although there may not be any real materials corresponding to such sets). In this chapter, a general method is presented to systematically obtain sets of material parameters with identical force-displacement relationships. The method serves as a tool to verify the existence and systematic study of non-uniqueness of force-displacement relationships for selected indentation geometries and material models.

The method is based on attempting to represent the force-displacement relationship with a few (two or three) shape functions and then comparing the selected shape functions to identify material parameter sets with identical values of those shape functions.

The method is illustrated by obtaining sets of materials with identical force-displacement relationship for wide range of indenter/substrate geometries and material models. It can thus be concluded that single indentation cannot provide unique material properties for a wide range of indenter/substrate geometries and material types. Thus alternate methodologies such as dual indentation technique are necessary. It is shown that in most cases two shape functions, the loading energy,  $W_t$ , and the unloading energy,  $W_e$ , of two materials can be compared to guarantee identical force-displacement relationship. In such cases, an existence map of such materials can be created using the concept of iso- $(W_t/W_e)$  lines and surfaces for visual demonstration of such materials in the material space. In some cases, such as spherical indentation with high depth-to-radius ratio, materials with identical force-displacement relationships could be obtained by comparing the loading energy,  $W_t$ , maximum load,  $P_m$  and the unloading energy,  $W_e$  instead of just  $W_t$  and  $W_e$ . The methodologies are applied to a

real indentation experiment reported in the literature, to identify materials with force-displacement relationship identical to the experimental material.

## Chapter 4

### ASSESSMENT OF THE SENSITIVITY OF INDENTATION TESTING USING CONDITION NUMBER AND SENSITIVITY ANALYSIS

In the previous chapters, we showed that several materials can result in identical force-displacement relationships when more than two material properties are involved. Therefore a single indentation technique cannot be used to determine the material properties uniquely. To overcome this difficulty, dual indentation methodologies can be utilized as discussed in Chapter 1, section 1.6. However, dual indentation methodologies can be quite sensitive to experimental error; that is, a small deviation in the experimental measurement can lead to a significant deviation in the determined material properties from the original material properties. Examples of common sources of error in an indentation experiment includes include instrument compliance (Van Vliet et al., 2004), imperfect indenter tip (Field and Swain, 1995), substrate surface roughness (Kim et al., 2007), size effect arising from increase in the density of dislocations (Huang et al., 2006), presence of small degree of material inhomogeneity (Higuchi et al., 2010) and thermal drift (Feng and Ngan, 2002). A range of combinations of shape functions, half-angles (conical indentation) and depth-to-radius ratios (spherical indentation) have been used for dual indentation tests in the literature. However, a systematic study to select combinations that minimize the sensitivity to experimental error is not available in the open literature. In this chapter, a systematic study of the sensitivity of indentation testing for isotropic and

transversely isotropic materials will be presented. A broader review of the background of this chapter can be found in Chapter 1, section 1.6.

In this chapter, conical and spherical indentation of a half-space composed of isotropic, linear-elastic, power-law hardening material or transversely isotropic, linear elastic, perfectly-plastic material is considered. In section 4.1, a methodology is presented to understand the uniqueness and sensitivity of an indentation system using condition number. In section 4.2, condition numbers are computed for isotropic materials for a range of dual indentation tests. Various combinations of shape functions, half-angles and depth-to-radius ratios are considered and the combinations are ranked according to the sensitivity of experimental error. In section 4.3, an explicit sensitivity analysis is presented to verify the findings using the condition number and to derive some further insights regarding sensitivity. In section 4.4, sensitivity of dual indentation testing of transversely isotropic materials is discussed. The work contained in this chapter is based on our work reported in Phadikar et al, 2013b, 2013c and 2013e.

The finite element models and the functional forms of used in this chapter are described in Chapter 3, section 3.3.

#### **4.1 Application of Condition Number to Indentation Technique**

In this section, a method will be presented first to determine the material properties of an isotropic, linear-elastic, power-law hardening material based on a conical dual indentation test. Then, the uniqueness and sensitivity of the determined material properties to experimental error will be discussed in a manner similar to the examples of Chapter 1, section 1.1.1.

As discussed in section 1.4, for conical indentation of a half-space composed of isotropic, linear-elastic, power law hardening material, several authors have shown that only two of the five shape functions listed in Eq. (1.12) are independent. Thus, for a single indentation test, two materials (materials 1 and 2) will have identical force-displacement relationships if both of them have the same values of maximum load,  $P_m$  and unloading slope,  $S_u$ . That also holds if they have the same  $P_m$  and the same  $P_m/S_u$ . Thus, the two conditions for identical force-displacement relationship can be written as (subscripts 1 and 2 correspond to two materials):

$$(P_m)_1 = (P_m)_2 \quad (4.2a)$$

$$(P_m / S_u)_1 = (P_m / S_u)_2 \quad (4.2b)$$

Using the relation of normalized  $P_m$  in Eq. (1.14b), Chapter 1, section 1.4, the first condition can be written as:

$$Y_1 h_m^2 \bar{G}_2 \left( \frac{E_1}{Y_1}, n_1 \right) = Y_2 h_m^2 \bar{G}_2 \left( \frac{E_2}{Y_2}, n_2 \right) \quad (4.3)$$

The above relationship can be used to obtain the ratio of the yield strengths of the two materials, as follows:

$$r = \frac{Y_1}{Y_2} = \bar{G}_2 \left( \left( \frac{E}{Y} \right)_2, n_2 \right) / \bar{G}_2 \left( \left( \frac{E}{Y} \right)_1, n_1 \right) \quad (4.4)$$

The two materials can be made to satisfy the second condition, Eq. (4.2b), by deriving non-dimensional relations involving  $P_m$  and  $S_u$  in Eq. (1.14b), which gives

$$\frac{P_m}{S_u h_m} = \bar{G}_6 \left( \frac{E}{Y}, n \right) \quad (4.5)$$

Eq. (4.2b) can be rewritten using Eq. (4.5) as:

$$\bar{G}_6\left(\left(\frac{E}{Y}\right)_1, n_1\right) = \bar{G}_6\left(\left(\frac{E}{Y}\right)_2, n_2\right) \quad (4.6)$$

From Eq. (4.5), iso- $P_m/(S_u h_m)$  lines can be drawn in the  $E/Y - n$  space and for  $\alpha = 50^\circ$ , such lines are shown in Figure 4.1a. Since all the materials lying on a particular iso- $P_m/(S_u h_m)$  line correspond to identical value of  $P_m/(S_u h_m)$ , it follows that any two materials selected from a particular iso- $P_m/(S_u h_m)$  line will satisfy the second condition for identical force-displacement relationship, Eq. (4.6). From Figure 4.1a, pairs of materials having identical force-displacement relationship can be obtained in the following steps:

**Step 1:** Select any two points on a particular iso-  $P_m/(S_u h_m)$  curve (as illustrated in Figure 4.1a). Thus obtain  $(E/Y)$  and  $n$  of two materials that satisfy the second condition of identical force-displacement relationship (Eq. (4.2b)).

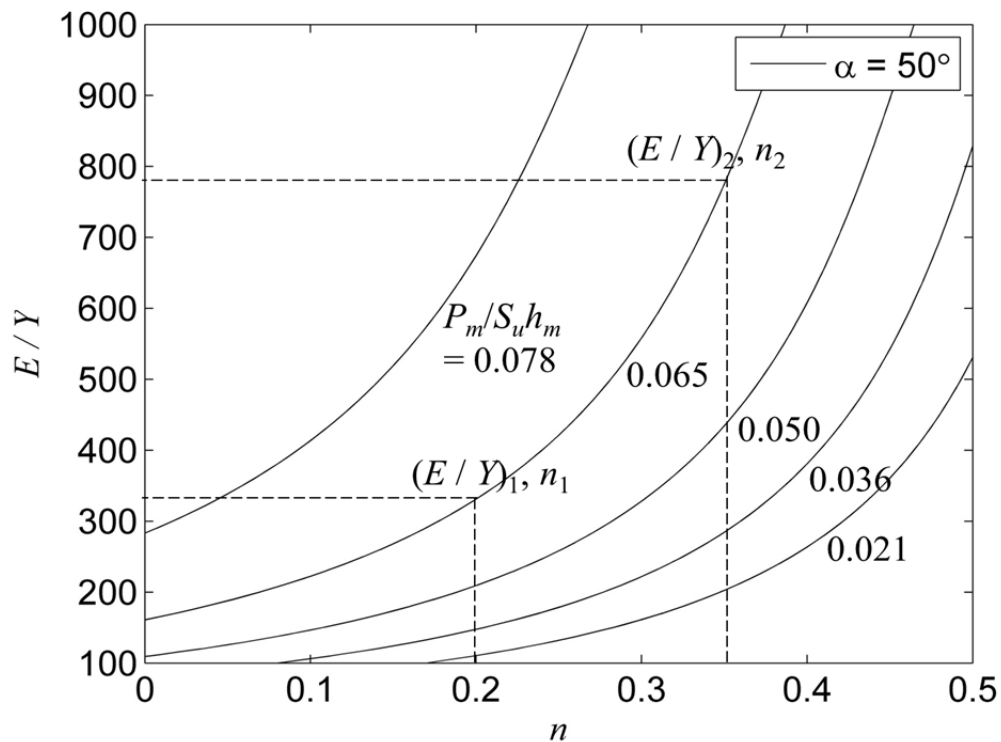
**Step 2:** Determine the ratio  $r = Y_1/Y_2$  from Eq. (4.4) using  $(E/Y)_1, n_1, (E/Y)_2$  and  $n_2$  obtained in Step 1. Since Eq. (4.4) is derived from Eq. (4.2a), the materials now satisfy the first condition (Eq. 4.2a) as well.

**Step 3:** Assume any value of  $Y_2$  and determine  $Y_1$  using  $Y_1 = rY_2$ , from Step 2.

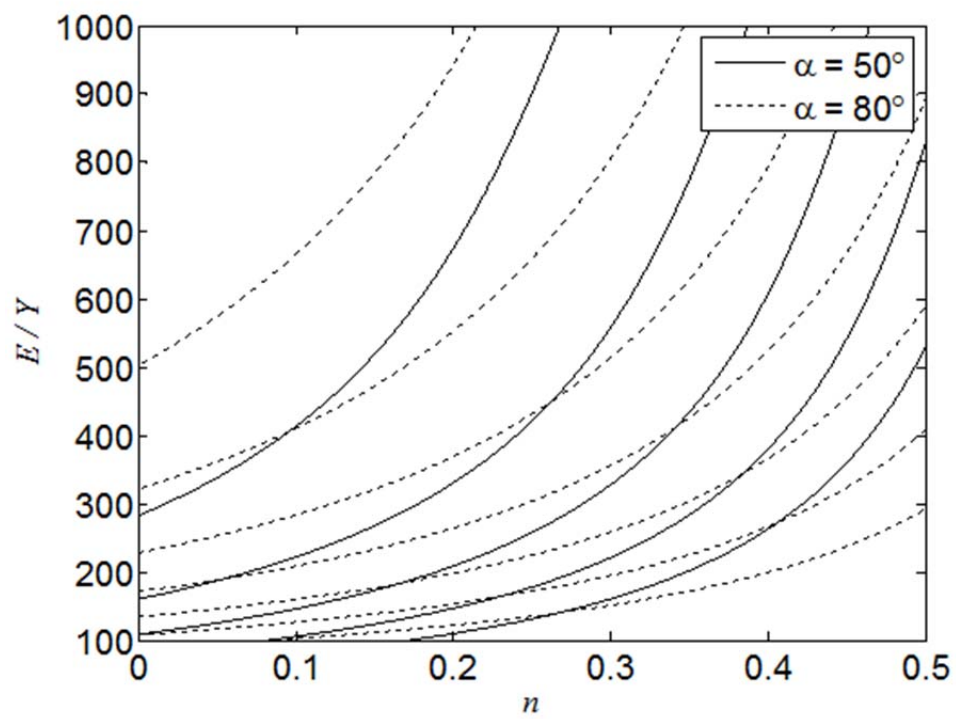
**Step 4:** Using  $Y_1$  and  $Y_2$ , and  $(E/Y)_1$  and  $(E/Y)_2$  obtained in Step 1, determine  $E_1$  and  $E_2$ . Since  $Y_2$  is selected arbitrarily, there are an infinite number of materials having the same force displacement relationship corresponding to any two points of an iso- $P_m/(S_u h_m)$  line.

For dual indentation testing, two different half-angles are used. Using the same approach discussed above, the iso-lines for the other indenter can be generated. In Figures 4.1b, 4.1c and 4.1d, iso-lines corresponding to indenters with  $\alpha = 80^\circ, 70^\circ$  and  $60^\circ$ , respectively are shown together with the iso-lines from  $\alpha = 50^\circ$ . These iso-lines can be used to determine the material properties of a material based on a dual

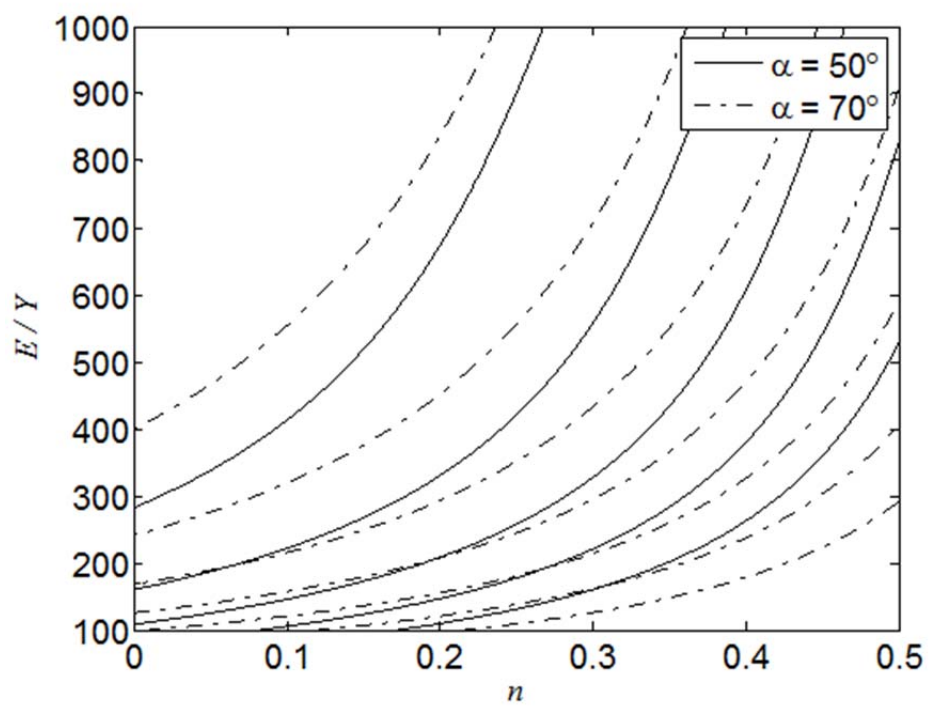
indentation test using the following procedure (described for  $\alpha_1 = 50^\circ$  and  $\alpha_2 = 80^\circ$ ): conduct the dual indentation test with  $\alpha_1 = 50^\circ$  and  $\alpha_2 = 80^\circ$ . Obtain the force-displacement relationships and thereby the quantities  $P_m/S_u h_m$  for the two tests. Draw the two particular iso-lines corresponding to the two tests in the  $E/Y-n$  space using finite element analysis and the procedure described in the previous paragraphs. Since both the iso-lines correspond to the same material, the intersection of the two lines will give the values of  $E/Y$  and  $n$  for the material. The elastic modulus,  $E$  can be determined using the commonly used “Oliver-Pharr method” (Oliver and Pharr, 1992). Thereafter, the yield strength,  $Y$  can be calculated using the values of  $E$  and  $E/Y$ .



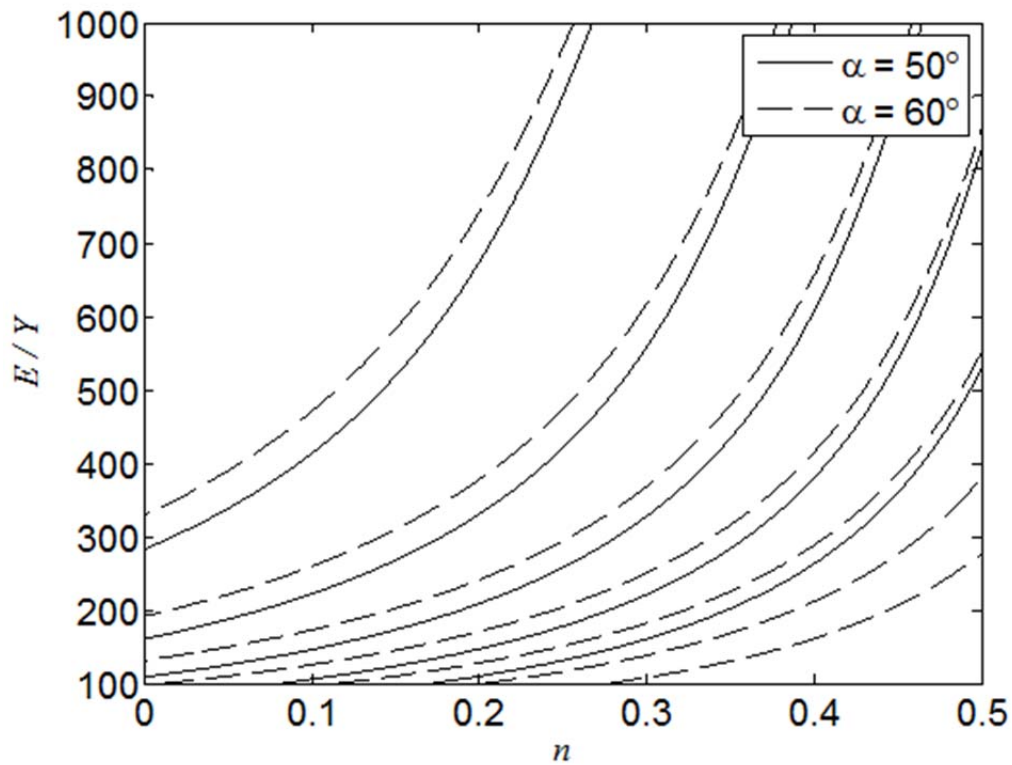
(a)



(b)



(c)



(d)

Figure 4.1: Selected iso- $(P_m/S_u h_m)$  lines for (a)  $\alpha = 50^\circ$ ; (b)  $\alpha = 50^\circ$  and  $\alpha = 80^\circ$ ; (c)  $\alpha = 50^\circ$  and  $\alpha = 70^\circ$ ; (d)  $\alpha = 50^\circ$  and  $\alpha = 60^\circ$ . As the iso-lines from two tests approach each other, the system becomes increasingly sensitive to experimental errors.

The concept of condition number and the method of iso- $P_m/(S_u h_m)$  lines can be used to demonstrate the sensitivity of dual indentation techniques due to experimental error. Figures 4.1b, 4.1c and 4.1d can be compared with Figures 1.3a, 1.3b, 1.3c. Here  $E/Y$  and  $n$  are equivalent to the elements of  $\mathbf{x}$  (solution), and values of  $P_m/(S_u h_m)$  corresponding to two different indentation tests are equivalent to the elements of  $\mathbf{y}$  (data) in Chapter 1, section 1.1.1. The sensitivity of the determined material properties

due to experimental error and the condition number of the system increase as the iso-lines get closer to each other, similar to the discussion of linear systems in section 1.1.1 (Figure 1.3). For a clearer illustration, in Figure 4.2, the iso-lines passing through the point  $E/Y = 500$ ,  $n = 0.25$  corresponding to the four indenter half-angles are shown. As the difference between the half-angle decreases, the iso-lines become closer which means that the indentation tests will be more sensitive to the experimental error and thus the viability of the determined material parameters will be questionable. Although, condition numbers are not explicitly computed for the examples presented in this section, it can be understood from the discussion in section 1.1.1, that as the indentation system becomes increasingly sensitive and approaches non-uniqueness, the condition number of the system will increase.

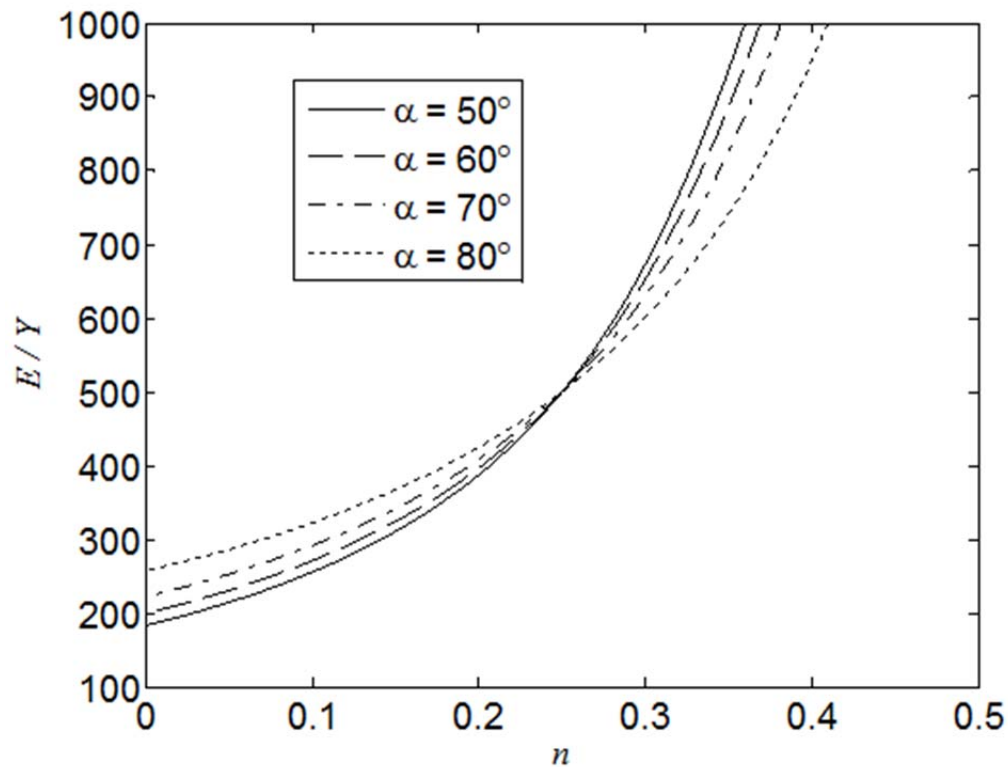


Figure 4.2: Selected iso- $(P_m/S_u h_m)$  lines passing through the point  $E/Y = 500$ ,  $n = 0.25$  for four selected conical indenters

Condition numbers can be computed for the indentation systems and different dual indentation tests can be ranked according to the sensitivity due to experimental error. This will be discussed next.

#### 4.2 Condition Numbers of Single and Dual Indentation Techniques

So far, the uniqueness and sensitivity of indentation systems have been discussed in qualitative terms. We will now attempt to quantify them using the concept of condition numbers. To compute the condition numbers for indentation

systems, indentation tests are to be simulated numerically and the functional relationships between the shape functions (data of the system) and material properties (solution of the system) need to be established. Such relationships between the normalized shape functions and the material properties are described in Eqs. (1.14)-(1.15) (Chapter 1, section 1.4) for isotropic materials. The functional forms of  $\bar{G}_i^{ph}$  and  $\bar{G}_i^{lh}$  are described in section 3.3, Chapter 3 and sections A.1 and A.2, Appendix A for various indentation geometries.

#### 4.2.1 Modified condition number

A brief overview of the condition number is provided in section 1.1.1. Considering large differences in the numerical values among the material properties (elastic modulus,  $E$ , yield strength,  $Y$ , and strain hardening exponent,  $n$ ), a new definition of the condition number is introduced in this section. In this definition, the relative change is measured on an element by element basis which is given by (for vector  $\mathbf{z}$ ):  $\|\mathbf{A}\mathbf{z} ./ \mathbf{z}\|$  instead of  $\|\mathbf{A}\mathbf{z}\| / \|\mathbf{z}\|$  used in the original definition (Eq. (1.1)). Here the definition of the “./” operation is

$$\mathbf{m} ./ \mathbf{n} = (m_1, m_2, m_3 \dots m_k) ./ (n_1, n_2, n_3 \dots n_k) = (m_1 / n_1, m_2 / n_2, m_3 / n_3 \dots m_k / n_k) \quad (4.8)$$

Consider the equation  $\mathbf{y} = \mathbf{f}(\mathbf{x})$ , where  $\mathbf{x}$  denotes the material property vector<sup>3</sup>,  $\mathbf{x} = (E, Y, n)$ , and  $\mathbf{y}$  denotes the vector of shape functions,  $\mathbf{y} = (\text{shape functions})$ . As discussed further in the paragraph following Eq. (4.9), the modified condition number accommodating the new definition of relative change is given by

$$\kappa_m = 1 / u_3(\mathbf{f}, C, \mathbf{z}) \quad (4.9a)$$

---

<sup>3</sup> The material properties that are used in this expression are the original properties used in the FE model, and not the ones that are obtained from reverse analysis.

with

$$u_3(\mathbf{f}, C, \mathbf{z}) = \sup_{\mathbf{x} \text{ in } C} \left\{ t \text{ in } [0, \infty); \left\| \frac{\mathbf{f}(\mathbf{x}) - \mathbf{f}(\mathbf{z})}{\mathbf{f}(\mathbf{z})} \right\| \leq t \left\| \frac{\mathbf{x} - \mathbf{z}}{\mathbf{z}} \right\| \right\} \quad (4.9b)$$

where  $\mathbf{z}$  is the point in material space where the condition number is computed and  $C$  is a user-defined domain enclosing  $\mathbf{z}$ .

A small  $\kappa_m$  implies that the relative error of the material properties,  $\|\Delta \mathbf{x} / \mathbf{x}\|$ , is small for a given error in shape functions,  $\|\Delta \mathbf{y} / \mathbf{y}\|$ , and vice versa. It can be understood as follows: from Eq. (4.9a), a small  $\kappa_m$  implies large  $u_3(\mathbf{f}, C, \mathbf{z})$ . Note that in Eq. (4.9b),  $\|\Delta \mathbf{x} / \mathbf{x}\|$  is denoted as  $\|(\mathbf{x} - \mathbf{z}) / \mathbf{z}\|$  and  $\|\Delta \mathbf{y} / \mathbf{y}\|$  is denoted as  $\|(\mathbf{f}(\mathbf{x}) - \mathbf{f}(\mathbf{z})) / \mathbf{f}(\mathbf{z})\|$ . From Eq. (4.9b),  $u_3(\mathbf{f}, C, \mathbf{z})$  roughly denotes the maximum value of  $\|\Delta \mathbf{y} / \mathbf{y}\| / \|\Delta \mathbf{x} / \mathbf{x}\|$ . Thus, for a given  $\|\Delta \mathbf{y} / \mathbf{y}\|$ , a large  $u_3(\mathbf{f}, C, \mathbf{z})$  implies a small  $\|\Delta \mathbf{x} / \mathbf{x}\|$ . It follows that a small  $\kappa_m$  results in small  $\|\Delta \mathbf{x} / \mathbf{x}\|$  for a given  $\|\Delta \mathbf{y} / \mathbf{y}\|$ .

#### 4.2.2 Computational procedure

The computational procedure of the modified condition number,  $\kappa_m$ , for an indentation test will be described in this section.

The relationships between the normalized shape functions and the material properties, Eq. (1.14b) (the functional forms are presented in section 3.3), represent the mapping between the space of material parameters (input space) and the space of shape functions (output space). The specific material for which the condition number is computed is considered as the origin of the input space and denoted by  $\mathbf{z} = (E_0, Y_0, n_0)$ . The set of shape functions corresponding to that material is considered as the origin of the output space. The perturbation region or the subdomain,  $C$ , (in Eq. (4.9)) enclosing the origin of the input space is selected as:

$$C = \{0.9z_i < z_i < 1.1z_i\}; i = 1-3; \mathbf{z} = (z_1, z_2, z_3)$$

A uniform grid is constructed in the input perturbation region which consists of  $50 \times 50 \times 50 = 125000$  material points. Using the mapping equations (Eqs. (1.14b)), the corresponding output perturbation region is determined. For both the input and output perturbation region, the relative differences (Eq. (4.8)) between the grid points and the origin are computed. For each grid point in the input perturbation region, the ratios of the relative differences in output and input region yield the parameter  $t$  of Eq. (4.9b). The maximum value of the parameter  $t$  is  $u_3(\mathbf{f}, C, \mathbf{z})$ . Its reciprocal,  $\kappa_m$  (Eq. (4.9a)) gives the value of the condition number at the material point.

Dimensional analysis shows that the condition number only depends on  $E/Y$  and  $n$ , instead of three material parameters independently. Thus, denoting the functional relation by  $J$ ,

$$\kappa_m = J\left(\frac{E}{Y}, n\right) \quad (4.10)$$

For a given indentation geometry, the condition numbers have been calculated at 45 points of the  $E/Y - n$  space, numerically, with  $E_0/Y_0 = 100, 200, 300, 400, 500, 600, 700, 800, 900$  and  $n_0 = 0.05, 0.15, 0.25, 0.35, 0.45$ . The average condition number for a particular indentation geometry is determined from these 45 cases, and used as the condition number for the indentation geometry,  $\kappa_m^{avg}$ .

### 4.2.3 Condition numbers for single indentation

In the previous sections, we have discussed that for single indentation, several materials can result in identical force-displacement relationship. Thus, the condition number for the single indentation technique should be infinite since it is a non-unique system (Datta, 2010). To investigate this, we computed the average modified

condition number,  $\kappa_m^{avg}$ , for conical indentation with  $\alpha = 70^\circ$  and spherical indentation with  $h_m/R = 20\%$ . The resulting condition numbers are tabulated in Table 4.1. As discussed in section 1.1.1, well-conditioned systems have a condition number close to 1. In this case, the condition numbers are quite large but finite. The condition numbers are finite since the subdomain,  $C$  is numerically discretized and the computation therefore does not account for all the infinite points. Also, the force-displacement relationships are not truly non-unique, but there are very small differences among the force-displacement relationships of different materials (Tho et al., 2004; Alkorta et al., 2005). Consequently, finite but very large condition numbers are obtained.

Table 4.1: Condition numbers for single indentation technique for various combinations of shape functions

Shape function combination	$\kappa_m^{avg}$	
	Conical Indentation	Spherical Indentation
$S_u, W_e, h_f$	88.6	87.0
$P_m, W_e, h_f$	131	131
$P_m, S_u, h_f$	125	100
$P_m, S_u, W_e$	99.8	94.2
$W_t, W_e, h_f$	109	117
$W_t, S_u, h_f$	106	105
$W_t, S_u, W_e$	88.6	44.0
$W_t, P_m, h_f$	445	76.4
$W_t, P_m, W_e$	153	50.9
$W_t, P_m, S_u$	165	44.2

#### 4.2.4 Condition numbers for dual indentation

Next, the condition numbers for dual indentation is presented. First, condition numbers will be presented for a range of shape function combinations and then for various combinations of half-angles and depth-to-radius ratios. For dual conical indentation, the condition numbers were computed for indenters with  $\alpha_1 = 50^\circ$  and  $\alpha_2 = 80^\circ$ . These half-angles may be considered as the limits of the range of half-angles that are of practical use. For spherical indentation, condition numbers were computed for indentation tests with  $(h_m/R)_1 = 10\%$  and  $(h_m/R)_2 = 40\%$ . A simple calculation shows that there are one hundred ways in which three shape functions can be selected from two half-angles (or depth-to-radius ratios). In fifty of them, two shape functions are selected from  $\alpha_1$  or  $(h_m/R)_1$  and one shape function is selected from  $\alpha_2$  or  $(h_m/R)_2$ . In the other fifty combinations, one shape functions is selected from  $\alpha_1$  or  $(h_m/R)_1$  and two shape functions are selected from  $\alpha_2$  or  $(h_m/R)_2$ . The condition numbers of those combinations are arranged in ascending order and are listed in Table 4.2 and 4.3. The condition numbers ranges from about 5.8 to 322 for dual conical indentation and from 7.6 to 253 for spherical indentation. Thus the dual indentation tests are highly dependent on the shape function combination used. Interestingly, condition numbers for many combinations of the shape functions for dual indentation are of the same order as single indentation technique. Small differences in condition number between two combinations may exist due to inaccuracy of regression. Thus, no conclusions can be drawn about the effectiveness of the combinations involved for such cases. Only a few combinations have condition numbers less than 10 and thus it appears only few combinations may result in moderate sensitivity behavior.

For dual spherical indentation, a part of the loading curve from indentation test with higher depth-to-radius ratio  $(h_m/R)_2$  is identical to the loading curve from

indentation with lower depth-to-radius ratio  $(h_m/R)_1$  (assuming constant radius). However, the unloading curves appear to contain significant information. The combinations containing the unloading energy,  $W_e$  from depth-to-radius ratio  $(h_m/R)_1$  have lower condition numbers (e.g. ranks 1-5 of Table 4.2), whereas combinations containing  $W_t$ 's from both depth-to-radius ratios have higher condition numbers (e.g. ranks 81, 95, 99). This is corroborated by the fact that, unloading curves of the materials which lead to identical force-displacement relationship for depth-to-radius ratio  $(h_m/R)_2$  are significantly different for indentation with depth-to-radius ratio  $(h_m/R)_1$ . For example, the maximum difference between elastic energies for the five material parameter sets (tabulated in Table 3.2) which lead to identical force-displacement relationship for  $(h_m/R)_2 = 20\%$  was computed to be 0.74% for  $(h_m/R)_2 = 20\%$  whereas it was computed to be 10.2% for  $(h_m/R)_1 = 10\%$ .

Table 4.2a: Condition numbers for various combinations of shape functions of dual conical indentation arranged in ascending order (rank 1-50).

Combination #	Shape function combination	Condition number ( $\kappa_m^{avg}$ )	Combination #	Shape function combination	Condition number ( $\kappa_m^{avg}$ )
1	$W_e^1, S_u^2, W_e^2$	5.629	26	$S_u^1, W_e^1, W_t^2$	12.20
2	$W_e^1, S_u^1, W_e^2$	5.825	27	$P_m^1, W_e^1, P_m^2$	17.22
3	$W_e^1, P_m^1, W_e^2$	5.862	28	$P_m^1, W_e^1, W_t^2$	17.46
4	$W_t^1, W_e^1, W_e^2$	5.870	29	$W_t^1, W_e^1, P_m^2$	17.47
5	$W_e^1, P_m^2, W_e^2$	6.687	30	$W_t^1, W_e^1, W_t^2$	17.72
6	$W_e^1, W_t^2, W_e^2$	6.697	31	$W_e^1, W_e^2, h_f^2$	24.85
7	$P_m^1, S_u^1, W_e^2$	7.681	32	$W_t^1, P_m^2, h_f^2$	26.79
8	$W_t^1, S_u^1, W_e^2$	7.747	33	$P_m^1, P_m^2, h_f^2$	26.91
9	$P_m^1, S_u^2, W_e^2$	7.880	34	$W_t^1, W_t^2, h_f^2$	27.04
10	$W_t^1, S_u^2, W_e^2$	7.908	35	$P_m^1, W_t^2, h_f^2$	27.31
11	$P_m^1, P_m^2, W_e^2$	9.287	36	$W_e^1, S_u^2, h_f^2$	29.29
12	$P_m^1, W_t^2, W_e^2$	9.349	37	$S_u^1, W_e^1, S_u^2$	32.19
13	$W_t^1, P_m^2, W_e^2$	9.446	38	$W_t^1, S_u^2, h_f^2$	33.41
14	$W_t^1, W_t^2, W_e^2$	9.513	39	$P_m^1, S_u^1, S_u^2$	34.06
15	$W_e^1, P_m^2, S_u^2$	10.10	40	$W_t^1, S_u^1, S_u^2$	34.08
16	$W_e^1, W_t^2, S_u^2$	10.17	41	$P_m^1, S_u^2, h_f^2$	34.53
17	$P_m^1, P_m^2, S_u^2$	10.56	42	$W_t^1, W_e^1, S_u^2$	34.73
18	$W_t^1, P_m^2, S_u^2$	10.59	43	$W_e^1, h_f^1, S_u^2$	36.31
19	$P_m^1, W_t^2, S_u^2$	10.64	44	$P_m^1, W_e^1, S_u^2$	36.93
20	$W_t^1, W_t^2, S_u^2$	10.67	45	$W_t^1, h_f^1, S_u^2$	39.99
21	$P_m^1, S_u^1, P_m^2$	11.71	46	$P_m^1, h_f^1, S_u^2$	40.65
22	$W_t^1, S_u^1, P_m^2$	11.73	47	$S_u^1, W_e^1, h_f^2$	42.72
23	$P_m^1, S_u^1, W_t^2$	11.81	48	$W_t^1, P_m^1, S_u^2$	42.80
24	$W_t^1, S_u^1, W_t^2$	11.82	49	$P_m^1, W_e^2, h_f^2$	47.04
25	$S_u^1, W_e^1, P_m^2$	12.11	50	$W_t^1, W_e^2, h_f^2$	48.61

Table 4.2b: Condition numbers for various combinations of shape functions of dual conical indentation arranged in ascending order (rank 51-100).

Combination #	Shape function combination	Condition number ( $\kappa_m^{avg}$ )	Combination #	Shape function combination	Condition number ( $\kappa_m^{avg}$ )
51	$W_t^1, S_u^1, h_f^2$	53.50	76	$S_u^1, h_f^1, S_u^2$	100.0
52	$P_m^1, S_u^1, h_f^2$	54.55	77	$h_f^1, S_u^2, h_f^2$	100.9
53	$S_u^1, S_u^2, W_e^2$	56.32	78	$P_m^1, h_f^1, P_m^2$	101.0
54	$W_e^1, W_t^2, h_f^2$	57.44	79	$P_m^1, h_f^1, W_t^2$	102.5
55	$W_e^1, P_m^2, h_f^2$	58.92	80	$S_u^1, P_m^2, h_f^2$	103.7
56	$h_f^1, S_u^2, W_e^2$	64.48	81	$W_t^1, h_f^1, W_t^2$	110.1
57	$S_u^1, W_t^2, S_u^2$	65.06	82	$h_f^1, S_u^1, h_f^2$	113.1
58	$W_t^1, W_e^1, h_f^2$	65.51	83	$W_t^1, h_f^1, P_m^2$	113.9
59	$P_m^1, W_e^1, h_f^2$	65.77	84	$W_e^1, h_f^1, P_m^2$	117.6
60	$S_u^1, h_f^1, W_e^2$	66.87	85	$W_e^1, h_f^2, W_t^2$	120.7
61	$S_u^1, P_m^2, S_u^2$	69.92	86	$h_f^1, P_m^2, h_f^2$	131.6
62	$S_u^1, W_e^2, h_f^2$	72.57	87	$h_f^1, W_t^2, h_f^2$	134.0
63	$W_t^1, h_f^1, W_e^2$	73.07	88	$h_f^1, W_e^2, h_f^2$	168.2
64	$S_u^1, S_u^2, h_f^2$	74.57	89	$W_t^1, h_f^1, h_f^2$	174.2
65	$h_f^1, W_t^2, S_u^2$	76.10	90	$W_t^1, P_m^1, W_e^2$	179.2
66	$S_u^1, W_t^2, W_e^2$	77.20	91	$P_m^1, h_f^1, h_f^2$	183.4
67	$S_u^1, P_m^2, W_e^2$	77.48	92	$W_e^1, h_f^1, h_f^2$	194.0
68	$P_m^1, h_f^1, W_e^2$	77.86	93	$S_u^1, W_t^2, P_m^2$	205.9
69	$h_f^1, W_t^2, S_u^2$	79.58	94	$W_e^1, W_t^2, P_m^2$	225.7
70	$h_f^1, P_m^2, W_e^2$	82.01	95	$W_t^1, P_m^1, W_t^2$	292.1
71	$W_e^1, h_f^1, W_e^2$	82.64	96	$W_t^1, P_m^1, h_f^2$	312.3
72	$h_f^1, W_t^2, W_e^2$	83.89	97	$W_t^1, P_m^1, h_f^2$	322.1
73	$S_u^1, h_f^1, W_t^2$	89.59	98	$P_m^1, W_t^2, P_m^2$	390.5
74	$S_u^1, h_f^1, P_m^2$	94.21	99	$W_t^1, W_t^2, P_m^2$	393.3
75	$S_u^1, W_t^2, h_f^2$	98.65	100	$h_f^1, P_m^1, W_t^2$	852.1

Table 4.3a: Condition numbers for various combinations of shape functions of dual spherical indentation arranged in ascending order (rank 1-50).

Combination #	Shape function combination	Condition number ( $\kappa_m^{avg}$ )	Combination #	Shape function combination	Condition number ( $\kappa_m^{avg}$ )
1	$W_e^1, S_u^2, W_e^2$	7.657	26	$P_m^1, S_u^1, W_t^2$	20.42
2	$W_e^1, S_u^1, W_e^2$	7.684	27	$P_m^1, W_t^2, S_u^2$	20.55
3	$W_e^1, P_m^2, W_e^2$	7.735	28	$P_m^1, P_m^2, W_e^2$	21.43
4	$W_e^1, W_t^2, W_e^2$	7.901	29	$W_t^1, W_t^2, W_e^2$	27.05
5	$P_m^1, W_e^1, W_e^2$	8.447	30	$W_e^1, h_f^1, W_e^2$	31.06
6	$W_t^1, W_e^1, W_e^2$	8.568	31	$S_u^1, W_t^2, P_m^2$	31.10
7	$S_u^1, W_e^1, P_m^2$	10.23	32	$W_e^1, P_m^2, W_t^2$	32.76
8	$W_e^1, P_m^2, S_u^2$	10.31	33	$P_m^1, W_t^2, W_e^2$	33.43
9	$W_t^1, W_e^1, P_m^2$	11.25	34	$S_u^1, W_t^2, W_e^2$	34.56
10	$W_t^1, S_u^1, P_m^2$	12.41	35	$S_u^1, h_f^1, W_e^2$	46.39
11	$W_t^1, P_m^2, S_u^2$	12.42	36	$W_e^1, W_e^2, h_f^2$	50.41
12	$W_t^1, S_u^2, W_e^2$	12.54	37	$h_f^1, S_u^2, W_e^2$	51.22
13	$W_t^1, S_u^1, W_e^2$	12.73	38	$S_u^1, h_f^1, P_m^2$	51.98
14	$P_m^1, W_e^1, P_m^2$	13.18	39	$W_t^1, h_f^1, P_m^2$	54.26
15	$P_m^1, S_u^1, P_m^2$	14.00	40	$W_t^1, P_m^1, S_u^2$	56.41
16	$P_m^1, S_u^2, W_e^2$	14.08	41	$W_t^1, W_e^1, S_u^2$	57.29
17	$P_m^1, P_m^2, S_u^2$	14.13	42	$h_f^1, P_m^2, S_u^2$	58.57
18	$P_m^1, S_u^1, W_e^2$	14.13	43	$W_t^1, P_m^2, h_f^2$	60.69
19	$S_u^1, W_e^1, W_t^2$	15.24	44	$S_u^1, h_f^1, W_t^2$	62.43
20	$W_e^1, W_t^2, S_u^2$	15.27	45	$P_m^1, h_f^1, W_t^2$	62.89
21	$W_t^1, W_e^1, W_t^2$	15.58	46	$S_u^1, S_u^2, W_e^2$	63.04
22	$W_t^1, W_t^2, S_u^2$	16.83	47	$h_f^1, W_t^1, W_e^2$	63.64
23	$W_t^1, S_u^1, W_t^2$	16.96	48	$W_t^1, h_f^1, W_t^2$	65.83
24	$W_t^1, P_m^2, W_e^2$	16.99	49	$S_u^1, W_e^2, h_f^2$	68.65
25	$P_m^1, W_e^1, W_t^2$	19.67	50	$h_f^1, W_t^2, W_e^2$	68.88

Table 4.3b: Condition numbers for various combinations of shape functions of dual spherical indentation arranged in ascending order (rank 51-100).

Combination #	Shape function combination	Condition number ( $\kappa_m^{avg}$ )	Combination #	Shape function combination	Condition number ( $\kappa_m^{avg}$ )
51	$P_m^1, h_f^1, P_m^2$	71.23	76	$S_u^1, S_u^2, h_f^2$	97.28
52	$h_f^1, W_t^2, W_e^2$	71.58	77	$P_m^1, W_e^1, h_f^2$	98.35
53	$S_u^1, P_m^2, S_u^2$	72.30	78	$W_t^1, W_e^1, h_f^2$	99.38
54	$S_u^1, W_e^1, S_u^2$	73.19	79	$W_t^1, S_u^2, h_f^2$	102.1
55	$W_t^1, W_t^2, h_f^2$	74.12	80	$h_f^1, S_u^1, S_u^2$	102.4
56	$S_u^1, W_e^2, P_m^2$	75.28	81	$P_m^1, S_u^2, h_f^2$	106.6
57	$h_f^1, P_m^1, W_e^2$	76.39	82	$P_m^1, W_e^1, S_u^2$	111.3
58	$P_m^1, P_m^2, h_f^2$	76.71	83	$W_t^1, W_e^2, h_f^2$	115.7
59	$h_f^1, W_t^2, S_u^2$	77.21	84	$W_e^1, W_t^2, h_f^2$	118.2
60	$S_u^1, W_t^2, S_u^2$	77.26	85	$h_f^1, W_e^1, W_t^2$	118.8
61	$W_t^1, S_u^1, S_u^2$	78.96	86	$W_t^1, P_m^1, W_e^2$	123.1
62	$S_u^1, W_e^1, h_f^2$	79.58	87	$S_u^1, h_f^1, h_f^2$	123.1
63	$h_f^1, P_m^2, W_e^2$	79.67	88	$P_m^1, W_e^2, h_f^2$	134.7
64	$W_e^1, P_m^2, h_f^2$	79.83	89	$h_f^1, S_u^2, h_f^2$	149.1
65	$S_u^1, P_m^2, h_f^2$	80.52	90	$W_t^1, P_m^1, P_m^2$	166.0
66	$P_m^1, S_u^1, h_f^2$	80.57	91	$W_t^1, P_m^1, W_t^2$	187.5
67	$S_u^1, W_t^2, h_f^2$	82.42	92	$W_t^1, h_f^1, h_f^2$	192.2
68	$W_e^1, h_f^1, S_u^2$	82.65	93	$P_m^1, W_t^1, h_f^2$	204.0
69	$W_e^1, h_f^1, P_m^2$	85.57	94	$P_m^1, h_f^1, h_f^2$	211.8
70	$S_u^1, P_m^1, S_u^2$	85.76	95	$h_f^1, W_e^2, h_f^2$	243.3
71	$W_e^1, S_u^2, h_f^2$	87.50	96	$W_e^1, h_f^1, h_f^2$	253.1
72	$h_f^1, W_t^1, S_u^2$	88.95	97	$h_f^1, P_m^2, h_f^2$	254.2
73	$P_m^1, h_f^2, W_t^2$	93.93	98	$h_f^1, W_t^2, h_f^2$	255.1
74	$W_t^1, S_u^1, h_f^2$	94.28	99	$W_t^1, W_t^2, P_m^2$	282.0
75	$h_f^1, P_m^1, S_u^2$	95.87	100	$P_m^1, W_t^2, P_m^2$	295.1

We considered four half-angles,  $50^\circ$ ,  $60^\circ$ ,  $70^\circ$  and  $80^\circ$  to determine how sensitivity depends on the combination of the half-angles (for conical indentation). Table 4.2 and 4.3 show that the shape function combination giving the lowest condition number is  $W_e^2, S_u^1, W_e^1$ . Thus, for various choices of  $\alpha_1$  and  $\alpha_2$  among the four angles, condition numbers are computed for the shape function combination  $W_e^2, S_u^1, W_e^1$  and are tabulated in Table 4.4. We can see from Table 4.4 that the condition number decreases as the difference between half-angle increases (for example, the  $50^\circ$ - $80^\circ$  combination has lower condition number than the  $50^\circ$ - $60^\circ$  combination). Thus, the sensitivity of indentation tests can be decreased by increasing the difference between the half-angles. Table 4.4 also shows that for an identical difference between the two half-angles, the sensitivity of the system decreases as the smaller angle increases. For spherical indentation, we considered four depth-to-radius ratios, 10%, 20%, 30% and 40%. The condition numbers for the shape function combination  $W_e^2, S_u^1, W_e^1$  are tabulated in Table 4.4. The following observations are made with respect to the effect of depth-to-radius ratios on the sensitivity: i) sensitivity can be decreased by increasing the difference between the depth-to-radius ratios and ii) sensitivity can be decreased for the smaller depth-to-radius ratio for identical difference in depth-to-radius ratios. The conclusions regarding the effect of half-angles and depth-to-radius ratio combinations on sensitivity have been demonstrated for selected cases by previous researchers (Cao and Lu, 2004a, Cao and Lu, 2004b, Chen et al., 2007) and here we have shown them to be valid for a wider range.

Table 4.4: Condition numbers for various choices of half-angles (for conical indentation) and depth-to-radius ratios (for spherical indentation) for the shape function combination

Conical Indentation			Spherical Indentation		
$\alpha_1$	$\alpha_2$	$\kappa_m^{avg}$	$(h_m/R)_1$	$(h_m/R)_2$	$\kappa_m^{avg}$
50°	80°	5.62	10%	40%	7.66
60°	80°	7.17	10%	30%	9.67
50°	70°	9.45	20%	40%	12.9
70°	80°	10.7	10%	20%	15.1
60°	70°	15.8	20%	30%	20.9
50°	60°	16.6	30%	40%	24.4

### 4.3 Sensitivity Analysis

Condition number quantifies the sensitivity of indentation testing but does not give information about the actual amount of error that can occur in the determined material properties due to experimental error. Therefore, although the condition number can give guidelines about the relative sensitivity behavior of different indentation protocols, explicit sensitivity analysis is required to evaluate the practical reliability of indentation methodologies. This will be considered in the following section.

#### 4.3.1 Analysis procedure

In a sensitivity analysis scheme, the material properties are first determined via the (numerically) correct shape functions. These will be denoted by  $E_{ts}$ ,  $Y_{ts}$  and  $n_{ts}$ , where  $ts$  indicates the “true solution” (e.g. the solution obtained with the reverse analysis based on the numerically correct, unperturbed shape functions). Next, the shape functions are slightly perturbed, simulating an experimental error, and the material properties are determined. These will be denoted by  $E_{ps}$ ,  $Y_{ps}$  and  $n_{ps}$ , where  $ps$

indicates the perturbed solution. The quantity,  $\delta_{mp}$ , is defined below to measure in the difference between the true and perturbed solutions (material properties):

$$\delta_{mp} = \sqrt{\left(\frac{E^{ts} - E^{ps}}{E^{ts}}\right)^2 + \left(\frac{Y^{ts} - Y^{ps}}{Y^{ts}}\right)^2 + \left(\frac{n^{ts} - n^{ps}}{n^{ts}}\right)^2} \quad (4.11)$$

In different sensitivity analysis schemes, the perturbations are imposed on the shape functions in different ways. A popular scheme is the so called "one factor at a time" (One Factor scheme) (Chollacoop et al., 2003; Lan and Venkatesh, 2007; Le, 2008). In this scheme, one shape function is varied while the two others are kept constant. However, in a real experiment, errors may occur in all the shape functions simultaneously. Thus, the One Factor scheme is ineffective to capture the errors that may occur in a real experiment. In an alternative scheme (Hyun et al., 2011), all shape functions are increased or decreased uniformly by the same percentage amount (Uniform Factors scheme). However, neither does this scheme realistically represent errors as they occur in a real experiment since it appears unlikely that all measured data contain the same amount of error. A more effective sensitivity analysis scheme is to vary all the shape functions simultaneously by different amounts but keeping all of them within in a fixed limit (Cao and Lu, 2004a; Swaddiwudhipong et al., 2005). This is known as a Monte Carlo sensitivity analysis scheme. To the author's knowledge, so far the experimental errors in the shape functions from indentation testing have been reported to be within 5.1% (Wang et al., 2005; Chollacoop et al., 2003). We investigated sensitivity for three error ranges of  $\pm 1\%$ ,  $\pm 5\%$  and  $\pm 10\%$  with step sizes of 0.5%, 2.5% and 5% respectively. For example, for the  $\pm 5\%$  error range, each of the three shape functions is perturbed with 5 errors: 5%, -2.5%, 0%, 2.5% and 5% which gives a total of 125 possible combinations. The perturbations will be denoted as

follows: a perturbation of 5%, 2.5% and 0% error in the three selected shape functions respectively, will be denoted as (5, 2.5, 0). The procedure for the sensitivity analysis is as follows:

**Step 1:** A specific material (material properties denoted by  $E_{ts}$ ,  $Y_{ts}$  and  $n_{ts}$ ) is considered for sensitivity analysis. Finite element simulations of a dual indentation test (conical or spherical) for this material are conducted to obtain numerically correct shape functions.

**Step 2:** Reverse analysis and the algorithm outlined in section 1.1.3 (Figure 1.5) are used to determine the material properties using the shape functions obtained in the previous step. This gives the material properties based on the reverse analysis.

**Step 3:** Impose perturbations on the numerically correct shape functions (as obtained in step 1) according to Monte Carlo scheme, simulating the experimental errors.

Compute the material properties  $E_{ps}$ ,  $Y_{ps}$  and  $n_{ps}$  for all perturbations combinations. The combination which gives the largest  $\delta_{mp}$  is recorded along with the associated solution  $E_{ps}$ ,  $Y_{ps}$ ,  $n_{ps}$  for that particular combination.

**Step 4:** Finally, determine the differences (expressed in percentage) between the true and perturbed elastic modulus, yield strength and strain hardening exponent. These percentage differences illustrate how much the material properties can deviate for a given uncertainty in the experimental measurements of the shape functions.

#### **4.3.2 Sensitivity of dual indentation techniques**

In the following sections, the sensitivity analysis procedure described in the previous section is applied to various dual indentation scenarios. These studies will reveal the practical effectiveness of the various dual indentation methodologies. The

material considered has the following properties: elastic modulus,  $E^{ts} = 180$  GPa, yield strength,  $Y^{ts} = 300$  MPa and strain hardening exponent,  $n^{ts} = 0.25$ .

#### 4.3.2.1 Dual conical indentation ( $\alpha_1 = 50^\circ$ , $\alpha_2 = 80^\circ$ )

To test how well the condition number,  $\kappa_m^{avg}$ , correlates to the sensitivity analysis, the sensitivity analysis is applied for three shape functions combinations (Table 4): (i)  $(W_e^2, S_u^1, W_e^1)$ ,  $\kappa_m^{avg} = 5.8248$ ; (ii)  $(h_f^2, S_u^1, W_e^1)$ ,  $\kappa_m^{avg} = 42.715$ ; and (iii)  $(h_f^2, W_t^1, P_m^1)$ ,  $\kappa_m^{avg} = 322.06$ .

The results of the sensitivity analysis for the shape function combination  $(W_e^2, S_u^1, W_e^1)$  are tabulated in Table 4.5, where the (unperturbed) reverse analysis results are included for comparison. For small experimental error (perturbations of  $\pm 1\%$ ), this dual indentation method predicts the material properties quite well. However, for larger experimental error, significant errors in the determined material properties can occur. For example, the deviation in the material properties is more than 40% for the error combination of  $(-5, 2.5, 5)$ . The One Factor and Uniform Factors schemes do not predict as large a deviation in material properties as that predicted by the Monte Carlo sensitivity analysis procedure. This confirms that these two schemes are not able to capture the full regime of sensitivity behavior. It is interesting to note that the error case  $(-5, 2.5, 5)$  gives larger deviation than the error cases  $(10, 10, 10)$  or  $(-10, -10, -10)$ . In the first error case, both positive and negative perturbations are present whereas in the two later error cases, perturbations are of the same sign. This large sensitivity due to the presence of perturbations of different signs has been observed earlier (Hyun et al., 2011).

Table 4.5: Errors in calculated material properties based on Monte Carlo, One Factor and Uniform Factors sensitivity analysis for conical dual indentation with  $\alpha_1 = 50^\circ$  and  $\alpha_2 = 80^\circ$  and shape function combination  $(W_e^2, S_u^1, W_e^1)$ ,  $\kappa_m^{avg} = 5.8248$ .

Sensitivity Analysis	Material props	Percentage error in determined material properties			
		0%	$\pm 1\%$ (1, -1, 1)	$\pm 5\%$ (-5, 2.5, 5)	$\pm 10\%$ (-5, 10, -10)
Monte Carlo	<i>E</i>	-0.152	-1.40	8.96	-6.27
	<i>Y</i>	0.727	4.67	-45.7	-54.6
	<i>n</i>	-0.735	-4.51	41.9	50.7
One Factor	<i>E</i>	(10, 0, 0)	(0, 10, 0)	(0, 0, 10)	
	<i>Y</i>	-1.32	1.09	9.94	
	<i>n</i>	24.7	-13.1	0.616	
Uniform Factors	<i>E</i>	(10, 10, 10)	(-10, -10, -10)		
	<i>Y</i>	9.83	-10.1		
	<i>n</i>	10.8	-9.35		
	<i>n</i>	-0.735	-0.734		

The results that are obtained by applying the Monte Carlo sensitivity analysis procedure on the shape function combinations with larger condition numbers,  $(h_f^2, S_u^1, W_e^1)$ ,  $\kappa_m^{avg} = 42.715$  and  $(h_f^2, W_t^1, P_m^1)$ ,  $\kappa_m^{avg} = 322.06$  are tabulated in Table 4.6. For the combination  $(h_f^2, S_u^1, W_e^1)$ , when no perturbations are imposed on the shape functions, the dual indentation technique can determine the material properties quite

accurately. However, a small error in the experimental measurement can create large errors in the determined material properties. For the combination  $(h_f^2, W_t^1, P_m^1)$ , even with the exact values of the shape functions, the deviations in the determined material properties are very large. This seems to be due to the very large condition number: the problem is close to non-uniqueness and more than one material gives almost identical values of the shape functions. Due to the numerical fluctuations, the code picks up a material other than the original material. The sensitivity analysis results suggest that this is not a suitable dual indentation technique as suggested by large  $\kappa_m^{avg}$ .

From these examples, the correlation between the condition number and the Monte Carlo sensitivity analysis can be seen clearly. For the three shape function combinations considered, as the condition number increases, the sensitivity to the experimental errors increases.

Table 4.6: Errors in calculated material properties based on Monte Carlo sensitivity analysis procedure for conical dual indentation with  $\alpha_1 = 50^\circ$  and  $\alpha_2 = 80^\circ$  and shape function combination  $(h_f^2, S_u^1, W_e^1), \kappa_m^{avg} = 42.715$  and  $(h_f^2, W_t^1, P_m^1), \kappa_m^{avg} = 322.06$ .

Shape Function	Material props	Percentage error in determined material properties			
		0%	$\pm 1\%$	$\pm 5\%$	$\pm 10\%$
			(-1, -1, 1)	(-5, 5, 5)	(-10, 5, 5)
$(h_f^2, S_u^1, W_e^1),$ $\kappa_m^{avg} = 42.715$	<i>E</i>	-0.050	-1.75	-2.79	1.67
	<i>Y</i>	-1.27	49.6	181	189
	<i>n</i>	0.800	-34.2	-99.2	-99.9
$(h_f^2, W_t^1, P_m^1),$ $\kappa_m^{avg} = 322.06$		0%	$\pm 1\%$	$\pm 5\%$	$\pm 10\%$
			(1, -0.5, 1)	(0, 2.5, 5)	(-10, 5, 10)
	<i>E</i>	-7.27	37.4	73.4	-35.1
	<i>Y</i>	-33.3	158	155	183
	<i>n</i>	32.0	-100	-100	-88.7

#### 4.3.2.2 Dual spherical indentation: $(h_m/R_i)_1 = 10\%$ , $(h_m/R_i)_2 = 40\%$

A similar study is done for spherical indentation to verify the correlation between the condition number and spherical indentation. The three shape function combinations (Table 4.3c and 4.3d) considered are: (i)  $(W_e^2, S_u^1, W_e^1), \kappa_m^{avg} = 7.6837$ ; (ii)  $(W_t^2, W_t^1, h_f^1), \kappa_m^{avg} = 65.825$ ; and (iii)  $(h_f^2, W_e^1, h_f^1), \kappa_m^{avg} = 253.09$ .

The results of the sensitivity analysis for the shape function combination  $(W_e^2, S_u^1, W_e^1)$  are tabulated in Table 4.7, where the (unperturbed) reverse analysis

results are included for comparison. For experimental error within  $\pm 1\%$ , this dual indentation method can predict the material properties with errors less than 10%. However, for larger experimental error, significant errors are obtained. Neither the One Factor nor Uniform Factors schemes predict the largest deviation in the material properties as predicted by the Monte Carlo sensitivity analysis procedure.

For the combination  $(W_t^2, W_t^1, h_f^1)$ ,  $\kappa_m^{avg} = 65.825$  and  $(h_f^2, W_e^1, h_f^1)$ ,  $\kappa_m^{avg} = 253.09$ , the results of the Monte Carlo sensitivity analysis are tabulated in Table 4.8. The dual indentation technique with the shape function combination  $(W_t^2, W_t^1, h_f^1)$ , will perform well if there are no errors in the experimental measurement. However, a slight error in the experimental measurement can create large deviation in the determined material properties. For the combination  $(h_f^2, W_e^1, h_f^1)$ , even when the exact values of shape functions are used, the deviations in the determined material properties are very large. Thus this is not a suitable dual indentation technique, as suggested by the large value of  $\kappa_m^{avg}$ .

Table 4.7: Errors in calculated material properties based on Monte Carlo, One Factor and Uniform Factors sensitivity analysis procedure for spherical dual indentation with  $(h_m/R_i)_1 = 10\%$  and  $(h_m/R_i)_2 = 40\%$  and shape function combination  $(W_e^2, S_u^1, W_e^1)$ ,  $\kappa_m^{avg} = 7.6837$ .

Sensitivity Analysis	Material props	Percentage error in determined material properties			
		0%	$\pm 1\%$ (1, -1, 1)	$\pm 5\%$ (-5, 2.5, 5)	$\pm 10\%$ (-5, 10, -10)
Monte Carlo	<i>E</i>	1.33	1.83	7.20	7.40
	<i>Y</i>	3.12	9.45	-47.4	67.3
	<i>n</i>	-2.12	-7.03	41.4	-44.9
One Factor	<i>E</i>	(10, 0, 0)	(0, 10, 0)	(0, 0, 10)	
	<i>Y</i>	3.76	-0.657	11.6	
	<i>n</i>	-19.8	37.3	4.07	
Uniform Factors	<i>E</i>	(10, 10, 10)	(-10, -10, -10)		
	<i>Y</i>	11.5	-8.80		
	<i>n</i>	13.4	-7.19		
	<i>n</i>	-2.12	-2.12		

Table 4.8: Errors in calculated material properties based on Monte Carlo sensitivity analysis procedure for spherical dual indentation with  $(h_m/R_i)_1 = 10\%$  and  $(h_m/R_i)_2 = 40\%$  and shape function combination  $(W_t^2, W_t^1, h_f^1), \kappa_m^{avg} = 65.825$  and  $(h_f^2, W_e^1, h_f^1), \kappa_m^{avg} = 253.09$ .

Shape Function	Material props	Percentage error in determined material properties			
		<b>0%</b>	<b>± 1%</b>	<b>± 5%</b>	<b>± 10%</b>
$(W_t^2, W_t^1, h_f^1),$ $\kappa_m^{avg} = 65.825$			<b>(-1, -1, 1)</b>	<b>(-5, -5, 5)</b>	<b>(0, -10, 10)</b>
	<i>E</i>	-2.23	-8.80	-29.3	-38.3
	<i>Y</i>	2.21	23.3	125	178
	<i>n</i>	-0.912	-16.3	-82.4	-100
$(h_f^2, W_e^1, h_f^1),$ $\kappa_m^{avg} = 253.09$		<b>0%</b>	<b>± 1%</b>	<b>± 5%</b>	<b>± 10%</b>
			<b>(1, 0.5, 1)</b>	<b>(2.5, 2.5, 0)</b>	<b>(-10, -10, 5)</b>
	<i>E</i>	-0.890	10.2	65.6	-70.8
	<i>Y</i>	21.0	139	175	-71.9
	<i>n</i>	-18.7	-99.1	-94.8	91.3

Thus for spherical indentation as well, as the condition number increases, the sensitivity to experimental errors increases.

#### 4.3.2.3 Dual spherical indentation: $(h_m/R_i)_1 = 10\%$ and $1\%$ , $(h_m/R_i)_2 = 100\%$

In the previous section it was seen that, for dual spherical indentation with  $(h_m/R_i)_1 = 10\%$ ,  $(h_m/R_i)_2 = 40\%$ , when conducted even with the best shape function combination  $(W_e^2, S_u^1, W_e^1)$ , large deviation in the material properties results for the  $\pm 5\%$  error range. So, we considered two indentation protocols by increasing the

difference between the depth-to-radius ratios further, in hope of obtaining indentation protocols with moderate sensitivity due to experimental error<sup>4</sup>.

For dual spherical indentation with  $(h_m/R_i)_1 = 10\%$ ,  $(h_m/R_i)_2 = 100\%$ , and shape function combination  $(W_e^2, S_u^1, W_e^1)$ , the condition number is computed to be 4.1113.

With same shape function combination, the dual indentation with  $(h_m/R_i)_1 = 1\%$ ,  $(h_m/R_i)_2 = 100\%$  has a condition number of 2.6237, which is even smaller. The results obtained by applying the Monte Carlo sensitivity analysis procedure for these cases are tabulated in Table 4.9. These techniques will give good results when the experiments are conducted perfectly; and the sensitivity behaviors have improved compared to the previous case ( $(h_m/R_i)_1 = 10\%$ ,  $(h_m/R_i)_2 = 40\%$ ). However, for the dual indentation with  $(h_m/R_i)_1 = 10\%$ ,  $(h_m/R_i)_2 = 100\%$ , the error in the determined material properties can be more than 30% for  $\pm 10\%$  error range. For the combination  $(h_m/R_i)_1 = 1\%$ ,  $(h_m/R_i)_2 = 100\%$ , the error can be around 20% for  $\pm 10\%$  error range.

---

<sup>4</sup> Depth-to-radius ratio of 100% can be achieved by using a spherical indenter of sufficiently small radius ( $R_i$ ). If  $R_i$  is large, indentation depth will be large which may result in cracking (Chen et al., 2007) thus making the indentation analysis incorrect. Similarly depth-to-radius ratio of 1% can be achieved by keeping  $R_i$  large. If  $R_i$  is small, indentation depth will be small which will result in surface roughness effect (Kim et al., 2007) and size effect (Xu and Li, 2006), thus making the indentation analysis incorrect.

Table 4.9: Errors in calculated material properties based on Monte Carlo sensitivity analysis procedure for spherical dual indentation with  $(h_m/R_i)_1 = 10\%$ ;  $(h_m/R_i)_2 = 100\%$ ; shape function combination  $(W_e^2, S_u^1, W_e^1)$ ,  $\kappa_m^{avg} = 4.1113$  and  $(h_m/R_i)_1 = 1\%$ ;  $(h_m/R_i)_2 = 100\%$ ; shape function combination  $(W_e^2, S_u^1, W_e^1)$ ,  $\kappa_m^{avg} = 2.6237$ .

Shape Function	Material props	Percentage error in determined material properties			
$(h_m/R_i)_1 = 10\%$ and $(h_m/R_i)_2 = 100\%$  $(W_e^2, S_u^1, W_e^1)$ , $\kappa_m^{avg} = 4.1113$		0%	$\pm 1\%$ (1, -1, 1)	$\pm 5\%$ (5, -5, 5)	$\pm 10\%$ (10, -10, -5)
	$E$	1.78	3.08	8.33	-0.283
	$Y$	-1.52	-4.63	-17.2	-37.7
	$n$	2.20	4.84	15.7	32.9
$(h_m/R_i)_1 = 1\%$ and $(h_m/R_i)_2 = 100\%$  $(W_e^2, S_u^1, W_e^1)$ , $\kappa_m^{avg} = 2.6237$		0%	$\pm 1\%$ (1, -1, 1)	$\pm 5\%$ (5, -5, 5)	$\pm 10\%$ (10, -10, 10)
	$E$	0.778	1.86	5.77	9.88
	$Y$	-1.76	-3.74	-11.3	-22.4
	$n$	2.15	4.04	11.2	21.8

#### 4.3.2.4 Dual conical-spherical indentation: $\alpha_1 = 80^\circ$ , $(h_m/R_i)_2 = 100\%$ ; and $(h_m/R_i)_1 = 1\%$ , $\alpha_2 = 50^\circ$

Finally, we considered the possibility of using a combination of conical and spherical indentation to reduce the sensitivity due to experimental error. Liu et al, (2008) demonstrated that sharp and blunt half-angles of conical indentation may be considered equivalent to high and low depth-to-radius ratio of spherical indentation, respectively. Thus, we considered two combinations: i) combination of blunt half-

angle,  $\alpha_1 = 80^\circ$  and high depth-to-radius ratio,  $(h_m/R_i)_2 = 100\%$  and ii) combination of low-depth-to-radius ratio,  $(h_m/R_i)_1 = 1\%$  and sharp half-angle,  $\alpha_2 = 50^\circ$ . For these two cases, the condition numbers for the shape function combination  $(W_e^2, S_u^1, W_e^1)$  are computed to be 4.1599 and 4.7386, respectively. The results of Monte Carlo sensitivity analysis for these two cases are tabulated in Table 4.10. It can be seen that this technique will give good results when the experiments are conducted perfectly. However the sensitivity due to experimental error has increased compared to the case with  $(h_m/R_i)_1 = 1\%$ ,  $(h_m/R_i)_2 = 100\%$ .

Table 4.10: Errors in calculated material properties based on Monte Carlo sensitivity analysis for dual conical-spherical indentation with  $\alpha_1 = 80^\circ$ ,  $(h_m/R_i)_2 = 100\%$ ; and  $(h_m/R_i)_1 = 1\%$ ,  $\alpha_2 = 50^\circ$  with shape function combination  $(W_e^2, S_u^1, W_e^1)$ . Condition numbers are 4.1599 and 4.7386 respectively.

Shape Function	Material props	Percentage error in determined material properties			
		0%	$\pm 1\%$	$\pm 5\%$	$\pm 10\%$
$\alpha_1 = 80^\circ$ and $(h_m/R_i)_2 = 100\%$  $(W_e^2, S_u^1, W_e^1)$ , $\kappa_m^{avg} = 4.1599$					
	<i>E</i>	0.192	1.26	5.58	11.5
	<i>Y</i>	-1.90	-4.38	-13.8	-28.5
	<i>n</i>	2.12	4.33	12.9	27.1
$(h_m/R_i)_1 = 1\%$ and $\alpha_2 = 50^\circ$  $(W_e^2, S_u^1, W_e^1)$ , $\kappa_m^{avg} = 4.7386$					
	<i>E</i>	0.696	1.80	-5.13	-9.83
	<i>Y</i>	-0.499	-3.14	13.9	29.1
	<i>n</i>	0.409	3.17	-14.3	-29.4

#### 4.3.2.5 Sensitivity behavior across material range

As discussed in section 1.1.1, the condition number and thereby the sensitivity of a dual indentation technique due to experimental error depends on the material being considered. Based on our investigation of various dual indentation protocols presented in previous section, the dual spherical indentation with  $(h_m/R_i)_1 = 1\%$  and  $(h_m/R_i)_2 = 100\%$  and shape function combination  $(W_e^2, S_u^1, W_e^1)$  is found to be least sensitive to experimental errors. To investigate the effectiveness of this dual

indentation technique over a range of materials, the Monte Carlo sensitivity analysis ( $\pm 5\%$  error range) is applied to this technique for 9 materials, which are situated in a rectangular grid of the  $E/Y-n$  space considered (see Table 4.11). For some materials, the deviation in the determined material properties from the actual material properties can be seen to be quite high (more than 80%), whereas for some materials, the deviation is about 10%. Since the actual material properties of the tested material are not known a priori, the reliability of the determined material properties from an indentation test is therefore questionable. Thus, it is more suitable to construct a confidence domain (Moussa et al., 2014) where a range of material parameter sets is determined in which the actual material properties will lie. Nevertheless, caution has to be exercised in doing an indentation test to ensure that experimental errors are sufficiently small.

Table 4.11: Errors in calculated material properties based on Monte Carlo sensitivity analysis for 9 selected materials spanning the  $E/Y-n$  space for spherical dual indentation with  $(h_m/R_i)_1 = 1\%$  and  $(h_m/R_i)_2 = 100\%$  and shape function combination  $(W_e^2, S_u^1, W_e^1)$ .

Material Properties					Percentage error in		
$E$ (GPa)	$Y$ (MPa)	$E/Y$	$n$	Error case	$E$	$Y$	$n$
180	1200	150	0.45	(-5, 5, -5)	-7.30	23.6	-9.83
180	360	500	0.45	(-5, 5, -5)	-3.29	18.3	-5.98
180	189	950	0.45	(5, -5, 5)	20.8	-8.72	0.358
180	1200	150	0.25	(-5, 5, -5)	-4.95	15.3	-17.8
180	360	500	0.25	(5, -5, 5)	5.39	-11.6	11.2
180	189	950	0.25	(-5, 5, 5)	5.84	16.9	-11.7
180	1200	150	0.05	(5, -5, 5)	3.86	-11.3	88.2
180	360	500	0.05	(-5, 5, -5)	-2.79	11.9	-76.9
180	189	950	0.05	(5, 2.5, -5)	-7.35	-9.98	39.1

#### **4.4 Sensitivity of Dual Indentation for Transversely Isotropic, Linear-elastic, Perfectly-plastic Materials**

A literature review regarding the available indentation methodologies for determining the material properties of anisotropic materials is presented in Chapter 1, section 1.7. Systematic dual indentation protocols with selected combinations of shape functions, half-angles (for conical indentation) and depth-to-radius ratios (for spherical indentation) can be developed for transversely isotropic, linear-elastic, perfectly-plastic material and is described in sections 1.4 and 1.6. Sensitivity behavior of such dual indentation protocols due to experimental error is investigated using the concept of condition number similar to that previously presented for isotropic materials. For this analysis, the functional forms of  $\bar{G}_i^p$  ( $i = 1-5$ ) used in Eqs. (1.16) of section 1.7 are required and are described in section 3.3, Chapter 3.

##### **4.4.1 Condition numbers and sensitivity**

In section 4.2, the concept of condition number was used to assess the sensitivity of dual indentation methodologies for isotropic materials. As the condition number increased, sensitivity of the indentation system due to experimental error increased. The grid for computing the modified condition number,  $\kappa_m$  consisted of 200 points for each material parameters thus in total,  $8 \times 10^6$  grid points were used (there were three material parameters). For transversely isotropic material, since there are four material parameters, 200 points for each material parameter would imply in total,  $1.6 \times 10^9$  points. With such a large number of grid points, a typical computation of  $\kappa_m$  requires a CPU time of around 20 hours (in a DELL OPTIPLEX 990 personal computer with Intel Core™ i5-2500 3.30 GHz Processor), and thus it will take around 330 days to do all the computations required for this study (around 400). Instead, 50 grid points are used, which resulted in CPU time of around 5 minutes. The average

modified condition number,  $\kappa_m^{avg}$  is computed by taking average over the following 64 (4 x 4 x 4) material points:  $E_z/E_x=10, 20, 30, 40$ ;  $E_x/G_{xz}= 2, 2.5, 3, 3.5$ ;  $E_x/\sigma_Y= 45, 115, 185, 255$ .

Considering the conical indenter (and similarly for spherical indentation), the four shape functions required to obtain the material properties can be selected from two indentation geometries in three ways: i) selecting one shape function from half-angle  $\alpha_1$  and three shape functions from half-angle  $\alpha_2$ ; ii) two from  $\alpha_1$  and two from  $\alpha_2$ ; and iii) three from  $\alpha_1$  and one from  $\alpha_2$ . Since five shape functions can be obtained from each test, a simple calculation shows that altogether 200 such combinations of shape functions are possible. Shape functions selected from half-angle  $\alpha_1$  and  $\alpha_2$  ( $(h_m/R)_1$  and  $(h_m/R)_2$  for spherical indentation) will be denoted by superscripts 1 and 2, respectively, similar to the case of isotropic materials.

For isotropic materials, as discussed in section 4.2.5, the sensitivity of the dual indentation tests to experimental error can be decreased by increasing the difference between half-angles (for conical indentation) or depth-to-radius ratios (for spherical indentation). The condition numbers for various combinations of half-angles and depth-to-radius ratios are tabulated in Table 4.12. Similarly, for transversely isotropic materials, condition number decreases as the difference between half-angles or depth-to-radius ratios increases.

Table 4.12: Condition numbers for various combinations of half-angles (conical indentation) and depth-to-radius ratios (spherical indentation). As the difference between half-angles or depth-to-radius ratio increases, sensitivity to experimental error decreases.

Conical Indentation ( $W_t^1, W_e^1, S_u^2, W_e^2$ )			Spherical Indentation ( $S_u^1, W_e^1, P_m^2, W_e^2$ )		
$\alpha_1$	$\alpha_2$	$\kappa_{m2}^{avg}$	$(h_m/R_i)_1$	$(h_m/R_i)_2$	$\kappa_{m2}^{avg}$
50°	80°	11.14669	20%	40%	10.49528
60°	80°	12.3324	20%	60%	9.320865
70°	80°	17.7795	20%	80%	8.935374

For  $\alpha_1 = 45^\circ$ ,  $\alpha_2 = 80^\circ$  (conical indentation) and  $(h_m/R_i)_1 = 1\%$ ,  $(h_m/R_i)_2 = 100\%$  (spherical indentation), condition numbers for various combinations of shape functions are tabulated in Table 4.13 (only selected combinations are shown for brevity). The half-angles and depth-to-radius ratios are selected to consider maximum possible differences among themselves. The shape functions  $S_u$  and  $W_e$  occur frequently in the first few combinations, and the shape function  $h_f$  occurs frequently in the last few combinations (similar to isotropic materials, section 4.2.5). Further, the condition numbers are more than 10. From the definition of the condition number, using a large number (e.g. 200) of grid points would result in even larger values. The condition number,  $\kappa_m^{avg}$  for two combinations giving minimum condition numbers, ( $P_m^2, W_e^1, S_u^1, W_e^2$ ) for conical indentation and ( $S_u^1, W_e^1, P_m^2, W_e^2$ ) for spherical indentation (Table 4.14)) are computed to be 23.2 and 27.6, respectively. From section 4.2.5, the dual indentation tests with  $\kappa_m^{avg} \sim 6$ , can determine the material properties accurately only when the experimental error is in the order of 1%. Thus, indentation tests of transversely isotropic materials are in general more sensitive to experimental errors compared to isotropic materials.

In the present study, it is assumed that both the indentations (for dual indentation) are performed perpendicular to the plane of isotropy. Several researchers (McAllister et al., 2012; Ebenstein and Wahl, 2006) have attempted two indentation tests along two different directions (perpendicular and parallel to the plane of isotropy). It is likely that the elastic modulus in the direction of the indentation will affect the response in that direction more strongly. Therefore, the sensitivities of such dual indentation tests are expected to be less than the sensitivity of the tests which consider two indentations along the same direction. Such dual indentation scenarios were not considered here due to computational limitations, as three-dimensional models are required to simulate indentation parallel to the plane of isotropy.

Table 4.13: Condition numbers for various combinations of shape functions arranged in ascending order

Combination #	Conical indentation $\alpha_1 = 45^\circ, \alpha_2 = 80^\circ$		Spherical indentation $(h_m/R_i)_1 = 1\%, (h_m/R_i)_2 = 100\%$	
	Shape function combination	$\kappa_m^{avg}$	Shape function combination	$\kappa_m^{avg}$
1	$S_u^1, W_e^1, P_m^2, W_e^2$	11.06	$P_m^1, W_e^1, S_u^2, W_e^2$	12.47
2	$P_m^1, S_u^1, P_m^2, W_e^2$	12.38	$P_m^1, S_u^1, W_e^1, W_e^2$	13.28
3	$S_u^1, W_e^1, P_m^2, S_u^2$	12.68	$W_t^1, W_e^1, S_u^2, W_e^2$	13.38
4	$S_u^1, W_e^1, S_u^2, W_e^2$	12.94	$S_u^1, W_e^1, S_u^2, W_e^2$	14.41
5	$S_u^1, W_e^1, W_t^2, W_e^2$	13.70	$W_t^1, S_u^1, W_e^1, W_e^2$	14.77
6	$P_m^1, P_m^2, S_u^2, W_e^2$	13.99	$W_e^1, W_t^2, S_u^2, W_e^2$	15.05
7	$P_m^1, S_u^1, S_u^2, W_e^2$	14.06	$W_e^1, P_m^2, S_u^2, W_e^2$	15.07
8	$P_m^1, S_u^1, W_t^2, W_e^2$	14.15	$P_m^1, W_e^1, S_u^2, h_f^2$	16.15
9	$W_t^1, S_u^1, P_m^2, W_e^2$	14.17	$W_t^1, W_e^1, S_u^2, h_f^2$	16.15
10	$P_m^1, S_u^1, h_f^2, W_e^2$	14.36	$P_m^1, S_u^1, W_e^1, S_u^2$	16.30
:	:	:	:	:
98	$S_u^1, W_t^2, P_m^2, W_e^2$	27.91	$P_m^1, S_u^1, h_f^1, P_m^2$	31.20
99	$S_u^1, h_f^1, W_t^2, h_f^2$	27.98	$P_m^1, h_f^1, P_m^2, S_u^2$	31.40
100	$W_t^1, h_f^1, P_m^2, W_e^2$	28.27	$P_m^1, S_u^1, W_t^2, h_f^2$	31.45
101	$W_t^1, h_f^1, W_t^2, S_u^2$	28.50	$W_t^1, W_e^1, P_m^2, h_f^2$	31.56
102	$S_u^1, W_t^2, S_u^2, h_f^2$	28.62	$W_t^1, W_e^1, W_t^2, h_f^2$	31.65
:	:	:	:	:
196	$S_u^1, W_t^2, P_m^2, h_f^2$	69.89	$h_f^1, W_t^2, P_m^2, S_u^2$	90.68
197	$W_e^1, W_t^2, P_m^2, h_f^2$	79.33	$S_u^1, W_t^2, P_m^2, h_f^2$	98.52
198	$h_f^1, W_t^2, P_m^2, h_f^2$	104.4	$W_e^1, h_f^1, W_t^2, P_m^2$	112.25
199	$P_m^1, W_t^2, P_m^2, h_f^2$	110.5	$W_t^1, P_m^1, W_t^2, P_m^2$	165.23
200	$W_t^1, W_t^2, P_m^2, h_f^2$	121.6	$h_f^1, W_t^2, P_m^2, h_f^2$	183.30

## 4.5 Summary

A systematic investigation of the uniqueness and sensitivity to experimental error for dual indentation methodologies is presented in this chapter. The observations can be summarized as follows.

The concept of condition number and iso- $(P_m/S_u h_m)$  lines are used to provide a comprehensive quantitative description of the uniqueness and sensitivity issues in indentation tests. In fact, non-uniqueness may be considered an extreme case of sensitivity for experimental errors. The concept of condition number is used to rank different choices of half-angles (dual conical indentation), depth-to-radius ratios (dual spherical indentation) and shape functions in terms of sensitivity due to experimental error. While condition numbers are easier to compute than performing sensitivity analyses and can provide a preliminary guideline about the sensitivity of an indentation technique, they are not a complete substitute for the sensitivity analysis. Thus different sensitivity analysis techniques are used to gain deeper insight.

Some dual indentation protocols with shape function combinations such as  $(h_f^2, W_e^1, h_f^1)$  and  $(h_f^2, P_m^1, h_f^1)$  are even more ineffective than single indentation protocols. The Monte Carlo sensitivity analysis procedure is demonstrated to be more effective in taking into account the errors occurring in a real experiment than both the One Factor (shape functions varied one at a time) and the Uniform Factors (all shape functions increased or decreased by same amount) scheme.

For isotropic materials, the most effective (least sensitive) dual indentation technique is suggested to be spherical dual indentation with  $(h_m/R_i)_1 = 1\%$  and  $(h_m/R_i)_2 = 100\%$  and shape function combination  $(W_e^2, S_u^1, W_e^1)$ . It appears that many dual indentation protocols are reliable when the experimental error is within  $\pm 1\%$ . However, for the error range of  $\pm 5\%$ , all three material properties cannot be determined with moderate

sensitivity even using the best dual indentation technique. New dual indentation protocols need to be developed to overcome the problem of sensitivity to experimental error.

Based on the computed condition numbers, it appears that indentation of transversely isotropic material is, in general, more sensitive to experimental errors compared to isotropic materials (when both indentations are along the direction perpendicular to the plane of isotropy). This result is likely related to the need for four material properties to be determined from the force-displacement relationships instead of three (for isotropic materials). By comparing the computed condition numbers, it appears that if dual indentation tests are conducted along the same direction of anisotropy, the experiments need to be highly accurate for determining the material properties accurately. Thus, dual indentation techniques with two tests performed in two different directions of anisotropy need to be investigated as a means for reducing the sensitivity due to experimental error.

## Chapter 5

### CONCLUDING REMARKS AND FUTURE WORK

In this thesis, contributions have been made to advance the evaluation of indentation testing in three areas:

1. **Geometry:** Most indentation techniques are limited to flat substrates. This thesis attempts to extend this geometric limitation and investigate indentation of a spherical object. Methodologies for other non-flat substrates can be developed following a similar approach.
2. **Reliability:** Non-uniqueness and sensitivity due to experimental errors of indentation testing are important practical problems. An investigation of these two issues for selected indentation geometries and material types are presented. Different indentation protocols are ranked according to sensitivity. The results suggest that indentation tests need to be very accurate to measure the material properties accurately.
3. **Material properties:** Few studies have been conducted to advance the understanding of indentation of anisotropic materials. A study of sensitivity due to experimental error of selected indentation protocols for transversely isotropic, linear-elastic, perfectly-plastic material is presented in this thesis.

#### 5.1 Concluding Remarks

Some of the key observations from this work are as follows:

##### 5.1.1 Geometry

To expand the prevailing indentation testing of flat surfaces, conical indentation of a sphere made of isotropic, linear-elastic, perfectly-plastic material was considered. Two methodologies were proposed to determine the material properties. The first methodology was based on finite element based reverse analysis technique,

which is typically used to determine the material properties of flat substrates using indentation testing. The second methodology was a semi-analytical method in which the problem was divided into two sub-problems and the analytical solutions of those two contact problems were utilized. In this method, the concept of elastic unloading was used to determine the elastic modulus similar to the Oliver-Pharr method for flat substrates.

As an extension of the work on conical indentation of a half-space, a semi-analytical method to determine the force-displacement relationship for conical indentation of a viscoelastic sphere was discussed in this thesis. The proposed technique is based on the method of functional equations that was developed to obtain the viscoelastic solution of a problem from the corresponding elastic solution. In the work of Vandamme and Ulm (2006), the Galin-Sneddon's analytical solution for the elastic problem was utilized. However for the conical indentation of a sphere, no such analytical solution is available. Thus for this problem, the elastic solution of the problem was obtained from finite element analysis.

### **5.1.2 Reliability**

When using a material model that includes plastic hardening during yielding, several materials can give identical force-displacement relationships. A methodology was presented to systematically identify the material parameter sets that will give identical force-displacement relationships. The methodology is based on comparing a limited set of shape functions of the force-displacement relationship. The methodology was illustrated for various indentation geometries and material models. It was concluded that a single indentation test, although simpler compared to a dual

indentation test, cannot be used to determine the material properties of a material uniquely.

Sensitivity to errors in the experimental measurements of an indentation test determines the practical usefulness of the experiment. This work illustrated that non-uniqueness of force-displacement relationship and sensitivity due to experimental error are not independent phenomena in that non-uniqueness is an extreme case of sensitivity. Selected test conditions (such as shape functions, half-angles and depth-to-radius ratios) resulting in different amount of sensitivities were ranked using condition numbers. This results in a set of guidelines for the experimentalists involving suitable selection of geometrical parameters and shape functions to improve the reliability of the experiment. It appears that, in general, the indentation experiments need to be very accurate to determine the material properties accurately. Since the reliability of the determined material parameter set depends on the actual material properties, which are not known a priori, it is suggested that a confidence domain is used to evaluate the reliability of the determined material parameter set.

### **5.1.3 Material properties**

Dual indentation of transversely isotropic, linear-elastic, perfectly-plastic material was considered. Condition numbers for several dual indentation protocols were computed. Similar to isotropic materials, and for transversely isotropic materials as well, the experiments need to be highly accurate to determine the material properties accurately. Further, the values of the computed condition numbers suggest that sensitivity for transversely isotropic materials is more than that for isotropic materials (assuming both indentations are performed along the direction perpendicular to the plane of isotropy). This might be due to the fact that for transversely isotropic,

linear-elastic, perfectly-plastic materials, more material parameters are involved compared to isotropic, linear-elastic, and power-law hardening materials.

In addition to the specific findings listed above, we also found that dimensional analysis (Buckingham PI theorem) can be a very important tool to reduce the computational costs involved in indentation analysis. In this work, the relationships between the shape functions of the force-displacement relationship and the material properties were determined numerically using extensive finite element simulations. The computational cost involved in such finite element analyses could be reduced greatly by using the non-dimensional forms of such relationships.

## **5.2 Suggested Future Work**

The following directions for future studies may be noted:

In section 2.1, conical indentation of a sphere made of linear-elastic, perfectly-plastic material was considered. It was shown that the basic principle involved in the finite element based reverse analysis methodologies remain the same for flat and non-flat substrates. Consequently, the proposed methodologies can be extended for other non-flat substrates as well. For example, for conical indentation of an infinitely long cylinder (e.g. micro-fiber), non-dimensional relationships between the shape functions and the material properties can be derived for fixed values of half-angle and depth-to-radius ratio, using a procedure similar to that outlined in section 2.1.2.3. The obtained relationships can be inverted to express the material properties in terms of shape functions using a procedure similar to that outlined in section 2.1.2.3. Thus, an algorithm similar to that depicted in Figure 2.8 can be obtained for determining the material properties of a micro-fiber. However, a three-dimensional model would be

required for this case instead of the axisymmetric two-dimensional model, resulting in a significant increase in computational cost.

The method presented in section 2.2, to obtain the force-displacement relationship for conical indentation of a viscoelastic sphere, can be easily extended to other indenter/substrate geometries for which no analytical solutions are available. For example, for spherical indentation of a cylinder, the elastic solution can be obtained using finite element simulations and regression analysis using a procedure similar to as outlined in section 2.2.1.1. Then, the method of functional equations can be applied to obtain the corresponding viscoelastic solution using a procedure similar to that outlined in section 2.2.1.2.

The method presented in Chapter 3 for identifying materials with identical force-displacement relationships, was shown to be independent of any specific indentation geometry or material model. Consequently, the method can be extended to more complicated indentation geometries and material models. For example, for conical indentation of a half-space made of viscoelastic material, the non-dimensional relationships between the shape functions and the material properties can be obtained using procedures similar to that described in section 1.4. Thereafter, a fixed material can be considered and the materials with force-displacement relationship identical to that of the fixed material can be obtained by comparing the shape functions using a procedure similar to that outlined in section 3.4.1. However, the regression analysis will be more extensive for this case.

In this work, indentation of transversely isotropic materials along only one direction of anisotropy was considered. Dual indentation with indentation on two different directions of anisotropy may reduce the sensitivity and could be a subject of

future study. For example, for transversely isotropic, elastic, perfectly-plastic materials, four shape functions need to be selected from indentation tests in both directions. Then, a procedure similar to that outlined in section 4.4.1 can be used to determine the condition numbers and assess the relative sensitivity due to experimental error. A three-dimensional model would be required instead of the two-dimensional axisymmetric model, again resulting in a significant increase in computational cost.

In Chapter 4, sensitivity of indentation methodologies which utilize only the force-displacement relationship from an indentation test is considered. Several indentation methodologies (Tabor, 1951; Taljat et al., 1998; Kang et al., 2013; Xu and Chen, 2010) have been developed which utilize the projected contact radius at maximum depth of penetration to extract the material properties. Sensitivity of such methodologies can be a subject of future study. The constitutive relationships between the contact radius and the material properties can be obtained using a procedure similar to as presented in section 3.3, where the relationships between the shape functions and the material properties are derived. Then, the condition number for different combinations can be computed and Monte Carlo sensitivity analysis can be carried out to assess the sensitivity similar to as done in Chapter 4 for force-displacement relationship based methodologies.

Similar to dual indentation tests for time-independent materials discussed in Chapter 4, recently a multi-curve method (Zhai and McKenna, 2014) has been proposed for efficient extraction of the material properties of time-dependent materials. In this method, several force-displacement relationships with different indentation and loading rates are utilized. Application of condition number for suitable

selection of the indentation and loading rates for minimizing sensitivity due to experimental error can be a subject of future study. For this, condition numbers for various combinations of indentation and loading rates can be computed utilizing the relationship between the material properties and force-displacement relationship. However, the computational cost involved in this case will be much higher compared to the present work since the number of material parameters involved in modeling time-dependent materials can be much larger than for time-independent materials.

It is discussed that the deviation in the determined material properties from the actual material properties depends on the actual material properties which are not known a priori in an indentation test. Therefore, instead of determining a single material parameter set, Moussa et al. (2014) proposed the construction of a confidence domain for the material parameters (assuming experimental error to be within a fixed amount) in which the actual material properties will lie. Relationship of such confidence domain with the condition number of the adopted methodology and its extension to transversely isotropic materials can be a subject of future study. A reasonable speculation is that the confidence domain will become narrower as condition number decreases. The procedure for the study will be similar to the procedure adopted in establishing the correlation between condition number and Monte Carlo sensitivity analysis (section 4.3.2).

### **5.3 Summary**

The work presented in this dissertation expands the scope of instrumented indentation technique for determining the mechanical properties for a wider range of substrate geometries (e.g. spherical substrates) and material types (e.g. viscoelastic and transversely isotropic materials). Furthermore, it provides cautions and guidelines

to the experimentalists regarding proper utilization of the indentation test data for determining the mechanical properties with improved accuracy.

The work opens up opportunities for future researchers to expand the utility of indentation technique for reliable characterization of a large number of material systems.

## REFERENCES

- Abaqus Theory Manual, 2009. Version 6.9-2. Dassault Systemes
- Aguilar-Santillan, J., 2008, "Elastic and hardness anisotropy and the indentation size effect of pyrite (FeS<sub>2</sub>) single crystal", *Acta Materialia*, Vol 56, pp 2476-2487.
- Alkorta, J., Martínez-Esnaola, J.M., Sevillano, J.G., 2005, "Absence of one-to-one correspondence between elastoplastic properties and sharp-indentation load-penetration data", *Journal of Materials Research*, Vol 20, pp 432-437.
- Amitay-Sadovsky, E., Cohen, S.R., Wagner, H.D., 1999, "Anisotropic nanoindentation of transcrystalline polypropylene by scanning force microscope using blade-like tips", *Applied Physics Letters*, Vol 74, pp 2966-2968.
- Arora, J., 2012, "Introduction to Optimum Design", Elsevier
- Bowden, F. P., Tabor, D., 2001, "The Friction and Lubrication of Solids", Oxford University Press.
- Bower, A. F., 2011, "Applied Mechanics of Solids", CRC Press
- Brookes, C.A., O'Neill, J.B., Redfern, B.A.W., 1971, "Anisotropy in the Hardness of Single Crystals", *Proceedings of the Royal Society of London. A. Mathematical and Physical Sciences*, Vol 322, pp 73-88.
- Bucaille, J.L., Stauss, S., Felder, E., Michler, J., 2003, "Determination of plastic properties of metals by instrumented indentation using different sharp indenters", *Acta Materialia*, Vol 51, pp 1663-1678.
- Buckingham, E., 1914, "On physically similar systems; illustrations of the use of dimensional equations", *Physics Review*, Vol 4, pp 345-376.
- Cao, Y.P., Lu, J., 2004, "Depth-sensing instrumented indentation with dual sharp indenters: stability analysis and corresponding regularization schemes", *Acta Materialia*, Vol 52, pp 1143-1153.
- Cao, Y.P., Lu, J., 2004, "A new method to extract the plastic properties of metal materials from an instrumented spherical indentation loading curve", *Acta Materialia*, Vol 52, pp 4023-4032.

- Cao, Y.P., Qian, X.Q., Lu, J., Yao, Z.H., 2005, "An energy-based method to extract plastic properties of metal materials from conical indentation tests", *Journal of Materials Research*, Vol 20, pp 1194-1206.
- Cao, Y., Huber, N., 2006, "Further investigation on the definition of the representative strain in conical indentation", *Journal of Materials Research*, Vol 21, pp 1810-1821.
- Capehart, T.W., Cheng, Y.-T., 2003, "Determining constitutive models from conical indentation: Sensitivity analysis", *Journal of Materials Research*, Vol 18, pp 827-832.
- Carnelli, D., Lucchini, R., Ponzoni, M., Contro, R., Vena, P., 2011, "Nanoindentation testing and finite element simulations of cortical bone allowing for anisotropic elastic and inelastic mechanical response", *Journal of Biomechanics*, Vol 44, pp 1852-1858.
- Chollacoop, N., Dao, M., Suresh, S., 2003, "Depth-sensing instrumented indentation with dual sharp indenters", *Acta Materialia*, Vol 51, pp 3713-3729.
- Cheng, Y.T., Cheng, C.M., 1998, "Scaling approach to conical indentation in elastic-plastic solids with work hardening", *Journal of Applied Physics*, Vol 84, pp 1284-1291
- Cheng, Y.T., Cheng, C.M., 1999, "Can stress-strain relationships be obtained from indentation curves using conical and pyramidal indenters?", *Journal of Materials Research*, Vol 14, pp 3493-3496.
- Cheng, Y.T., Cheng, C.M., 2004, "Scaling, dimensional analysis, and indentation measurements. *Materials Science and Engineering: R: Reports*", Vol 44, pp 91-149.
- Cheng Y.T., Cheng C.M., 2005, "General relationship between contact stiffness, contact depth, and mechanical properties for indentation in linear viscoelastic solids using axisymmetric indenters of arbitrary profiles", *Applied Physics Letters*, Vol 87, article # 111914.
- Cheng L., Xia X., Scriven L.E., Gerberich W.W., 2005, "Spherical-tip indentation of viscoelastic material", *Mechanics of Materials*, Vol 37, pp 213-226.
- Chen, X., Yan, J., Karlsson, A., 2006, "On the determination of residual stress and mechanical properties by indentation", *Materials Science and Engineering*, Vol 416, pp 139-149.

- Chen, X., Ogasawara, N., Zhao, M., Chiba, N., 2007, "On the uniqueness of measuring elastoplastic properties from indentation: the indistinguishable mystical materials", *Journal of Mechanics and Physics of Solids*, Vol 55, pp 1618-1660.
- Cox, M.A.J., Driessen, N.J.B., Boerboom, R.A., Bouten, C.V.C., Baaijens, F.P.T., 2008, "Mechanical characterization of anisotropic planar biological soft tissues using finite indentation: Experimental feasibility", *Journal of Biomechanics*, Vol 41, pp 422-429.
- Cui, F.Z., Wen, H.B., Zhang, H.B., Li, H.D., Liu, D.C., 1994, "Anisotropic indentation morphology and hardness of natural ivory", *Materials Science and Engineering: C*, Vol 2, pp 87-91.
- Dao, M., Chollacoop, N., Van Vliet, K.J., Venkatesh, T.A., Suresh, S., 2001, "Computational modeling of the forward and reverse problems in instrumented sharp indentation", *Acta Materialia*, Vol 49, pp 3899-3918.
- Dao, M., Lim, C., Suresh, S., 2003, "Mechanics of the human red blood cell deformed by optical tweezers", *Journal of Mechanics and Physics of Solids*, Vol 51, pp 2259-2280.
- Datta, B.N., 2010, "Numerical Linear Algebra and Applications", Society for Industrial and Applied Mathematics
- Delafargue, A., Ulm, F.-J., 2004, "Explicit approximations of the indentation modulus of elastically orthotropic solids for conical indenters", *International Journal of Solids and Structures*, Vol 41, pp 7351-7360.
- Dieter, G., 1976, "Mechanical Metallurgy", Second ed., McGraw-Hill, New York
- Ebenstein, D.M., Wahl, K.J., 2006, "Anisotropic nanomechanical properties of *Nephila clavipes* dragline silk", *Journal of Materials Research*, Vol 21, pp 2035-2044.
- Fan, Z., Swadener, J.G., Rho, J.Y., Roy, M.E., Pharr, G.M., 2002, "Anisotropic properties of human tibial cortical bone as measured by nanoindentation", *Journal of Orthopaedic Research*, Vol 20, pp 806-810.
- Feng, G., and Ngan, A. H. W., 2002, "Effects of Creep and Thermal Drift on Modulus Measurement Using Depth-Sensing Indentation," *Journal of Materials Research*, 17(03), pp. 660-668.
- Field, J. S., and Swain, M. V., 1995, "Determining the Mechanical Properties of Small Volumes of Material from Submicrometer Spherical Indentations," *Journal of Materials Research*, 10(01), pp. 101-112.

- Francius G., Hemmerlé J., Ball V., Lavallo P., Picart C., Voegel J.C., 2007, "Stiffening of soft polyelectrolyte architectures by multilayer capping evidenced by viscoelastic analysis of AFM indentation measurements", *Journal of Physical Chemistry C*, Vol 111, pp 8299-8306.
- Franzoso, G., 2008, "Elastic anisotropy of lamellar bone measured by nanoindentation", PhD Dissertation, Politecnico Di Milano
- Fu, G., 2007, "An Extension of Hertz's Theory in Contact Mechanics", *Journal of Applied Mechanics*, Vol 74, pp 373-374.
- Galin, L.A., 1961, "Contact problems in the theory of elasticity", I.N. (Ed.) North Carolina State University
- Green, I., 2005, "Poisson ratio effects and critical values in spherical and cylindrical Hertzian contacts", *International Journal of Applied Mechanics and Engineering*, Vol 10, pp 451-462
- Gindl, W., Gupta, H.S., 2002, "Cell-wall hardness and Young's modulus of melamine-modified spruce wood by nano-indentation", *Composites Part A: Applied Science and Manufacturing*, Vol 33, pp 1141-1145.
- Gindl, W., Schöberl, T., 2004, "The significance of the elastic modulus of wood cell walls obtained from nanoindentation measurements", *Composites Part A: Applied Science and Manufacturing*, Vol 35, pp 1345-1349.
- Haddad Y., 1995, "Viscoelasticity of engineering materials", Springer.
- Heinrich, C., Waas, A.M., Wineman, A.S., 2009, "Determination of material properties using nanoindentation and multiple indenter tips", *International Journal of Solids and Structures*, Vol 46, pp 364-376.
- Higham, N.J., 1996, "Accuracy and stability of numerical algorithms", Society for Industrial and Applied Mathematics
- Higuchi, R., Mochizuki, M., and Toyoda, M., 2010, "A Method for Evaluating the Stress-Strain Relationship of Materials in the Microstructural Region Using a Triangular Pyramidal Indenter," *Welding International*, 24(8), pp. 611-619.
- Hill, R., 1998, "The mathematical theory of plasticity", Oxford University Press, USA.
- Huang, Y., Zhang, F., Hwang, K. C., Nix, W. D., Pharr, G. M., and Feng, G., 2006, "A Model of Size Effects in Nano-Indentation," *Journal of the Mechanics and Physics of Solids*, 54(8), pp. 1668-1686.

- Hyun, H.C., Kim, M., Lee, J.H., Lee, H., 2011, "A dual conical indentation technique based on FEA solutions for property evaluation", *Mechanics of Materials*, Vol 43, pp 313-331.
- Jackson, R.L., Green, I., 2005, "A Finite Element Study of Elasto-Plastic Hemispherical Contact Against a Rigid Flat", *Journal of Tribology*, Vol 127, pp 343-354.
- Jackson, R.L., Green, I., Marghitu, D.B., 2010, Predicting the coefficient of restitution of impacting elastic-perfectly plastic spheres, *Nonlinear Dynamics*, Vol 60, pp 217-229
- Johnson, K.L., 1987, "Contact mechanics", Cambridge university press.
- Juárez-de la Rosa, B.A., Muñoz-Saldaña, J., Torres-Torres, D., Ardisson, P.L., Alvarado-Gil, J.J., 2012, "Nanoindentation characterization of the micro-lamellar arrangement of black coral skeleton", *Journal of Structural Biology*, Vol 177, pp 349-357.
- Kearney, C., Zhao, Z., Bruet, B.J.F., Radovitzky, R., Boyce, M.C., Ortiz, C., 2006, "Nanoscale Anisotropic Plastic Deformation in Single Crystal Aragonite", *Physical Review Letters*, Vol 96, article # 255505.
- Kim, J.-Y., Kang, S.-K., Lee, J.-J., Jang, J.-i., Lee, Y.-H., Kwon, D., 2007, "Influence of surface-roughness on indentation size effect", *Acta Materialia*, Vol 55, pp 3555-3562.
- Kristiansen, H., Shen, Y., Liu, J., 2001, "Characterisation of mechanical properties of metal-coated polymer spheres for anisotropic conductive adhesive", *IEEE*, pp. 344-348.
- Kucharski S., Mróz Z., 2007, "Identification of yield stress and plastic hardening parameters from a spherical indentation test", *International Journal of Mechanical Sciences*, Vol 49, pp 1238-1250.
- Kwon W.S., Paik K.W., 2006, "Experimental analysis of mechanical and electrical characteristics of metal-coated conductive spheres for anisotropic conductive adhesives (ACAs) interconnection", *IEEE Transactionson Componentsand Packaging Technologies*, Vol 29, pp 528-534.
- Lan, H., Venkatesh, T.A., 2007, "Determination of the elastic and plastic properties of materials through instrumented indentation with reduced sensitivity", *Acta Materialia*, Vol 55, pp 2025-2041.

- Lan, H., Venkatesh, T.A., 2007, "On the sensitivity characteristics in the determination of the elastic and plastic properties of materials through multiple indentation", *Journal of Materials Research*, Vol 22, pp 1043-1063.
- Lan, H., Venkatesh, T.A., 2007, "On the uniqueness and sensitivity issues in determining the elastic and plastic properties of power-law hardening materials through sharp and spherical indentation", *Philosophical Magazine*, Vol 87, pp 4671-4729.
- Le, M.Q., 2008, "A computational study on the instrumented sharp indentations with dual indenters", *International Journal of Solids and Structures*, Vol 45, pp 2818-2835.
- Le, M.Q., 2009, "Material characterization by dual sharp indenters", *International Journal of Solids and Structures*, Vol 46, pp 2988-2998
- Le, M.Q., 2011, "Improved reverse analysis for material characterization with dual sharp indenters", *International Journal of Solids and Structures*, Vol 48, pp 1600-1609
- Lee E.H., Radok J.R.M., 1960, "The contact problem for viscoelastic bodies", *Journal of Applied Mechanics*, Vol 27, pp 438-444.
- Lichinchi, M., Lenardi, C., Haupt, J., Vitali, R., 1998, "Simulation of Berkovich nanoindentation experiments on thin films using finite element method", *Thin Solid Films*, Vol 312, pp 240-248.
- Lin, L.P., Lin, J.F., 2006, "A New Method for Elastic-Plastic Contact Analysis of a Deformable Sphere and a Rigid Flat", *Journal of Tribology*, Vol 128, pp 221-229.
- Liu, L., Ogasawara, N., Chiba, N., Chen, X., 2009, "Can indentation technique measure unique elastoplastic properties", *Journal of Materials Research*, Vol 24, pp 784.
- Lubliner, J., 1990, "Plasticity Theory", Macmillan, New York
- Malayalamurthi, R., Marappan, R., 2008, "Elastic-plastic Contact Behavior of a Sphere Loaded against a Rigid Flat", *Mechanics of Advanced Materials and Structures*, Vol 15, pp 364-370.
- Martha M. McCann, 2004, "Nanoindentation of gold single crystals", PhD Dissertation, Virginia Polytechnic Institute and State University

- MATLAB R2011a, 2010, Natick, Massachusetts: The MathWorks Inc..
- McAllister, Q.P., Gillespie, J.W., VanLandingham, M.R., 2012, "Evaluation of the three-dimensional properties of Kevlar across length scales", *Journal of Materials Research*, Vol 27, pp 1824-1837.
- Mesarovic, S.D., Fleck, N.A., 1999, "Spherical indentation of elastic-plastic solids", *Proceedings of the Royal Society London A*, Vol 455, pp 2707–2728
- Misawa, H., Koshioka, M., Sasaki, K., Kitamura, N., Masuhara, H., 1991, "Three dimensional optical trapping and laser ablation of a single polymer latex particle in water", *Journal of Applied Physics*, Vol 70, pp 3829-3836.
- Moussa, C., Hernot, X., Bartier, O., Delattre, G., Mauvoisin, G., 2014. Evaluation of the tensile properties of a material through spherical indentation: definition of an average representative strain and a confidence domain. *J Mater Sci* 49, 592-603.
- Nakamura, T., Gu, Y., 2007, "Identification of elastic–plastic anisotropic parameters using instrumented indentation and inverse analysis", *Mechanics of Materials*, Vol 39, pp 340-356.
- Ogasawara, N., Chiba, N., Chen, X., 2009, "A simple framework of spherical indentation for measuring elastoplastic properties", *Mechanics of Materials*, Vol 41, pp 1025-1033.
- Oliver, W.C., Pharr, G.M., 1992, "An improved technique for determining hardness and elastic modulus using load and displacement sensing indentation experiments", *Journal of Materials Research*, Vol 7, pp 1564-1583.
- Oliver, W., Pharr, G., 2004, "Measurement of hardness and elastic modulus by instrumented indentation: Advances in understanding and refinements to methodology", *Journal of Materials Research*, Vol 19, pp 3-20.
- Pharr, G., 1998, "Measurement of mechanical properties by ultra-low load indentation", *Materials Science and Engineering A*, Vol 253, pp 151-159.
- Phadikar, J. K., Bogetti, T. A., Karlsson, A. M., 2012, "On Establishing Elastic-plastic Properties of a Sphere by Indentation Testing", *International Journal of Solids and Structures*, Vol 49, pp 1961-1972.
- Phadikar, J. K., Bogetti, T. A., Kaliakin V. N., Karlsson, A. M., 2013, "Conical Indentation of a Viscoelastic Sphere", *Journal of Engineering Materials and Technology*, Vol 135, article # 041001.

- Phadikar, J. K., Bogetti, T. A., Karlsson, A. M., 2013, "On the Uniqueness and Sensitivity of Indentation Testing of Isotropic Materials", *International Journal of Solids and Structures*, Vol 50, pp 3242-3253.
- Phadikar, J. K., Bogetti, T. A., Karlsson, A. M., 2014, "Aspects of experimental errors and data reduction schemes from spherical indentation of isotropic materials", *Journal of Engineering Materials and Technology*, Vol 136, 031005.
- Phadikar, J. K., Bogetti, T. A., Karlsson, A. M., 2013, "A general methodology to establish the non-unique systems for instrumented indentation testing", *Computational Material Science* (submitted).
- Phadikar, J. K., Bogetti, T. A., Karlsson, A. M., 2013, "Aspects of experimental errors from dual indentation on transversely isotropic materials", *Journal of Materials Research* (submitted).
- Philips, J. R., 2013, [www.zunzun.com](http://www.zunzun.com)
- Reisinger, A., Pahr, D., Zysset, P., 2011, "Elastic anisotropy of bone lamellae as a function of fibril orientation pattern", *Biomechanics and Modeling in Mechanobiology*, Vol 10, pp 67-77.
- Rheinboldt, W.C., 1976, "On measures of ill-conditioning for nonlinear equations", *Mathematics of Computation*, Vol 30, pp 104-111
- Sahoo, P., Chatterjee, B., Adhikary, D., 2009, "Finite Element based Elastic-Plastic Contact Behaviour of a Sphere against a Rigid Flat—Effect of Strain Hardening", *International Journal of Engineering and Technology*, Vol 2, pp 1-6
- Sneddon, I.N., 1965, "The relation between load and penetration in the axisymmetric Boussinesq problem for a punch of arbitrary profile", *International Journal of Engineering Science*, Vol 3, pp 47-57.
- Swadener, J.G., Rho, J.-Y., Pharr, G.M., 2001, "Effects of anisotropy on elastic moduli measured by nanoindentation in human tibial cortical bone", *Journal of Biomedical Materials Research*, Vol 57, pp 108-112.
- Swaddiwudhipong, S., Tho, K.K., Liu, Z.S., Zeng, K., 2005, "Material characterization based on dual indenters", *International Journal of Solids and Structures*, Vol 42, pp 69-83.

- Tamai, H., Hasegawa, M., Suzawa, T., 1989, "Surface characterization of hydrophilic functional polymer latex particles", *Journal of Applied Polymer Science*, Vol 38, pp 403-412.
- Taljat, B., Zacharia, T., Kosel, F., 1998, "New analytical procedure to determine stress-strain curve from spherical indentation data", *International Journal of Solids and Structures*, Vol 35, pp 4411-4426.
- Tatara, Y., 1989, "Extensive Theory of Force-Approach Relations of Elastic Spheres in Compression and in Impact", *Journal of Engineering Materials and Technology*, Vol 111, pp 163-168.
- Tatara, Y., 1991, "On Compression of Rubber Elastic Sphere Over a Large Range of Displacements---Part 1: Theoretical Study", *Journal of Engineering Materials and Technology*, Vol 113, pp 285-291.
- Tho, K.K., Swaddiwudhipong, S., Liu, Z.S., Zeng, K., Hua, J., 2004, "Uniqueness of reverse analysis from conical indentation tests", *Journal of Materials Research*, Vol 19, pp 2498-2502.
- Vandamme M., Ulm F.J., 2006, "Viscoelastic solutions for conical indentation", *International Journal of Solids and Structures*, Vol 43, pp 3142-3165.
- Van Vliet, K. J., Prchlik, L., and Smith, J. F., 2004, "Direct Measurement of Indentation Frame Compliance," *Journal of Materials Research*, 19(01), pp. 325-331.
- Vinson, J. R., 1993, "The Behavior of Sandwich Structures of Isotropic and Composite Materials", CRC Press
- Viswanath, B., Raghavan, R., Ramamurty, U., Ravishankar, N., 2007, "Mechanical properties and anisotropy in hydroxyapatite single crystals", *Scripta Materialia*, Vol 57, pp 361-364.
- Vlassak, J.J., Nix, W.D., 1994, "Measuring the elastic properties of anisotropic materials by means of indentation experiments", *Journal of Mechanics of Physics and Solids*, Vol 42, pp 1223-1245.
- Wang, L., Ganor, M., Rokhlin, S.I., 2005, "Inverse scaling functions in nanoindentation with sharp indenters: Determination of material properties", *Journal of Materials Research*, Vol 20, pp 987-1001.

- Wang, J.S., Zheng, X.J., Zheng, H., Song, S.T., Zhu, Z., 2010, "Identification of elastic parameters of transversely isotropic thin films by combining nanoindentation and FEM analysis", *Computational Materials Science*, Vol 49, pp 378-385.
- Xu, Z.H., Li, X., 2005, "Influence of equi-biaxial residual stress on unloading behaviour of nanoindentation", *Acta Materialia*, Vol 53, pp 1913-1919.
- Yan, J., Karlsson, A., Chen, X., 2007, "Determining plastic properties of a material with residual stress by using conical indentation", *International Journal of Solids and Structures*, Vol 44, pp 3720-3737.
- Yan, J., Chen, X., Karlsson, A., 2007, "Determining equi-biaxial residual stress and mechanical properties from the force-displacement curves of conical microindentation", *Journal of Engineering Materials and Technology*, Vol 129, pp 200.
- Yeap, K.B., Hangen, U.D., Raabe, D., Zschech, E., 2011, "Nanoindentation Study Of Elastic Anisotropy Of Cu Single Crystals And Grains In TSVs", *AIP Conference Proceedings*, Vol 1378, pp 121-128.
- Yonezu, A., Kuwahara, Y., Yoneda, K., Hirakata, H., Minoshima, K., 2009, "Estimation of the anisotropic plastic property using single spherical indentation—An FEM study", *Computational Materials Science*, Vol 47, pp 611-619.
- Yonezu, A., Yoneda, K., Hirakata, H., Sakihara, M., Minoshima, K., 2010, "A simple method to evaluate anisotropic plastic properties based on dimensionless function of single spherical indentation – Application to SiC whisker-reinforced aluminum alloy. *Materials Science and Engineering: A*", Vol 527, pp 7646-7657.
- Zambaldi, C., Raabe, D., 2010, "Plastic anisotropy of  $\gamma$ -TiAl revealed by axisymmetric indentation", *Acta Materialia*, Vol 58, pp 3516-3530.
- Zambaldi, C., Yang, Y., Bieler, T.R., Raabe, D., 2012, "Orientation informed nanoindentation of  $\alpha$ -titanium: Indentation pileup in hexagonal metals deforming by prismatic slip", *Journal of Materials Research*, Vol 27, pp 356-367.
- Zhao, M., Chen, X., Ogasawara, N., Razvan, A.C., Chiba, N., Lee, D., Gan, Y.X., 2006, "New sharp indentation method of measuring the elastic-plastic properties of compliant and soft materials using the substrate effect", *Journal of Materials Research*, Vol 21, pp 3134-3151.

- Zhao, M., Ogasawara, N., Chiba, N., Chen, X., 2006, "A new approach to measure the elastic-plastic properties of bulk materials using spherical indentation", *Acta Materialia*, Vol 54, pp 23-32.
- Zhao, M., Chen, X., Xiang, Y., Vlassak, J.J., Lee, D., Ogasawara, N., Chiba, N., Gan, Y.X., 2007, "Measuring elastoplastic properties of thin films on an elastic substrate using sharp indentation", *Acta Materialia*, Vol 55, pp 6260-6274.
- Zhou Z., Lu H., 2010, "On the measurements of viscoelastic functions of a sphere by nanoindentation", *Mechanics of Time-Dependent Materials*, Vol 14, pp 1-24.
- Zhai, M., McKenna, G.B., 2014. Viscoelastic modeling of nanoindentation experiments: A multicurve method. *J. Polym. Sci., Part B: Polym. Phys.* 52, 633-639.

## Appendix A

### FUNCTIONAL FORMS AND FITTING COEFFICIENTS

The fitting coefficients used in the regression analysis for various indenter/substrate geometries and material models are tabulated in this appendix.

#### A.1 Isotropic, Linear-elastic, Power-law Strain Hardening Plastic Materials

The normalized shape functions are related to the normalized material properties for fixed indenter/substrate geometry. As discussed in Chapter 1, section 1.4, the fixed geometric parameter(s) for various indentation geometries are as follows: i) conical indentation of a half-space: indenter half-angle,  $\alpha$ ; ii) spherical indentation of a half-space: depth-to-indenter radius ratio,  $h_m/R_i$ ; iii) conical indentation of a sphere: indenter half-angle,  $\alpha$ , and depth-to-substrate radius ratio,  $h_m/R_s$ ; and iii) spherical indentation of a sphere: depth-to-substrate radius ratio,  $h_m/R_s$  and indenter radius-to-substrate radius ratio:  $R_i/R_s$ . Following Eq. (3.11), the following functional form is used for regression:

$$\Psi_i = \bar{G}_i^{ph} \left( \frac{E}{Y}, n \right) = \sum_{j=0}^{j_u} \sum_{k=0}^{k_u} \mathbb{C}_p^{jk} \left( \frac{E}{Y} \right)^{5-j} n^{5-k}; \quad i = 1-5 \quad (\text{A.1})$$

where  $j_u$  and  $k_u$  are upper limits of  $j$  and  $k$  which and are different for different shape functions and indenter/substrate geometries. The subscript  $p$  indicates power-law hardening material. The fitting coefficients  $\mathbb{C}_p^{jk}$ , are tabulated in the following tables for various indentation geometries.

### A.1.1 Conical indentation of a half-space

The fitting coefficients for various shape functions are tabulated in this section for the range of half-angles used in the study,  $\alpha = 50^\circ, 60^\circ, 70^\circ$  and  $80^\circ$ .

Table A.1: Fitting coefficients for Eq. (A.1) for the normalized total energy,  $W_t$ , for  $\alpha = 50^\circ$

$\mathbb{C}_p^{jk}$	$j=0$	$j=1$	$j=2$	$j=3$	$j=4$	$j=5$
$i=1$	-8.635E-14	-3.249E-13	1.873E-13	-3.899E-14	9.296E-14	2.216E-14
$i=2$	4.508E-10	7.556E-10	-4.200E-10	6.442E-11	-3.047E-10	-7.046E-11
$i=3$	-7.188E-07	-6.762E-07	3.357E-07	1.200E-08	3.956E-07	8.671E-08
$i=4$	6.129E-04	2.054E-04	-9.416E-05	-1.059E-04	-2.640E-04	-5.225E-05
$i=5$	-1.961E-01	1.255E-01	5.070E-02	1.308E-01	1.046E-01	1.654E-02
$i=6$	1.760E+01	-1.657E+01	1.695E+00	-3.516E+00	1.800E+00	4.000E+00

Table A.2: Fitting coefficients for Eq. (A.1) for the normalized maximum load,  $P_m$ , for  $\alpha = 50^\circ$

$\mathbb{C}_p^{jk}$	$j=0$	$j=1$	$j=2$	$j=3$	$j=4$	$j=5$
$i=1$	-1.599E-10	2.119E-10	-1.013E-10	2.042E-11	-1.200E-12	7.144E-14
$i=2$	4.692E-07	-6.217E-07	2.976E-07	-6.026E-08	3.467E-09	-2.274E-10
$i=3$	-5.133E-04	6.795E-04	-3.258E-04	6.638E-05	-3.660E-06	2.790E-07
$i=4$	2.503E-01	-3.308E-01	1.592E-01	-3.288E-02	1.615E-03	-1.659E-04
$i=5$	-4.628E+01	6.212E+01	-3.012E+01	6.714E+00	-1.683E-01	5.035E-02
$i=6$	2.229E+03	-3.066E+03	1.541E+03	-3.495E+02	3.300E+01	1.153E+01

Table A.3: Fitting coefficients for Eq. (A.1) for the normalized unloading slope,  $S_u$ , for  $\alpha = 50^\circ$

$\mathbb{C}_p^{jk}$	$j=0$	$j=1$	$j=2$	$j=3$	$j=4$	$j=5$
$i=1$	-1.378E-08	1.898E-08	-9.454E-09	2.016E-09	-1.550E-10	-8.556E-14
$i=2$	3.678E-05	-5.082E-05	2.542E-05	-5.450E-06	4.221E-07	1.320E-10
$i=3$	-3.664E-02	5.070E-02	-2.545E-02	5.492E-03	-4.295E-04	5.174E-08
$i=4$	1.631E+01	-2.261E+01	1.141E+01	-2.486E+00	1.976E-01	-1.870E-04
$i=5$	-2.474E+03	3.519E+03	-1.841E+03	4.187E+02	-3.611E+01	3.167E+00
$i=6$	8.883E+04	-1.352E+05	7.660E+04	-1.898E+04	1.745E+03	-2.504E+01

Table A.4: Fitting coefficients for Eq. (A.1) for the normalized elastic energy,  $W_e$ , for  $\alpha = 50^\circ$

$\mathbb{C}_p^{jk}$	$j=0$	$j=1$	$j=2$	$j=3$	$j=4$	$j=5$
$i=1$	-1.207E-11	1.559E-11	-6.994E-12	1.355E-12	-8.467E-14	-6.843E-15
$i=2$	3.171E-08	-4.113E-08	1.850E-08	-3.642E-09	2.332E-10	2.185E-11
$i=3$	-3.011E-05	3.934E-05	-1.773E-05	3.572E-06	-2.380E-07	-2.703E-08
$i=4$	1.232E-02	-1.640E-02	7.389E-03	-1.543E-03	1.115E-04	1.639E-05
$i=5$	-1.678E+00	2.538E+00	-1.158E+00	2.626E-01	-2.448E-02	-5.094E-03
$i=6$	6.437E+01	-9.840E+01	5.276E+01	-8.790E+00	3.270E+00	7.952E-01

Table A.5: Fitting coefficients for Eq. (A.1) for the normalized final depth,  $h_f$ , for  $\alpha = 50^\circ$

$\mathbb{C}_p^{jk}$	$j=0$	$j=1$	$j=2$	$j=3$	$j=4$	$j=5$
$i=1$	-6.551E-12	8.918E-12	-4.432E-12	9.580E-13	-7.643E-14	2.506E-15
$i=2$	1.767E-08	-2.412E-08	1.202E-08	-2.604E-09	2.073E-10	-7.558E-12
$i=3$	-1.687E-05	2.324E-05	-1.170E-05	2.561E-06	-2.041E-07	8.656E-09
$i=4$	6.515E-03	-9.197E-03	4.759E-03	-1.069E-03	8.569E-05	-4.698E-06
$i=5$	-8.322E-01	1.269E+00	-7.084E-01	1.693E-01	-1.326E-02	1.186E-03
$i=6$	1.324E+01	-3.548E+01	2.727E+01	-8.265E+00	5.562E-01	8.514E-01

Table A.6: Fitting coefficients for Eq. (A.1) for the normalized unloading slope,  $S_u$ , for  $\alpha = 60^\circ$

$\mathbb{C}_p^{jk}$	$j=0$	$j=1$	$j=2$	$j=3$	$j=4$	$j=5$
$i=1$	8.699E-09	-9.101E-09	2.962E-09	-3.563E-10	3.262E-11	-1.976E-12
$i=2$	-2.637E-05	3.015E-05	-1.155E-05	1.856E-06	-1.649E-07	5.808E-09
$i=3$	2.896E-02	-3.580E-02	1.537E-02	-2.847E-03	2.491E-04	-6.328E-06
$i=4$	-1.398E+01	1.838E+01	-8.521E+00	1.702E+00	-1.459E-01	3.063E-03
$i=5$	2.761E+03	-3.765E+03	1.818E+03	-3.747E+02	2.878E+01	4.105E+00
$i=6$	-1.539E+05	2.138E+05	-1.052E+05	2.197E+04	-1.734E+03	-2.296E+01

Table A.7: Fitting coefficients for Eq. (A.1) for the normalized unloading energy,  $W_e$ , for  $\alpha = 60^\circ$

$\mathbb{C}_p^{jk}$	$j=0$	$j=1$	$j=2$	$j=3$	$j=4$	$j=5$
$i=1$	7.170E-13	-9.694E-13	8.655E-13	-2.410E-13	7.086E-14	-1.621E-14
$i=2$	-3.901E-09	5.376E-09	-3.830E-09	9.245E-10	-2.205E-10	5.182E-11
$i=3$	6.100E-06	-8.467E-06	5.595E-06	-1.231E-06	2.508E-07	-6.434E-08
$i=4$	-3.845E-03	5.210E-03	-3.410E-03	6.892E-04	-1.228E-04	3.939E-05
$i=5$	1.358E+00	-1.440E+00	9.080E-01	-1.598E-01	2.044E-02	-1.259E-02
$i=6$	-8.062E+01	9.686E+01	-4.993E+01	1.607E+01	2.961E+00	2.113E+00

Table A.8: Fitting coefficients for Eq. (A.1) for the normalized total energy,  $W_e$ , for  $\alpha = 70^\circ$

$\mathbb{C}_p^{jk}$	$j=0$	$j=1$	$j=2$	$j=3$	$j=4$	$j=5$
$i=1$	-1.440E-11	1.960E-11	-9.639E-12	1.749E-12	5.684E-14	1.377E-13
$i=2$	4.462E-08	-6.129E-08	3.076E-08	-5.835E-09	-1.573E-10	-4.519E-10
$i=3$	-5.078E-05	7.036E-05	-3.618E-05	7.200E-06	2.281E-07	5.801E-07
$i=4$	2.478E-02	-3.437E-02	1.827E-02	-3.906E-03	-2.692E-04	-3.718E-04
$i=5$	-4.260E+00	5.998E+00	-3.086E+00	9.594E-01	2.505E-01	1.269E-01
$i=6$	2.179E+02	-3.089E+02	1.582E+02	-4.594E+01	1.134E+00	1.244E+01

Table A.9: Fitting coefficients for Eq. (A.1) for the normalized maximum load,  $P_m$ , for  $\alpha = 70^\circ$

$\mathbb{C}_p^{jk}$	$j=0$	$j=1$	$j=2$	$j=3$	$j=4$	$j=5$
$i=1$	-3.051E-10	3.333E-10	-1.193E-10	1.478E-11	1.750E-14	4.195E-13
$i=2$	7.440E-07	-8.062E-07	2.832E-07	-3.266E-08	-8.893E-10	-1.367E-09
$i=3$	-6.505E-04	6.998E-04	-2.419E-04	2.585E-05	1.916E-06	1.748E-06
$i=4$	2.508E-01	-2.684E-01	9.278E-02	-9.811E-03	-1.602E-03	-1.121E-03
$i=5$	-4.150E+01	4.465E+01	-1.496E+01	2.335E+00	8.918E-01	3.843E-01
$i=6$	2.889E+03	-3.295E+03	1.222E+03	-1.885E+02	3.425E-01	3.587E+01

Table A.10: Fitting coefficients for Eq. (A.1) for the normalized unloading slope,  $S_u$ , for  $\alpha = 70^\circ$

$\mathbb{C}_p^{jk}$	$j=0$	$j=1$	$j=2$	$j=3$	$j=4$	$j=5$
$i=1$	4.901E-09	-1.002E-08	6.346E-09	-1.467E-09	9.283E-11	-4.415E-13
$i=2$	-1.126E-05	2.431E-05	-1.600E-05	3.853E-06	-2.649E-07	2.416E-09
$i=3$	1.043E-02	-2.260E-02	1.510E-02	-3.754E-03	2.820E-04	-4.503E-06
$i=4$	-4.612E+00	9.581E+00	-6.358E+00	1.613E+00	-1.317E-01	3.544E-03
$i=5$	7.678E+02	-1.566E+03	1.037E+03	-2.643E+02	1.845E+01	6.346E+00
$i=6$	-9.521E+03	4.120E+04	-3.530E+04	1.022E+04	-7.723E+02	-5.983E+01

Table A.11: Fitting coefficients for Eq. (A.1) for the normalized unloading energy,  $W_e$ , for  $\alpha = 70^\circ$

$\mathbb{C}_p^{jk}$	$j=0$	$j=1$	$j=2$	$j=3$	$j=4$	$j=5$
$i=1$	-2.453E-11	2.716E-11	-9.773E-12	1.493E-12	3.693E-14	-2.680E-14
$i=2$	6.699E-08	-7.427E-08	2.658E-08	-4.139E-09	-1.320E-10	8.764E-11
$i=3$	-6.629E-05	7.364E-05	-2.609E-05	4.230E-06	1.735E-07	-1.130E-07
$i=4$	2.872E-02	-3.215E-02	1.111E-02	-1.963E-03	-9.974E-05	7.402E-05
$i=5$	-4.586E+00	5.682E+00	-1.826E+00	3.990E-01	1.824E-02	-2.689E-02
$i=6$	3.035E+02	-3.811E+02	1.471E+02	-1.765E+01	8.793E+00	5.761E+00

Table A.12: Fitting coefficients for Eq. (A.1) for the normalized final depth,  $h_f$ , for  $\alpha = 70^\circ$

$\mathbb{C}_p^{jk}$	$j=0$	$j=1$	$j=2$	$j=3$	$j=4$	$j=5$
$i=1$	4.181E-12	-5.603E-12	2.704E-12	-5.531E-13	4.169E-14	2.422E-15
$i=2$	-1.280E-08	1.699E-08	-8.109E-09	1.639E-09	-1.221E-10	-7.729E-12
$i=3$	1.468E-05	-1.930E-05	9.103E-06	-1.817E-06	1.340E-07	9.502E-09
$i=4$	-7.761E-03	1.010E-02	-4.704E-03	9.259E-04	-6.798E-05	-5.665E-06
$i=5$	1.841E+00	-2.371E+00	1.091E+00	-2.116E-01	1.580E-02	1.706E-03
$i=6$	-1.472E+02	1.873E+02	-8.525E+01	1.608E+01	-1.396E+00	7.467E-01

Table A.13: Fitting coefficients for Eq. (A.1) for the normalized total energy,  $W_t$ , for  $\alpha = 70.3^\circ$

$\mathbb{C}_p^{jk}$	$j=0$	$j=1$	$j=2$	$j=3$	$j=4$	$j=5$
$i=1$	-3.593E-10	4.494E-10	-1.902E-10	3.152E-11	-1.580E-12	1.468E-13
$i=2$	1.021E-06	-1.286E-06	5.497E-07	-9.224E-08	4.625E-09	-4.790E-10
$i=3$	-1.061E-03	1.348E-03	-5.835E-04	9.946E-05	-4.927E-06	6.123E-07
$i=4$	4.849E-01	-6.222E-01	2.736E-01	-4.765E-02	2.205E-03	-3.911E-04
$i=5$	-9.049E+01	1.176E+02	-5.249E+01	9.600E+00	-2.407E-01	1.332E-01
$i=6$	4.980E+03	-6.548E+03	2.970E+03	-5.470E+02	2.895E+01	1.248E+01

Table A.14: Fitting coefficients for Eq. (A.1) for the normalized elastic energy,  $W_e$ , for  $\alpha = 70.3^\circ$

$\mathbb{C}_p^{jk}$	$j=0$	$j=1$	$j=2$	$j=3$	$j=4$	$j=5$
$i=1$	-2.318E-10	2.832E-10	-1.195E-10	2.041E-11	-1.038E-12	-2.688E-14
$i=2$	6.548E-07	-8.020E-07	3.390E-07	-5.813E-08	2.938E-09	8.852E-11
$i=3$	-6.741E-04	8.280E-04	-3.510E-04	6.054E-05	-3.030E-06	-1.150E-07
$i=4$	3.043E-01	-3.751E-01	1.594E-01	-2.778E-02	1.369E-03	7.585E-05
$i=5$	-5.537E+01	6.903E+01	-2.935E+01	5.224E+00	-2.559E-01	-2.774E-02
$i=6$	2.787E+03	-3.466E+03	1.492E+03	-2.557E+02	2.241E+01	5.985E+00

Table A.15: Fitting coefficients for Eq. (A.1) for the normalized total energy,  $W_t$ , for  $\alpha = 80^\circ$

$\mathbb{C}_p^{jk}$	$j=0$	$j=1$	$j=2$	$j=3$	$j=4$	$j=5$
$i=1$	2.722E-11	-2.778E-11	7.208E-12	-5.355E-14	-2.054E-13	5.265E-13
$i=2$	-7.070E-08	7.272E-08	-1.914E-08	6.676E-10	3.425E-10	-1.716E-09
$i=3$	6.863E-05	-7.283E-05	2.070E-05	-2.105E-06	2.077E-07	2.195E-06
$i=4$	-3.074E-02	3.496E-02	-1.120E-02	2.085E-03	-7.685E-04	-1.423E-03
$i=5$	5.094E+00	-5.908E+00	2.073E+00	3.910E-02	7.161E-01	5.220E-01
$i=6$	-2.515E+02	2.910E+02	-1.050E+02	-3.733E+00	-1.749E+01	2.890E+01

Table A.16: Fitting coefficients for Eq. (A.1) for the normalized maximum load,  $P_m$ , for  $\alpha = 80^\circ$

$\mathbb{C}_p^{jk}$	$j=0$	$j=1$	$j=2$	$j=3$	$j=4$	$j=5$
$i=1$	-1.507E-10	2.606E-10	-1.638E-10	4.275E-11	-4.140E-12	1.614E-12
$i=2$	3.749E-07	-6.486E-07	4.117E-07	-1.083E-07	1.050E-08	-5.282E-09
$i=3$	-3.426E-04	5.894E-04	-3.771E-04	9.872E-05	-8.833E-06	6.765E-06
$i=4$	1.309E-01	-2.237E-01	1.464E-01	-3.768E-02	1.829E-03	-4.371E-03
$i=5$	-1.994E+01	3.447E+01	-2.283E+01	7.460E+00	1.409E+00	1.592E+00
$i=6$	9.495E+02	-1.671E+03	1.117E+03	-3.819E+02	-1.241E+01	8.575E+01

Table A.17: Fitting coefficients for Eq. (A.1) for the normalized unloading slope,  $S_u$ , for  $\alpha = 80^\circ$

$\mathbb{C}_p^{jk}$	$j=0$	$j=1$	$j=2$	$j=3$	$j=4$	$j=5$
$i=1$	-1.403E-08	1.729E-08	-7.520E-09	1.335E-09	-8.029E-11	3.620E-13
$i=2$	2.991E-05	-3.739E-05	1.673E-05	-3.154E-06	2.246E-07	-2.204E-09
$i=3$	-2.127E-02	2.749E-02	-1.300E-02	2.696E-03	-2.299E-04	1.991E-06
$i=4$	5.306E+00	-7.406E+00	3.887E+00	-9.190E-01	9.012E-02	1.510E-03
$i=5$	-2.613E+02	5.321E+02	-3.883E+02	1.200E+02	-1.998E+01	1.307E+01
$i=6$	-6.170E+03	-5.708E+03	1.202E+04	-5.159E+03	9.535E+02	-1.680E+02

Table A.18: Fitting coefficients for Eq. (A.1) for the normalized elastic energy,  $W_e$ , for  $\alpha = 80^\circ$

$\mathbb{C}_p^{jk}$	$j=0$	$j=1$	$j=2$	$j=3$	$j=4$	$j=5$
$i=1$	5.702E-11	-7.232E-11	3.130E-11	-4.907E-12	7.638E-13	-1.381E-14
$i=2$	-1.520E-07	1.951E-07	-8.542E-08	1.317E-08	-2.292E-09	6.096E-11
$i=3$	1.444E-04	-1.886E-04	8.393E-05	-1.244E-05	2.607E-06	-1.126E-07
$i=4$	-5.831E-02	7.804E-02	-3.591E-02	4.750E-03	-1.399E-03	1.125E-04
$i=5$	1.042E+01	-1.323E+01	6.682E+00	-5.485E-01	3.372E-01	-6.702E-02
$i=6$	-5.632E+02	7.023E+02	-3.468E+02	5.127E+01	1.167E+01	2.596E+01

Table A.19: Fitting coefficients for Eq. (A.1) for the normalized final depth,  $h_f$ , for  $\alpha = 80^\circ$

$\mathbb{C}_p^{jk}$	$j=0$	$j=1$	$j=2$	$j=3$	$j=4$	$j=5$
$i=1$	4.088E-12	-3.903E-12	1.054E-12	-4.648E-14	-7.805E-15	4.271E-15
$i=2$	-1.142E-08	1.061E-08	-2.666E-09	4.879E-11	2.868E-11	-1.347E-11
$i=3$	1.155E-05	-1.032E-05	2.289E-06	7.113E-08	-3.924E-08	1.640E-08
$i=4$	-4.998E-03	4.141E-03	-6.742E-04	-1.249E-04	2.484E-05	-9.714E-06
$i=5$	7.709E-01	-4.978E-01	-3.538E-02	6.106E-02	-7.126E-03	2.926E-03
$i=6$	-4.138E+00	-2.787E+01	3.001E+01	-9.535E+00	5.687E-01	5.548E-01

### A.1.2 Spherical indentation of a half-space

The fitting coefficients for various shape functions are tabulated in this section for the range of depth-to-radius ratios used in the study,  $(h_m/R_s) = 1\%$ ,  $10\%$ ,  $20\%$ ,  $30\%$ ,  $40\%$  and  $100\%$ .

Table A.20: Fitting coefficients for Eq. (A.1) for the normalized unloading slope,  $S_u$ , for  $(h_m/R_s) = 1\%$

$\mathbb{C}_p^{jk}$	$j=0$	$j=1$	$j=2$	$j=3$	$j=4$	$j=5$
$i=1$	1.893E-09	-2.378E-09	1.080E-09	-2.183E-10	1.869E-11	-3.082E-13
$i=2$	-6.215E-06	7.538E-06	-3.269E-06	6.280E-07	-5.239E-08	9.554E-10
$i=3$	7.920E-03	-9.192E-03	3.737E-03	-6.612E-04	5.247E-05	-1.106E-06
$i=4$	-4.947E+00	5.447E+00	-2.026E+00	3.119E-01	-2.212E-02	5.820E-04
$i=5$	1.570E+03	-1.642E+03	5.508E+02	-6.769E+01	3.547E+00	-1.339E-01
$i=6$	-2.250E+05	2.263E+05	-6.900E+04	6.218E+03	-1.123E+02	4.320E+01
$i=7$	1.065E+07	-1.049E+07	3.009E+06	-2.018E+05	-5.504E+03	-7.981E+02

Table A.21: Fitting coefficients for Eq. (A.1) for the normalized unloading energy,  $W_e$ , for  $(h_m/R_s) = 1\%$

$\mathbb{C}_p^{jk}$	$j=0$	$j=1$	$j=2$	$j=3$	$j=4$	$j=5$
$i=1$	-2.000E-11	2.033E-11	-5.242E-12	-2.958E-13	1.768E-13	-9.639E-15
$i=2$	7.219E-08	-7.675E-08	2.251E-08	-1.457E-10	-5.034E-10	3.298E-11
$i=3$	-1.014E-04	1.129E-04	-3.711E-05	2.056E-06	5.003E-07	-4.382E-08
$i=4$	6.865E-02	-8.026E-02	2.911E-02	-2.708E-03	-1.913E-04	2.826E-05
$i=5$	-2.247E+01	2.756E+01	-1.085E+01	1.311E+00	1.340E-02	-8.875E-03
$i=6$	3.197E+03	-4.089E+03	1.720E+03	-2.386E+02	5.413E+00	9.807E-01
$i=7$	-1.469E+05	1.932E+05	-8.439E+04	1.253E+04	-2.642E+02	1.842E+02

Table A.22: Fitting coefficients for Eq. (A.1) for the normalized total energy,  $W_t$ , for  $(h_m/R_s) = 10\%$

$\mathbb{C}_p^{jk}$	$j=0$	$j=1$	$j=2$	$j=3$	$j=4$	$j=5$
$i=1$	4.436E-11	-6.276E-11	3.043E-11	-6.565E-12	8.523E-13	5.280E-13
$i=2$	-1.147E-07	1.617E-07	-7.701E-08	1.656E-08	-2.535E-09	-1.709E-09
$i=3$	1.037E-04	-1.452E-04	6.649E-05	-1.404E-05	2.967E-06	2.165E-06
$i=4$	-3.935E-02	5.506E-02	-2.284E-02	4.297E-03	-1.943E-03	-1.370E-03
$i=5$	6.497E+00	-9.245E+00	4.066E+00	1.193E-01	1.053E+00	4.615E-01
$i=6$	-2.982E+02	4.376E+02	-2.146E+02	-1.260E+00	-1.390E+01	4.152E+01

Table A.23: Fitting coefficients for Eq. (A.1) for the normalized maximum load,  $P_m$ , for  $(h_m/R_s) = 10\%$

$\mathbb{C}_p^{jk}$	$j=0$	$j=1$	$j=2$	$j=3$	$j=4$	$j=5$
$i=1$	8.723E-10	-1.331E-09	7.645E-10	-1.976E-10	2.094E-11	6.369E-13
$i=2$	-1.849E-06	2.856E-06	-1.665E-06	4.369E-07	-4.753E-08	-2.491E-09
$i=3$	1.365E-03	-2.134E-03	1.260E-03	-3.344E-04	3.806E-05	3.672E-06
$i=4$	-4.293E-01	6.799E-01	-4.022E-01	1.058E-01	-1.401E-02	-2.565E-03
$i=5$	5.113E+01	-8.390E+01	5.186E+01	-1.142E+01	3.478E+00	8.838E-01
$i=6$	6.714E+02	1.185E+01	-6.969E+02	2.025E+02	-3.140E+01	9.763E+01

Table A.24: Fitting coefficients for Eq. (A.1) for the normalized unloading slope,  $S_u$ , for  $(h_m/R_s) = 10\%$

$\mathbb{C}_p^{jk}$	$j=0$	$j=1$	$j=2$	$j=3$	$j=4$	$j=5$
$i=1$	6.752E-08	-9.577E-08	4.988E-08	-1.139E-08	1.003E-09	-1.683E-11
$i=2$	-1.571E-04	2.233E-04	-1.165E-04	2.662E-05	-2.334E-06	4.139E-08
$i=3$	1.307E-01	-1.861E-01	9.723E-02	-2.219E-02	1.925E-03	-3.616E-05
$i=4$	-4.692E+01	6.717E+01	-3.518E+01	8.009E+00	-6.836E-01	1.417E-02
$i=5$	6.741E+03	-9.755E+03	5.135E+03	-1.159E+03	8.925E+01	9.254E+00
$i=6$	-2.614E+05	3.918E+05	-2.124E+05	4.860E+04	-3.636E+03	-5.147E+01

Table A.25: Fitting coefficients for Eq. (A.1) for the normalized elastic energy,  $W_e$ , for  $(h_m/R_s) = 10\%$

$\mathbb{C}_p^{jk}$	$j=0$	$j=1$	$j=2$	$j=3$	$j=4$	$j=5$
$i=1$	-4.454E-11	5.006E-11	-1.485E-11	7.876E-13	7.194E-13	-1.337E-13
$i=2$	1.427E-07	-1.660E-07	5.473E-08	-5.691E-09	-1.807E-09	4.273E-10
$i=3$	-1.635E-04	1.947E-04	-6.807E-05	9.453E-06	1.689E-06	-5.383E-07
$i=4$	8.314E-02	-1.007E-01	3.581E-02	-6.120E-03	-7.236E-04	3.442E-04
$i=5$	-1.725E+01	2.279E+01	-7.794E+00	1.669E+00	1.097E-01	-1.211E-01
$i=6$	1.434E+03	-1.913E+03	7.529E+02	-1.025E+02	3.568E+01	2.409E+01

Table A.26: Fitting coefficients for Eq. (A.1) for the normalized final depth,  $h_f$ , for  $(h_m/R_s) = 10\%$

$\mathbb{C}_p^{jk}$	$j=0$	$j=1$	$j=2$	$j=3$	$j=4$	$j=5$
$i=1$	8.622E-12	-9.998E-12	3.915E-12	-6.088E-13	3.934E-14	3.226E-15
$i=2$	-2.224E-08	2.588E-08	-1.020E-08	1.611E-09	-1.099E-10	-1.028E-11
$i=3$	2.081E-05	-2.436E-05	9.698E-06	-1.571E-06	1.154E-07	1.273E-08
$i=4$	-8.574E-03	1.015E-02	-4.116E-03	6.953E-04	-5.657E-05	-7.783E-06
$i=5$	1.484E+00	-1.796E+00	7.568E-01	-1.375E-01	1.303E-02	2.474E-03
$i=6$	-8.271E+01	1.048E+02	-4.762E+01	9.332E+00	-1.284E+00	6.019E-01

Table A.27: Fitting coefficients for Eq. (A.1) for the normalized total energy,  $W_t$ , for  $(h_m/R_s) = 20\%$

$\mathbb{C}_p^{jk}$	$j=0$	$j=1$	$j=2$	$j=3$	$j=4$	$j=5$
$i=1$	-3.057E-11	4.190E-11	-2.192E-11	4.924E-12	-1.339E-13	2.732E-13
$i=2$	8.814E-08	-1.209E-07	6.379E-08	-1.443E-08	2.146E-10	-8.755E-10
$i=3$	-8.744E-05	1.200E-04	-6.455E-05	1.490E-05	2.157E-07	1.088E-06
$i=4$	3.229E-02	-4.352E-02	2.459E-02	-6.114E-03	-6.933E-04	-6.633E-04
$i=5$	-3.119E+00	3.732E+00	-1.747E+00	1.037E+00	6.195E-01	2.076E-01
$i=6$	6.641E+01	-4.942E+01	-4.469E+00	-1.857E+01	-2.891E+00	2.629E+01

Table A.28: Fitting coefficients for Eq. (A.1) for the normalized maximum load,  $P_m$ , for  $(h_m/R_s) = 20\%$

$\mathbb{C}_p^{jk}$	$j=0$	$j=1$	$j=2$	$j=3$	$j=4$	$j=5$
$i=1$	-1.407E-09	1.724E-09	-7.298E-10	1.276E-10	-8.104E-12	4.928E-13
$i=2$	3.788E-06	-4.665E-06	1.989E-06	-3.509E-07	2.174E-08	-1.564E-09
$i=3$	-3.682E-03	4.567E-03	-1.968E-03	3.514E-04	-2.049E-05	1.914E-06
$i=4$	1.568E+00	-1.953E+00	8.491E-01	-1.533E-01	7.321E-03	-1.134E-03
$i=5$	-2.757E+02	3.422E+02	-1.464E+02	2.722E+01	-7.506E-02	3.362E-01
$i=6$	1.422E+04	-1.757E+04	7.417E+03	-1.309E+03	7.561E+01	6.235E+01

Table A.29: Fitting coefficients for Eq. (A.1) for the normalized unloading slope,  $S_u$ , for  $(h_m/R_s) = 20\%$

$\mathbb{C}_p^{jk}$	$j=0$	$j=1$	$j=2$	$j=3$	$j=4$	$j=5$
$i=1$	-3.100E-08	3.420E-08	-1.208E-08	1.576E-09	-9.730E-11	-9.933E-13
$i=2$	8.448E-05	-9.480E-05	3.453E-05	-4.776E-06	3.038E-07	2.923E-09
$i=3$	-8.346E-02	9.582E-02	-3.630E-02	5.374E-03	-3.524E-04	-3.280E-06
$i=4$	3.628E+01	-4.264E+01	1.680E+01	-2.648E+00	1.784E-01	1.747E-03
$i=5$	-6.474E+03	7.727E+03	-3.127E+03	5.173E+02	-4.043E+01	7.845E+00
$i=6$	3.370E+05	-4.034E+05	1.640E+05	-2.720E+04	2.024E+03	-6.940E+01

Table A.30: Fitting coefficients for Eq. (A.1) for the normalized unloading energy,  $W_e$ , for  $(h_m/R_s) = 20\%$

$\mathbb{C}_p^{jk}$	$j=0$	$j=1$	$j=2$	$j=3$	$j=4$	$j=5$
$i=1$	-3.050E-11	4.082E-11	-1.828E-11	3.954E-12	-1.592E-13	-8.135E-14
$i=2$	8.535E-08	-1.143E-07	5.090E-08	-1.122E-08	4.153E-10	2.618E-10
$i=3$	-8.822E-05	1.178E-04	-5.171E-05	1.172E-05	-3.846E-07	-3.276E-07
$i=4$	4.214E-02	-5.593E-02	2.351E-02	-5.534E-03	1.617E-04	2.022E-04
$i=5$	-7.380E+00	1.093E+01	-4.173E+00	1.081E+00	-4.561E-02	-6.462E-02
$i=6$	3.429E+02	-5.175E+02	2.239E+02	-2.680E+01	2.176E+01	1.040E+01

Table A.31: Fitting coefficients for Eq. (A.1) for the normalized final depth,  $h_f$ , for  $(h_m/R_s) = 20\%$

$\mathbb{C}_p^{jk}$	$j=0$	$j=1$	$j=2$	$j=3$	$j=4$	$j=5$
$i=1$	1.075E-11	-1.469E-11	7.078E-12	-1.383E-12	8.843E-14	3.316E-15
$i=2$	-3.140E-08	4.260E-08	-2.038E-08	3.960E-09	-2.528E-10	-1.049E-11
$i=3$	3.373E-05	-4.543E-05	2.158E-05	-4.165E-06	2.656E-07	1.281E-08
$i=4$	-1.605E-02	2.148E-02	-1.013E-02	1.944E-03	-1.242E-04	-7.620E-06
$i=5$	3.151E+00	-4.202E+00	1.974E+00	-3.771E-01	2.461E-02	2.287E-03
$i=6$	-1.807E+02	2.402E+02	-1.125E+02	2.092E+01	-1.617E+00	6.730E-01

Table A.32: Fitting coefficients for Eq. (A.1) for the normalized unloading slope,  $S_u$ , for  $(h_m/R_s) = 30\%$

$\mathbb{C}_p^{jk}$	$j=0$	$j=1$	$j=2$	$j=3$	$j=4$	$j=5$
$i=1$	2.666E-08	-3.170E-08	1.277E-08	-1.989E-09	9.397E-11	7.973E-13
$i=2$	-7.722E-05	9.219E-05	-3.724E-05	5.795E-06	-2.723E-07	-2.205E-09
$i=3$	7.908E-02	-9.479E-02	3.837E-02	-5.953E-03	2.761E-04	2.196E-06
$i=4$	-3.351E+01	4.025E+01	-1.627E+01	2.499E+00	-1.118E-01	-9.565E-04
$i=5$	5.507E+03	-6.605E+03	2.649E+03	-3.960E+02	1.307E+01	6.740E+00
$i=6$	-2.868E+05	3.451E+05	-1.390E+05	2.095E+04	-8.116E+02	-6.180E+01

Table A.33: Fitting coefficients for Eq. (A.1) for the normalized elastic energy,  $W_e$ , for  $(h_m/R_s) = 30\%$

$\mathbb{C}_p^{jk}$	$j=0$	$j=1$	$j=2$	$j=3$	$j=4$	$j=5$
$i=1$	2.429E-11	-3.128E-11	1.423E-11	-2.201E-12	1.917E-13	-5.281E-14
$i=2$	-6.143E-08	8.067E-08	-3.767E-08	5.726E-09	-5.162E-10	1.687E-10
$i=3$	5.225E-05	-7.070E-05	3.460E-05	-5.051E-06	4.789E-07	-2.087E-07
$i=4$	-1.629E-02	2.304E-02	-1.263E-02	1.640E-03	-1.613E-04	1.261E-04
$i=5$	2.433E+00	-2.553E+00	1.817E+00	-1.553E-01	-1.511E-03	-3.874E-02
$i=6$	-1.230E+02	1.420E+02	-7.323E+01	2.615E+01	1.333E+01	5.745E+00

Table A.34: Fitting coefficients for Eq. (A.1) for the normalized total energy,  $W_t$ , for  $(h_m/R_s) = 40\%$

$\mathbb{C}_p^{jk}$	$j=0$	$j=1$	$j=2$	$j=3$	$j=4$	$j=5$
$i=1$	3.746E-11	-5.038E-11	2.361E-11	-4.734E-12	6.509E-13	1.026E-13
$i=2$	-1.083E-07	1.466E-07	-6.912E-08	1.399E-08	-2.086E-09	-3.239E-10
$i=3$	1.172E-04	-1.602E-04	7.613E-05	-1.556E-05	2.620E-06	3.942E-07
$i=4$	-5.690E-02	7.956E-02	-3.842E-02	7.877E-03	-1.664E-03	-2.327E-04
$i=5$	1.094E+01	-1.560E+01	8.242E+00	-1.436E+00	6.006E-01	6.883E-02
$i=6$	-5.713E+02	8.088E+02	-4.309E+02	8.750E+01	-7.512E+00	1.598E+01

Table A.35: Fitting coefficients for Eq. (A.1) for the normalized maximum load,  $P_m$ , for  $(h_m/R_s) = 40\%$

$\mathbb{C}_p^{jk}$	$j=0$	$j=1$	$j=2$	$j=3$	$j=4$	$j=5$
$i=1$	-8.870E-11	6.149E-11	-4.711E-12	-3.506E-12	1.466E-12	1.236E-13
$i=2$	1.770E-07	-7.581E-08	-3.269E-08	1.901E-08	-5.267E-09	-3.870E-10
$i=3$	-4.140E-05	-1.056E-04	1.180E-04	-3.562E-05	7.426E-06	4.641E-07
$i=4$	-9.607E-02	1.964E-01	-1.209E-01	2.844E-02	-5.108E-03	-2.667E-04
$i=5$	5.205E+01	-7.965E+01	4.308E+01	-8.341E+00	1.742E+00	7.489E-02
$i=6$	-4.872E+03	6.904E+03	-3.477E+03	6.895E+02	-4.095E+01	3.496E+01

Table A.36: Fitting coefficients for Eq. (A.1) for the normalized unloading slope,  $S_u$ , for  $(h_m/R_s) = 40\%$

$\mathbb{C}_p^{jk}$	$j=0$	$j=1$	$j=2$	$j=3$	$j=4$	$j=5$
$i=1$	-6.967E-09	7.873E-09	-3.335E-09	6.880E-10	-5.990E-11	-2.639E-13
$i=2$	1.619E-05	-1.770E-05	7.275E-06	-1.508E-06	1.384E-07	5.853E-10
$i=3$	-1.210E-02	1.225E-02	-4.659E-03	9.759E-04	-1.017E-04	-3.466E-07
$i=4$	2.210E+00	-1.361E+00	1.728E-01	-6.003E-02	2.053E-02	-9.052E-05
$i=5$	5.781E+02	-1.018E+03	5.539E+02	-1.030E+02	1.758E+00	5.526E+00
$i=6$	-7.909E+04	1.174E+05	-5.928E+04	1.155E+04	-6.533E+02	-3.053E+01

Table A.37: Fitting coefficients for Eq. (A.1) for the normalized elastic energy,  $W_e$ , for  $(h_m/R_s) = 40\%$

$\mathbb{C}_p^{jk}$	$j=0$	$j=1$	$j=2$	$j=3$	$j=4$	$j=5$
$i=1$	-1.019E-11	9.076E-12	-1.832E-12	2.760E-13	1.029E-15	-3.628E-14
$i=2$	2.297E-08	-1.859E-08	1.922E-09	-2.880E-10	-1.983E-11	1.151E-10
$i=3$	-1.642E-05	1.037E-05	2.313E-06	-3.436E-07	3.254E-08	-1.408E-07
$i=4$	2.765E-03	6.397E-04	-3.836E-03	5.624E-04	-8.017E-06	8.373E-05
$i=5$	1.864E+00	-2.183E+00	1.735E+00	-2.542E-01	-1.220E-02	-2.505E-02
$i=6$	-2.156E+02	2.862E+02	-1.473E+02	4.191E+01	9.085E+00	3.538E+00

Table A.38: Fitting coefficients for Eq. (A.1) for the normalized final depth,  $h_f$ , for  $(h_m/R_s) = 40\%$

$\mathbb{C}_p^{jk}$	$j=0$	$j=1$	$j=2$	$j=3$	$j=4$	$j=5$
$i=1$	-6.381E-12	7.472E-12	-2.996E-12	4.747E-13	-2.171E-14	2.236E-15
$i=2$	1.703E-08	-2.001E-08	8.071E-09	-1.291E-09	5.918E-11	-7.123E-12
$i=3$	-1.632E-05	1.931E-05	-7.869E-06	1.280E-06	-5.867E-08	8.773E-09
$i=4$	6.793E-03	-8.152E-03	3.392E-03	-5.690E-04	2.594E-05	-5.265E-06
$i=5$	-1.201E+00	1.486E+00	-6.456E-01	1.150E-01	-5.079E-03	1.593E-03
$i=6$	7.537E+01	-9.863E+01	4.571E+01	-9.247E+00	2.730E-01	7.739E-01

Table A.39: Fitting coefficients for Eq. (A.1) for the normalized unloading slope,  $S_u$ , for  $(h_m/R_s) = 100\%$

$\mathbb{C}_p^{jk}$	$j=0$	$j=1$	$j=2$	$j=3$	$j=4$	$j=5$	$j=6$
$i=1$	-9.087E-10	0.000E+00	-3.194E-10	7.585E-10	-3.190E-10	3.770E-11	-2.161E-13
$i=2$	2.112E-06	0.000E+00	8.431E-07	-1.891E-06	7.947E-07	-9.456E-08	5.479E-10
$i=3$	-1.528E-03	0.000E+00	-9.829E-04	1.790E-03	-7.299E-04	8.636E-05	-4.393E-07
$i=4$	1.588E-01	0.000E+00	7.158E-01	-8.569E-01	3.121E-01	-3.514E-02	-1.562E-05
$i=5$	2.490E+02	0.000E+00	-3.545E+02	2.587E+02	-7.192E+01	7.417E+00	2.751E+00
$i=6$	-3.148E+04	0.000E+00	3.642E+04	-2.308E+04	5.297E+03	-4.665E+02	6.325E+00

Table A.40: Fitting coefficients for Eq. (A.1) for the normalized elastic energy,  $W_e$ , for  $(h_m/R_s) = 100\%$

$\mathbb{C}_p^{jk}$	$j=0$	$j=1$	$j=2$	$j=3$	$j=4$	$j=5$	$j=6$
$i=1$	-1.722E-12	0.000E+00	6.176E-13	5.705E-13	-2.655E-13	6.528E-15	-5.436E-15
$i=2$	4.976E-09	0.000E+00	-2.734E-09	-9.475E-10	6.100E-10	-4.577E-12	1.717E-11
$i=3$	-5.043E-06	0.000E+00	3.872E-06	3.153E-07	-4.982E-07	-1.328E-08	-2.090E-08
$i=4$	1.998E-03	0.000E+00	-2.326E-03	1.575E-04	1.796E-04	1.863E-05	1.234E-05
$i=5$	8.592E-02	0.000E+00	5.245E-01	-7.419E-02	-3.510E-02	-8.850E-03	-3.656E-03
$i=6$	8.856E+00	0.000E+00	-2.147E+01	1.748E+01	5.453E+00	2.058E+00	5.085E-01

### A.1.3 Conical indentation of a sphere

The fitting coefficients for various shape functions are tabulated in this section for the range of depth-to-radius ratios used in the study,  $(h_m/R_s) = 1\%$ ,  $10\%$ ,  $20\%$ ,  $30\%$ ,  $40\%$  and  $100\%$ .

Table A.41: Fitting coefficients for Eq. (A.1) for the normalized total energy,  $W_t$ , for  $\alpha = 70.3^\circ$  and  $(h_m/R_s) = 20\%$

$\mathbb{C}_p^{jk}$	$j=0$	$j=1$	$j=2$	$j=3$	$j=4$	$j=5$	$j=6$
$i=1$	9.591E-14	0.000E+00	-8.898E-14	4.805E-14	-8.403E-15	2.491E-16	-9.906E-17
$i=2$	-3.206E-10	0.000E+00	2.987E-10	-1.616E-10	2.822E-11	-7.459E-13	3.645E-13
$i=3$	4.177E-07	0.000E+00	-3.912E-07	2.120E-07	-3.692E-08	7.825E-10	-5.400E-10
$i=4$	-2.666E-04	0.000E+00	2.508E-04	-1.363E-04	2.366E-05	-2.695E-07	4.134E-07
$i=5$	8.512E-02	0.000E+00	-8.036E-02	4.383E-02	-7.632E-03	-8.698E-05	-1.751E-04
$i=6$	-1.216E+01	0.000E+00	1.160E+01	-6.263E+00	1.191E+00	1.052E-01	4.108E-02

Table A.42: Fitting coefficients for Eq. (A.1) for the normalized elastic energy,  $W_e$ , for  $\alpha = 70.3^\circ$  and  $(h_m/R_s) = 20\%$

$\mathbb{C}_p^{jk}$	$j=0$	$j=1$	$j=2$	$j=3$	$j=4$	$j=5$	$j=6$
$i=1$	1.834E-14	0.000E+00	-1.691E-14	8.648E-15	-1.658E-15	3.368E-17	3.374E-17
$i=2$	-5.976E-11	0.000E+00	5.486E-11	-2.786E-11	5.425E-12	-1.037E-13	-1.245E-13
$i=3$	7.463E-08	0.000E+00	-6.819E-08	3.425E-08	-6.845E-09	1.229E-10	1.852E-10
$i=4$	-4.445E-05	0.000E+00	4.051E-05	-1.997E-05	4.183E-06	-7.447E-08	-1.427E-07
$i=5$	1.273E-02	0.000E+00	-1.177E-02	5.583E-03	-1.281E-03	2.998E-05	6.104E-05
$i=6$	-1.376E+00	0.000E+00	1.554E+00	-6.637E-01	1.805E-01	-1.119E-02	-1.449E-02

### A.1.4 Spherical indentation of a sphere

The fitting coefficients for various shape functions are tabulated in this section for the range of depth-to-radius ratios used in the study,  $(h_m/R_s) = 1\%$ ,  $10\%$ ,  $20\%$ ,  $30\%$ ,  $40\%$  and  $100\%$ .

Table A.43: Fitting coefficients for Eq. (A.1) for the normalized total energy,  $W_t$ , for  $h_m/R_i = 38.33\%$  and  $h_m/R_s = 5\%$ .

$\mathbb{C}_p^{jk}$	$j=0$	$j=1$	$j=2$	$j=3$	$j=4$	$j=5$	$j=6$
$i=1$	8.593E-20	0.000E+00	-6.564E-20	2.842E-20	-2.973E-21	1.480E-21	-1.920E-21
$i=2$	-7.718E-16	0.000E+00	7.020E-16	-3.694E-16	6.188E-17	-9.092E-18	8.774E-18
$i=3$	2.155E-12	0.000E+00	-2.055E-12	1.129E-12	-2.031E-13	2.108E-14	-1.694E-14
$i=4$	-2.853E-09	0.000E+00	2.769E-09	-1.547E-09	2.845E-10	-2.424E-11	1.801E-11
$i=5$	2.024E-06	0.000E+00	-1.971E-06	1.107E-06	-2.039E-07	1.453E-08	-1.153E-08
$i=6$	-7.767E-04	0.000E+00	7.496E-04	-4.200E-04	7.581E-05	-3.926E-06	4.579E-06
$i=7$	1.471E-01	0.000E+00	-1.376E-01	7.602E-02	-1.286E-02	-9.866E-05	-1.123E-03
$i=8$	-1.062E+01	0.000E+00	8.816E+00	-4.345E+00	7.034E-01	3.562E-01	1.654E-01
$i=9$	1.662E+02	0.000E+00	-8.059E+01	9.093E+00	5.899E+00	-7.205E+00	7.214E+00

Table A.44: Fitting coefficients for Eq. (A.1) for the normalized elastic energy,  $W_e$ , for  $h_m/R_i = 38.33\%$  and  $h_m/R_s = 5\%$ .

$\mathbb{C}_p^{jk}$	$j=0$	$j=1$	$j=2$	$j=3$	$j=4$	$j=5$	$j=6$
$i=1$	-2.472E-18	0.000E+00	2.696E-18	-1.625E-18	3.424E-19	-2.761E-20	4.422E-22
$i=2$	1.109E-14	0.000E+00	-1.220E-14	7.385E-15	-1.563E-15	1.261E-16	-2.087E-18
$i=3$	-2.130E-11	0.000E+00	2.358E-11	-1.432E-11	3.037E-12	-2.443E-13	4.190E-15
$i=4$	2.289E-08	0.000E+00	-2.541E-08	1.545E-08	-3.273E-09	2.613E-10	-4.673E-12
$i=5$	-1.501E-05	0.000E+00	1.662E-05	-1.009E-05	2.128E-06	-1.678E-07	3.176E-09
$i=6$	6.086E-03	0.000E+00	-6.690E-03	4.043E-03	-8.465E-04	6.561E-05	-1.357E-06
$i=7$	-1.457E+00	0.000E+00	1.583E+00	-9.513E-01	1.970E-01	-1.497E-02	3.639E-04
$i=8$	1.794E+02	0.000E+00	-1.920E+02	1.149E+02	-2.352E+01	1.744E+00	-5.965E-02
$i=9$	-8.018E+03	0.000E+00	8.498E+03	-5.062E+03	1.043E+03	-6.589E+01	5.716E+00

## A.2 Isotropic, Linear-elastic, Linear-hardening Material

Similar to Eq. (A1.1), the following function is used to relate the normalized shape functions to the material properties, following Eq. (3.12):

$$\Psi_i = \bar{G}_i^{lh} \left( \frac{E}{Y}, n \right) = \sum_{j=0}^4 \sum_{k=0}^4 \mathbb{C}_i^{jk} \left( \frac{E}{Y} \right)^{5-j} n^{5-k}; \quad i=1-5 \quad (\text{A.2})$$

where  $l$  indicates linear hardening. The fitting coefficients are tabulated in the following tables for two different indenter geometries.

### A.2.1 Conical indentation of a half-space

Fitting coefficients for two shape functions,  $W_t$  and  $W_e$  are tabulated in this section for  $\alpha = 70.3^\circ$ .

Table A.45: Fitting coefficients for Eq. (A.2) for the normalized total energy,  $W_t$ , for  $\alpha = 70.3^\circ$ .

$\mathbb{C}_l^{jk}$	$j=0$	$j=1$	$j=2$	$j=3$	$j=4$
$i=1$	-2.594E-09	3.195E-09	-1.374E-09	3.053E-10	-8.113E-11
$i=2$	6.328E-06	-7.779E-06	3.308E-06	-7.403E-07	2.191E-07
$i=3$	-4.628E-03	5.582E-03	-2.246E-03	5.202E-04	-2.194E-04
$i=4$	-3.188E+00	4.378E+00	-2.488E+00	1.281E+00	1.017E-01
$i=5$	1.953E+02	-2.475E+02	1.186E+02	-4.024E+01	1.428E+01

Table A.46: Fitting coefficients for Eq. (A.2) for the normalized elastic energy,  $W_e$ , for  $\alpha = 70.3^\circ$ .

$\mathbb{C}_l^{jk}$	$j=0$	$j=1$	$j=2$	$j=3$	$j=4$
$i=1$	5.815E-10	-8.438E-10	5.749E-10	-2.356E-10	1.564E-11
$i=2$	-1.737E-06	2.426E-06	-1.603E-06	6.547E-07	-4.315E-08
$i=3$	1.867E-03	-2.498E-03	1.626E-03	-6.879E-04	4.474E-05
$i=4$	-4.106E-01	2.399E-01	3.915E-01	3.698E-01	-2.214E-02
$i=5$	3.186E+01	-2.215E+01	-1.739E+01	1.099E+01	5.680E+00

### A.2.2 Spherical indentation of a half-space

Fitting coefficients for two shape functions,  $W_t$  and  $W_e$  are tabulated in this section for  $(h_m/R_s) = 3\%$ .

Table A.47: Fitting coefficients for Eq. (A.2) for the normalized total energy,  $W_t$ , for  $h_m/R_s = 3\%$ .

$C_l^{jk}$	$j=0$	$j=1$	$j=2$	$j=3$	$j=4$
$i=1$	-2.432E-08	3.063E-08	-1.363E-08	3.293E-09	-8.686E-10
$i=2$	6.885E-05	-8.577E-05	3.750E-05	-8.861E-06	2.384E-06
$i=3$	-6.817E-02	8.346E-02	-3.536E-02	8.211E-03	-2.461E-03
$i=4$	3.326E-01	2.673E+00	-4.767E+00	4.563E+00	1.228E+00
$i=5$	1.131E+02	-3.151E+02	3.237E+02	-2.274E+02	9.837E+01

Table A.48: Fitting coefficients for Eq. (A.2) for the normalized elastic energy,  $W_e$ , for  $h_m/R_s = 3\%$ .

$C_l^{jk}$	$j=0$	$j=1$	$j=2$	$j=3$	$j=4$
$i=1$	-1.585E-09	-5.784E-10	3.325E-09	-2.045E-09	8.774E-11
$i=2$	-1.014E-06	7.475E-06	-1.143E-05	6.102E-06	-2.929E-07
$i=3$	6.072E-03	-1.316E-02	1.400E-02	-6.927E-03	3.751E-04
$i=4$	-2.244E+00	3.404E+00	-1.864E+00	4.089E+00	-2.393E-01
$i=5$	-1.438E+02	1.515E+02	-1.095E+02	-3.038E+01	8.579E+01

### A.3 Transversely Isotropic, Linear-elastic, Perfectly-plastic Material

The procedure to obtain the functional forms of the equations relating normalized shape functions with material properties for transversely isotropic, linear-elastic, perfectly-plastic material is discussed in section 3.3 and depicted in Figure 3.4. In that procedure, one of  $E_z/E_x$ ,  $E_x/G_{xz}$  and  $E_x/Y$  is kept fixed and a surface is selected to express the normalized shape function with the rest of the two parameters. As stated in section 3.3, seven equations (tabulated in Table A.49) were found to be sufficient for all the indenter/substrate geometries considered in this study. The variables  $x$ ,  $y$  and  $z$  of the equations in Table A.49 can be either of  $E_z/E_x$ ,  $E_x/G_{xz}$  or  $E_x/Y$ . Such assignments will be identified by three “xyz-selection” numbers and are tabulated in

Table A.50. The coefficients of the selected surface are expressed as polynomials of the fixed parameter,  $z$ , as follows:

$$\mathbb{C}_{ip}^i = \sum_{j=0}^{j_u} \mathbb{C}_{ip}^{ij} z^j; \quad i = 1-10 \quad (\text{A.3})$$

where  $j_u$  is the degree of the polynomial (upper limit of  $j$ ). For different half-angles (conical indentation) and depth-to-radius ratios (spherical indentation), the equation of the surface, fixed parameters and the degree of the polynomials are tabulated in Table A.51. The coefficients  $\mathbb{C}_{ip}^{ij}$  for the polynomials are tabulated in Table A.53-88.

Table A.49: Equations of the seven surfaces used in the regression analysis (Figure 3.4) for transversely isotropic, linear-elastic, perfectly plastic material.

Equation #	Equation
1	$f = \mathbb{C}_{ip}^1(z) + \mathbb{C}_{ip}^2(z)x + \mathbb{C}_{ip}^3(z)y + \mathbb{C}_{ip}^4(z)x^2 + \mathbb{C}_{ip}^5(z)y^2 + \mathbb{C}_{ip}^6(z)x^3 + \mathbb{C}_{ip}^7(z)y^3 + \mathbb{C}_{ip}^8(z)xy + \mathbb{C}_{ip}^9(z)x^2y + \mathbb{C}_{ip}^{10}(z)xy^2$
2	$f = \mathbb{C}_{ip}^1(z) + \mathbb{C}_{ip}^2(z)\log(x) + \mathbb{C}_{ip}^3(z)\log(y) + \mathbb{C}_{ip}^4(z)\log(x)^2 + \mathbb{C}_{ip}^5(z)\log(y)^2 + \mathbb{C}_{ip}^6(z)\log(x)^3 + \mathbb{C}_{ip}^7(z)\log(y)^3 + \mathbb{C}_{ip}^8(z)\log(x)\log(y) + \mathbb{C}_{ip}^9(z)\log(x)^2\log(y) + \mathbb{C}_{ip}^{10}(z)\log(x)\log(y)^2$
3	$f = \mathbb{C}_{ip}^1(z) + \mathbb{C}_{ip}^2(z)x + \mathbb{C}_{ip}^3(z)y + \mathbb{C}_{ip}^4(z)x^2 + \mathbb{C}_{ip}^5(z)y^2 + \mathbb{C}_{ip}^6(z)x^3 + \mathbb{C}_{ip}^7(z)y^3$
4	$f = \mathbb{C}_{ip}^1(z) + x^{\mathbb{C}_{ip}^2(z)} + y^{\mathbb{C}_{ip}^3(z)}$
5	$f = \mathbb{C}_{ip}^1(z) + \mathbb{C}_{ip}^2(z)x + \mathbb{C}_{ip}^3(z)y + \mathbb{C}_{ip}^4(z)x^2 + \mathbb{C}_{ip}^5(z)y^2 + \mathbb{C}_{ip}^6(z)xy$
6	$f = \mathbb{C}_{ip}^1(z) + \mathbb{C}_{ip}^2(z)\log(x) + \mathbb{C}_{ip}^3(z)y + \mathbb{C}_{ip}^4(z)\log(x)^2 + \mathbb{C}_{ip}^5(z)y^2 + \mathbb{C}_{ip}^6(z)\log(x)y$
7	$f = \mathbb{C}_{ip}^1(z) + \mathbb{C}_{ip}^2(z)\log(x) + \mathbb{C}_{ip}^3(z)\log(y) + \mathbb{C}_{ip}^4(z)\log(x)^2 + \mathbb{C}_{ip}^5(z)\log(y)^2 + \mathbb{C}_{ip}^6(z)\log(x)\log(y)$

Table A.50: The assignment of  $x$ ,  $y$  and  $z$  of the equations in Table A.49 to the non-dimensional material properties groups  $(E_z/E_x)$ ,  $(E_x/G_{xz})$  and  $(E_x/Y)$ .

<b>xyz-selection #</b>	<b><math>x</math></b>	<b><math>y</math></b>	<b><math>z</math></b>
1	$\frac{E_z}{E_x}$	$\frac{E_x}{G_{xz}}$	$\frac{E_x}{Y}$
	$E_x$	$G_{xz}$	$\sigma_Y$
2	$\frac{E_z}{E_x}$	$\frac{E_x}{Y}$	$\frac{E_x}{G_{xz}}$
	$E_x$	$\sigma_Y$	$G_{xz}$
3	$\frac{E_x}{G_{xz}}$	$\frac{E_x}{Y}$	$\frac{E_z}{E_x}$
	$G_{xz}$	$\sigma_Y$	$E_x$

Table A.51: The equations used in the regression analysis for various shape functions for conical indentation of a half-space

Half-angle	Normalized shape function	Equation # (of Table A.49)	xyz-selection # (of Table A.50)	Degree of polynomial ( $j_u$ ) of Eq. (A1.3)
45°	$W_t/(E_x h_m^3)$	4	1	6
	$P_m/(E_x h_m^3)$	4	1	6
	$S_u/(E_x h_m)$	1	3	6
	$W_e/(E_x h_m^3)$	6	1	7
	$h_f/(E_x h_m^3)$	4	1	6
50°	$W_t/(E_x h_m^3)$	4	1	6
	$W_e/(E_x h_m^3)$	6	1	7
60°	$W_t/(E_x h_m^3)$	4	1	6
	$W_e/(E_x h_m^3)$	6	1	7
70°	$W_t/(E_x h_m^3)$	1	1	6
	$W_e/(E_x h_m^3)$	6	1	7
80°	$W_t/(E_x h_m^3)$	1	1	6
	$P_m/(E_x h_m^3)$	1	1	6
	$S_u/(E_x h_m)$	5	3	6
	$W_e/(E_x h_m^3)$	6	1	7
	$h_f/(E_x h_m^3)$	5	3	6

Table A.52: The equations used in the regression analysis for various shape functions for spherical indentation of a half-space.

Depth-to-radius ratio	Normalized shape function	Equation # (of Table A.49)	xyz-selection # (of Table A.50)	Degree of polynomial ( $j_u$ ) of Eq. (A1.3)
1%	$W_t/(E_x h_m^3)$	6	1	7
	$P_m/(E_x h_m^3)$	6	1	7
	$S_u/(E_x h_m)$	7	3	7
	$W_e/(E_x h_m^3)$	6	1	6
	$h_f/(E_x h_m^3)$	6	1	6
20%	$S_u/(E_x h_m)$	5	3	7
	$W_e/(E_x h_m^3)$	6	1	7
40%	$P_m/(E_x h_m^3)$	4	1	6
	$W_e/(E_x h_m^3)$	6	1	7
60%	$P_m/(E_x h_m^3)$	4	1	6
	$W_e/(E_x h_m^3)$	6	1	7
80%	$P_m/(E_x h_m^3)$	4	1	6
	$W_e/(E_x h_m^3)$	6	1	7
100%	$W_t/(E_x h_m^3)$	4	1	6
	$P_m/(E_x h_m^3)$	4	1	6
	$S_u/(E_x h_m)$	1	3	6
	$W_e/(E_x h_m^3)$	6	1	7
	$h_f/(E_x h_m^3)$	4	1	6

Table A.53: Polynomial fitting coefficients for the coefficients of the surface for the normalized total energy,  $W_t$ , for  $\alpha = 45^\circ$ .

$C_{tp}^{ij}$	$j=0$	$j=1$	$j=2$	$j=3$	$j=4$	$j=5$	$j=6$
$i=1$	1.889E-15	-2.223E-12	1.078E-09	-2.786E-07	4.137E-05	-3.557E-03	-1.828E+00
$i=2$	7.507E-17	-8.632E-14	4.055E-11	-9.994E-09	1.376E-06	-1.029E-04	3.526E-03
$i=3$	-2.643E-16	3.062E-13	-1.450E-10	3.602E-08	-4.994E-06	3.742E-04	-1.282E-02

Table A.54: Polynomial fitting coefficients for the coefficients of the surface for the normalized maximum load,  $P_m$ , for  $\alpha = 45^\circ$ .

$C_{tp}^{ij}$	$j=0$	$j=1$	$j=2$	$j=3$	$j=4$	$j=5$	$j=6$
$i=1$	4.671E-15	-5.651E-12	2.828E-09	-7.558E-07	1.161E-04	-1.025E-02	-1.500E+00
$i=2$	5.894E-16	-6.636E-13	3.002E-10	-6.943E-08	8.613E-06	-5.463E-04	1.470E-02
$i=3$	-1.840E-15	2.025E-12	-8.955E-10	2.031E-07	-2.493E-05	1.596E-03	-4.514E-02

Table A.55: Polynomial fitting coefficients for the coefficients of the surface for the normalized unloading slope,  $S_u$ , for  $\alpha = 45^\circ$ .

$C_{tp}^{ij}$	$j=0$	$j=1$	$j=2$	$j=3$	$j=4$	$j=5$	$j=6$
$i=1$	-2.971E-08	4.269E-06	-2.416E-04	7.063E-03	-1.244E-01	1.991E+00	2.880E+00
$i=2$	3.083E-08	-4.177E-06	2.145E-04	-5.267E-03	6.821E-02	-7.485E-01	-1.204E+00
$j=3$	-6.029E-11	8.519E-09	-4.548E-07	1.120E-05	-1.301E-04	1.179E-04	9.514E-03
$j=4$	-8.893E-09	1.134E-06	-5.269E-05	1.065E-03	-8.926E-03	7.785E-02	6.108E-01
$j=5$	1.153E-12	-1.713E-10	9.824E-09	-2.741E-07	3.884E-06	-2.632E-05	3.696E-05
$j=6$	8.087E-10	-9.557E-08	3.813E-06	-4.899E-05	-2.921E-04	5.167E-03	-9.700E-02
$j=7$	-2.056E-15	3.037E-13	-1.729E-11	4.753E-10	-6.539E-09	4.239E-08	-6.677E-08
$j=8$	-8.116E-11	1.257E-08	-7.618E-07	2.299E-05	-3.624E-04	2.992E-03	-9.964E-03
$j=9$	1.454E-11	-2.235E-09	1.348E-07	-4.076E-06	6.533E-05	-5.459E-04	1.768E-03
$i=10$	-2.502E-14	3.549E-12	-1.974E-10	5.674E-09	-9.523E-08	8.576E-07	-1.446E-06

Table A.56: Polynomial fitting coefficients for the coefficients of the surface for the normalized elastic energy,  $W_e$ , for  $\alpha = 45^\circ$ .

$\mathbb{C}_{tp}^{ij}$	$j=0$	$j=1$	$j=2$	$j=3$	$j=4$	$j=5$
$i=1$	-5.833E-19	9.852E-16	-6.864E-13	2.580E-10	-5.702E-08	7.515E-06
$i=2$	-2.737E-20	-7.645E-17	1.132E-13	-5.888E-11	1.570E-08	-2.342E-06
$i=3$	-1.388E-18	1.756E-15	-9.290E-13	2.662E-10	-4.479E-08	4.464E-06
$i=4$	7.521E-20	-7.604E-17	2.797E-14	-3.694E-12	-2.977E-10	1.492E-07
$i=5$	1.922E-19	-2.358E-16	1.200E-13	-3.273E-11	5.160E-09	-4.705E-07
$i=6$	8.419E-20	-1.125E-16	6.306E-14	-1.921E-11	3.447E-09	-3.675E-07

$\mathbb{C}_{tp}^{ij}$	$j=6$	$j=7$
$i=1$	-5.612E-04	1.957E-02
$i=2$	1.913E-04	-7.143E-03
$i=3$	-2.504E-04	6.547E-03
$i=4$	-1.740E-05	7.766E-04
$i=5$	2.323E-05	-5.013E-04
$i=6$	2.215E-05	-6.268E-04

Table A.57: Polynomial fitting coefficients for the coefficients of the surface for the normalized final depth,  $h_f$ , for  $\alpha = 45^\circ$ .

$\mathbb{C}_{tp}^{ij}$	$j=0$	$j=1$	$j=2$	$j=3$	$j=4$	$j=5$	$j=6$
$i=1$	6.739E-15	-7.065E-12	2.842E-09	-5.366E-07	4.484E-05	-1.083E-03	-1.066E+00
$i=2$	2.699E-16	-1.372E-13	-9.660E-12	1.699E-08	-3.357E-06	1.891E-04	5.223E-03
$i=3$	-8.855E-15	8.950E-12	-3.500E-09	6.611E-07	-6.218E-05	3.024E-03	-7.918E-02

Table A.58: Polynomial fitting coefficients for the coefficients of the surface for the normalized total energy,  $W_t$ , for  $\alpha = 80^\circ$ .

$C_{tp}^{ij}$	$j=0$	$j=1$	$j=2$	$j=3$	$j=4$	$j=5$	$j=6$
$i=1$	2.36E-14	-2.85E-11	1.42E-08	-3.79E-06	0.0005822	-0.0523652	2.8522068
$i=2$	1.53E-15	-1.73E-12	7.92E-10	-1.90E-07	2.55E-05	-0.0018658	0.0645295
$i=3$	-6.21E-15	7.56E-12	-3.78E-09	9.99E-07	-0.0001483	0.0120847	-0.467896
$i=4$	-4.58E-17	5.16E-14	-2.37E-11	5.70E-09	-7.66E-07	5.64E-05	-0.001987
$i=5$	7.28E-16	-9.62E-13	5.17E-10	-1.45E-07	2.24E-05	-0.0018504	0.0698096
$i=6$	4.77E-19	-5.38E-16	2.47E-13	-5.92E-11	7.95E-09	-5.85E-07	2.07E-05
$i=7$	-1.09E-17	2.73E-14	-2.05E-11	7.05E-09	-1.25E-06	0.0001131	-0.004564
$i=8$	-2.84E-18	-5.58E-16	2.52E-12	-1.32E-09	3.04E-07	-3.52E-05	0.0018591
$i=9$	-1.99E-19	2.46E-16	-1.25E-13	3.36E-11	-5.12E-09	4.42E-07	-1.97E-05
$i=10$	2.01E-18	-2.03E-15	7.77E-13	-1.37E-10	9.44E-09	1.47E-07	-3.66E-05

Table A.59: Polynomial fitting coefficients for the coefficients of the surface for the normalized maximum load,  $P_m$ , for  $\alpha = 80^\circ$ .

$C_{tp}^{ij}$	$j=0$	$j=1$	$j=2$	$j=3$	$j=4$	$j=5$	$j=6$
$i=1$	1.93E-13	-2.06E-10	8.94E-08	-2.04E-05	0.0026457	-0.2000544	9.3081339
$i=2$	2.92E-15	-3.45E-12	1.67E-09	-4.30E-07	6.22E-05	-0.0048998	0.1802284
$i=3$	-1.25E-13	1.26E-10	-5.07E-08	1.05E-05	-0.0011815	0.0711491	-2.004859
$i=4$	-1.53E-16	1.68E-13	-7.56E-11	1.79E-08	-2.38E-06	0.0001741	-0.006078
$i=5$	3.75E-14	-3.71E-11	1.46E-08	-2.92E-06	0.0003141	-0.0174052	0.4187966
$i=6$	1.63E-18	-1.82E-15	8.28E-13	-1.98E-10	2.63E-08	-1.92E-06	6.61E-05
$i=7$	-3.98E-15	3.94E-12	-1.54E-09	3.07E-07	-3.26E-05	0.0017528	-0.039352
$i=8$	1.02E-15	-1.03E-12	4.09E-10	-8.22E-08	8.86E-06	-0.0005052	0.0135734
$i=9$	1.23E-18	6.53E-17	-6.42E-13	2.74E-10	-4.73E-08	3.75E-06	-0.000124
$i=10$	-1.45E-16	1.33E-13	-4.71E-11	8.13E-09	-7.13E-07	3.07E-05	-0.000585

Table A.60: Polynomial fitting coefficients for the coefficients of the surface for the normalized unloading slope,  $S_u$ , for  $\alpha = 80^\circ$ .

$C_{tp}^{ij}$	$j=0$	$j=1$	$j=2$	$j=3$	$j=4$	$j=5$	$j=6$
$i=1$	-8.77E-08	1.37E-05	-0.0008671	0.0287606	-0.5667772	10.086864	6.113212
$i=2$	2.98E-08	-4.45E-06	0.0002681	-0.0085136	0.1609952	-2.7142624	-0.098368
$i=3$	3.05E-10	-4.70E-08	2.78E-06	-7.89E-05	0.001081	-0.0048307	0.038376
$i=4$	-1.87E-09	2.62E-07	-1.56E-05	0.0005389	-0.0122161	0.2697575	-0.011075
$i=5$	-2.18E-13	3.82E-11	-2.55E-09	8.15E-08	-1.29E-06	8.69E-06	-6.75E-05
$i=6$	-8.56E-11	1.28E-08	-7.29E-07	2.00E-05	-0.0002686	0.001441	-0.003288

Table A.61: Polynomial fitting coefficients for the coefficients of the surface for the normalized elastic energy,  $W_e$ , for  $\alpha = 80^\circ$ .

$C_{tp}^{ij}$	$j=0$	$j=1$	$j=2$	$j=3$	$j=4$	$j=5$	$j=6$
$i=1$	-1.67E-16	2.21E-13	-1.23E-10	3.75E-08	-6.81E-06	0.0007485	-0.047884
$i=2$	4.25E-17	-5.64E-14	3.15E-11	-9.65E-09	1.77E-06	-0.0002001	0.0135129
$i=3$	-4.70E-18	5.65E-15	-2.91E-12	8.57E-10	-1.61E-07	2.03E-05	-0.001682
$i=4$	-7.58E-19	1.07E-15	-6.55E-13	2.27E-10	-4.97E-08	7.09E-06	-0.000647
$i=5$	1.84E-18	-2.34E-15	1.25E-12	-3.60E-10	6.13E-08	-6.22E-06	0.0003623
$i=6$	-3.24E-18	4.22E-15	-2.28E-12	6.54E-10	-1.07E-07	9.70E-06	-0.000426

$C_{tp}^{ij}$	$j=7$
$i=1$	1.532309
$i=2$	-0.47968
$i=3$	0.081405
$i=4$	0.032929
$i=5$	-0.01043
$i=6$	0.003758

Table A.62: Polynomial fitting coefficients for the coefficients of the surface for the normalized final depth,  $h_f$ , for  $\alpha = 80^\circ$ .

$C_{tp}^{ij}$	$j=0$	$j=1$	$j=2$	$j=3$	$j=4$	$j=5$	$j=6$
$i=1$	5.90E-11	7.52E-10	-8.38E-07	6.04E-05	-0.0019004	0.0309202	0.7332771
$i=2$	-1.88E-10	2.95E-08	-1.85E-06	5.90E-05	-0.0010024	0.0086618	-0.046889
$i=3$	1.12E-12	-2.65E-10	2.34E-08	-1.03E-06	2.45E-05	-0.0003258	0.0021757
$i=4$	3.00E-11	-4.87E-09	3.14E-07	-1.01E-05	0.0001641	-0.0012125	0.0034537
$i=5$	-1.89E-15	4.71E-13	-4.37E-11	2.01E-09	-5.06E-08	7.14E-07	-4.84E-06
$i=6$	-1.29E-13	2.57E-11	-1.87E-09	6.26E-08	-9.26E-07	3.53E-06	4.41E-05

Table A.63: Polynomial fitting coefficients for the coefficients of the surface for the normalized total energy,  $W_t$ , for  $(h_m/R) = 1\%$ .

$C_{tp}^{ij}$	$j=0$	$j=1$	$j=2$	$j=3$	$j=4$	$j=5$	$j=6$
$i=1$	-6.277E-16	7.832E-13	-4.090E-10	1.173E-07	-2.065E-05	2.394E-03	-1.970E-01
$i=2$	6.711E-17	-1.913E-14	-3.856E-11	3.042E-08	-9.620E-06	1.579E-03	-1.375E-01
$i=3$	-9.913E-17	9.367E-14	-2.731E-11	-8.536E-10	2.196E-06	-5.182E-04	5.561E-02
$i=4$	-4.126E-17	5.049E-14	-2.428E-11	5.614E-09	-5.559E-07	-7.883E-06	6.216E-03
$i=5$	-2.653E-18	7.530E-15	-6.608E-12	2.810E-09	-6.655E-07	9.137E-05	-7.102E-03
$i=6$	2.896E-17	-3.954E-14	2.222E-11	-6.590E-09	1.095E-06	-9.849E-05	3.961E-03

$C_{tp}^{ij}$	$j=7$
$i=1$	1.330E+01
$i=2$	5.599E+00
$i=3$	-2.784E+00
$i=4$	-4.354E-01
$i=5$	2.712E-01
$i=6$	-8.198E-03

Table A.64: Polynomial fitting coefficients for the coefficients of the surface for the normalized maximum load,  $P_m$ , for  $(h_m/R) = 1\%$ .

$C_{tp}^{ij}$	$j=0$	$j=1$	$j=2$	$j=3$	$j=4$	$j=5$	$j=6$
$i=1$	7.938E-15	-1.017E-11	5.392E-09	-1.524E-06	2.452E-04	-2.192E-02	9.104E-01
$i=2$	7.433E-15	-8.521E-12	3.963E-09	-9.536E-07	1.242E-04	-8.015E-03	1.423E-01
$i=3$	-7.160E-15	8.623E-12	-4.280E-09	1.128E-06	-1.686E-04	1.400E-02	-5.581E-01
$i=4$	-3.884E-15	4.689E-12	-2.334E-09	6.175E-07	-9.297E-05	7.860E-03	-3.352E-01
$i=5$	-6.431E-16	7.901E-13	-4.016E-10	1.091E-07	-1.707E-05	1.544E-03	-7.620E-02
$i=6$	3.986E-15	-4.865E-12	2.453E-09	-6.597E-07	1.015E-04	-8.866E-03	4.010E-01

$C_{tp}^{ij}$	$j=7$
$i=1$	2.830E+00
$i=2$	6.710E+00
$i=3$	5.518E+00
$i=4$	4.950E+00
$i=5$	1.669E+00
$i=6$	-6.932E+00

Table A.65: Polynomial fitting coefficients for the coefficients of the surface for the normalized unloading slope,  $S_u$ , for  $(h_m/R) = 1\%$ .

$C_{tp}^{ij}$	$j=0$	$j=1$	$j=2$	$j=3$	$j=4$	$j=5$	$j=6$
$i=1$	1.601E-08	-3.885E-06	3.674E-04	-1.796E-02	4.967E-01	-7.897E+00	7.482E+01
$i=2$	3.247E-08	-5.701E-06	4.173E-04	-1.645E-02	3.756E-01	-4.894E+00	2.989E+01
$i=3$	-1.090E-08	2.355E-06	-2.061E-04	9.507E-03	-2.499E-01	3.744E+00	-2.969E+01
$i=4$	1.508E-11	-1.319E-07	1.886E-05	-1.087E-03	3.209E-02	-5.161E-01	4.898E+00
$i=5$	1.585E-09	-3.273E-07	2.768E-05	-1.243E-03	3.197E-02	-4.701E-01	3.668E+00
$i=6$	-6.585E-09	1.196E-06	-9.047E-05	3.680E-03	-8.661E-02	1.174E+00	-8.490E+00

$C_{tp}^{ij}$	$j=7$
$i=1$	-1.674E+02
$i=2$	-1.113E+02
$i=3$	9.661E+01
$i=4$	-1.442E+01
$i=5$	-1.178E+01
$i=6$	2.543E+01

Table A.66: Polynomial fitting coefficients for the coefficients of the surface for the normalized elastic energy,  $W_e$ , for  $(h_m/R) = 1\%$ .

$C_{tp}^{ij}$	$j=0$	$j=1$	$j=2$	$j=3$	$j=4$	$j=5$	$j=6$
$i=1$	-9.210E-15	-9.041E-12	1.517E-08	-7.014E-06	1.542E-03	-1.760E-01	9.489E+00
$i=2$	2.343E-14	-2.175E-11	7.349E-09	-9.534E-07	-2.337E-05	1.968E-02	-1.954E+00
$i=3$	4.833E-14	-5.156E-11	2.209E-08	-4.836E-06	5.675E-04	-3.415E-02	9.808E-01
$i=4$	4.771E-15	-4.990E-12	2.060E-09	-4.240E-07	4.552E-05	-2.678E-03	1.352E-01
$i=5$	9.008E-16	-8.595E-13	3.021E-10	-4.467E-08	1.303E-06	3.704E-04	-3.961E-02
$i=6$	-1.878E-14	1.965E-11	-8.181E-09	1.716E-06	-1.880E-04	9.850E-03	-1.881E-01

Table A.67: Polynomial fitting coefficients for the coefficients of the surface for the normalized final depth,  $h_f$ , for  $(h_m/R) = 1\%$ .

$C_{tp}^{ij}$	$j=0$	$j=1$	$j=2$	$j=3$	$j=4$	$j=5$	$j=6$
$i=1$	5.760E-14	-6.478E-11	2.883E-08	-6.348E-06	6.926E-04	-2.961E-02	7.434E-01
$i=2$	-8.201E-14	8.710E-11	-3.671E-08	7.748E-06	-8.394E-04	4.082E-02	-3.967E-01
$i=3$	3.615E-14	-3.454E-11	1.265E-08	-2.204E-06	1.804E-04	-5.188E-03	-7.931E-02
$i=4$	1.441E-14	-1.527E-11	6.431E-09	-1.359E-06	1.482E-04	-7.415E-03	9.237E-02
$i=5$	-6.018E-15	5.817E-12	-2.180E-09	3.984E-07	-3.666E-05	1.555E-03	-2.067E-02
$i=6$	-1.270E-15	1.213E-12	-4.204E-10	5.836E-08	-7.284E-07	-5.417E-04	4.019E-02

Table A.68: Polynomial fitting coefficients for the coefficients of the surface for the normalized total energy,  $W_t$ , for  $(h_m/R) = 100\%$ .

$C_{tp}^{ij}$	$j=0$	$j=1$	$j=2$	$j=3$	$j=4$	$j=5$	$j=6$
$i=1$	4.116E-15	-4.829E-12	2.332E-09	-5.989E-07	8.806E-05	-7.429E-03	-1.661E+00
$i=2$	8.703E-17	-1.012E-13	4.809E-11	-1.197E-08	1.658E-06	-1.233E-04	4.023E-03
$i=3$	-2.897E-16	3.348E-13	-1.580E-10	3.911E-08	-5.401E-06	4.033E-04	-1.351E-02

Table A.69: Polynomial fitting coefficients for the coefficients of the surface for the normalized maximum load,  $P_m$ , for  $(h_m/R) = 100\%$ .

$C_{tp}^{ij}$	$j=0$	$j=1$	$j=2$	$j=3$	$j=4$	$j=5$	$j=6$
$i=1$	7.598E-15	-8.875E-12	4.262E-09	-1.086E-06	1.581E-04	-1.311E-02	-1.422E+00
$i=2$	5.118E-17	-5.817E-14	2.710E-11	-6.656E-09	9.169E-07	-6.848E-05	2.263E-03
$i=3$	-3.805E-16	4.133E-13	-1.827E-10	4.237E-08	-5.514E-06	3.937E-04	-1.299E-02

Table A.70: Polynomial fitting coefficients for the coefficients of the surface for the normalized unloading slope,  $S_u$ , for  $(h_m/R) = 100\%$ .

$C_{tp}^{ij}$	$j=0$	$j=1$	$j=2$	$j=3$	$j=4$	$j=5$	$j=6$
$i=1$	-1.837E-09	8.271E-07	-9.245E-05	4.665E-03	-1.268E-01	2.314E+00	3.443E+00
$i=2$	-8.997E-09	1.072E-06	-3.787E-05	-1.038E-04	3.442E-02	-8.795E-01	-4.966E-01
$i=3$	1.415E-11	-5.274E-09	4.743E-07	-1.778E-05	3.288E-04	-4.193E-03	3.708E-03
$i=4$	6.500E-09	-9.227E-07	4.786E-05	-1.040E-03	5.735E-03	1.221E-01	1.780E-01
$i=5$	-1.933E-13	3.506E-11	-2.328E-09	7.208E-08	-1.124E-06	1.100E-05	-1.056E-05
$i=6$	-1.343E-09	1.961E-07	-1.077E-05	2.703E-04	-2.879E-03	3.748E-03	-4.124E-02
$i=7$	1.459E-15	-2.090E-13	1.151E-11	-3.059E-10	4.080E-09	-2.804E-08	4.423E-08
$i=8$	-1.001E-11	2.901E-09	-2.442E-07	8.811E-06	-1.513E-04	1.508E-03	-2.629E-03
$i=9$	1.676E-11	-2.523E-09	1.463E-07	-4.099E-06	5.728E-05	-3.979E-04	8.094E-04
$i=10$	-2.272E-13	3.017E-11	-1.532E-09	3.747E-08	-4.525E-07	2.206E-06	-5.066E-06

Table A.71: Polynomial fitting coefficients for the coefficients of the surface for the normalized elastic energy,  $W_e$ , for  $(h_m/R) = 100\%$ .

$C_{tp}^{ij}$	$j=0$	$j=1$	$j=2$	$j=3$	$j=4$	$j=5$	$j=6$
$i=1$	-5.382E-18	6.827E-15	-3.636E-12	1.056E-09	-1.818E-07	1.875E-05	-1.101E-03
$i=2$	2.143E-18	-2.710E-15	1.438E-12	-4.157E-10	7.116E-08	-7.294E-06	4.252E-04
$i=3$	7.594E-21	9.482E-17	-1.154E-13	5.547E-11	-1.394E-08	1.961E-06	-1.503E-04
$i=4$	-1.508E-19	1.993E-16	-1.116E-13	3.443E-11	-6.352E-09	7.077E-07	-4.505E-05
$i=5$	1.229E-19	-1.505E-16	7.600E-14	-2.044E-11	3.160E-09	-2.827E-07	1.397E-05
$i=6$	-3.056E-19	3.513E-16	-1.631E-13	3.883E-11	-4.917E-09	2.951E-07	-3.511E-06

$C_{tp}^{ij}$	$j=6$
$i=1$	3.027E-02
$i=2$	-1.156E-02
$i=3$	5.216E-03
$i=4$	1.335E-03
$i=5$	-3.241E-04
$i=6$	-2.929E-04

Table A.72: Polynomial fitting coefficients for the coefficients of the surface for the normalized final depth,  $h_f$ , for  $(h_m/R) = 100\%$ .

$C_{tp}^{ij}$	$j=0$	$j=1$	$j=2$	$j=3$	$j=4$	$j=5$	$j=6$
$i=1$	8.772E-15	-8.910E-12	3.581E-09	-7.160E-07	7.166E-05	-2.773E-03	-1.051E+00
$i=2$	-3.541E-15	3.650E-12	-1.493E-09	3.075E-07	-3.301E-05	1.659E-03	-2.042E-02
$i=3$	2.923E-15	-2.708E-12	9.148E-10	-1.272E-07	3.277E-06	8.269E-04	-6.931E-02

Table A.73: Polynomial fitting coefficients for the coefficients of the surface for the normalized total energy,  $W_t$ , for  $\alpha = 50^\circ$ .

$C_{tp}^{ij}$	$j=0$	$j=1$	$j=2$	$j=3$	$j=4$	$j=5$	$j=6$
$i=1$	2.499E-15	-2.944E-12	1.429E-09	-3.697E-07	5.499E-05	-4.747E-03	-1.768E+00
$i=2$	1.145E-16	-1.309E-13	6.117E-11	-1.503E-08	2.070E-06	-1.559E-04	5.413E-03
$i=3$	-3.988E-16	4.616E-13	-2.186E-10	5.441E-08	-7.580E-06	5.736E-04	-1.985E-02

Table A.74: Polynomial fitting coefficients for the coefficients of the surface for the normalized elastic energy,  $W_e$ , for  $\alpha = 50^\circ$ .

$\mathbb{C}_{tp}^{ij}$	$j=0$	$j=1$	$j=2$	$j=3$	$j=4$	$j=5$	$j=6$
$i=1$	-2.700E-18	3.694E-15	-2.155E-12	6.970E-10	-1.356E-07	1.601E-05	-1.088E-03
$i=2$	5.212E-19	-8.414E-16	5.691E-13	-2.093E-10	4.539E-08	-5.848E-06	4.237E-04
$i=3$	-8.725E-19	1.201E-15	-6.918E-13	2.167E-10	-4.002E-08	4.409E-06	-2.756E-04
$i=4$	7.713E-20	-6.296E-17	1.056E-14	5.147E-12	-2.605E-09	4.793E-07	-4.233E-05
$i=5$	1.402E-19	-1.725E-16	8.812E-14	-2.422E-11	3.883E-09	-3.676E-07	1.962E-05
$i=6$	-7.230E-20	6.408E-17	-1.763E-14	-2.045E-13	1.038E-09	-2.177E-07	1.952E-05

$\mathbb{C}_{tp}^{ij}$	$j=7$
$i=1$	3.506E-02
$i=2$	-1.419E-02
$i=3$	8.122E-03
$i=4$	1.598E-03
$i=5$	-4.912E-04
$i=6$	-7.284E-04

Table A.75: Polynomial fitting coefficients for the coefficients of the surface for the normalized total energy,  $W_t$ , for  $\alpha = 60^\circ$ .

$\mathbb{C}_{tp}^{ij}$	$j=0$	$j=1$	$j=2$	$j=3$	$j=4$	$j=5$	$j=6$
$i=1$	4.465E-15	-5.240E-12	2.535E-09	-6.537E-07	9.716E-05	-8.443E-03	-1.573E+00
$i=2$	2.658E-16	-3.080E-13	1.459E-10	-3.635E-08	5.083E-06	-3.898E-04	1.389E-02
$i=3$	-1.022E-15	1.179E-12	-5.561E-10	1.379E-07	-1.916E-05	1.454E-03	-5.073E-02

Table A.76: Polynomial fitting coefficients for the coefficients of the surface for the normalized elastic energy,  $W_e$ , for  $\alpha = 60^\circ$ .

$C_{tp}^{ij}$	$j=0$	$j=1$	$j=2$	$j=3$	$j=4$	$j=5$	$j=6$
$i=1$	-7.090E-18	9.784E-15	-5.725E-12	1.847E-09	-3.570E-07	4.190E-05	-2.844E-03
$i=2$	2.215E-18	-3.232E-15	1.993E-12	-6.741E-10	1.357E-07	-1.644E-05	1.143E-03
$i=3$	-2.159E-18	2.814E-15	-1.537E-12	4.564E-10	-7.988E-08	8.354E-06	-5.033E-04
$i=4$	-1.768E-20	7.790E-17	-7.932E-14	3.700E-11	-9.383E-09	1.353E-06	-1.077E-04
$i=5$	2.368E-19	-2.986E-16	1.558E-13	-4.352E-11	7.049E-09	-6.719E-07	3.645E-05
$i=6$	6.249E-20	-8.375E-17	5.013E-14	-1.732E-11	3.683E-09	-4.767E-07	3.553E-05

$C_{tp}^{ij}$	$j=6$
$i=1$	9.277E-02
$i=2$	-3.799E-02
$i=3$	1.511E-02
$i=4$	4.000E-03
$i=5$	-9.625E-04
$i=6$	-1.315E-03

Table A.77: Polynomial fitting coefficients for the coefficients of the surface for the normalized total energy,  $W_t$ , for  $\alpha = 70^\circ$ .

$C_{tp}^{ij}$	$j=0$	$j=1$	$j=2$	$j=3$	$j=4$	$j=5$	$j=6$
$i=1$	1.470E-14	-1.667E-11	7.721E-09	-1.886E-06	2.619E-04	-2.098E-02	9.858E-01
$i=2$	1.960E-16	-2.274E-13	1.079E-10	-2.695E-08	3.774E-06	-2.908E-04	1.069E-02
$i=3$	-6.332E-15	6.814E-12	-2.941E-09	6.502E-07	-7.801E-05	4.938E-03	-1.424E-01
$i=4$	-8.827E-18	1.004E-14	-4.646E-12	1.120E-09	-1.499E-07	1.091E-05	-3.763E-04
$i=5$	1.437E-15	-1.508E-12	6.299E-10	-1.333E-07	1.503E-05	-8.677E-04	2.184E-02
$i=6$	9.869E-20	-1.125E-16	5.213E-14	-1.257E-11	1.678E-09	-1.213E-07	4.135E-06
$i=7$	-1.175E-16	1.218E-13	-5.012E-11	1.040E-08	-1.145E-06	6.397E-05	-1.546E-03
$i=8$	5.861E-17	-6.385E-14	2.775E-11	-6.117E-09	7.187E-07	-4.313E-05	1.108E-03
$i=9$	-2.334E-19	2.726E-16	-1.283E-13	3.110E-11	-4.091E-09	2.815E-07	-8.569E-06
$i=10$	-7.446E-18	7.884E-15	-3.302E-12	6.922E-10	-7.568E-08	4.059E-06	-8.447E-05

Table A.78: Polynomial fitting coefficients for the coefficients of the surface for the normalized elastic energy,  $W_e$ , for  $\alpha = 70^\circ$ .

$\mathbb{C}_{tp}^{ij}$	$j=0$	$j=1$	$j=2$	$j=3$	$j=4$	$j=5$	$j=6$
$i=1$	-1.960E-17	2.769E-14	-1.662E-11	5.498E-09	-1.085E-06	1.288E-04	-8.750E-03
$i=2$	4.001E-18	-6.044E-15	3.919E-12	-1.409E-09	3.035E-07	-3.935E-05	2.915E-03
$i=3$	-4.977E-18	5.863E-15	-2.866E-12	7.595E-10	-1.204E-07	1.195E-05	-7.486E-04
$i=4$	1.075E-18	-1.136E-15	4.549E-13	-7.794E-11	1.859E-09	1.277E-06	-1.820E-04
$i=5$	2.041E-18	-2.325E-15	1.087E-12	-2.698E-10	3.847E-08	-3.183E-06	1.466E-04
$i=6$	-2.001E-18	2.243E-15	-1.029E-12	2.483E-10	-3.357E-08	2.454E-06	-7.795E-05

$\mathbb{C}_{tp}^{ij}$	$j=7$
$i=1$	2.849E-01
$i=2$	-1.035E-01
$i=3$	2.659E-02
$i=4$	8.968E-03
$i=5$	-3.217E-03
$i=6$	-1.600E-04

Table A.79: Polynomial fitting coefficients for the coefficients of the surface for the normalized unloading slope,  $S_u$ , for  $\alpha = 80^\circ$ .

$\mathbb{C}_{tp}^{ij}$	$j=0$	$j=1$	$j=2$	$j=3$	$j=4$	$j=5$	$j=6$
$i=1$	-8.774E-08	1.374E-05	-8.671E-04	2.876E-02	-5.668E-01	1.009E+01	6.113E+00
$i=2$	2.981E-08	-4.453E-06	2.681E-04	-8.514E-03	1.610E-01	-2.714E+00	-9.836E-02
$i=3$	3.054E-10	-4.703E-08	2.782E-06	-7.889E-05	1.081E-03	-4.831E-03	3.838E-02
$i=4$	-1.869E-09	2.622E-07	-1.562E-05	5.389E-04	-1.222E-02	2.698E-01	-1.108E-02
$i=5$	-2.184E-13	3.816E-11	-2.547E-09	8.154E-08	-1.285E-06	8.687E-06	-6.753E-05
$i=6$	-8.565E-11	1.275E-08	-7.288E-07	1.999E-05	-2.686E-04	1.441E-03	-3.288E-03

Table A.80: Polynomial fitting coefficients for the coefficients of the surface for the normalized elastic energy,  $W_e$ , for  $\alpha = 80^\circ$ .

$C_{tp}^{ij}$	$j=0$	$j=1$	$j=2$	$j=3$	$j=4$	$j=5$	$j=6$
$i=1$	-1.672E-16	2.211E-13	-1.231E-10	3.754E-08	-6.814E-06	7.485E-04	-4.788E-02
$i=2$	4.253E-17	-5.635E-14	3.147E-11	-9.649E-09	1.774E-06	-2.001E-04	1.351E-02
$i=3$	-4.702E-18	5.650E-15	-2.913E-12	8.574E-10	-1.613E-07	2.029E-05	-1.682E-03
$i=4$	-7.583E-19	1.073E-15	-6.546E-13	2.272E-10	-4.969E-08	7.093E-06	-6.468E-04
$i=5$	1.838E-18	-2.343E-15	1.248E-12	-3.604E-10	6.126E-08	-6.218E-06	3.623E-04
$i=6$	-3.236E-18	4.224E-15	-2.278E-12	6.535E-10	-1.066E-07	9.700E-06	-4.261E-04

$C_{tp}^{ij}$	$j=7$
$i=1$	1.532E+00
$i=2$	-4.797E-01
$i=3$	8.141E-02
$i=4$	3.293E-02
$i=5$	-1.043E-02
$i=6$	3.758E-03

Table A.81: Polynomial fitting coefficients for the coefficients of the surface for the normalized unloading slope,  $S_u$ , for  $(h_m/R) = 20\%$ .

$C_{tp}^{ij}$	$j=0$	$j=1$	$j=2$	$j=3$	$j=4$	$j=5$	$j=6$
$i=1$	-5.225E-10	8.513E-08	-4.768E-06	7.393E-05	2.989E-03	-1.638E-01	4.739E+00
$i=2$	6.782E-10	-1.171E-07	7.933E-06	-2.619E-04	4.026E-03	-7.693E-03	-9.865E-01
$i=3$	-6.499E-13	5.299E-11	2.238E-10	-1.602E-07	7.588E-06	-1.853E-04	2.099E-03
$i=4$	-1.751E-10	2.961E-08	-1.994E-06	6.760E-05	-1.180E-03	8.414E-03	6.951E-02
$i=5$	-2.867E-14	4.790E-12	-3.224E-10	1.124E-08	-2.185E-07	2.410E-06	-1.562E-05
$i=6$	3.088E-12	-5.014E-10	3.286E-08	-1.115E-06	2.081E-05	-2.087E-04	1.074E-03

$C_{tp}^{ij}$	$j=7$
$i=1$	7.731E+00
$i=2$	-1.961E+00
$i=3$	1.396E-02
$i=4$	2.788E-01
$i=5$	1.376E-06
$i=6$	-3.066E-03

Table A.82: Polynomial fitting coefficients for the coefficients of the surface for the normalized elastic energy,  $W_e$ , for  $(h_m/R) = 20\%$ .

$C_{tp}^{ij}$	$j=0$	$j=1$	$j=2$	$j=3$	$j=4$	$j=5$	$j=6$
$i=1$	1.330E-18	5.394E-15	-7.419E-12	3.744E-09	-9.719E-07	1.406E-04	-1.110E-02
$i=2$	5.566E-18	-1.021E-14	7.408E-12	-2.818E-09	6.159E-07	-7.871E-05	5.620E-03
$i=3$	-3.399E-17	4.255E-14	-2.219E-11	6.236E-09	-1.019E-06	9.727E-05	-5.104E-03
$i=4$	3.611E-19	-7.486E-17	-2.068E-13	1.461E-10	-4.271E-08	6.534E-06	-5.314E-04
$i=5$	3.299E-18	-4.141E-15	2.161E-12	-6.058E-10	9.821E-08	-9.189E-06	4.613E-04
$i=6$	2.219E-18	-2.700E-15	1.370E-12	-3.769E-10	6.109E-08	-5.942E-06	3.356E-04

$C_{tp}^{ij}$	$j=7$
$i=1$	4.033E-01
$i=2$	-1.873E-01
$i=3$	1.224E-01
$i=4$	1.978E-02
$i=5$	-9.914E-03
$i=6$	-9.552E-03

Table A.83: Polynomial fitting coefficients for the coefficients of the surface for the normalized maximum load,  $P_m$ , for  $(h_m/R) = 40\%$ .

$C_{tp}^{ij}$	$j=0$	$j=1$	$j=2$	$j=3$	$j=4$	$j=5$	$j=6$
$i=1$	1.977E-14	-2.324E-11	1.128E-08	-2.930E-06	4.399E-04	-3.850E-02	-1.287E-01
$i=2$	-1.477E-15	1.400E-12	-4.958E-10	7.732E-08	-3.961E-06	-1.998E-04	2.033E-02
$i=3$	2.174E-15	-1.887E-12	5.552E-10	-4.506E-08	-7.468E-06	1.579E-03	-8.208E-02

Table A.84: Polynomial fitting coefficients for the coefficients of the surface for the normalized elastic energy,  $W_e$ , for  $(h_m/R) = 40\%$ .

$C_{tp}^{ij}$	$j=0$	$j=1$	$j=2$	$j=3$	$j=4$	$j=5$	$j=6$
$i=1$	-2.807E-17	3.658E-14	-2.004E-11	5.992E-09	-1.061E-06	1.125E-04	-6.784E-03
$i=2$	1.506E-17	-1.933E-14	1.040E-11	-3.046E-09	5.259E-07	-5.410E-05	3.147E-03
$i=3$	-3.000E-18	3.914E-15	-2.162E-12	6.592E-10	-1.210E-07	1.361E-05	-8.994E-04
$i=4$	-2.332E-18	2.957E-15	-1.567E-12	4.505E-10	-7.607E-08	7.620E-06	-4.302E-04
$i=5$	-3.290E-19	3.859E-16	-1.824E-13	4.389E-11	-5.476E-09	2.902E-07	2.631E-06
$i=6$	1.099E-18	-1.368E-15	7.090E-13	-1.986E-10	3.260E-08	-3.180E-06	1.768E-04

$C_{tp}^{ij}$	$j=6$
$i=1$	1.912E-01
$i=2$	-8.521E-02
$i=3$	2.911E-02
$i=4$	1.132E-02
$i=5$	-6.866E-04
$i=6$	-4.720E-03

Table A.85: Polynomial fitting coefficients for the coefficients of the surface for the normalized maximum load,  $P_m$ , for  $(h_m/R) = 60\%$ .

$C_{tp}^{ij}$	$j=0$	$j=1$	$j=2$	$j=3$	$j=4$	$j=5$	$j=6$
$i=1$	1.497E-14	-1.757E-11	8.485E-09	-2.179E-06	3.202E-04	-2.694E-02	-7.838E-01
$i=2$	4.722E-16	-5.318E-13	2.429E-10	-5.759E-08	7.491E-06	-5.115E-04	1.471E-02
$i=3$	-1.529E-15	1.728E-12	-7.929E-10	1.892E-07	-2.484E-05	1.723E-03	-5.128E-02

Table A.86: Polynomial fitting coefficients for the coefficients of the surface for the normalized elastic energy,  $W_e$ , for  $(h_m/R) = 60\%$ .

$C_{tp}^{ij}$	$j=0$	$j=1$	$j=2$	$j=3$	$j=4$	$j=5$	$j=6$
$i=1$	-8.430E-18	1.132E-14	-6.430E-12	2.009E-09	-3.748E-07	4.214E-05	-2.701E-03
$i=2$	3.847E-18	-5.075E-15	2.832E-12	-8.690E-10	1.592E-07	-1.761E-05	1.111E-03
$i=3$	-2.816E-18	3.631E-15	-1.968E-12	5.829E-10	-1.025E-07	1.084E-05	-6.570E-04
$i=4$	-4.368E-19	5.803E-16	-3.265E-13	1.012E-10	-1.876E-08	2.104E-06	-1.350E-04
$i=5$	3.432E-19	-4.233E-16	2.173E-13	-6.022E-11	9.742E-09	-9.270E-07	4.898E-05
$i=6$	1.287E-19	-1.881E-16	1.155E-13	-3.870E-11	7.680E-09	-9.131E-07	6.177E-05

$C_{tp}^{ij}$	$j=7$
$i=1$	8.045E-02
$i=2$	-3.260E-02
$i=3$	1.885E-02
$i=4$	4.045E-03
$i=5$	-1.173E-03
$i=6$	-1.956E-03

Table A.87: Polynomial fitting coefficients for the coefficients of the surface for the normalized maximum load,  $P_m$ , for  $(h_m/R) = 80\%$ .

$C_{tp}^{ij}$	$j=0$	$j=1$	$j=2$	$j=3$	$j=4$	$j=5$	$j=6$
$i=1$	1.057E-14	-1.238E-11	5.963E-09	-1.525E-06	2.227E-04	-1.853E-02	-1.180E+00
$i=2$	1.049E-16	-1.203E-13	5.617E-11	-1.369E-08	1.848E-06	-1.330E-04	4.151E-03
$i=3$	-4.057E-16	4.654E-13	-2.182E-10	5.372E-08	-7.385E-06	5.485E-04	-1.821E-02

Table A.88: Polynomial fitting coefficients for the coefficients of the surface for the normalized elastic energy,  $W_e$ , for  $(h_m/R) = 80\%$ .

$C_{tp}^{ij}$	$j=0$	$j=1$	$j=2$	$j=3$	$j=4$	$j=5$	$j=6$
$i=1$	-3.799E-18	5.198E-15	-3.011E-12	9.601E-10	-1.829E-07	2.103E-05	-1.382E-03
$i=2$	1.970E-18	-2.624E-15	1.477E-12	-4.566E-10	8.421E-08	-9.363E-06	5.941E-04
$i=3$	-2.158E-18	2.767E-15	-1.488E-12	4.357E-10	-7.535E-08	7.773E-06	-4.534E-04
$i=4$	-2.485E-19	3.335E-16	-1.892E-13	5.897E-11	-1.096E-08	1.227E-06	-7.817E-05
$i=5$	2.194E-19	-2.702E-16	1.382E-13	-3.801E-11	6.073E-09	-5.670E-07	2.919E-05
$i=6$	1.488E-19	-2.025E-16	1.163E-13	-3.655E-11	6.809E-09	-7.567E-07	4.730E-05

$C_{tp}^{ij}$	$j=7$
$i=1$	4.231E-02
$i=2$	-1.747E-02
$i=3$	1.226E-02
$i=4$	2.301E-03
$i=5$	-6.775E-04
$i=6$	-1.354E-03





